SOLID STATE AND MECHANISTIC STUDY OF SCHIFF-BASE COMPLEXES OF MIDDLE TRANSITION AND PLATINUM GROUP ELEMENTS

by

PETRUS PENNIE MOKOLOKOLO

A thesis submitted to meet the requirements for the degree of

PHILOSOPHIAE DOCTOR

In the

DEPARTMENT OF CHEMISTRY

FACULTY OF NATURAL AND AGRICULATURAL SCIENCES

At the

UNIVERSITY OF THE FREE STATE

PROMOTER: PROF. ANDREAS ROODT

CO-PROMOTOR: DR. A. BRINK

FEBRUARY 2018

Acknowledgements

First of all, all glory to God, my foundation, the very breath of my life. Thank You Lord for all that You have bestowed upon my life. I am nothing without You.

To Prof Andreas Roodt, I am truly short for words to describe how grateful I am for the opportunities, the support and guidance you have given me over the years. I am in awe of your willingness to have sleepless nights making sure that this work is complete and I will forever be grateful.

To Alice, thank you for your hard work, your support and patience with me, you set an example for all of us. You did it with such grace and wit and such passion. Thank you for always having my back. I will always be grateful for that.

To Deon and Marietjie, thank you for your support, enthusiasm and for always making time to listen and guide. I will always be grateful for that.

Thank you to Prof Alberto for the opportunities to spend some time in Zurich. Thank you for your support, your enthusiasm and inputs. Thank you to Angelo, Giuse and Dr Braband for always being on standby to help.

Thank you to the all the Inorganic chemistry group for all your help and also for making the lab hours fun and enjoyable

Thank you Dr Linnet for always being there whenever I need your assistance

To my family, my strengths and to my life partner Kutlwano, thank you guys for your unconditional love and unwavering support

To all my friends and the Yose's, de Wet's and Karen, I am grateful thank you are part of my life.

Financial assistance from SASOL, University of the Free State and the South African National Research Foundation is gratefully acknowledged.

Table of Contents

Chapter 3

Chapter 7

Kinetic Study of the Iodomethane Oxidative Addition to [Rh(N,O-Schiff-Base)(CO)(PPh_3)] Complexes .....

Chapter 8

Preliminary Solid-State NMR Investigation on [Rh(L,L'-Bid)(CO)(PX_3)] Complexes .....

Chapter 9

Evaluation of Study .....

Abbreviations and Symbols

Abbreviation	Meaning
L,L'-Bid	Bidentate ligand
Sal	Salicylidene
PPX_3	Tertiary phosphine
Me	Methyl
α	Alpha
β	Beta
γ	Gamma
°	Degrees
°C	Degrees Celsius
$\Delta S^{\neq}$	Entropy of activation
$\Delta H^{\neq}$	Enthalpy of activation
k_B	Boltzmann's constant
π	Pi
Z	Number of molecules in a unit cell
IR	Infrared spectroscopy
UV	Ultraviolet region in light spectrum
Vis	Visible region in light spectrum
NMR	Nuclear magnetic resonance spectroscopy
XRD	X-ray diffraction
v	Stretching frequency on IR
CO	Carbonyl
ppm	(Units of chemical shift) parts per million
RMS	Root Mean Square
MeOH	Methanol
EtPh	phenylethyl
*m*Tol	Tolyl
CycHex	Cyclohexylamine
iProp	Isopropyl

CyPent	Cyclopentyl
k_{obs}	Observed pseudo first-order rate constant
Ox	8-hydroxyquinoline
PPh_3	Triphenylphosphine
PPh_2Cy	Cyclohexyldiphenylphosphine
$PPhCy_2$	Dicyclohexylphosphine
PCy_3	tricyclohexylphosphine

Abstract

The principle aim of this study was to investigate the coordination behavior of N,O Schiff-base and oxine-type ligand systems to selected middle and late transition metal carbonyl cores. Firstly, the coordination behavior of Schiff-base bidentate ligands to the *fac*-$[M^{I}(CO)_3]^+$ (M = manganese, technetium or rhenium) was investigated in the context of radiopharmaceutical models. A bidentate ligand can be used in combination with a monodentate ligand utilizing the [2+1] labeling approach, wherein a biologically active component is appended to either the bidentate or the monodentate ligands. Secondly, due to the structural relevance of these ligands systems, the study was extended to investigate their coordination to rhodium(I) as potential supramolecular building blocks for the construction of infinite one dimensional metal chains in the solid state. The oxine ligands systems were incorporated in the investigation to investigate their steric and electronic influence on the assembly of metal-metal chains due to their excellent chelating ability. Moreover, they are known to introduce variations in the metallocycle formed with the rhodium centre (five-membered in oxines *vs*. six membered for the Schiff-base ligands).

With the above in mind, a range of bidentate Schiff-base ligands (5-Me-Sal-CyPentH = 2-(cyclopentyl)methyl-5-methylphenol, (Sal-CyHexH = 2-(cyclohexyliminomethyl-)phenol, 5-Me-Sal-EtPhH = 5-methyl-2-(phenylethyliminimethyl)-phenol and Sal-*m*TolH = 2-(*m*-Tolyliminomethyl)phenol, with varying electronic and steric properties were coordinated to the *fac*-$[M(CO)_3]^+$ { M = manganese(I), technetium(I) or rhenium(I)}. Single crystal structures were obtained for complexes *fac*-$[Mn(5\text{-}Me\text{-}Sal\text{-}CyPent)(CO)_3]_2$ **(1)**, *fac*-$[Re(Sal\text{-}CyHex)(CO)_3]_2$ **(2)**, *fac*-$[Re(5\text{-}Me\text{-}Sal\text{-}EtPh)(CO)_3\text{-}(MeOH)]$ **(3),** *fac*-$[^{99}Tc(Sal\text{-}m\text{Tol})(CO)_3]_2$ **(4)**, *fac*-$[^{99}Tc(5\text{-}Me\text{-}Sal\text{-}CyPent)(CO)_3]_2$ **(5)** and *fac*-$[^{99}Tc(5\text{-}Me\text{-}Sal\text{-}EtPh)(CO)_3]$ **(6)**. The study illustrated that the nuclearity of the rhenium(I) complexes can be manipulated to produce either mono- or dinuclear structures. However, only dinuclear complexes could be isolated with manganese(I) and technetium(I) in spite of employing similar synthesis procedures as for the

rhenium(I) complexes. It is postulated that the rhenium mononuclear compound is an intermediate which can be isolated due to the slower reactivity in rhenium complexes, while the increased reactivity in manganese and technetium prevents the isolation of the mononuclear complex. The basic coordination geometry of the mononuclear complex resembles that of the dinuclear one with the metal atom sitting at the centre of an octahedron coordinated by three facially carbonyl ligands, the oxygen and nitrogen atoms of the bidentate chelate. The coordination is completed by a methanol molecule in the mononuclear complex **(3)**, or by the bridging phenolato oxygen atom of the bidentate ligands forming a rigid coplanar system in the dinuclear compound.

Rhodium(I) complexes [Rh(5,7-Diido-Ox)$(CO)_2$] **(7)**, [Rh(5,7-DiMe-Ox)$(CO)_2$] **(8)** and [Rh(5-Me-Sal-iProp)$(CO)_2$] **(9)** {where 5,7-diido-OxH = 5,7-Diido-8-hydroxyquinoline, 5,7-Dimethyl-OxH = 5,7-Dimethy-8-hydroxyquinoline and (5-Me-Sal-iPropH = 5-Methyl-2-(isopropyliminomethyl)phenol} were synthesized and the electronic and steric effects on the potential assembly of one dimensional metallophilic interactions in the solid state were evaluated. Two classes of rhodium-rhodium interactions were observed from the single X-ray diffraction results. In the one type of interaction, an infinite array of metal-metal interactions occurs in the crystal lattice with a Rh···Rh distance of 3.4602(24) Å for complex **(7)**. In the other type, the rhodium-rhodium interactions are restricted between two neighboring molecules forming pseudo dimeric pairs with the intermolecular Rh···Rh distance of 3.1345(17) Å and 3.6007(10) Å for complexes **(8)** and **(9)** respectively.

The [Rh(L,L-Bid)(CO)(PPh_3)] complexes, where L,L'-Bid is a monocharged bidentate ligand, are fairly well-behaved models in solution for study by ^{31}P NMR, to correlate Rh-P bond distances from solid-state X-ray structural data with observed solution behavior. This study was extended to include solid-state ^{31}P data and a reasonable correlation was obtained.

Finally, a kinetic study was conducted to evaluate the reactivity of the rhodium(I) Schiff-base complexes of the form [Rh(Schiff-base)(CO)(PPh_3)] towards the oxidative addition of iodomethane thereon. The Schiff-base ligands have varying

electronic and steric parameters as informed by the cyclopentyl, isopropyl, cyclohexyl and the methyl substituents attached to the imine nitrogen atom. The effects of these varying factors on the rate of oxidative addition were evaluated in order to further understand the role of the coordinated ligand in this process. Only the formation of the rhodium(III) alkyl species could be observed with no subsequent formation of the rhodium(III) acyl species noted. This is assumed to be due to the slow rate of formation of the acyl species relative to the alkyl(III) product. No significant changes of the activity of the Schiff-base substituents on the rhodium(I) complexes towards the oxidative addition of iodomethane were observed as indicated by the second-order rate constants (k_1, $M^{-1}.s^{-1}$) [Rh(5-Me-Sal-CyPent)(CO)(PPh_3)], 0.072(2); [Rh(5-Me-Sal-Iso)(CO)(PPh_3)], 0.058(1) and [Rh(Sal-CyHex)(CO)(PPh_3)], 0.054(1) in spite of the different substituents incorporated on the ligand backbone. The effect of the tertiary phosphine ligands on the rates of oxidative addition of iodomethane was also evaluated in the complexes [Rh(Schiff-base)(CO)(PPX_3)], where PPX_3 = PPh_3, PPh_2Cy, $PPhCy_2$ and PCy_3, containing a systematic variation on the substituents of the PPX_3. The second-order rate constants (k_1, $M^{-1}.s^{-1}$) for the alkyl formation in the oxidative addition of iodomethane were determined to be [Rh(5-Me-SalCyPent)(CO)(PPh_3)], 0.072(2); [Rh(5-Me-SalCyPent)(CO)(PPh_2Cy)] 0.146(1); [Rh(5-Me-SalCyPent)(CO)($PPhCy_2$)], 0.026(5) and [Rh(5-Me-SalCyPent)(CO)(PCy_3)], 0.082(1). It was anticipated that the rates would increase with the systematic substitution of the weaker donating phenyl rings on the tertiary phosphine by the more electron-rich cyclohexyl rings. However, the results obtained indicated a somewhat competing effect between the steric and electronic parameters of the phosphine ligands: the observed rates are not in correlation with the electron donating capabilities of the tertiary phosphine ligands. The activation parameters for the oxidative addition of iodomethane to the complex [Rh(5-Me-Sal-CyPent)($CO)_2$(PPh_3)] were determined from a variable temperature study in dichloromethane. An associative type mechanism was assigned for the oxidative addition reaction due to the relatively small $\Delta H^{\neq}$ = 36(1) kJ mol^{-1} and a large negative $\Delta S^{\neq}$ = -145(5) (J K^{-1} mol) values which are characteristic of an associative type mechanism.

1 Introduction and Aim

1.1 Introduction

Since the seminal development in synthetic methods for the preparation of the *fac*-$[M(CO)_3(H_2O)_3)]^+$ (where M = Tc, Re) core for potential radiopharmaceutical application, much attention has been given to designing ligands that can provide *in vivo* stability to the tricarbonyl core. The precursor synthon comprises of kinetically stable carbonyl ligands and three labile water molecules. The coordinated water ligands can be readily sacrificed by various mono-, bi- or tridentate ligand systems that can also serve as anchors for a biomolecule.[1,2,3,4] Due to the versatile nature of the *fac*-$[M(CO)_3]^+$ core, many synthetic variations have been developed for optimization of the properties and activity of the model radiopharmaceuticals. One of the widely sought after strategies is the [2+1] mixed ligand approach,[5,6,7,8] which is applicable under certain conditions. This concept involves a combination of a bidentate and monodentate ligands to form a fully coordinated stable tricarbonyl complex for potential application as imaging/ therapeutic agent. A biomolecule can also be appended within the ligand framework and the characteristics thereof can be manipulated by variations on either the bidentate or monodentate ligand backbone.

In addition to their use in radiopharmaceutical design, bidentate ligands have potential in the development of organometallic complexes of the platinum group

[1] R. Alberto, R. Schibli, A. Egli, A. P. Schubiger, *J. Am. Chem. Soc*. 120 (1998) 7987-7988.
[2] R. Alberto, R. Schibli, R. Waibel, U. Abram, U.P. Schubiger, Coord. *Chem. Rev*. 190-192 (1999) 901-919.
[3] R. Alberto, R. Schibli, A. Egli, P.A. Schubiger, W.A. Hermann, G. Artus, U. Abram, T.A. Kaden, *J. Organomet. Chem*. 493 (1995) 119-127.
[4] R. Alberto R, P.J. Kyong, D. van Staveren, S. Mundwiler, P. Benny, *Peptide Science*.76 (2004) 324-333.
[5] S. Mundwiler, M. Kündig, K. Ortner, R. Alberto, *Dalton Trans*. 9 (2004) 1320-1328.
[6] T. R. Hayes, S. C. Bottorff, W. S. Slocumb, C. L. Barnes, A. E. Clarka, P. D. Benny, *Dalton Trans*. 46 (2017) 1134-1144.
[7] F. Tisato, M. Porchia, C. Bolzati, F. Refosco, A. Vittadini . *Coord. Chem. Rev*. 250 (2006) 2034–2045.
[8] S. Mundwiler, M. Kündig, K. Ortner, R. Alberto, *Dalton Trans*. 9 (2004) 1320-1328.

metals (PGMs) as chemotherapeutic agents and potential catalysts for a number of chemical processes in heterogeneous and homogeneous catalysis.[9,10,11] Square planar rhodium(I) carbonyl complexes of the type [Rh(CO)(L,L'-Bid)(PR_3)], where L,L'-Bid = bidentate ligands; PR_3 = tertiary phosphine) have been investigated as potential precursors in a number of catalytic reactions such as the rhodium catalyzed carbonylation of methanol to acetic acid and methyl acetate.[12,13,14,15] The activity and selectivity of the catalyst can be optimized by incorporating substituents on the ligand skeleton thereby providing a useful range of steric and electronic properties essential for the fine-tuning of structure and reactivity. This study serves to continue the investigations of how the steric and electronic contributions of the coordinated ligands may affect the rate of oxidative addition to the rhodium centre.[16,17]

Apart from the catalytic application, these square planar rhodium(I) complexes display one-dimensional metal-metal interactions in the solid state.[18,19,20] These metallophilic interactions have attracted attention due to their added special properties such as conductivity, magnetism, photophysical properties and catalytic properties.[21,22,23,24] There are in principle two strategies employed for building the linear arrays of these metal atoms, where the one approach entails the linking via supporting ligands and the other approach involves the *direct* metal-metal

[9] B. Breit*, Angew. Chem. Int. Ed*. 44 (2005) 6816-6825.
[10] E.G. Moschetta, K.M. Gans, R.M. Rioux, *J. Catal*. 309 (2014) 11-20.
[11] W.Keim, J*. Mol. Catal. Chem*. 224 (2004) 11-16.
[12] P.P. Sarmah, B. Deb, B.J. Borah, A.L.Fullar, A.M.Z. Slawin, J.D. Woollins, D.K.Dutta *J. Organomet. Chem*. 695 (2010) 2603-2608.
[13]A. Haynes, P.M. Maitlis, G.E. Morris, G.J.Sunley, H. Adams, P.W. Badger, C.M. Bowers, D.B. Cook,P.I.P. Elliott, T. Ghaffar,H. Green, T.R. Griffin, M. Payne, J.M.Pearson, M.J. Taylor, P.W. Vickers, R.J. Watt, *J. Am. Chem. Soc.* 126 (2004), 2847-286.
[14] A Brink, A. Roodt, G. Steyl, H.G. Visser, *Dalton Trans*. 39 (2010) 5572–5578.
[15] S. Warsink, F.G. Fessha, W. Purcell, J.A. Venter, *J. Organomet. Chem*. 726 (2013) 14-20.
[16] D.K. Dutta, P. Chutia, B.J. Sarmah, B.J. Borah, B. Deb, J.D. Woollins, *J. Mol. Catal. A. Chem*. 300 (2009) 29-35.
[17] P.M. Maitlis, A. Haynes, G.J. Sunley, M.J. Howard, J*. Chem. Soc. Dalton Trans.* (1996) 2187-2196.
[18] K. Jang, I.G. Jung, H.J. Nam, D.-Y.Jung, S.U. Son, *J. Am. Chem. Soc*. 131 (2009)12046-12047.
[19] A.K.-W. Chan, K.M.-C. Wong, V.W.-W. Yam, *J. Am. Chem. Soc*.137 (2015) 6920-6931.
[20] M.M. Conradie, P.H. P.H. van Rooyen, C. Pretorius, A. Roodt, J. Conradie, *J. Mol. Struct*. 1144 (2017) 280-289.
[21] M. Jakonen, L. Oresmaa, M. Haukka, *Cryst. Growth Des*. 7 (2007) 2620-2626.
[22] Y. Chen, K. Li, H.O. Loyd, W. Lu, S.S.-Y. Chui, C.-M. Che*. Angew. Chem. Int. Ed*. 49 (2010) 9968-9971.
[23] L. Zang, Y. Che, J.S. Moore, *Acc. Chem. Res*. 41 (2008) 1596-1608.
[24] M-L. Kontkanen, L. Oresmaa, M.A. Moreno, J. Jänis, E. Laurila, M. Haukka, *Appl. Cat*. 365 (2009) 130-134.

interaction.[25] The focus in this PhD study is on the latter. These complexes containing direct metal-metal interactions can have discrete or infinite number of directly interacting metal atoms arranged in linear chains throughout the crystal lattice. The linear arrays of metal atoms are often further stabilised by synergistic effects with other noncovalent interactions such as hydrogen bonding, π-π interactions, electrostatics and even halogen interactions. This study aims to evaluate the contribution of steric and electronic properties of the coordinated ligands on the metallophilic interactions in model complexes of Rh(I). This will contribute to the understanding of the fundamentals that govern the construction of these one dimensional chains and consequently potentially contribute to the modeling and design of effective materials using these intermolecular interactions.

1.2 Aim of study

In order to gain more insight into the coordination of *fac*-$[M(CO)_3]^+$ (M = Mn, Re and Tc) to various bidentate ligands for the development of the [2+1] labeling approach in radiopharmaceutical design, a range of Schiff-base ligands containing nitrogen and oxygen donor atoms were selected. The ligands have systematic variations in steric and electronic parameters and their coordination behavior to the tricarbonyl core will be evaluated. These structurally flexible ligands have the potential to bind to one or more metal centres in various coordination modes allowing synthesis of homo and/or heteronuclear metal complexes with diverse chemistry. The structural behavior associated with the other 3d congener *i.e*. manganese, will also be evaluated in order to expand the knowledge base within the manganese triad (Mn, Tc and Re). Only a small number of example structures with identical ligand systems are reported in the literature for the Mn-triad metal complexes containing with the *fac*-$[M(CO)_3]^+$ core. This will build towards the understanding of the dynamics and influence of the Schiff-base ligands on the geometry and reactivity of the tricarbonyl complexes of the Mn-triad.

An additional aim of this study is to investigate the coordination and kinetic behavior induced by the N,O Schiff-base and oxine ligands on the square planar rhodium(I)

[25] J.K. Bera, K.R. Dunbar, *Angew. Chem. Int. Ed*. 41 (2002) 4453-4457.

complexes. The 8-hydroxyquinoline ligands incorporated in these investigations have somewhat structural similarities to Schiff-base ligands derived from the salicyaldehyde in that both these systems contain at least one hydroxyl group and a nitrogen donor group, see Figure 1.1. The effect of the 5-membered ring formed by the 8-hydroxyquinoline chelation with the rhodium(I) metal centre relative to the 6-membered ring formed by the Schiff-base ligands will be evaluated.

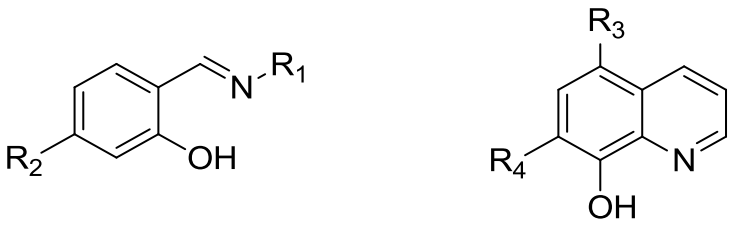

Figure 1.1 Illustration of the backbone of the Schiff-base and 8-hydroxyquinoline ligands used in this study. R_1, R_2, R_3, R_4 represents a variety of electron withdrawing or donating groups, as well as steric factors.

The metallophillic interactions displayed by square planar rhodium(I) complexes are dependent on a number of factors such as coordination modes, the ligand's electronic nature, steric effects, etc. The relationship between structural characteristics and the formation of these metallophilic interactions within rhodium(I) complexes containing a series of Schiff-base and 8-hydroxyquinoline ligands will thus be evaluated in detail.

With the above in mind, the overall stepwise aims and objectives are listed below:

(i) Synthesis and characterisation of carbonyl complexes of the type [Rh (L,L'-Bid) $(CO)_2$] and *fac*-$[M(CO)_3(L,L'\text{-Bid})_a(X)_b]_c$, where M(I) = Mn^I, Tc^I, Re^I and Rh^I, L,L'-Bid = monocharged bidentate ligands with Schiff-base or oxine-type architectures, X = solvent molecule, a = 1/2, b = 0/1 and c = 1/2.

(ii) Characterization of all the synthesized complexes by NMR (using solution and solid-state where appropriate), UV/Vis and Infrared spectroscopy.

(iii) Obtain the solid-state structures of a systematic range of the synthesized carbonyl complexes using single crystal X-ray diffraction to obtain a broad correlation and knowledge-base of relevant structural properties in particular in the manganese triad complexes.

(iv) Study metallophillic interactions in a range of Rh(I) complexes by detailed solid-state X-ray investigations.

(v) Kinetic investigations of the oxidative addition of iodomethane to the rhodium(I) complexes, [Rh(L,L'-Bid)(CO)(PR_3)]. This study will provide insight into the reactivity of the rhodium(I) complexes. It is important to not only have knowledge of the structural properties but also kinetic behaviour of these complexes in order to understand all the influences for the development of compounds with relevance in optoelectronics, catalysis and medicine.

The next chapter will present a brief overview of the literature related to this study followed by the presentation and discussion of the experimental results in Chapter 3, where after a number of topic-specific Chapters will follow which address the different aims and experiments associated therewith in a step-wise manner.

2 Literature Study

2.1 Introduction

Through a judicious selection and design of a ligand, one can influence the overall chemical and physicochemical properties of the metal complexes utilized in many useful applications such as radiopharmaceuticals, supramolecular assemblies, catalysis, surfaces and nano-materials. The properties of the metal complexes can be manipulated via covalent attachment of electron withdrawing or donating groups on the ligand skeleton or by incorporating groups with varying degrees of steric bulkiness.[1,2] Schiff-base and quinoline-type ligands have both contributed a great deal in the development of coordination chemistry and their importance transfers to significant technological and biochemical processes.[3,4] These ligand systems are capable of stabilizing different transition metals in various oxidation states offering the prospect of synthesizing materials with a broad range of properties.[5,6]

In the forthcoming sections, a brief overview of the ligand systems and their metal complexes in the fields of relevance will be discussed.

2.2 Radiopharmaceuticals

Radiopharmaceuticals are medicinal formulations consisting of radiolabeled molecules used in clinical areas for non-invasive diagnostic imaging or to deliver therapeutic doses of radiation to a specific target. Thus, depending on their medical application, radiopharmaceuticals can be classified into diagnostic and therapeutic. These compounds are further categorized based on their biodistribution characteristics; those whose biodistribution is determined by their chemical and

[1] A. Brink, H.G. Visser, A. Roodt, *J. Coord. Chem*. 64 (2011) 122-133.
[2] C.D. Duarte, E.J. Barreiro, C. A. Fraga, *Mini. Rev. Med. Chem*. 11 (2007) 1108-1119.
[3] P.G. Cozzi, *Chem. Soc. Rev*. 33 (2004) 410-421.
[4] K. Li, G.S.M. Tong, Q. Wan, G. Cheng, W.-Y. Tong, W.-H. Ang, W.-L. Kwong, C.-M. Che, *Chem. Sci*. 7 (2016) 1653-1673.
[5] Y. Song, H. Xu, W. Chen, P. Zhan, X. Liu. *Med. Chem. Commun*. 6 (2015) 61-74.
[6] M.D. Bartholoma, A.S. Louie, J.F. Valliant, J. Zubieta, *Chem. Rev.* 110 (2010) 2903-2920.

physical properties and those whose biodistribution is determined by their receptor binding and other biological interactions. These compounds are systematically administered in the body utilising different methods, the most common being via intravenous injection. For diagnostic imaging, the goal is to have a radioisotope that emits radiation sufficient enough to be readily detected but have minimal effect on the surrounding tissues. Gamma (γ) or positron-emitting (β^+) radioisotopes are used in this regard. For therapy, Auger but more importantly beta (β^-) emitting radioisotope is used to systematically deliver a high energy sterilizing dose of radiation to the specific disease areas while having minimal effect on the surrounding tissues and organs.[7,8]

Diagnostics radiopharmaceuticals are labelled with gamma emitters for single photon emission computed tomography (SPECT) and alternatively with a positron emitting radioisotope for positron emission tomography (PET).[9] Both these imaging strategies have the capacity to map out physiological and metabolic activity thus providing important information relating to the functioning and/or dysfunction of organs or tissues. Therapeutic radiopharmaceuticals are designed to deliver a sterilizing dose of radiation to the disease site with effective tumor uptake and rapid clearance from the blood and tissues to prevent damage of healthy tissues and organs. The radiation can be introduced in different external and internal methods depending on the type of therapy best suited for the patient.[10]

The design and development of radiopharmaceuticals for diagnosis and therapy has many intricacies. Some of the main aspects include: type of radionuclide, half-life, mode of decay, cost, availability and handling of the radioisotope. At the centre of radiopharmaceutical development is the fundamental understanding of the structure and reactivity of the compounds. The process encompasses the identification of biological targets and the design of bifunctional chelators, the radiolabeling kinetics, stability, modification of pharmacokinetics etc. All these

[7] S.M. Qaim, *Radiochim. Acta*. 89 (2001) 223-232.
[8] W.A. Volkert and T. J. Hoffman, *Chem. Rev.* 99 (1999) 2269-2292.
[9] O.O. Sogbein, J. F. Valliant, in Metallotherapeutic Drugs and Metal-Based Diagnostic Agents:the Use of Metals in Medicine, ed. M. Gielen and E. R. T. Tiekink, Wiley-VCH, Weinheim, 2005.
[10] P.S. Donnelly, *Dalton Trans*. 40 (2011) 999-1010.

factors are subjected to the fundamental understanding of the coordination chemistry associated with the particular agent.[16]

2.2.1 Rhenium and technetium radiopharmaceuticals with specific reference to the *fac*-$[M(CO)_3]^+$ core

There has been much development in diagnostic and therapeutic drugs that are based on the technetium and rhenium compounds of the type *fac*-$[M(CO)_3(H_2O)_3]^+$ where M = $^{186/188}$Re(I) or ^{99m}Tc (I).[11,12,13,14,15] Rhenium has two radioisotopes that have the potential to be employed in radiopharmaceuticals, the ^{186}Re and ^{188}Re. The isotope ^{186}Re ($t_{1/2}$ = 3.68 d, β^-_{max} = 1.07 MeV, 91 % abundance) is obtained from irradiation of ^{185}Re with neutrons (^{185}Re; n, γ). The properties of ^{186}Re makes it suitable for the treatment of small tumours. The radionuclide ^{188}Re ($t_{1/2}$ = 16.98 h, β^-_{max} = 2.12 MeV, 85 % abundance) is generated by neutron radiation of ^{185}W.[16] The Tc-99m radioisotope ($t_{1/2}$ = 6 h, γ= 140 keV, 89% abundance) can be obtained conveniently from ^{98}Mo/^{99m}Tc generators at reasonable cost.[16] The precursor *fac*-$[^{99m}Tc(CO)_3(H_2O)_3]^+$ is prepared via a one-step synthesis through the direct reduction of $[^{99m}TcO_4]^-$ with sodium borohydride in saline under 1 atm carbon monoxide, see Scheme 1. Alternatively, the precursor can be obtained from a commercially available Tc-99m formulation, the “Isolink kit”, based on disodium boronocarbonate (BC), $Na_2[H_3BCO_2]$, which serves as an *in situ* source of CO and at the same time, reduces the metal centre.[17]

[11] L. Helm, A.E. Merbach, *Chem. Rev*. 105 (2005) 1923-1959.
[12] S. Liu, Adv. *Drug Delivery Rev*. 60 (2008) 1347-1370.
[13] J.D. Correia, A. Paulo, I. Santos, *Curr. Radiopharm*. 2 (2009) 277-294.
[14] R. Schibli, P. A. Schubiger, *Eur. J. Nucl. Med. Mol. Imaging*, 29 (2002) 1529-1542.
[15] M.P. Coogan, R.P. Doyle, J.F. Valliant, J.W. Babich, J. Zubieta, J. Labelled. Compd. Radiopharm. 57 (2014) 255-261.
[16] S. Liu, *Chem. Soc. Rev*. 33 (2004) 445-461.

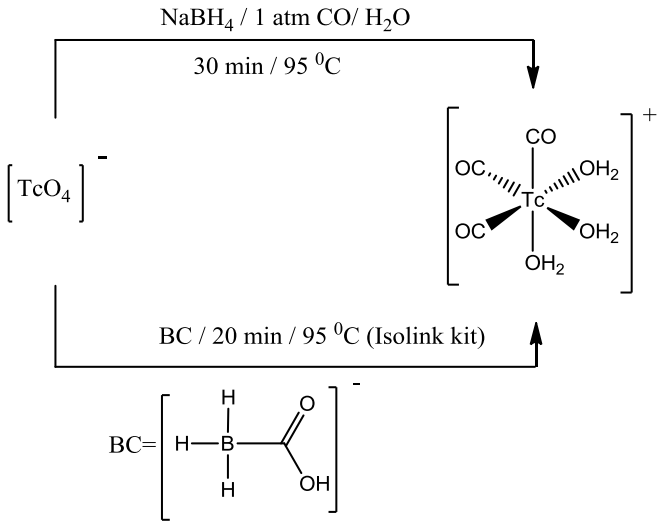

Scheme 2.1: The synthesis of the *fac*-[^{99m}Tc(CO)$_3$(H$_2$O)$_3$]$^+$ labelling precursor.[17]

The *fac*-[M(CO)$_3$(H$_2$O)$_3$]$^+$ (M = Re or Tc) complex primarily features three tightly bound carbonyl ligands stabilising the low oxidation state metal centre via backbonding and three labile water ligands which can be readily substituted by a variety of mono-, bi- and tridentate systems, or a combination thereof.[18] Figure 2.1 illustrates some examples of the bi- and tridentate chelates explored with the *fac*-[M(CO)$_3$]$^+$ core.[18] The low spin d^6 *fac*-[M(CO)$_3$]$^+$ configuration renders the metal centre inert with respect to the carbonyl ligands, and thus, provide complexes with high *in vivo* stability important for medicinal applications. In addition, the octahedral complexes *fac*-[M(CO)$_3$]$^+$ are in general more compact in size and therefore less likely to interfere with the bioactivity and physicochemical properties of the biomolecule.

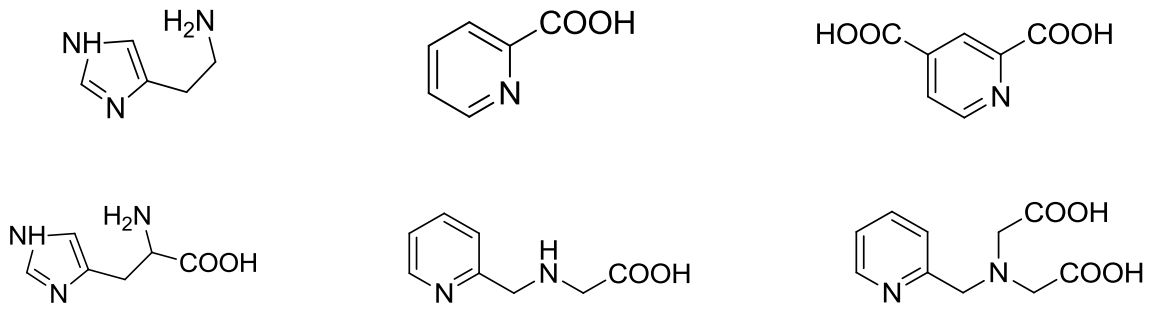

Figure 2.1: Representative examples of tridentate and bidentate ligand systems used for tricarbonyl complexes, where M = Re, Tc.[18]

[17] R. Alberto, R. Schibli, A. Egli, A.P. Schubiger, U. Abram, T.A. Kaden, *J. Am. Chem. Soc*. 120 (1998) 7987-7988.
[18] R. Schibli, R. La Bella, R. Alberto, E. Garcia-Garayoa, K. Ortner, U. Abram, P.A. Schubiger *Bioconjugate Chem.* 11 (2000) 345-351.

It has been illustrated through many examples that higher denticity chelates provide good stability to the ^{99m}Tc core, and tridentate ligands occupy directly the three vacant sites, forming thermodynamically stable compounds. There is however some challenges associated with these chelating systems such as the complexity of introducing a linking group for the biomolecule.[20] Alternative strategies are under development in order to overcome the need for the multistep functionalization of the tridentate chelators. One of the strategies proving efficient is the [2+1] mixed ligand approach. The [2+1] concept entails the combination of a mono- and bidentate ligand, see Scheme 2.2. A bio-active component can be attached within the ligand skeleton to improve the biodistribution of the radiopharmaceutical. In the one system, the biomolecule can be attached to the bidentate chelate and the properties of the complexes can be influenced by the introduction of various monodentate ligands into the coordination sphere. In the other system, the biomolecule is then appended on the monodentate and the variable portion in then represented by the bidentate ligand.[19,20,21]

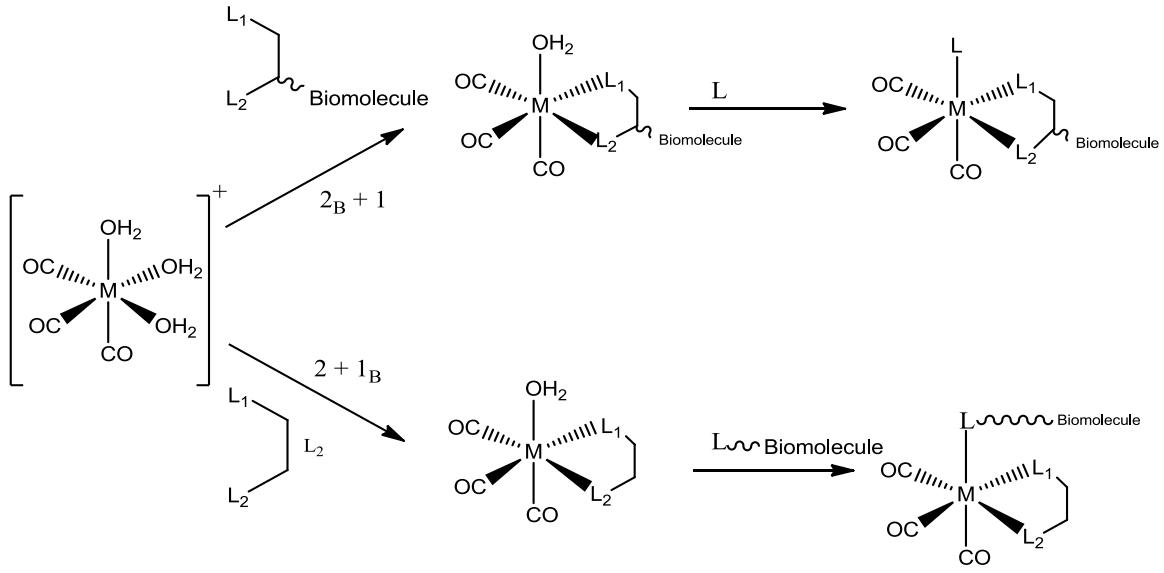

Scheme 2.2: Illustration of the [2+1] mixed ligand approach, L_1, L_2 = different donating atoms of the bidentate ligand; L = monodentate ligand.[20]

[19] N.I. Gorshkov, R. Schibli, A.P. Schubiger, A.A. Lumpov, A.E. Miroslavov, D.N. Suglobov, *J. Organomet. Chem*. 689 (2004) 4757-4763.
[20] S. Mundwiler, M. Kündig, K. Ortner, R. Alberto, *Dalton Trans*. 9 (2004) 1320-1328.
[21] M. Riondato, D. Camporese, D. Martín, J. Suades, A. Alvarez-Larena, U. Mazzi, *Eur. J. Inorg. Chem*. 44 (2005) 4048-4055.

There is considerable amount of interest addressed towards developing suitable, tailor made, ligand systems for the *fac*-$[M(CO)_3]^+$ fragment. It is thus important to evaluate extensively the effect of the ligands on the reactivity of the *fac*-$[M(CO)_3]^+$ complexes in order to foster advances in the design of directing ligand systems, as well as to improve on the stabilities of the labelled complexes, especially in the diverse [2+1] mixed ligand approach. In addition, the chemistries of rhenium and technetium draw some parallels and complementing features are being explored in the development of theranostics.[22,23,24] Theranostics are essentially a matched-pair constellation for imaging and therapeutic application taking advantage of the radio-cytotoxicity of rhenium complexes and the ^{99m}Tc molecular imaging agents.[25,26]

2.3 Substitution kinetics of *fac*-$[M(CO)_3(L,L'\text{-Bid})(X)]^n$ in the Mn-Triad

Since the development of pioneering synthetic methods of the *fac*-$[M(CO)_3(H_2O)_3]^+$ (where M = $^{186/188}$Re(I) or ^{99m}Tc (I)) precursors, the coordination behaviour of a range of ligand systems towards the *fac*-$[M(CO)_3]^+$ have been investigated as models for developing novel radiopharmaceutical compounds. The aim of the complex design is to influence biodistribution and lipophilicity features through alterations of the ligand's steric and electronic properties. Rhenium, the third row congener of technetium is often used as a non-radioactive analogue for developing technetium chemistry.[27,28,16] The translation of rhenium chemistry to technetium however requires careful investigations of the fundamentals. It is thus imperative to study the structural behaviour and kinetics associated with these model complexes. Important information with regards to the preparation, administration in patients, uptake and clearance of the radiopharmaceutical agents can be drawn from

[22] N. Agorastos, L. Borsig, A. Renard, P. Antoni, G. Viola, B. Spingler, P. Kurz, R. Alberto, Chem. Eur. J. 13 (2007) 3842-3852.
[23] A. Boulay, M. Artigau, Y. Coulais, C. Picard, B. Mestre-Voegtle, Dalton Trans. 40 (2011) 6206-6209.
[24] C.A. Kluba, A. Bauman, I.E. Valverde, S. Vomstein, T.L. Mindt, Org. Biomol. Chem.10 (2012) 7594-76023.

[25] N. Drude, L. Tienken, F. M.Mottaghy, Methods. 130 (2017) 14-22.
[26] M.D. Gott, C.R. Hayes. D.E. Wycoff, E.R. Balkin, B.E. Smith, P.J. Pauzauskie, M.E. Fassbender, C.S. Cutler, A.R. Ketring, D.S. Wilbur, S.S. Jurisson, Appl. Radiat. Isot. 114 (2016) 159-166.
[27] R. Alberto, Eur. J. Nucl. Med. Mol. Imaging. 30 (2003) 1299-1302.
[28] J.R. Ballinger, M.S. Cooper, S.J. Mather, Eur. J. Nucl. Med. Mol. Imaging. 31 (2004) 304-305.

mechanistic studies. To further expand on the knowledge of coordinative and kinetic behaviour of the *fac*-$[M(CO)_3]^+$ core, manganese, the 3rd row congener of technetium, is evaluated as a potential model towards the development of more effective radiopharmaceuticals which is reliant on the understanding of the structural and kinetic behaviour associated therein.

Investigative studies on the lability and mechanism of substitution of the methanol ligand by various nucleophiles such as bromide (Br^-), pyridine (Py) and thiourea (TU), in the complexes of the type *fac*-$[M(CO)_3(L,L'\text{-Bid})(MeOH)]^n$ (where M = Mn, Re and L,L'-Bid= N,N', N,O' and also O,O'-bidentate ligands) has been conducted.[29,30,31,32,33] Understanding the substitution behaviour in the complexes, i.e the rates of substitution, reactivity of the CO ligands and the effects of the entering ligands will provide more insight for the development of the [2+1] mixed ligand approach mentioned earlier. The ligands were carefully selected in order to bring about systematic electronic and steric changes onto the metal centre.

The results obtained for the substitution reactions in the N,N-bidentate metal complexes, *fac*-$[M(CO)_3(bipy)(MeOH)]^+$ (bipy = 2,2-bipyridine) and *fac*-$[M(CO)_3(phen)(MeOH)]^+$ (phen = 1,10-phenanthroline), M = Re/Mn, with the entering nucleophiles bromide (Br^-) and pyridine (Py), indicated an increase in substitution rate in the order of $k_1(Br^-) > k_1(Py)$. The order of reactivity is similar in both rhenium and manganese complexes. Comparing the rates of substitution of Br^- and Py monodentate ligands in rhenium against those of manganese analogous, about one order-of-magnitude increase in the substitution rates in manganese in comparison to rhenium complexes was observed.

A reactivity trend with the order $k_1(Py) > k_1(Br^-)$ was obtained for substitution reactions in the corresponding rhenium and manganese N,O'-bidentate metal complexes, *fac*-$[M(CO)_3(Pico)(MeOH)]^+$ (picoH = 2-picolinic acid) and *fac*-$[M(CO)_3(2,4\text{-QuinH})(MeOH)]^+$ (quinoline-2,4-dicarboxylic acid), where M = Re, Mn.

[29] A. Manicum, M. Schutte-Smith, G. kemp, H. G. Visser, *Polyhedron.* 85 (2015) 190-195.
[30] T.N. Twala, M. Schutte-Smith, A. Roodt, H. G. Visser, *Dalton Trans*. 44 (2015) 3278-3288.
[31] A. Brink, H.G. Visser and A. Roodt, *Inorg. Chem*. 52 (2013) 8950-8961.
[32] M. Schutte, H.G. Visser, A. Roodt, *Inorg. Chem*. 51 (2012) 11996-12006.
[33] M. Schutte, G. Kemp, H.G. Visser, A. Roodt, *Inorg. Chem*. 50 (2011) 12486-12498.

The observed order of reactivity is in contrast that obtained for the substitution reactions in N,O'-bidentate metal complexes. The change in reactivity might be attributed to the net positive charge on the complexes when N,N'= Bid ligands are used and neutral in with respect of N,O' ligands.

Another observation made when comparing the $k_1(Br^-)$ rates in manganese complexes for the neutral complexes against the positively charged complexes is that the rates are only around 1-1.5 orders-of-magnitude faster in the positively charged N,N'-bidentate ligand complexes, in comparison to the complexes containing the mono-anionic N,O'-bidentate ligands (neutral complexes). Similar results were obtained in corresponding rhenium complexes. An opposite effect was observed in the rates obtained for N,N'-bidentate and N,O'-bidentate complexes with Py and TU. A k_1(Py) rate of about 3.1 orders-of-magnitude higher was obtained for the complex *fac*-$[Re(CO)_3(2.4\text{-QuinH})(MeOH)]^+$ and a rate of about 3 orders-of-magnitude higher for the (TU) in the same neutral N,O'-bidentate metal complex. A similar behavior was obtained in corresponding rhenium complexes with Py as the entering nucleophile.

An underlying factor outlined by the methanol substitution reactions in manganese and rhenium complexes by various nucleophiles is the general increase in substitution rate when going from rhenium to manganese. The results are consistent with those obtained for the water substitution in the complexes *fac*-$[M(CO)_3(H_2O)_3)]^+$ where (M = Mn, Tc and Re). The water substitution increased in the order of Mn > Tc > Re.[34,35] The activation parameters obtained for the substitution kinetics in *fac*-$[M(CO)_3(L,L'\text{-Bid})(CH_3OH)]$ highlighted that the substitution reactions proceed via an interchange mode of activation with the N,N'-Bid positively charged metal complexes potentially favoring an associative mechanism I_a , while the neutral O,O'-Bid and N,O'-Bid complexes are suggestive of a more dissociative type mechanism I_d.

The influence of N,O bidentate Schiff-base ligands on the reactivity of the rhenium(I) complexes has also been investigated and the results indicated that

[34] B. Salignac, P.V. Grundler, S. Cayemittes, U. Frey, R. Scopelliti, A.E. Merbach, *Inorg. Chem*. 42 (2003) 3516-352.
[35] P.V. Grundler, L. Helm, R. Alberto, A. E. Merbach, *Inorg. Chem.* 2006, *45*, 10378-10390.

these N,O Schiff-base ligands activate the metal centre substantially when compared to the reported N,O'-, N,N'- and the O,O'-bidentate rhenium complexes reported by Schutte et al.[31,32,36,37] The results also pointed out that the substitution rates are primarily influenced by both the electronic and steric parameters of the coordinated bidentate ligands with the entering nucleophiles having only a minimal contribution. As part of continuing studies towards the development of the 2+1 ligand approach in radiopharmaceutical design, this study aims to further investigate the coordination behavior of bidentate Schiff-base ligands bearing nitrogen and oxygen donor atoms on the *fac*-$[M(CO)_3]^+$ (M = Mn, Tc and Re).

The forthcoming section gives a general overview of the Schiff-base ligands. The structural flexibility of these ligands systems can potentially allow the inclusion of biological directing molecule on their backbone.

2.4 Schiff-base ligands

Schiff-bases are organic compounds containing a carbon-nitrogen double bond functional group with the nitrogen atom connected to an alkyl or an aryl group. Schiff-base ligands fall within a class of the most widely used ligand systems, due to their facile synthesis and excellent chelating abilities. The structural flexibility of these ligand systems offer prospects of controlling the (i) denticity of the final ligands, (ii) nature of donor atoms, and (iii) the number of chelating moieties. These chelating ligands can stabilise many different transition metals in various oxidation states, hence they have been a subject of intense interest in the design of new materials in numerous fields such as catalysis, photo-physical chemistry and also radiopharmaceutical design.[38,39,40,41,42,43,44] The structural and stereo-electronic

[36] B. Salignac, P.V. Grundler, S. Cayemittes, U. Frey, R. Scopelliti, A.E. Merbach, R. Hedinger, K. Hegetschweiler, R. Alberto, U. Prinz, G. Raabe, U. Kolle, S. Hall, *Inorg. Chem.* 42 *(*2003) 3516-3526
[37] P.V. Grundler, B. Salignac, S. Cayemittes, R. Alberto, A. E. Merbach, *Inorg. Chem*. 43 (2004) 865-873
[38] X. Liu, C. Manzur, N. Novoa. S. Celedón, D. Carrillo, J-R. Hamon, *Coord. Chem. Rev*. 357 (2018) 144-172.
[39] D.N. Dhar, C.L. Taploo, *J. Sci. Ind. Res*. 41 (1982) 501-506.
[40] W. Rehman, M.K. Baloch, B. Muhammad, A. Badshah, K.M. Khan, *Chin. Sci. Bull.* 49 (2004) 119-22.
[41] S. Mandal, D.K. Poria, D.K. Seth, P.S. Ray, P. Gupta, *Polyhedron*.73 (2014) 12-21.
[42] W.W. Wang, B. Spingler, R. Alberto, R, *Inorg. Chim. Acta.* 355 (2003) 386-393.

diversity of these ligands are desirable for optimisation of the properties and activity of the metal complexes.

Scheme 2.3 illustrates a general synthesis of Schiff-base ligands via the condensation reaction of primary amines with aldehyde or ketone precursors.[3] For a more effective coordination, these ligands usually contain a functional group nearer to the condensation site forming a five or six membered chelate ring with the metal ion. The modern day focus in the design of Schiff-bases is directed to variations in the azomethine to allow different chelating ring sizes and combinations.[45]

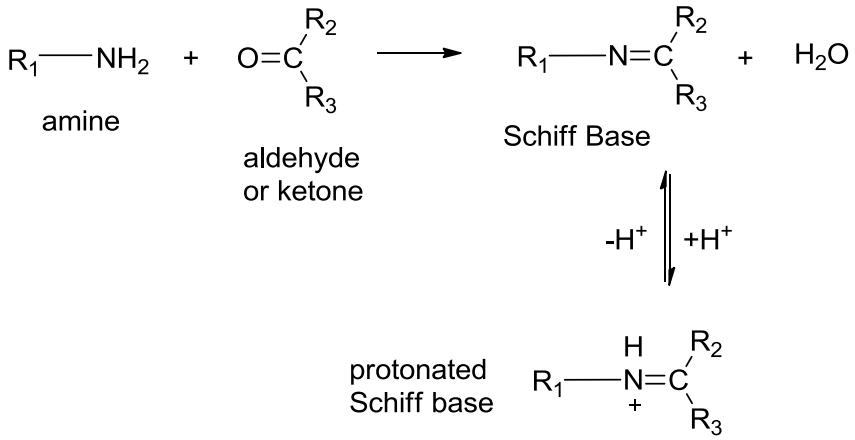

Scheme 2.3: **The general synthesis of Schiff-base ligands. The R groups represent a variety of substituents such as alkyl, aryl, cyclohexyl or other heterocyclic fragments.[45]**

There is a considerable amount of ongoing interest in exploiting the desirable properties of Schiff-base ligands for the development of novel metal complexes with a wide range of applications. In catalysis, ligands play a key role in manipulating the activity and selectivity of the catalyst through ligand optimization strategies. Schiff-base metal complexes have shown to be effective in some catalytic reactions such as polymerization, hydroformylation, hydrogenation, oxidation and reduction,

[43] A. Lehwess-Litzmann, P. Neumann, C.Parthier, S. Lüdtke, R. Golbik, R. Ficner, K.Tittmann, *Nat*. *Chem. Biol*. 7 (2011) 678-684.
[44] H. Naeimi, Z.S. Nazifi, S.M. Amininezhad,M. Amouheidari, *J. Antibiot*. 66 (2013) 687-689.
[45] A.M. Abu-Dief, I.M.A. Mohamed, *Beni*-Seuf. *Univ. J. Apll. Sc*. 4 (2015) 119-133.

carbonylation and epoxidation. Schiff-base metal complexes have also gained attention in the development of luminescence materials.

2.4.1 Schiff-base ligands in medicine

Schiff-base ligands and their metal complexes exhibit a broad range of biological activities such as antibacterial, antifungal, antiviral and anti-inflammatory and antitumor properties.[38,38,44,46] Figure 2.2 illustrates two examples of Schiff-base ligands with antibacterial and antifungal activity. The diverse nature of Schiff-base ligands offers an opportunity to incorporate a biologically active group on the complex molecule, whose properties can be enhanced by modifications of the steric and electronic properties of the ligand, consequently influencing the properties and activity of the (radio)pharmaceutical model.[1,2]

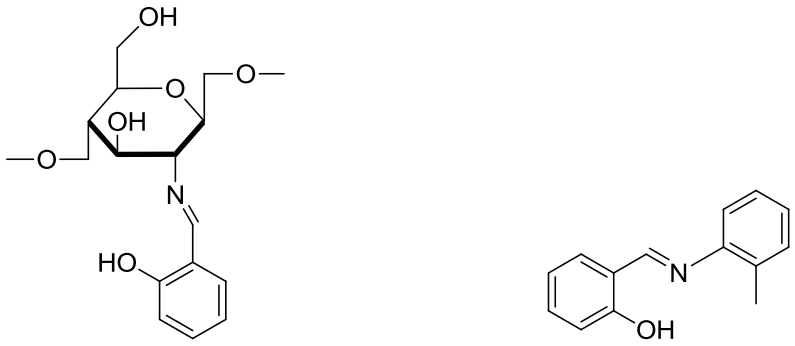

Figure 2.2: Examples of bioactive Schiff-base ligands derived from Chitosan and N-(salicylidene)-2-hydroxyaniline with primary amines.[47,48]

The ligand systems derived from salicylaldehyde are somewhat structurally similar to 8-hydroxyquinoline, the cornerstone ligand in the design of organic light emitting diodes (OLEDs). Both ligand systems contain at least one hydroxyl group, a coordinating nitrogen donor and a delocalised π-conjugate system. These ligand systems are structurally flexible and can form stable complexes with a wide range

[46] T. Aboul-Fadl, F.A. Mohammed, E.A. Hassan, *Arch. Pharm. Res.* 26 (2003) 778-784.
[47] A.O. de Souza, F.C.S. Galetti, C.L. Silva, B. Bicalho, M.M. Parma, S.F. Fonseca, A.J. Marsaioli, A.C.L.B. Trindade, R.P. Freitas, F.S. Bezerra, M. Andreda-Neto, M.C.F. De Oliveira, *Quim. Nova*. 30 (2007) 1563-1566.
[48] W. Rehman, M.K. Baloch, B. Muhammad, A. Badshah, K.M. Khan, *Chin. Sci. Bull.* 49 (2004) 119-122.

of metal ions for application in numerous fields. The forthcoming paragraphs give a general overview of 8-Hydroxyquinoline ligands and its derivatives.

2.5 8-Hydroxyquinoline ligands

Quinoline-bearing structures are well known due to their broad functions in areas such as medicine, catalysis, material design and electronics.[49,50,51] The continuing interest in these compounds is driven by their synthetic versatility which allows the creation of a library of structurally diverse derivatives. 8-Hydoxyquinoline, see Figure 2.3, and its derivatives is one of the mostly encountered quinolines, wherein the heterocyclic aromatic compound is characterized by a phenol ring fused with a pyridine. These bidentate chelators form metal complexes through the oxygen and nitrogen atoms resulting in the formation of five-membered chelate metallo-cycled systems. Different substituents can be introduced at various positions on the ligand scaffold to achieve fine-tuning of structural and chemical properties of the metal quinolinate complexes.

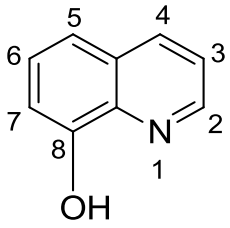

Figure 2.3: Illustration of the structure of 8-hydroxyquinoline.

A number of synthetic methodologies have been developed for the preparation of 8-hydroxyquinoline ligands. The most common methods are the Skraupor Friedlander methods and the Suzuki cross-coupling reaction.[52,53] Because of their metal complexing abilities, these ligand systems have played an important role in the development of organometallic chemistry. A library of 8-hydroxyquinoline ligand derivatives has been prepared and evaluated in order to optimize the chemical and biological properties of the metal complexes. The versatility of the ligand skeleton

[49] M. Azam, M.S. Islam, S.I. Al-Resayes, M.R. Siddiqui, A. Trzesowska-Kruszynska, R. Kruszynski, *Spectrochimica. Acta A. Mol. Biomol. Spectrosc*. 123 (2014) 1-6.
[50] P.P. Sarmah, D.K. Dutta, *J. Mol. Cat*. A. 372 (2013) 1-5.
[51] H. Xu, R. Chen, Q. Sun, W. Lai, Q. Su, W. Huang, X. Liu, *Chem. Soc. Rev. 43* (2014) 3259-3302.
[52] J.P. Heiskanen, O.E.O. Hormi, *Tetrahedron*. 65 (2009) 518-524.
[53] H. Gershon, D.D. Clarke, M. Gershon, *Monatsh. Chem*. 125 (1994) 51-59.

permits various electronic and steric alterations, for example, because of the strong ortho-/para-directing activation of the hydroxyl substituent group on the 8-hydroxyquinoline, the 5 and 7 positions can be readily functionalized. The nitrogen atom can be deprotonated, oxidised or alkylated in order to activate nucleophilic attack on the 2- or 4- positions.

The fabrication of the first thin film light-emitting diode using the compound tris(8-hydroxyquinoline) aluminium(III), Alq3, has pioneered the development of optoelectronic application such as photodetectors, OLEDs, flat and flexible colour display and also photovoltaic cells.[54,55,56] The aluminum(III) compound represents a class of materials with strong luminescence, high electric conductance, low cost and fabrication technologies. Extensive research has been undertaken in view of optimizing the device characteristics, improvement of structural stability and also understanding the charge transport mechanism.

2.5.1 8-Hydoxyquinoline ligands in medicine

Due to the distinctive chemical properties of 8-hydroxyquinoline and its derivatives, many metal compounds incorporating the ligand moieties have been widely explored for their biological effects such antimalarial, antifungal, anticancer, antibacterial as well as antituberculotic.[57,58,59] Figure 2.4 gives two examples of clinically used 8-hydroxyquinoline derivatives, clioquinol and nitroxoline.

Clioquinol nitroxoline

Figure 2.4: Examples of clinically used 8-hydroxyquinoline agents.[60]

[54] C.H. Chen, J. Shi, Coord. *Chem. Rev*. 171 (1998) 161-174.
[55] Y.G. Lee,Y. Kim, S.H. Yang, S.N. Kwon, K. Yoneg, *Appl. Phys. Lett*. 72 (1998) 1757-1771.
[56] P. Dalasiński, Z. Lukasiak, M. Wojdyla, M. Rebarz, W. Bala, *Opt. Mater*. 28 (2006) 98-101.
[57] R. Musiol, J. Jampilek, V. Buchta, L. Silva, H. Niedbala, B. Podeszwa, A. Palka, K. Majerz-Maniecka, B. Oleksyn, J. Polanski, Bioorg. *Med. Chem*. 14 (2006) 3592−3598.
[58] P. Palit, P. Paira, A. Hazra, S. Banerjee, A.D. Gupta, S.G. Dastidar, N.B. Mondal, *Eur. J. Med. Chem*. 44 (2009) 845-853.
[59] F. Zouhiri, M. Danet, C. Benard, M. Normand-Bayle, J.F. Mouscadet, H. Leh, C.M. Thomas, G. Mbemba, J. d'Angelo, D. Desmaele, *Tetrahedron Lett*. 46 (2005) 2201-2205.
[60] H. Jiang, J.E. Taggart, X. Zhang, D.M. Benbrook, S.E. Lind, W.Q. Ding, *Cancer Lett*. 312 (2011) 11-17.

Quinoline based metal complexes are a subject of considerable interest in the development of biological imaging/therapy agents due to their attractive luminescence properties, which are suitable for application as fluorescent and radioactive probes. These complexes exhibit long luminescence lifetimes, high photostability and large Stokes shifts. The high spatial resolution of the fluorescence imaging microscopy allows precise depiction of biological and metabolic processes.

In the preceding discussions, a general overview of the Schiff-base and quinoline as bidentate chelators was briefly presented. The structural diversity of these ligands makes them relevant in numerous fields of interest. More recently, these chelators are being explored as possible building blocks in supramolecular assemblies.[61,62,63] Supramolecular self-assembly entities are essentially polymeric systems in which molecular units or building blocks propagate infinitely in one-, two- or three dimensions. The formation of these high dimensionality structures are mediated by various types of non-covalent interactions in the crystal lattice. The rationale for exploring these multidimensional structures is driven by their intriguing properties that may be developed as a new generation of functional materials with potential applications in catalysis, therapeutic and diagnostic radiopharmaceuticals, and optoelectronics.[64,65,66] One of the keystones for generating functional materials by supramolecular self-assembly is the ability to sensibly increase structural dimensionality. Because of their versatile nature, Schiff-base and quinoline chelators may be used as building blocks for the enhancement of structural dimensionality.

A short description of the crystal engineering concept will be given in the forthcoming section.

---

[61] H. Xu, R. Chen, Q. Sun, W. Lai, Q. Su, W. Huang, X. Liu, *Chem. Soc. Rev.* 43 (2014) 3259-3302.
[62] N. Yoshida, H. Oshio, T. Ito, *J. Chem. Soc. Perkin Trans.* 2. (2001) 1674-1678.
[63] M. S. Ray, A. Ghosh, R. Bhattacharya, G. Mukhopadhyay, M. G. B. Drew , J. Ribas, *Dalton Trans.* (2004) 252-259.
[64] B. Gao, D. Zhang, Y. Li, *Opt. Mater*. 77 (2018) 77-86
[65] A.W. Jeevadason, K.K. Murugavel, M.A. Neelakantan, *Renew. Sustain. Energy. Rev*. 36 (2014) 220-227.
[66] Y.-W. Dong, R.-Q. Fan, P. Wang, L.G. Wei, X.-M. Wang, H.J Zhang, S. Gao, Y.L. Yang, Y.L. Wang, *Dalton Trans*. 44 (2015) 5306-5322.

2.6 Crystal engineering

The intrinsic properties of molecules are not only informed by the atoms used to construct/assemble them, but also the manner in which they are connected. These connections/chemical bonds are at the heart of (coordination) chemistry and provide the rational power of designing molecules through the making and breaking of these bonds. However, a shift occurred from one focused upon atoms and bonds to one focused upon molecules and bonds.[67] The focus in crystal engineering is now on the properties generated by the association of two or more chemical entities held together by intermolecular forces and also on the relationship(s) between these collective properties to that of individual building blocks.[68,69,70] If these intermolecular interactions can be predicted and controlled, then in principle the properties of the resulting solids can be dictated. This line of thinking is what gave birth to the concept of crystal engineering. A working description of crystal engineering is: "*the use of intermolecular interactions in the context of crystal packing to design functional material with premeditated properties*".[71]

There are intensive investigations towards the use of transition metal complexes to construct predictable, multi-dimensional networks where molecular or ionic components are linked via non-covalent interactions propagating in one-, two- or three dimensions. These interests are driven by the potential of creating new materials with tuneable optical characteristics, vapochromic, magnetic conducting and other interesting properties.[72,73,74] Central in this approach of material design is the realisation that the characteristics of the crystals are derived from their molecular components and the manner in which these components are arranged and interact in the crystalline state. Understanding the nature of these interactions is of crucial importance in the design of new functional materials with predefined chemical and physical properties. The next section gives a general overview of the

[67] D. Braga, *Acc. Chem. Res*. 33 (2000) 601-608.
[68] G.R. Desiraju, *Angew. Chem. Int. Ed. Engl*. 34 (1995) 2311-2327.
[69] Z. Zhang, M. Zaworotko, *J. Chem. Soc. Rev*. 43 (2014) 5444-5455.
[70] A.K.-W. Chan, K.M.-C. Wong, V.W.-W. Yam, *J. Am. Chem. Soc.*137 (2015) 6920-6931.
[71] G. R. Desiraju, Crystal Engineering: The Design of Organic Solids, Elsevier, Amsterdam, (1989).
[72] H. Sun, K. Ye, C. Wang, H. Qi, F. Li, Y. Wang, *J. Phys. Chem. A.* 110 (2006) 10750-1075.
[73] V.W.-W. Yam, E.C.-C. Cheng, *Top. Curr. Chem*. 281 (2007) 269 - 309.
[74] M.J. Frampton, H.L. Anderson, *Angew. Chem. Int. Ed*. 46 (2007) 1028-1064.

metal-metal interactions and the factors that influences the construction of these one dimensional networks.

2.6.1 Metal-metal interactions in complexes

Metallophilicity is described as the interaction between closed-shell or pseudo closed shell metal centres with an interatomic distance shorter than the sum of the van der Waals radii of the individual atoms.[75,76,77,78] The tendency of d^8, d^{10} and s^2 metal centres to form metallophilic interactions is increasingly being recognized as an important factor in ordering the arrangement as well as stabilizing the metal complexes in the solid state. These interactions can manifest themselves in the solid state as dimers, oligomers, extended chains or sheets of metal complexes. The metal-metal bonding interaction in the d^8 metal centres arise from the overlap between filled nd_z^2 and empty $(n + 1)p_z$ orbitals on adjacent metal centres.[76,79] Complexes containing direct metal-metal interactions can have a discrete number of directly interacting metal atoms, or an infinite number of directly interacting metal atoms arranged in linear chains throughout the crystal lattice. In general, these complexes consist of planar, or nearly planar, monomeric units stacked above one another to form long/infinite metal-metal chains. A typical identifier of the presence of metallophilic interaction is the appearance of a metallic lustre which arises from the reflection of polarized light parallel to the linear metal chains.

These interatomic interactions are influenced by a number of factors such as the nature of the metal ion, the supporting ligands, coordination modes and geometries, solvents, counterions and other complementary molecular interactions. It is thus important to derive a delicate balance in all the factors mentioned above in order to design highly functional materials for application is various fields. In the subsequent sections, a brief overview on most notable factors influencing these metal-metal interactions will be given.

[75] F. Scherbaum, A. Grohmann, B. Huber, C. Krueger, H. Schmidbaur, *Angew. Chem. Int. Ed. Engl*. 27 (1988) 1544-15446.
[76] Pyykkö, *Chem. Rev*. 97 (1997) 597-636.
[77] H. Schmidbaur, A. Schier, *Chem. Soc. Rev*. 37 (2008) 1931-1951.
[78] M.J. Katz, K. Sakai, D.B. Leznoff, *Chem. Soc. Rev*. 37 (2008) 1884-1895.
[79] P. Pyykkö, *Chem. Rev*. 88 (1988) 563-594.

2.6.2 Ligand influence

The choice of ligand is important in the formation of chain structures supported by metal-metal interactions. The metallophilic contacts can be affected by steric as well as electronic contributions of the supporting ligands. If one desires not just a single metallophilic contact, but rather an extended series of these interactions aligned in a 1-dimentional array, only certain coordination modes are permitted. Square planar and linear metal complexes are in general the preferred geometrical building blocks in the assembly of infinite linear chains of metal atoms in the solid state. Such geometries are limited to a ligand set that enforces a highly anisotropic environment in which ligands are only present in the xy-plane and not along the z-axis. Geometries that allow for effective overlap of orbitals between adjacent metal centres are represented in Figure 2.5.[80]

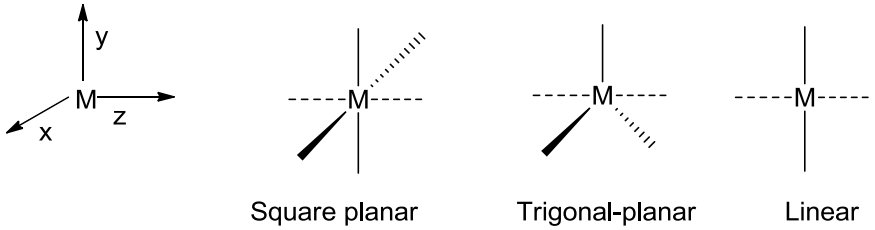

Figure 2.5: Complex geometries that generally support metal-metal interactions. [80]

2.6.3 Effects of substituents on the ligand on the interactions

The coordinating strength of ligands has a significant influence on the metal centres ability to facilitate interactions between neighbouring metal ions. Strong coordinating ligands can destabilize orbital overlap between metal centres thus preventing metallophillic interactions from occurring. The introduction of π-acceptor coordinating ligands will decrease the electron density on the metal centre and result in less repulsion between the metal centres of neighbouring molecules. This will in turn enable more effective orbital overlap between metal centres resulting in stronger and shorter interactions.[81]

[80] G. Gliemann, H. Yersin, *Struct. Bonding*. 62 (1985) 87-153.
[81] L. H. Doerrer, *Dalton Trans*. 39 (2010) 3543-3553.

Since metallophilic interactions result from interatomic overlap of electron density, any influencing factor on the electron density around the metal centre or its accessibility to another metal centre, can affect the presence, absence or the extent of metallophilic interaction in the complex. One can in principle modulate the electron density around the metal centre by altering the type and position of the substituent on the ligand backbone. The substituents can either be electron withdrawing or electron donating.

The overall effects of the substituent on the metallophilic interaction can be probed by evaluating the metal-metal bond distances in the complex. Increase or decrease in interatomic distance is in general indicated by a change in appearance of the physical crystal. Classic examples of square planar complexes with linear stacks include the Magnus green salts and Krogmann's salts. Some characteristic differences occur between the original Magnus green salt $[Pt(NH_3)_4[PtCl_4]$ and its derivatives $[Pt(NH_2R)4[PtCl_4]$ with bulkier R groups. The colour of the complexes change from green to pink and also the semiconducting properties are lost when employing bulky substituents, heptyl to tetradecyl on the amine.[82,83,84]

One should keep an account of different parameters that can influence the packing of the complex in the crystal lattice, which in turn depends on other factors such as the sterics, electronic, solvents, and other electrostatic attractions. A delicate balance between the nature of the transition metal centre, ligands, coordination modes, etc. grants the possibility to affect the final solid-state structure and also enhance the number of applications. In light of gaining understanding in the relationship between structural characteristics and properties of the metal complexes, it is important to study the solid and solution state properties of these compounds. The (PGMs) coordination chemistry is dominated by the strong tendency to adopt square planar geometries. It is thus important to study the kinetic behaviour of these complexes in order to understand all the influences for the development of compounds with relevance in medicine, catalysis and

[82] B.E.G. Lucier, K.E. Johnston, W. Xu, J.C. Hanson, S.D. Senanayake, S. Yao, M.W. Bourassa, M. Srebro, J. Autschbach, R.W. Schurko, *J. Am. Chem. Soc*. 136 (2004) 1333-1351.
[83] R.L. Musselman, *Inorg. Chim. Acta*. 361 (2008) 820-830.
[84] L. Interrante, R.P. Messmer, *Inorg. Chem*. 10 (1971) 1174-1180.

optoelectronics. The coming section will briefly discuss the basic ligand substitution kinetics and the oxidative addition in the d^8 metal complexes of the platinum groups metals (PGMs).

2.7 Ligand exchange in square planar PGMs

The understanding of fundamentals and prerequisites governing the structure and reactivity of these compounds is important in the development of new functioning materials. The kinetics and mechanism of substitution reactions of the d^8 metal complexes has been investigated in considerable detail.[85,86,87,88,89,90,91,92,93] Most of the principles derived for the mechanism of substitution reactions are pioneered by the Pt(II) complexes due to its suitable reaction times. The kinetics can be evaluated by conventional techniques such NMR and UV-Vis spectroscopies.

The development of more sophisticated techniques such as stopped flow has powered mechanistic studies of the other d^8 metal complexes. A wealth of information as pertaining to the drug design, the synthesis, administration uptake and clearance of the pharmaceutical can be obtained from the data acquired from these reactivity studies. Equation 2.1 illustrates the most elementary substitution reaction a coordination complex can undergo.

$$MX_n + Y \longrightarrow MX_{n-1}Y + X \qquad ...2.1$$

Here M represents the metal ion and X and Y represent the exchanging ligands. Substitution reactions are classified into nucleophilic and electrophilic type.

[85] T. Richens, *Chem. Rev.* 105 (2005) 1961-2002.
[86] S.F. Lincoln, D.T. Richens, A.G. Sykes, In Comprehensive Coordination Chemistry II, J.A. McCleverty, T.J. Meyer, Eds, Elsevier, Amsterdam, 1 (2003) 515-555.
[87] F. Basolo, R. G. Pearson, Mechanism of Inorganic Reactions, A Study of Metal Complexes in Solutions, 2nd edition, John Wiely and sons, Inc. New York, (1967).
[88] C.H. Langford, H.B. Gray, Ligand Substitution Processes, W. A. Benjamin Inc, New York, United States of America, 1965.
[89] F. Basolo, R.G. Pearson, The Mechanisms of Inorganic Reactions, Wiley, New York, 1958.
[90] F. Basolo, *Coord. Chem. Rev* .154 (1996) 151-161.
[91] D. Jaganyi, D. Reddy, J.A. Gertenbach, A. Hofmann, R. van Eldik, *Dalton Trans*. 11 (2004) 299-304.
[92] B. Pinter, V. Van Speybroeck, M. Waroquier, P. Geerlings, F. De Proft, *Phys. Chem. Chem. Phys*.15 (2013) 17354-17365
[93] L. Rigamonti, M. Rusconi, A. Forni, A. Pasini, *Dalton Trans*. 40 (2011) 10162-10173.

However, the scope of this work will only consider the nucleophilic substitution which is further divided in two classes, the dissociation and association substitution. For a **dissociation** type mechanism of substitution,

$$MX_n \underset{-X}{\overset{+X}{\rightleftharpoons}} \left[MX_{n-1}\right]^{+} \underset{-Y}{\overset{+Y}{\rightleftharpoons}} MX_{n-1}Y \qquad ...2.2$$

From Equation 2.2, the departing group X first dissociates from the coordination sphere and creates an intermediate state with decreased coordination number followed by the occupation of the vacant site by either a solvent molecule or the incoming ligand Y. The rate of substitution is (virtually) independent on the entering ligand. For an **associative** type mechanism of substitution;

$$MX_n \underset{-Y}{\overset{+Y}{\rightleftharpoons}} MX_nY \underset{+X}{\overset{-X}{\rightleftharpoons}} MX_{n-1}Y \qquad ...2.3$$

In an associative type mechanism, the entering ligand coordinates to the metal centre, rearranges into an intermediate state with increased coordination number and then the leaving group is cleaved from the coordination sphere. The overall rate of the process is controlled by the rate at which the incoming ligand can attack the metal centre.

The assignment of mechanism of substitution reactions is not always straight forward; complicating factors such as the existence of intermediate mechanism between the associative and dissociative mechanisms may arise. In cases like these, the substitution processes are classified based on the careful identification of the steps involved in the overall reaction and the magnitude of the rate constants for each of the individual steps. For an interchange type mechanism of substitution,

$$MX_n...Y \longrightarrow MX_{n-1}...Y...X \qquad ...2.4$$

In Eq. 2.4, the departing ligand is moving from the inner to the outer coordination sphere, while the entering nucleophile is moving from the outer to the inner coordination sphere, therefore no intermediate is observed. Although many transitions states may occur, there should be two well-defined transitions

approximating those of either an associative and dissociative reaction with the associative like transition denoted as I_a, and the dissociative like state indicated as I_d. The discrimination between the associative and dissociative mechanism can largely be classified in accordance to the dependency of the rate on the size and charge of the metal centre. Table 2.1 gives a summary of the contributing factors in the overall square planar substitution reactions.[92,93,94,95,96,97,98]

Table 2.1: Effects of size and charge on the substitution rate of the dissociative, associative and interchange mechanisms.[94,95,96,97]

Changes	Influence on rate		
	Dissociative	**Associative**	**Interchange**
Increase in size of metal ion	Increase	Increase	Increase
Increase in positive charge of metal ion	Decrease	Small change	Increase
Increase in size of incoming ligand	No effect	Decrease	Decrease
Increase in size of outgoing ligand	Increase	Small change	Decrease
Increase in negative charge of incoming ligand	No effect	Increase	Increase
Increase in negative charge of outgoing ligand	Decrease	Decrease	Decrease

A perfect model used in square planar d^8 metal complexes to evaluate the *trans* influence of the donor atoms in the coordinated ligands on the overall substitution reactions, is the substitution of one carbonyl ligand in the complexes of the type [Rh(L,L'-Bid)(CO_2)] by a tertiary monodentate phosphine ligand yielding the complex [Rh(CO)(L,L'-Bid)(PR_3)], where L,L'-Bid = bidentate ligands; PR_3 = tertiary phosphine). These monophosphine rhodium(I) complexes can undergo oxidative addition reactions and have been recognized as important systems in homogenous catalysis. The coming section briefly touches upon the oxidative addition reaction in these d^8 metal complexes.

[94] R.G. Pearson, H.B. Gray, F. Basolo, F, *J. Am. Chem. Soc*. 82 (1960) 787-792.
[95] R. J. Cross, *Chem. Soc. Rev*. 14 (1985). 197-223.
[96] R. J. Cross, *Adv. Inorg. Chem*. 34 (1989) 219-292.
[97] D. Minniti, G. Alibrandi, M.L. Tobe, R. Romeo, *Inorg. Chem*. 26 (1987) 3956-3958.
[98] P.W. Atkins, T.L. Overton, J.P. Rourke, M.T. Weller, F.A. Armstrong, F.A. Shriver & Atkins Inorganic Chemistry, Oxford University Press, Oxford, United Kingdom, (2010).

2.8 Oxidative addition

Oxidative addition reaction represents one of the most fundamental processes in inorganic and organometallic chemistry.[99,100,101] Principally, a substrate A-B is added oxidatively to a metal centre leading to an increase in coordination number of the complex due to the formation of two new bonds, the M-A and M-B upon the complete cleavage of A-B bond and a change of oxidation state by 2 units. An opposite process, the reductive elimination can reverse the dissociation of the A-B molecule. Oxidative addition plays a key role in many important synthetic and catalytic reactions such as carbonylation of alcohols, hydroformylation of alkenes etc.[102,103,]

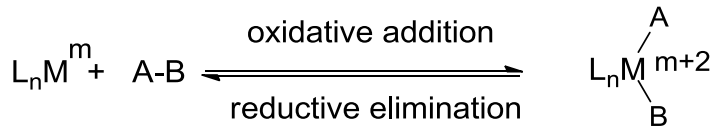

...2.5

The oxidative addition of alkyl halides can occur in different pathways yielding either the *cis*- or the *trans* product depending on a number of factors. In most cases, the reaction proceeds as an SN_2 type mechanism wherein the electron rich rhodium(I) complexes attacks the carbon atom of the iodomethane, forming a linear polar transition state leading to the *trans* addition. However, there is a possibility to form three–centred polar transition state via a concerted reaction, which can lead to the cis addition.[99,100,101]

A classic example of on oxidative addition is the industrially important carbonylation of methanol to acetic acid, where iodomethane is oxidatively added to cis-$[M(CO)_2I_2]^-$ (M = Rh or I).[104,105] The carbonylation catalyst consists of two components, a soluble rhodium(I) complex and an iodide source. The initial step of the catalytic cycle constitutes the rate-determining oxidative addition of

[99] J.J. Hartwig, Organotransition Metal Chemistry, *From Bonding to* Catalysis, University Science Books, Sausalito, CA, (2010).
[100] J.A. Labinger, *Organometallics*. 34 (2015) 4784-4795.
[101] L.M. Rendina, R. J. Puddephatt, *Chem. Rev*. 97 (1997) 1737-1754.
[102] J.F. Hartwig, F. Paul, *J. Am. Chem. Soc*. 117 (1995) 5373-5374.
[103] F.O. Arp, G.C. Fu, J*. Am. Chem. Soc*. 127 (2005) 10482-10483.
[104] P.M. Maitlis, A. Haynes, G.J. Sunley, M.J. Howard, *J. Chem. Soc. Dalton Trans*. (1996) 2187-2196.
[105] A. Haynes, P.M. Maitlis, G.E. Morris, G.J. Sunley, H. Adams, P.W. Badger, C.M. Bowers, C.D. Cook, P.I.P Elliot, T. Ghaffar, H. Green, T.R. Griff, M. Payne, J.-M. Pearson, M.J. Taylor, P.W. Vickers, R.J. Watt, *J. Am. Chem. Soc*. 126 (2004) 2847-2861.

iodomethane to the rhodium(I) centre, forming a cationic six coordinated intermediate, rhodium-alkyl(III). The subsequent steps involve the facile carbon monoxide insertion reaction forming the acyl-rhodium(III), followed by the reductive elimination step to generate the original rhodium(I) complex. Acetic acid is then obtained via the hydrolysis of the acetyl iodine.[106]

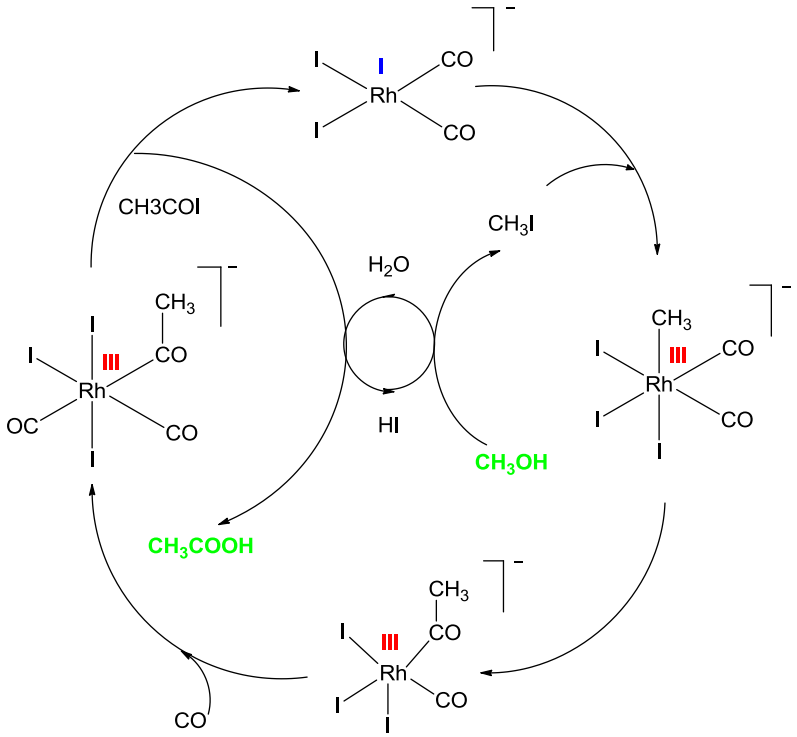

Scheme 2.3: The rhodium supported catalytic cycle for the carbonylation of methanol (the Monsanto Process).[106]

The Monsanto species $[Rh(CO)_2I_2]^-$, is the most widely used catalyst in the carbonylation reaction of methanol. Although the catalyst is effective, it requires drastic conditions for optimal performance.[107,108] The iodomethane oxidative addition to complexes of the type $[Rh(CO)(L,L'\text{-Bid})(PX_3)]$, where L,L'-Bid = mono anionic bidentate ligands; PX_3 = tertiary phosphine) have been studied at length; as part of ongoing interest in the development of novel robust catalytic species for the rhodium supported catalytic carbonylation of methanol to acetic acid and methyl acetate.[109,110,111,112,113,114,115,116,117] The steric and electronic properties can be

[106] C.M. Thomas, G. Süss-Fink, *Coord. Chem. Rev*. 243 (2003) 125-142.
[107] D. Foster, *J. Am. Chem. Soc*. 98 (1976) 846-848.
[108] P.P. Sarmah, B. Deb, B.J. Borah, A.L. Fuller, A.M.Z. Slawin, J.D. Woollins , D.K. Dutta, *J. Organomet. Chem.* 695 (2010) 2603-2608.
[109] S. Warsink, F.G. Fessha, W. Purcell, J.A. Venter, *J. Organomet. Chem*. 726 (2013) 14-20.
[110] A Brink, A. Roodt, G. Steyl, H.G. Visser, *Dalton Trans*. 39 (2010) 5572-5578.

manipulated to affect the reactivity of the rhodium metal centre. Excellent electron donating ligands enhance the rates of reaction, whilst sterically demanding ligands attached to the metal centre can retard the rate of iodomethane addition into the coordination sphere, consequently decreasing the rates of reaction. The accurate identification and characterization of these compounds, their reaction intermediates and products are essential for understanding the mechanisms in order to design a highly functioning catalyst.

Solution state nuclear magnetic resonance (NMR) spectroscopy and X-ray crystallography and UV-vis spectroscopy have been the most commonly used method and techniques to study molecular structure and in particular, dynamics. Developments in other complementing spectroscopic techniques such as solid state nuclear magnetic spectroscopy (SSNMR) is expanding the detailed knowledge and understanding of chemical and structural dynamics. A brief overview of the SSNMR spectroscopy will be given in the coming section

2.9 Solid State Nuclear Magnetic Resonance

The fundamental principle behind NMR spectroscopy is that many nuclei have spin and all nuclei are electrically charged. When an external magnetic field is applied, an energy transfer is possible between the base energy to a higher energy level (generally a single energy gap). The energy transfer takes place at a wavelength that corresponds to radio frequencies (Rf) and when the spin returns to its base level, energy is emitted at the same frequency. The signal that matches this transfer is measured in many ways and processed in order to yield an NMR spectrum for the nucleus concerned.[118,119,120] The technique has become an integral part in the

[111] M.M. Conradie, J. Conradie, *Dalton Trans*. 40 (2011) 8226-8237.
[112] J. Conradie, G.J. Lamprecht, A. Roodt, J.C. Swarts, *Polyhedron.* 23 (2007) 5075-5087.
[113] G. J. J. Steyn, A. Roodt, I. Poletaeva, Y.S. Varshavsky, *J. Organomet. Chem*. 536-537 (1997) 197-205.
[114] S.S. Basson, J.G. Leipoldt, J.A. Venter, *Acta Crystallogr*. C46 (1990) 1324-1326.
[115] S.S. Basson, J.G. Leipoldt, A. Roodt, J.A. Venter, *Inorg. Chim. Acta*. 128 (1987) 31-37.
[116] S.S. Basson, J.G. Leipoldt, A. Roodt, J.A. Venter, T.J. Van Der Walt, *Inorg. Chim. Acta*. 119 (1986) 35-38.
[117] J.G. Leipoldt, E.C. Steynberg, R. van Eldik, *Inorg. Chem*. 26 (1987) 3068-3070.
[118] M. Hunger, E. Brunner, NMR Spectroscopy. In: H.G. Karge J. Weitkamp (eds) Characterization I. Molecular Sieves – Science and Technology, Springer, Berlin, Heidelberg. 4 (2004).

elucidation of structural information in a diversity of fields. This spectroscopy technique is classified into two categories; solution and solid-state nuclear magnetic resonance depending on the state of matter.

Due to the advances in solution state NMR spectroscopy, investigations of structural dynamics in the solution state have become sometimes mundane, however still indispensible. The advances in high resolution solid-state NMR methodologies and techniques with varying complexities have afforded solid state studies the same liberties as solution state NMR. The difference between the two modes is reduced to simply the exchanging of probes from the same spectrometer in order to study either state. Some of the most commonly used techniques include the magic-angle spinning (MAS), decoupling and cross polarization. The fundamental difference between solution and solid-state NMR is essentially the molecular mobility in the sample. In solution state, fast rotational and translational motion of the molecules relative to the magnetic field averages the directional dependent interactions such as dipolar, chemical shift and scalar interactions, giving rise to narrow lines in the NMR spectra. By contrast, because the molecule is immobile in the solid state, the anisotropic or orientation dependent interactions are in full effect. As a result, the spectra appear broad and poorly resolved. In order to reduce or completely eliminate the spectral line-broadening, special spinning techniques must be employed.[121,122,123]

In the magic-angle spinning (MAS) methodology, the sample is spun at a significantly high speed about an axis at an angle of 54.44° with respect to the applied magnetic field which allows for some portions of the directionally dependent interactions to be averaged out, leaving narrower spectral lines. Cross-polarization is a method of enhancing sensitivity of less abundant nuclei through the transfer of polarization from abundant nuclei. The method makes use of the magnetic dipolar coupling of the abundant and the less abundant nuclei in the solid state. The two

[119] G. Davidson, B.E. Mann, Spectroscopic Properties of Inorganic and Organometallic Compounds, 31 (1998).
[120] V. Pattabhi, N. Gautham, *NMR Spectroscopy*. In: Biophysics. Springer, Dordrecht, (2002).
[121] S. Bai, W. Wang, C. Dybowski, *Anal. Chem*. 82 (2010) 4917-4924.
[122] A. Lesage, *Phys. Chem. Phys*. 11 (2009) 6876-6891.
[123] A.E. Alien, R.V. Law, *Nucl. Magn. Reson*. 37 (2008) 208-256.

methods are usually combined together with high decoupling techniques to yield well resolved spectra with good signal to noise ratio reminiscent of the solution state NMR.

Solid state NMR is now a much more developed field with many applications covering many fields in material science and nanotechnology, pharmaceuticals, catalysis and biomolecules.[124,125,126,127] A great majority of commercial drugs are solids, and by virtue of this, it is important to evaluate their molecular and physicochemical properties directly in the solid state. Several complementing methods and techniques are available for investigating the solid-state properties of drugs including X-ray diffraction, different scanning calorimetry (DSC), infrared (IR) and Raman spectroscopy, thermogravimetric analysis (TGA), optical and electron microscopy and solid state nuclear magnetic resonance (SSNMR). Solid state NMR spectroscopy is now one of the primary tools for analysis of structural and chemical dynamics in heterogeneous catalytic systems. The technique allows for an in-depth probing of the reaction pathways, catalytically active species and their functions. Knowledge of these entities will lead to a more strategic approach in the design of effective catalysts for different catalytic processes alternative to the classical trial-and-error approach.

The power of combining NMR and X-ray crystallography were clearly displayed in the study of different isomers resulting from the substitution of one carbonyl in the complex [Rh(L,L'-Bid)$(CO)_2$], with a monodentate tertiary phosphine. Figure 2.7 indicates the possible isomers obtained from the substitution of one carbonyl ligand of the parent complexes [Rh(L,L'-Bid)$(CO)_2$] by a tertiary phosphine. When there is a pronounced difference in the donating and accepting properties between the atoms L and L', NMR studies revealed the substitution to be highly selective. The atom with the lowest electronegativity with direct the substitution, i.e the principle isomer will contain the substitution in the trans position to the stronger donor e,g

[124] E. Ravera, T. Martelli, Y. Geiger, M. Fragai, G. Goobes, C. Luchinat, *Coord. Chem. Rev*. 327-328 (2016) 110-122.
[125] R.L. Musselman, R.W. Larsen, B.M. Hoffman, *Coord. Chem. Rev*. 257 (2013) 369-380.
[126] J. Blümel, *Coord. Chem. Rev*. 252 (2008) 2410-2423.
[127] A. Grelard A. Couvreux, C. Loudet, E.J. Dufourc, *Methods. Mol. Biol.* 462 (2009) 111-133.

(sulphur or nitrogen if O,S or O,N). If the donor atoms have similar properties, the isomers form in comparable rations.[128]

Figure 2.7: Illustration of the possible isomers in the substitution reaction of complex Rh(L,L'-Bid)(CO)$_2$] with a monodentate tertiary phosphines

2.10 Conclusion

The interest in coordination compounds of Schiff-bases and quinoline bidentate ligands has increased dramatically in past few years due to their attractive chemical and physical properties making them relevant in various fields. The ease of synthesis of these ligand systems, high coordination affinity toward a wide variety of metal ions makes these complexes attractive in the context of application in inorganic medicine, catalysis and electronic application.

In this study, the structural behavior of N,O'-bidentate Schiff-base ligands with the *fac*-[M(CO)$_3$]$^+$ (where M = Mn, Tc and Re) will be evaluated as model radiopharmaceuticals in the development of the [2+1] labeling strategy mentioned in the preceding section. The activity and properties of the metal complexes can be modified by variations on the ligand backbone. These ligands have the potential to form dinuclear metal complexes through the phenolate oxygen atoms. In this bridging disposition, the bidentate chelators bring in close proximity two metal ions to each other, consequently mimicking some biological sites, especially those where the two metal centres cooperate to form a more active centre. In addition, there is also the potential of preparing a bimetallic (Re/Tc) theranostic compounds.

A parallel aim of this study is to employ these structurally flexible ligand systems and investigate the propensity of square planar rhodium(I) [Rh(L,L'-Bid)(CO)$_2$]

[128] A. Roodt , H.G. Visser, A. Brink, *Crystallogr. Rev.* 17 (2011) 241-280.

(where N,O'-Bid = Schiff-base, 8-hydroxyquinoline) complexes to form one-dimensional chains via non-covalent metallophillic interactions. Moreover, the reactivity of complexes of the type [Rh(N,O'-Bid)(CO)(PX_3)] (where N,O'-Bid = Schiff-base bidentate ligands and PPX_3 = different monodentate tertiary phosphine) towards oxidative addition of iodomethane will be investigated. Corresponding studies with the 8-hydroxyquinoline and its derivatives have been previously reported. Schiff-base ligands form a 6-membered ring with the rhodium(I) centre in comparison to the five-membered chelate ring formed by the 8-hydroquinolline chelates. The effect of the chelate ring on the reactivity of square planar rhodium(I) complexes has been reported. The results from these studies indicated the correspondence of reactivity of the rhodium(I) complex towards oxidative addition to the bite angle of the ligand and thus the size of the chelate ring. Thus, the influence of the steric as well as electronic properties of the N,O'-bidentate Schiff-base ligands towards the oxidative addition reaction will be tailored and evaluated in this PhD study.

The understanding of the activities of the different metal complexes requires insight not only in structural information, but also the reactivity, pathways and the formation of intermediates are important in the design of more robust complexes. The advances in bridging the gap between solution and solid-state studies allow for in-depth evaluations in structural and reactivity dynamics and potentially fast-tracking the design and development of new functional material with desirable properties.

The following chapter presents the synthesis and characterization of the metal complexes containing the said N,O'-bidentate (Schiff and quinoline) ligands.

3 Synthesis of Complexes

3.1 Introduction

The primary aim of this study was to investigate the coordination behavior of Schiff-base and oxine bidentate ligands to the *fac*-$[M(CO)_3]^+$ (M = manganese, technetium, rhenium) as well as the rhodium(I) carbonyl cores. Firstly, the structural flexibility of Schiff-base ligands and their ease of preparation render them attractive for use in the development of radiopharmaceuticals derived from a combination of a bidentate and a monodentate ligand system. Biologically active molecules can be attached either directly on the periphery of the bidentate ligand or on the incorporated monodentate ligand. The physiochemical properties of the resulting complex such as lipophilicity, can thus be manipulated through modulation of the ligand backbone.[1,2,3] Secondly, this study aims to quantify the effects of the coordinated ligands on the assembly of one dimensional chains constructed via metal-metal interactions in rhodium(I) square planar complexes. The electronic and steric properties of the N,O bidentate ligands were varied and their effect on the metallophillic was evaluated by monitoring the Rh⊙⊙⊙Rh distances obtained in the single crystal X-ray diffraction analysis. The oxine ligand systems are included in the investigations of the influence of steric and electronic parameters on the metallophilic interactions because they offer an opportunity to introduce subtle variations in the periphery of the ligand without significantly varying the steric contribution within the system.

The synthesis and characterization of the complexes in this study are reported in this chapter. Their coordinative and kinetic properties will be discussed in succeeding chapters. The ligands used in this are illustrated in Figure 3.1.

1 T.R. Hayes, S.C. Bottorff, W. S. Slocumb, C.L. Barnes, A. E. Clarka, P.D. Benny, *Dalton Trans*. 46 (2017) 1134-1144.
2 R. Alberto, J.K. Pak, D. van Staveren, S. Mundwiler, P. Benny, *Biopolymers (Peptide Science).* 76 (2004) 324-333.
3 S. Mundwiler, M. Kündig, K. Ortner, R. Alberto, *Dalton Trans*. (2004) 1320-1328.

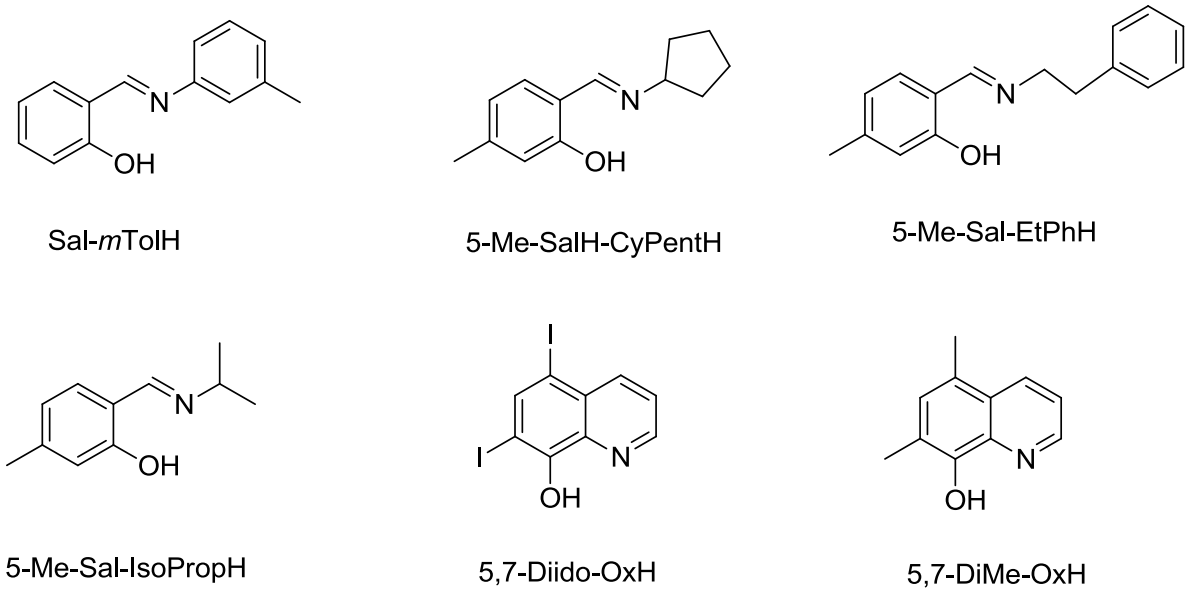

Figure 3.1: Schematic representation of the Schiff-base and oxine bidentate ligands used in this study. Where Sal-*m*TolH = 2-(*m*-Tolyliminomethyl)phenol; 5-Me-SalH-CyPentH = 2-(cyclopentyl)methyl-5-methylphenol; 5-Me-Sal-EtPhH = 5-methyl-2-(phenylethyliminimethyl)-phenol; 5-Me-Sal-IsoPropH = 5-Methyl-2 (isopropyliminomethyl)phenoline; 5,7-Diido-OxH =5,7-Diido-8-hydroxyquinoline; 5,7-Dimethyl-OxH = 5,7-Dimethy-8-hydroxyquinoline

3.2 Instrumentation and chemicals

All reagents used for the synthesis and characterisation were of analytical grade and were purchased from Sigma-Aldrich, unless otherwise stipulated. The reagents were used as received without further purification. All solvents used were of analytical grade. $[Re(CO)_5Br]$ was purchased from Strem Chemicals and was used as precursor to synthesize *fac*-$[Et_4N_2][ReBr_3(CO)_3]$ as described by Alberto *et al*.[4,5] Similarly, $[Mn(CO)_5Br]$ was used for all syntheses involving Mn(I) complexes.[6] The ^{13}C and ^{1}H NMR spectra of the ligands and metal complexes were recorded at 75.48 and 300.13 MHz respectively on a Bruker AXS 300 MHz or on a Bruker AXS 400 MHz (100.61 and 400.13 MHz respectively). The ^{31}P spectra were recorded on

[4] R. Alberto, A. Egli, U. Abram, K. Hegetschweiler, V. Gramlich, P.A. Schubiger, *J. Chem. Soc. Dalton Trans*. (1994) 2815-2820.
[5] R. Alberto, R. Schibli, P.A. Schubiger, *Polyhedron*. 15 (1996) 1079-1089.
[6] P.P. Mokolokolo, A. Brink, H.G. Visser, *Z. Kristallogr, NCS*. 231 (2016) 613-615.

a Bruker AXS 400 MHz at 161.98 MHz at ambient temperature (25 ± 1 °C). All chemical shifts are reported in ppm and coupling constants in Hz. Infrared spectra were recorded on a Bruker Tensor 27 Standard System spectrometer with a laser range of 4000-370 cm^{-1}, equipped with a temperature cell regulator accurate within ±0.3 °C.

The FT-IR spectra were recorded as liquid samples in dry dichloromethane in a NaCl cell in the range of 2350-1600 cm-1. The UV/visible measurements were performed on a Varian Cary 50 Conc spectrophotometer with thermostated automated multicell changers, equipped with a Julabo F12-mV temperature cell regulator and accurate within 0.1°C in 1.000(1) cm quartz tandem cuvette cells. Infrared spectra of the complexes were obtained on a Bruker Tensor 27 Standard System spectrometer with a laser range of 4000 – 370 cm^{-1}.

HPLC analysis of the ^{99}Tc complexes were performed on a Merck Hitachi LaChrom L 7100 pump coupled to a Merck Hitachi LaChrom L7200 tunable UV detector and a radiodetector. UV/Vis detection was performed at 250 nm. The detection of radioactive ^{99}Tc complexes was performed with a Berthold LB508 radiodetector equipped with BGO/YG cell. Separations were achieved on a Macherey-Nagel C18 reversed-phase column (Nucleosil 10 lm, 250 4 mm) using a gradient of MeOH/ 0.1 % CF_3COOH as eluent, and a flow rate of 0.5 mL/min. Gradient: t = 0 – 3 min: 0 % MeOH; 3 – 3.1 min: 0 – 25 % MeOH; 3.1 – 9 min: 25 % MeOH; 9 – 9.1 min: 25 – 34% MeOH; 9.1 – 18 min: 34 – 100 % MeOH; 18 – 25 min: 100 % MeOH, 25 – 25.1 min: 100 – 0 % MeOH; 25.1 – 30 min: 0 % MeOH.

Caution! ^{99}Tc is a weak β^- emitter with a half-life of 200 ky and should be handled in specially equipped laboratories only

3.3 Synthesis of Mn(I) and Re(I) tricarbonyl complexes

The mono- and dinuclear metal complexes were synthesized as illustrate in Scheme 3.1.

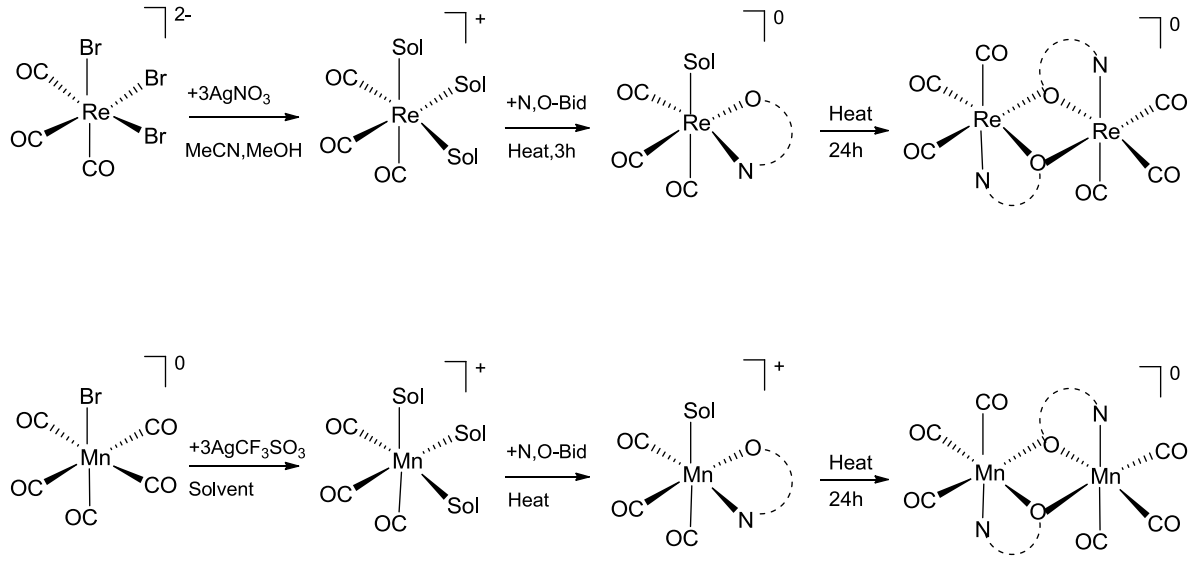

Scheme 3.1: General synthesis for the Mn(I) and Re(I) tricarbonyl complexes.

3.3.1 Synthesis of *fac*-[Mn(5-Me-Sal-CyPent)$(CO)_3]_2$

AgO_3SF_3 (0.093 g, 0.362 mmol) was added to a yellow solution of $[MnBr(CO)_5]$ (0.10 g, 0.362 mmol) in acetone (10 ml) solution and was refluxed for 2 h. AgBr precipitated and was filtered off. The solvent was removed under reduced pressure yielding a yellow oil to which 5-Me-SalH-Cypent (0.088 g, 0.438. mmol) in diethyl ether (20 ml) was added and the solution was heated at refluxed for 3 h. The majority of the solvent was removed under reduced pressure and suitable crystals were obtained through slow evaporation of the solvent in the dark at room temperature. Yield: (0.057 g, 17 %).

IR(KBr, cm^{-1}): ν_{CO} = 2013, 1905 cm^{-1}. ^{1}H NMR (300 MHz, $(CD_3)_2CO$ (ppm) 8.24 (s, 1H, HC=N), 7.03 (m, 1H, Ar), 6.58 (m, 1H, Ar), 6.30 (m, 1H, Ar) 4.49 (m, 1H, CH), 2.19 (s, 1H, CH3), 1.70-1.94 (m, 8H, Cyp). ^{13}C NMR (300 MHz, Acetone-*d6*) δ 163.33, 161.25, 131.85, 131.45, 119.16, 118.16, 116.48 (Ar), 67.18(CH), 34.20, 329.71, 25.33, 24.14 (Cyp).

3.3.2 Synthesis of *fac*-[Re(Sal-CyHex)(CO)$_3$]$_2$

$AgNO_3$ (0.033 g, 0.195 mmol) was added to an acetonitrile (10 ml) solution of *fac*-$(Et_4N)_2[ReBr_3(CO)_3]$ (0.05 g, 0.065 mmol) and heated at 80 ^oC for 20 minutes. AgBr precipitated and was removed by filtration. SalH-CyHex (0.0150 g, 0.0735 mmol) dissolved in acetonitrile (5 ml) was added to the solution. Triethylamine (50 µl) was added to the solution and heated at 80 ^oC for 3 hours. The solvent was removed under reduced pressure and suitable crystal for X-ray diffraction analysis were obtained through slow evaporation of a layered solution of dichloromethane/hexane. Yield (0.015 g, 24 %)

IR(KBr, cm^{-1}): ν_{CO} = 1851, 2006 cm^{-1}. ^1H NMR (400 MHz, DMSO) δ(ppm) 8.45 (s, 1H, HC=N), 7.30 (d, *J* = Hz, 2H, Ar), 6.73 (d, *J* = 8.4 Hz, 1H, Ar), 6.57 (m, 1H, Ar), 3.86 (m,1H, CH), 2.24 (s, 1H, C21), 2.01-1.65 (m,10H, Cyc). ^{13}C NMR (101 MHz, DMSO) δ 164.61, 164.03, 135.82, 134.45, 121.04, 120.91, 114.52 (Ar), 75.45 (CH), 33.74, 33.51, 25.47, 25.45, 24.94 (Cyc).

3.3.3 Synthesis of *fac*-[Re(5-Me-Sal-EtPh)(CO)$_3$(MeOH)]

fac-$(Et_4N)_2[ReBr_3(CO)_3]$ (0.051 g, 0.0666 mmol) was dissolved in methanol (10 ml) followed by the addition of 5-methyl-2-(phenylethyliminimethyl)-phenol = 5-Me-SalH-EtPh (0.016 g, 0.0649 mmol), also dissolved in methanol (10 ml). The solution was heated at 80 ^oC for 24 hours. The product was washed with THF and the solvent removed under reduced pressure. Suitable crystals for X-ray diffraction analysis were obtained through slow evaporation of methanol/acetone solution. (Yield 0.019 g, 56 %).

IR(KBr, cm^{-1}): ν_{CO} = 1863, 1999 cm^{-1}. ^1H NMR (400 MHz, CDCl3) : δ(ppm) 8.22 (s, 1H), 6.64 (d, *J* = 38.8 Hz, 2H), 3.52 (s, 2H), 2.25 (s, 3H), 1.72 (s, 2H). 13C NMR (100 MHz, CDCl3): δ(ppm) 21.85 (CH3), 21.66 (2 x CH), 23.56, 28.56, 32.02, 35.42 (2 x CH), 119.33 (Ar), 126.74, 128.40, 135.13, 138.55, 154.99, 162.56 (C=N).

3.4 Synthesis of Tc(I) tricarbonyl complexes

3.4.1 Synthesis of *fac*-[^{99}Tc(Sal-mTol)(CO)$_3$]$_2$

fac-([NEt$_4$]$_2$[^{99}Tc(CO)$_3$(Cl)$_3$]) (0.025 g, 0.05 mmol) was dissolved in 3 ml acetonitrile. 2-(*m*-Tolyliminomethyl)phenol = SalH-*m*Tol (0.015 mg, 0.07311 mmol) dissolved in 2 ml acetonitrile was added to the solution. An excess of trimethylamine was added to the solution and heated at 80 ˚C for 3 hours. The solution was filtered and the solvent removed under vacuum. The resulting yellow solution was crystallized from a DCM solution. The formation of *fac*-[^{99}Tc(Sal-*m*Tol)(CO)$_3$]$_2$ was confirmed by radiochemical/HPLC analysis.(yield: 4 %) Rt = 24.27 minutes.

3.4.2 Synthesis of *fac*-[^{99}Tc(5-Me-Sal-CyPent)(CO)$_3$]$_2$

([NEt$_4$]$_2$[^{99}Tc(CO)$_3$(Cl)$_3$]) (0.025 g, 0.05 mmol) was dissolved in (3 ml) acetonitrile. 2-(cyclopentane)methyl-5-methylphenol = 5-Me-SalH-CyPent (0.014 g, 0.0689 mmol) in (2 ml) acetonitrile was added to the solution. An excess of trimethylamine was added to the solution and heated at 80˚C for 3 hours. The solvent was removed under vacuum, and [Et$_4$N]$_2$ was removed with THF. The resulting yellow solution was crystallized in DCM solution. The formation of *fac*-[^{99}Tc(5-Me-Sal-CyPent)(CO)$_3$]$_2$ was confirmed by radiochemical/HPLC analysis. (Yield: 8 %) Rt = 24.17 minutes.

3.4.3 Synthesis of *fac*-[^{99}Tc(5-Me-SalH-EtPh)(CO)$_3$]$_2$

fac-([NEt$_4$]$_2$[^{99}Tc(CO)$_3$(Cl)$_3$]) (0.025 g, 0.05 mmol) was dissolved in (3 ml) acetonitrile. 5-methyl-2-(phenylethyliminimethyl)-phenol = 5-Me-SalH-EtPh (0.014 g, 0.058 mmol) was dissolved in (2 ml) acetonitrile was added to the solution. An excess of trimethylamine was added to the solution and heated at 80˚C for 3 hours. The solution was filtered and the solvent removed under vacuum. The resulting yellow solution was crystallized from a DCM solution. The formation of *fac*-[^{99}Tc(Sal-CyHex)(CO)$_3$]$_2$ was confirmed by radiochemical/HPLC analysis. (Yield: 6 %) Rt = 24.07 minutes.

3.5 Synthesis of Rh(I) dicarbonyl complexes

The general synthesis of the dinuclear precursor, $[Rh(\mu\text{-}Cl)(CO)_2]_2$, used for the synthesis of the rhodium(I) complexes is given in Scheme 3.2. The staring complex is prepared from refluxing $RhCl_3.xH_2O$ in DMF until the color changes from red to yellow, approximately 30 minutes. The chloro-bridged dimeric complex is used further without isolation.

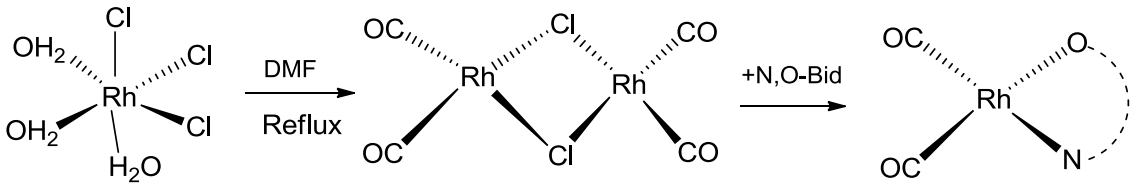

Scheme 3.2: Illustration of the rhodium(I) complex synthesis.

3.5.1 Synthesis of [Rh(5-Me-Sal-IsoProp)$(CO)_2$]

$RhCl_3.xH_2O$ (0.020 g, 0.076 mmol) was dissolved in 5 ml of DMF and the solution was refluxed for approximately 30 minutes. The solution was cooled and then 5-Methyl-2-(isopropyliminomethyl)phenol = 5Me-Sal-IsoProp (0.016 g, 0091 mmol) was added to the reaction mixture and stirred. After two minutes of stirring, the product was precipitated by ice water and isolated by centrifugation. The product was recrystallized by dissolving it in 1 ml acetone. Yield (0.016 g, 63%).

IR (ATR): ν_{CO} 2062, 1994 cm^{-1}. ^1H NMR (300 MHz, CD_2Cl_2) δ 8.22 (s, 1H, Ar), 7.16 (s, 1H, Ar), 6.78 (s, 1H, Ar), 6.54 (s, 1H, Ar), 4.26 (s, 1H, CH), 2.28 (s, 3H, CH_3), 1.4 (s, 6H, 2xCH_3). ^{13}C NMR (101 MHz, CD_2Cl_2) δ 163.66, 161.29, 146.51, 134.78, 120.61, 117.50, 116.33 (Ar), 67.46 (CH), 24.27 (CH_3), 21.34 (2 x CH_3).

3.5.2 Synthesis of [Rh(Sal-CyHex)(CO)$_2$]

$RhCl_3.xH_2O$ (0.020 g, 0.076 mmol) was dissolved in 5 ml of DMF and the solution was refluxed for approximately 30 minutes. The solution was cooled and 2-(Cyclohexyliminomethyl)phenol = SalH-CyHex (0.019 g, 0.091 mmol) was added to the cooled reaction mixture. After two minutes of stirring, the product was precipitated by ice water and isolated by centrifugation. The product was recrystallized by dissolving it in 1 ml acetone. Yield (0.018 g, 64 %).
IR (ATR): ν_{CO} 2062, 1988 cm^{-1}. ^{1}H NMR (400 MHz, CD_3CN) δ 8.37 (s, 1H, HC=N), 7.34 (s, 2H), 6.86 (s, 1H), 6.68 (s, 1H), 3.88 (m, 1H), 1.87-1.13 (m, 10H, Cyc). ^{13}C NMR (101 MHz, DMSO) δ 163.55, 163.02, 136.31, 135.62, 119.10, 116.05, 115.46 (Ar), 76.01 (CH), 34.87, 25.84, 25.32 (Cyc).

3.5.3 Synthesis [Rh(5-Me-Sal-CyPent)(CO)$_2$]

$RhCl_3.xH_2O$ (0.021 g, 0.079 mmol) was dissolved in 5ml of DMF and refluxed until the red colour turned yellow (approx. 30min). 2-(cyclopentane)methyl-5-methylphenol = 5-Me-Sal-CyPent (0.019 g, 0.095 mmol) was added to the cooled solution of $[Rh(\mu\text{-}Cl)(CO)_2]_2$. After two minutes of stirring, the product was precipitated by ice water and isolated by centrifugation. The product was recrystallized by dissolving it in 1 ml acetone. Yield (0.024 g, 80 %).
IR (ATR): ν_{CO} = 2066.18, 1986.47 cm^{-1}. ^{1}H NMR (400 MHz, CD_3CN) δ 8.33 (s, 1H, HC=N), 7.25 (s, 1H), 6.72 (s, 1H), 6.54 (s, 1H), 3.87 (m, 1H), 2.27 (s, 3H), 1.89-1.23 (m, 8H, Cyp). ^{13}C NMR (101 MHz, DMSO) δ 162.0, 160.25, 129.11, 128.54, 113.72, 76.01 (CH), 33.81, 24.26 (Cyp).

3.5.4 Synthesis of [Rh(Ox)(CO)$_2$]

$RhCl_3.xH2O$ (0.022 g, 0.083 mmol) was dissolved in 3 ml of DMF and the solution was refluxed for approximately 30 minutes. The solution was cooled and 8-hydroxyquinoline = Ox (0.039 g, 0.100 mmol) was added to the reaction mixture. After two minutes of stirring, the product was precipitated by ice water and isolated by centrifugation. The product was recrystallized by dissolving it in 1 ml acetone. Yield (0.035 g, 76 %).

IR (ATR): ν_{CO} 2074, 2005 cm^{-1}. ^{1}H NMR (300 MHz, CD_2Cl_2) δ 8.67 (s, 1H, Ar), 8.41 (s, 1H, Ar), 7.50 (s, 2H, Ar), 7.09 (s, 2H, Ar). ^{13}C NMR (75 MHz, DMSO) δ 155.40, 153.35, 151.32, 150.10 , 145.02, 140.35, 138.49, 130.08, 124.65.

3.5.5 Synthesis of [Rh(5,7-Diido-Ox)$(CO)_2$]

$RhCl_3$.xH2O (0.022 g, 0.083 mmol) was dissolved in 3 ml of DMF and the solution was refluxed for approximately 30 minutes. The solution was cooled and 5,7-Diido-8-hydroxyquinoline = 5.7-Diido-Ox (0.039 g, 0.100 mmol) was added to the reaction mixture. After two minutes of stirring, the product was precipitated by ice water and isolated by centrifugation. The product was recrystallized by dissolving it in 1 ml acetone. Yield (0.035 g, 76 %).
IR (ATR): ν_{CO} cm^{-1} 2055, 1982 cm^{-1}. ^{1}H NMR (300 MHz, CD_2Cl_2) δ 8.72 (s, 2H, Ar), 7.57 (s, 2H, Ar), 6.94 (s, 1H, Ar). ^{13}C NMR (75 MHz, DMSO) δ 159.41, 153.35, 151.32, 148.10 , 144.02, 134.35, 128.49, 120.08, 112.65.

3.5.6 Synthesis of [Rh(5,7-Dimethyl-Ox)$(CO)_2$]

$RhCl_3$.xH2O (0.02 g, 0.076 mmol) was dissolved in 3 ml of DMF and the solution was refluxed for approximately 30 minutes. The solution was cooled and 5,7-Dimethyl-8-hydroxyquinoline = 5,7-Dimethyl-Ox (0.016 g, 0.091 mmol) was added to the reaction mixture. The yellow product was precipitated by the addition of ice-water and isolated by centrifugation. The product was recrystallized by dissolving it in 1 ml acetone. Yield (0.021 g, 84 %).
IR (ATR): ν_{CO} 2051, 1981 cm^{-1}. ^{1}H NMR (300 MHz, DMSO) δ 8.82 (s, 1H), 8.65 (s, 1H), 7.61 (s, 1H), 7.29 (s,1H), 2.54 (s, 3H), 2.30 (s, 3H). ^{13}C NMR (75 MHz, DMSO) δ. 138.03, 133.27, 124.16, 120.11, 119.76, 114.51, 109.46 (s), 16.99, 16.28.

3.5.7 Synthesis of [Rh(acac)$(CO)_2$]

$RhCl_3$.xH2O (0.023 g, 0.087 mmol) was dissolved in 3 ml of DMF and the solution was refluxed for approximately 30 minutes. The solution was cooled and Acetylacetone = acac (0.0110 g, 0.105 mmol) was added to the reaction mixture.

The yellow product was precipitated by the addition of ice-water and isolated by centrifugation. The product was recrystallized by dissolving it in 1ml acetone. Yield (0.01 g, 70 %).
IR (ATR): ν_{CO} 1992, 2062 cm^{-1}. ^{1}H NMR (300 MHz, benzene) 5.08 (s, 1H, CH), 1.62 (s, 6H, 2 x CH3). ^{13}C NMR (75 MHz, benzene) δ 102.11 (CH), 26.22 (CH3).

3.6 Synthesis of rhodium(I) monophosphine complexes

A variety of rhodium(I) complexes were investigated via ^{31}P NMR spectroscopy. (CP/MAS) was used for the solid samples. The idea is to study the ligand effects in square planar [Rh(L,L'-Bid)(CO)PPX_3] complexes, formed by substituting one CO ligand in the complex of the type [Rh(L,L'-Bid)$(CO)_2$]. This study will allow us to better derive correlations such as bond distances, donating and accepting properties and the overall reactivity of the complexes.

The general synthesis of the rhodium(I) monophosphine complexes synthesized is illustrated by Scheme 3.3. The replacement of one carbonyl ligand from the parent complexes [Rh(L,L'-Bid)$(CO)_2$], may lead to the formation of either one or both isomers depending on the donor/acceptor properties of the donor atoms L,L' of the ligand as shown in Scheme 3.3. The dicarbonyl complex precursor is prepared from the reaction of the dimeric compound, [Rh(μ-Cl)$(CO)_2]_2$ and the bidentate ligand in question. The monophosphine complexes were prepared by dissolving dicarbonyl complexes in minimum acetone followed by the addition of the subjected tertiary phosphine ligand, PPX_3. The solid was then filtered and dried at room temperature.

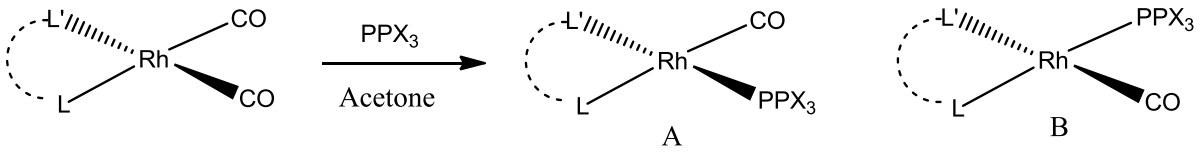

Scheme 3.3: General synthesis of the rhodium(I) monophosphine complexes.

3.6.1 Synthesis of [Rh(Ox)(CO)(PPh_3)]

[Rh(Ox)$(CO)_2$] (0.04 g, 0.132 mmol) was dissolved in 2 ml acetone to which PPh_3 (0.035 g, 0.158 mmol) was added. The reaction mixture was allowed to evaporate slowly resulting in a yellow product. Yield (0.060, 85 %).

IR (ATR): ν_{CO} 1991 cm^{-1}. ^1J(RH-P) = 161.6 Hz.

^{1}H NMR (300 MHz, CD_2Cl_2) δ 8.67 (s, 1H), 8.41 (s, 1H), 7.50 (s, 2H), 7.09 (s, 2H).

3.6.2 Synthesis of [Rh(5-Cl-Ox)(CO)(PCy_3)]

[Rh(Ox)$(CO)_2$] (0.041 g, 0.121 mmol) was dissolved in 2 ml acetone to which PCy_3 (0.035 g, 0.159 mmol) was added. The solvent was allowed to evaporate slowly resulting in a yellow product. Yield (0.051 g, 73%).

IR (ATR): ν_{CO} 1943 cm^{-1}. ^1J(Rh-P) = 157.0 Hz.

^{1}H NMR (300 MHz, DMSO) δ 8.73 (s, 1H), 8.47 (s, 1H), 7.57 (s, 1H), 7.35 (s, 1H), 7.01 (s, 1H), 1.89-1.50 (m, 33H).

3.6.3 Synthesis of [Rh(5,7-DiMe)(Ox)(CO)(PPh_3)]

[Rh(5,7-DiMe)(Ox)$(CO)_2$] (0.044 g, 0.133 mmol) was dissolved in 2 ml acetone to which PPh_3 (0.035 g, 0.159 mmol) was added. The solvent was allowed to evaporate slowly resulting in a yellow product. Yield (0.045 g, 60%).

IR (ATR): ν_{CO} 1952 cm^{-1}. ^1J(Rh-P) = 163.6 Hz.

^{1}H NMR (300 MHz, DMSO) δ 8.83 (s, 1H), 8.56 (s, 1H), 7.66-7.51(m, 6H), 7.34(m,10H), 7.19 (s, 1H), 2.07 (s, 6H).

3.6.4 Synthesis of [Rh(5,7-Dichloro)(Ox)(CO)(PPh_3)]

[Rh(5,7-Dichloro)(Ox)$(CO)_2$] (0.039 g, 0.11 mmol) was dissolved in 2 ml acetone to which PPh_3 (0.026 g, 0.260 mmol) was added. The solvent was allowed to evaporate slowly resulting in a yellow product. Yield (0.043 g, 67 %).

IR (ATR): ν_{CO} 1970 cm^{-1}. ^1J(Rh-P) = 165.2 Hz.

^{1}H NMR (300 MHz, DMSO) δ 8.98 (s, 1H), 8.69 (s, 1H), 7.82 (s, 2H), 7.76 (m, 6H), 7.35-7.17 (m, 9H).

3.6.5 Synthesis of [Rh(Ox)(CO)(PPh_2Cy)]

[Rh(8-Ox)$(CO)_2$] (0.036g mg, 0.12 mmol) was dissolved in 2 ml acetone to which PPh_2Cy (0.032 g, 0.143 mmol) was added. The solvent was allowed to evaporate slowly resulting in a yellow product. Yield (0.039 g, 61%).

IR (ATR): ν_{CO} 1953 cm^{-1}. ^1J(Rh-P) = 162.3 Hz.

^{1}H NMR (300 MHz, DMSO) δ 8.47 (s, 1H), 7.71-7.41(m, 12H), 7.25 (s, 1H),6.67 (s,1H), 6.34 (s,1H), 1.89-1.16(m,11H).

3.6.6 Synthesis of [Rh(5,7-Diido)(Ox)(CO)(PPh_3)]

[Rh(5,7-Diido)(Ox)$(CO)_2$] (0.042 g, 0.076 mmol) was dissolved in 2 ml acetone to which PPh_3 (0.019 g, 0.091 mmol) was added. The solvent was allowed to evaporate slowly resulting in a yellow product. Yield (0.052 g, 87 %).

IR (ATR): ν_{CO} 1956 cm^{-1}. ^1J(Rh-P) = 164.1.

^{1}H NMR (300 MHz, DMSO) δ 8.88 (s, 1H), 8.46 (s, 1H), 7.70 – 7.49 (m, 15H), 6.97 (s, 1H), 6.85 (s, 1H).

3.6.7 Synthesis of [Rh(Sal-CyHex)(CO)(PPh_3)]

[Rh(Sal-CyHex)$(CO)_2$] (0.044 g, 0.12 mmol) was dissolved in 2 ml acetone to which PPh_3 (0.032 g, 0.15 mmol) was added. The solvent was allowed to evaporate slowly resulting in a yellow product. Yield (0.048 g, 66%).

IR (ATR): ν_{CO} 1957 cm^{-1}. ^1J(Rh-P) = 157.6 Hz.

^{1}H NMR (400 MHz, DMSO) δ 8.56 (s,1H), 7.73 - 7.38 (m, 15H), 7.09 (s, 1H), 6.87 (s, 1H), 6.49 (s, 1H), 6.09 (s, 1H), 2.29 – 1.08 (m, 11H).

3.6.8 Synthesis of [Rh(5-Me-Sal-IsoProp)(CO)(PPh_3)]

[Rh(5-Me-Sal-CyPent)$(CO)_2$] (0.040 g, 0.07 mmol) was dissolved in 2 ml acetone to which PPh_3 (0.022 g, 0.08 mmol) was added. The solvent was allowed to evaporate slowly resulting in a yellow product. Yield (0.031 g, 65 %).

IR (ATR): ν_{CO} 1955 cm^{-1}. ^1J(Rh-P) = 158.7 Hz.

^{1}H NMR (400 MHz, Acetone) δ 8.48 (s,1H), 7.74(m, 6H), 7.43(m, 9H), 7.19(s, 1H), 6.34 (s, 1H), 6.07 (s, 1H), 3.96 (s, 1H), 2.30 (s, 3H), 1.92-1.24 (m 10H).

3.6.9 Synthesis of [Rh(5-Me-Sal-CyPent)(CO)(PPh_3)]

[Rh(5-Me-Sal-CyPent)$(CO)_2$] (0.040 g, 0.067 mmol) was dissolved in 2 ml acetone to which PPh_3 (0.021 g, 0.080 mmol) was added. The solvent was allowed to evaporate slowly resulting in a yellow product. Yield (0.039 g, 83 %).
IR (ATR): ν_{CO} 1955 cm^{-1}. ^1J(Rh-P) = 157.6 Hz.
^{1}H NMR (400 MHz, Acetone) δ 8.49 (s,1H), 7.72 (s, 6H), 7.48 (s, 9H), 7.20 (s, 1H), 6.33 (s, 1H), 6.09 (s, 1H), 4.36 (s, 1H), 1.55 (s, 2 x CH_3).

3.6.10 Synthesis of [Rh(5-Me-Sal-CyPent)(CO)(PPh_2Cy)]

[Rh(5-Me-Sal-CyPent)$(CO)_2$] (0.041 g, 0.068 mmol) was dissolved in 2 ml acetone to which PPh_2Cy (0.022 g, 0.081 mmol) was added. The solvent was allowed to evaporate slowly resulting in a yellow product. Yield (0.038 g, 77 %).
IR (ATR): ν_{CO} 1951 cm^{-1}. ^1J(Rh-P) = 157.2 Hz.
^{1}H NMR (400 MHz, Acetone) δ 8.43 (s,1H), 7.79 (m, 10H), 7.15 (s, 1H), 6.42 (s, 1H), 6.34 (s, 1H), 4.40 (m, 1H), 1.89-1.61 (m, 10H), 1.57-1.23 (m 10H).

3.6.11 Synthesis of [Rh(5-Me-Sal-CyPent)(CO)($PPhCy_2$)]

[Rh(5-Me-Sal-CyPent)$(CO)_2$] (0.042 g, 0.069 mmol) was dissolved in 2 ml acetone to which $PPhCy_2$ (0.023 g, 0.083 mmol) was added. The solvent was allowed to evaporate slowly resulting in a yellow product. Yield (0.031 g, 62 %).
IR (ATR): ν_{CO} 1948 cm^{-1}. ^1J(Rh-P) = 157.8 Hz.
^{1}H NMR (400 MHz, Acetone) δ 8.45 (s, 1H), 7.89 (s, 2H), 7.49 (s, 3H), 7.17 (s, 1H), 6.48 (s, 1H), 6.35 (s,1H), 4.46 (s,1H), 1.9-1.81 (m 9H), 1.74-1.10 (m, 22 H).

3.6.12 Synthesis of [Rh(5-Me-Sal-CyPent)(CO)(PCy_3)]

[Rh(5-Me-Sal-CyPent)$(CO)_2$] (0.040 g, 0.065 mmol) was dissolved in 2 ml acetone to which PCy_3 (0.022 g, 0.078 mmol) was added. The solvent was allowed to evaporate slowly resulting in a yellow product. Yield (0.043 g, 89 %).

IR (ATR): ν_{CO} 1938 cm^{-1}. ^1J(Rh-P) = 152.2 Hz.

^{1}H NMR (400 MHz, Acetone) δ 8.45 (s,1H), 7.89 (s, 1H), 6.58 (s, 1H), 6.33 (s, 1H), 4.44 (m, 1H), 2.44 (s, 3H), 1.95-1.78 (m, 9H), 1.65-1.25 (m, 33H).

3.6.13 Synthesis of [Rh(acac)(CO)(PPh_3)]

[Rh(acac)$(CO)_2$] (0.036 g, 0.21 mmol) was dissolved in 2 ml acetone to which (PCy_3)] (0.056 g, 0.25 mmol) was added. The solvent was allowed to evaporate slowly resulting in a yellow product. Yield (0.064 g, 75%).

IR (ATR): ν_{CO} 1988 cm^{-1}. ^1J(Rh-P) = 178.04 Hz.

^{1}H NMR (300 MHz, DMSO) δ 7.65-7.34 (m, 15H) 5.41 (s, 1H), 2.08 (s, 3H, CH_3), 1.62(s, CH_3).

3.6.14 Synthesis of [Rh(acac)(CO)(PCy_3)]

[Rh(acac)$(CO)_2$] (0.046 g, 0.27 mmol) was dissolved in 2 ml acetone to which (PCy_3)] (0.076 g, 0.32 mmol) was added. The solvent was allowed to evaporate slowly resulting in a yellow product. Yield (0.097 g, 85 %)

IR (ATR): ν_{CO} 1947 cm^{-1}. ^1J(Rh-P) = 163.72 Hz.

^{1}H NMR (300 MHz, DMSO) δ 5.48(s, 1H), 2.09 (s, 3H), 1.86 (s, 3H), 1.95 (s, CH_3) 1.86-1.60 (m, 33H)

3.6.15 Synthesis of [Rh(acac)(CO)(PPh_2Cy)]

[Rh(acac)$(CO)_2$] (0.042 g, 0.25 mmol) was dissolved in 2 ml acetone to which an equivalent amount of (PPh_2Cy)] (0.066 g, 0.30 mmol) was added. The solvent was allowed to evaporate slowly resulting in a yellow product. Yield (0.084 g, 83 %)

IR (ATR): ν_{CO} 1948 cm^{-1}. ^1J(Rh-P) = 167.23 Hz.

^{1}H NMR (300 MHz, DMSO) δ 7.91-7.67(m, 5H), 5.52 (s, 1H), 2.03 (s, 3H),1.78 (s, 3H), 2.33,1.78 -1.16 (m, 22H)

3.7 Discussion and Conclusion

One of the objective of this study is to evaluate the coordination behavior of N,O Schiff bidentate ligands towards the *fac*-$[M(CO)_3]^+$ (M= manganese, technetium and rhenium) core. The analogues complexes synthesized are reported in this chapter. A keen observation made is that, in spite of applying relatively similar synthetic procedures in the synthesis of the metal complexes, only dinuclear complexes manganese and technetium could be isolated, while we could dictate the nuclearity in regards to rhenium complexes. The single X-ray diffraction study of the crystals obtained for the *fac*-$[M(CO)_3]^+$ complexes will be discussed in forthcoming chapters. The stretching frequencies of all the complexes are given by Table 3.1. The data indicates the coordination of the three CO ligands with three distinctive peaks characteristic of facially coordinated CO ligands.

A range of N,O-bidentate ligands with variation in steric and electronic properties were coordinated to rhodium centre affording complexes of the type, $[Rh(CO)_2(N,O\text{-}Bid)]$(N,O-Bid= bidentate ligands). The influence of the ligands on the rhodium-rhodium interactions was evaluated. The synthesis of the complexes is in general straight forward as illustrated Scheme 3 above. The major challenge experienced is the difficulty in obtaining single crystals suitable for X-ray diffraction studies. Numerous crystallization methods were attempted and proved successful in some cases; however the various methods failed in some instances. More attempts will be made in future since the determination of the crystal structure is of central importance since the Rh⊙⊙⊙Rh distances can be used to quantify the effect of the coordinated ligands on the metal-metal interaction.

In order to evaluate the reactivity of the rhodium(I) complexes, complexes of the type $[Rh(CO)(L,L'\text{-}Bid)(PR_3)]$, where L,L'-Bid = Bidentate ligands; PR_3 = tertiary phosphine) were synthesized by replacing one carbonyl ligand from the parent complex $[Rh(CO)_2(L,L'\text{-}Bid)]$. The influence of the bidentate ligands on the rate of oxidative addition reaction will be investigated and presented in Chapter 7. Table 3.1 gives a summary of selected spectroscopic data for the complexes. The succeeding chapters will present the sold state and solution state characteristics of the complexes synthesized herein this chapter.

Table 3.1: Summary of selected spectroscopic data for the synthesized complexes.

Complex	ν_{CO} cm^{-1}	^{31}P(a) ppm	$^{1}J_{RhP}$ (a) Hz	^{31}P (b) ppm	$^{1}J_{Rh-P}$ (b) (Hz
***fac*-[Mn(5-Me-Sal-CyPent)$(CO)_3]_2$**	1908,1924				
***fac*-[Re(Sal-CyHex)$(CO)_3]_2$**	1905,2013				
***fac*-[Mn(5-Me-Sal-EtPh)$(CO)_3$(MeOH)$]_2$**	1863,2000				
[Rh(5-Me-Sal-CyPent)$(CO)_2$]	2066,1986				
[Rh(5-Me-Sal-IsoProp)$(CO)_2$]	2062,1984				
[Rh(Sal-CyHex)$(CO)_2$]	2062,1988				
[Rh(acac)$(CO)_2$]	1992,2062				
[Rh(Ox)$(CO)_2$]	2074,2005				
[Rh(5,7-Diido)$(CO)_2$]	2055,1982				
[Rh(5,7-DiMe)$(CO)_2$]	2051,1981				
[Rh(5-Cl-Ox)$(CO)_2$]	2070 1982				
[Rh(Trop)(CO)PPh_3]	1978	48.7	176.2	52.7	173.6
[Rh(Cup)(CO)PPh_3]	1982	48.9	171.1	53.6	170.3
[Rh(5-Me-Sal-IsoProp)(CO)(PPh_3)]	1955	41.5	158.7		
[Rh(5-Me-Sal-CyPent)(CO)PPh_3]	1955	41.3	157.6		
[Rh(5-Me-Sal-Cypent)(CO)(PPh_2Cy)]	1951	46.9	157.2		
[Rh(5-Me-Sal-CyPent)(CO)$PPhCy_2$]	1948	51.0	157.8		
[Rh(5-Me-Sal-Cypent)(CO)(PCy_3)]	1938	50.3	152.2		
[Rh(Sal-CyHex)(CO)(PPh_3)]	1957	41.6	156.9		152.9
[Rh(Ox)(CO)(PPh_3)]	1991	41.4	161.6	41.6	157.3
[Rh(5,7-DiChloro)(CO)(PPh_3)]	1970	41.1	165.2	45.6	157.5
Rh(Ox)(CO)(PPh_2Cy)]	1953	47.9	162.0	50.6	158.2
[Rh(5-Cl-Ox)(CO)(PCy_3)]	1964	40.7	157.0	41.1	155.9
[Rh(5,7-DiMe)(CO)(PPh_3)]	1952	-	163.6	41.4	161.1
[Rh(5,7-Diido)(CO)(PPh_3)]	1956	-	164.1	41.8	160.0
[Rh(acac)(CO)(PPh_3)]	1977	48.6	175.7	46.6	173.4
[Rh(acac)(CO)(PP_2Cy)]	1948	58.8	171.3	60.0	177.7
[Rh(acac)(CO)(PCy_3)]	1945	59.1	164.3	60.8	166.1

[a] Solution state ^{31}P NMR, [b] Solid state ^{31}P NMR

Where (5-Me-Sal-CyPent) = 2-(cyclopentyl)methyl-5-methylphenolato; (Sal-CyHexH) = 2-(cyclohexyliminomethyl)phenolato; (5-Me-Sal-EtPhH) = 5-methyl-2-(phenylethyliminimethyl)phenolate; (5,7-Diido-OxH) = 5,7-Diido-8-hydroxyquinoline; 5,7-Dimethyl-OxH = 5,7-Dimethy-8-hydroxyquinoline; 5,7-Dichloro-OxH = 5,7-Dichloro-8-hydroxyquinoline; 5-Chloro-OxH = 5-Chloro-8-hydroxyquinoline (5-Me-Sal-IsoPropH) = (5-Methyl-2-(isopropyliminomethyl)phenol; (TropH) = Tropolone; (CupH) = Cupferron; (acacH) = Acetylacetone.

4 Crystallographic Study of Dinuclear *fac*-Mn(I) and *fac*-Re(I) Tricarbonyl Complexes

4.1 Introduction

The design and synthesis of radiopharmaceutical drugs derived from the *fac*-$[M(CO)_3]^+$ (M = Tc, Re) core has continued to be a subject of great interest.[1,2,3,4,5] The nuclear properties of the ^{99m}Tc isotope such as the short half-life (6 hours) and low energy gamma rays (141 keV) are favorable for diagnostic imaging using single photon emission computed tomography. Due to the complementing coordination properties of rhenium to technetium, the former can be used as a model for the development of the technetium complexes.[6,7,8,9] The two elements have comparable ionic radia and often form isostructural complexes. In addition to the isostructural behavior to technetium, rhenium has two radioisotopes that have potential in radiopharmaceutical design, i.e., ^{186}Re and ^{188}Re. The isotope ^{186}Re ($t_{1/2}$ = 3.68 d, β^-_{max} = 1.07 MeV) can be obtained from irradiation of ^{185}Re with neutrons (^{185}Re; n, γ) and the radionuclide ^{188}Re ($t_{1/2}$ = 16.98 h, β^-_{max} = 2.12 MeV, 85 % abundance) is generated by neutron radiation of ^{186}W.[10,11,12,13]

[1] R. Alberto, R. Schibli, R. Waibel, U. Abram, A.P. Schubiger, *Coord. Chem. Rev*. 192 (1999) 901-919.
[2] R. Alberto R, P.J. Kyong, D. van Staveren, S. Mundwiler, P. Benny, *Peptide Science*. 76 (2004) 324-333
[3] M. Bartholomae, J. Valliant, K.P. Maresca, J. Babich, J. Zubieta, *Chem. Commun*. 5 (2009) 493-512.
[4] R. Schibli, P.A. Schubiger, *Eur. J. Nucl. Med*. 29 (2002) 1529-1542.
[5] S.R. Banerjee, P. Schaffer, J.W. Babich, J.F. Valliant, J. Zubieta*, Dalton Trans*. 24 (2005) 3886-3897.
[6] G.R. Morais, A. Paulo, I. Santos, *Organometallics*. 31 (2012) 5693-5714.
[7] J. Jia, K. Zhou, J. Dai, B. Liu, M. Cu, *Eur. J. Med. Chem*. 124 (2016) 763-772.
[8] T. Kaur, W.-Z. Lee, M. Ravikanth, *Inorg. Chem*. 55 (2016) 5305-5311.
[9] R.-R. Ye, C.-P. Tan, M.-H. Chen, L.Hao, L.-N. Ji, Z.-W. Mao. *Chem. Eur. J*. 22 (2016) 7800-7809
[10] S. Liu, Chem. Soc . Rev. 33 (2004) 445-461.
[11] A. Leonidova, G. Gasser, *ACS Chem. Biol.* 9 (2014) 2180-2193.

As part of the ongoing investigations on the tricarbonyl complexes of technetium and rhenium, this study investigates the coordination behavior of Schiff-base bidentate ligands [see Chapter 3, Par 3.3] as potential bio-linkers in the [2+1] labeling strategy used in radiopharmaceutical design. In the [2+1] labeling approach, a mono and a bidentate ligand are utilized to replace the facile water ligands in the complexes *fac*-$[M(CO)_3(H_2O)_3]^+$. A bio-active component can thus be appended within the ligand skeleton on either the bidentate or the monodentate ligand. The properties of the final complex can thus be modulated by the introduction of appropriate functions on the ligand skeleton, and in two separate steps.[14,15,16,17]

This study serves as a continuation of ongoing investigations on the effect which various Schiff-base bidentate ligands have on the *fac*-$[M(CO)_3]^+$(M = Mn, Tc, Re) core. These ligands were selected due to their rich coordination chemistry and their structural flexibility allowing variations of the electronic and steric parameters on the periphery of the ligand skeleton. The variations are manifested systematically in terms of cyclohexyl, cyclopentyl and phenyl substituents and methyl groups on the ligand backbone. Two dinuclear manganese complexes wherein the Schiff-base bidentate ligands acts as both a chelator and a bridge between two manganese atoms via the phenolato oxygen atoms, were previously reported.[18,19] In spite of utilizing similar synthetic procedures as in mononuclear rhenium tricarbonyl analogues, only dinuclear manganese complexes could be isolated.[20] In this chapter examples are thus reported to demonstrate the manipulation of nuclearity in the rhenium tricarbonyl system as possible model radiopharmaceuticals. Although dinuclear compounds are rare in radiopharmaceuticals, there is a potential to

[12] C.S. Cutler, H.M. Hennkens, N. Sisay, S. Huclier-Markai, S.S Jurisson, *Chem. Rev*. 113 (2013) 858- 883
[13] C.F. Ramogida, C. Orvig, *Chem. Commun*. 49 (2013) 4720-4739.
[14] T.R. Hayes, S.C. Bottorff, W.S. Slocumb, C.L. Barnes, A.E. Clarka, P.D. Benny, *Dalton Trans*. 46 (2017) 1134-1144.
[15] S. Mundwiler, M. Kündig, K. Ortner, R. Alberto, Dalton Trans, 9 (2004) 1320-1328.
[16] T.R. Hayes, S.C. Bottorff, W.S. Slocumb, C.L. Barnes, A.E. Clarka, P.D. Benny, *Dalton Trans*. 46 (2017) 1134-1144.
[17] F. Tisato, M. Porchia, C. Bolzati, F. Refosco, A. Vittadin, *Coord. Chem. Rev*. 250 (2006) 2034-2045.
[18] P.P. Mokolokolo, A. Frei, M.S. Tsosane, D.V. Kama, M. Schutte-Smith, A. Brink, H.G. Visser, G. Meola, R. Alberto, A. Roodt, *Inorganica. Chimica. Act*a. 471 (2018) 249-256.
[19] P.P. Mokolokolo, A. Brink, *Z. Kristallogr. NCS*. 231 (2016) 613-615.
[20] A. Brink, H.G. Visser, A. Roodt*, Inorg. Chem*. 52 (2013) 8950-8961.

develop multifunctional tricarbonyl radiopharmaceutical agents that can integrate both therapeutic and imaging capabilities.

This chapter presents and describes crystal structures of the *fac*-manganese(I) and rhenium(I) tricarbonyl complexes as illustrated in Figure 4.1.

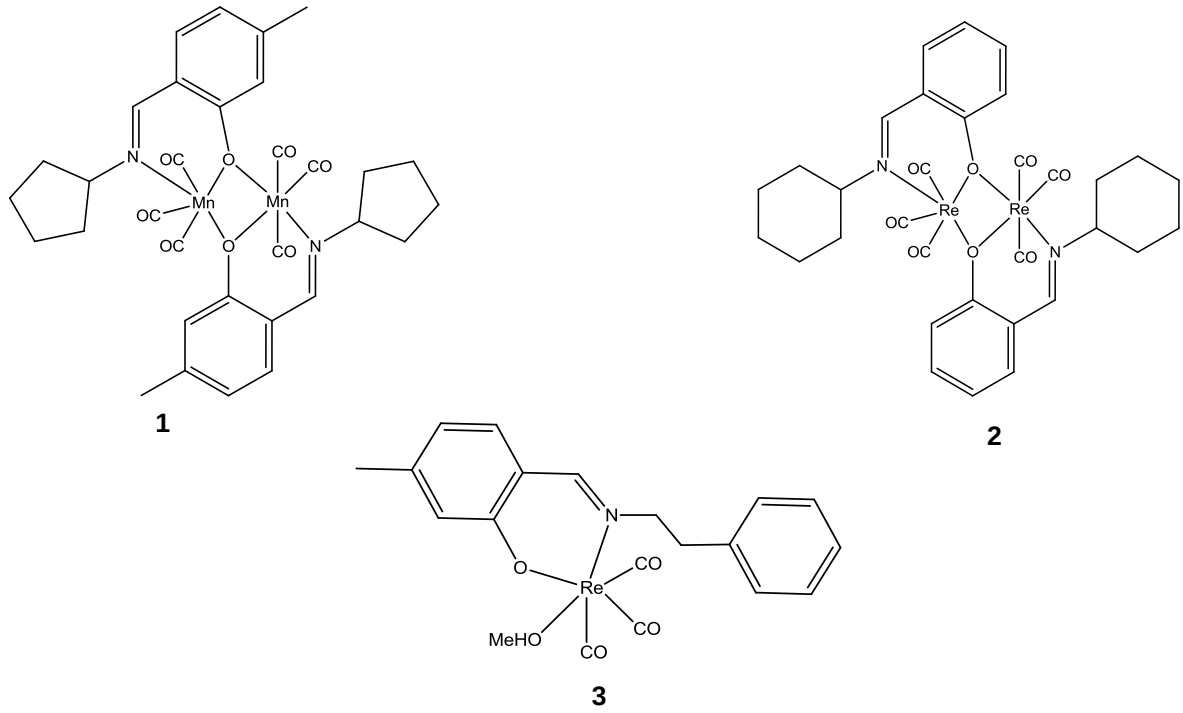

Figure 4.1: The two dimensional illustrations of *fac*-[Mn(5-Me-Sal-CyPent)$(CO)_3]_2$ (1), *fac*-[Re(Sal-CyHex)$(CO)_3]_2$ (2) and *fac*-[Re(5Me-Sal-EtPh)$(CO)_3$(MeOH)] (3), where (5-Me-Sal-Cypent = 2-(cyclopentyl)methyl-5-methylphenolate, (Sal-CyHex = 2-(cyclohexyliminomethyl)phenolate) and (5Me-Sal-EtPh = 5-methyl-2-(phenylethyliminimethyl)phenolate).

4.2 Experimental

Diffraction data of *fac*-[Mn(5Me-Sal-CyPent)$(CO)_3]_2$ (**1**), *fac*-[Re(Sal-CyHex)$(CO)_3]_2$ (**2**), and *fac*-[Re(5Me-Sal-EtPh)$(CO)_3$(MeOH)] (**3**), were collected at 100(2) K on a Bruker X8 Apex II 4K diffractometer using MoKα radiation (λ = 0.71073 Å).[21] The Apex II software package was utilized along with the optimum measurement method in collecting more than a hemisphere of reciprocal space as predicted by COSMO[22]. The cell parameters were refined by the SAINT-Plus[23] program while SADABS[24] was used for the absorption corrections. The structures were solved by direct methods and refined on F^2 using anisotropic displacement parameters for all non-hydrogen atoms. SHELXL-97[25,26] and WinGX[27] were used for structure solutions and refinements respectively, while the molecular graphics were prepared with DIAMOND.[28] All hydrogen atoms were refined with anisotropic displacement parameters, while the methyl, methane and aromatic H atoms were placed in geometrically idealised positions and constrained to ride of their parent atoms, with (C-H distances of 0.98 – 0.95 Å and U_{iso}(H) = 1.2U_{eq}(C) and U_{iso}(H) = 1.5U_{eq}(C)) respectively. The N-bound hydrogen atom was located from the electron density map and refined without any constraints.

Table 4.1 gives a summary of the general crystal data and refinement parameters for the rhenium(I) and manganese(I) tricarbonyl Schiff-base complexes (**1**-**3**). The supplementary data for the atomic coordinates, bond distances and bond angles and anisotropic displacement parameters are given in the Appendix for each individual dataset.

[21] Apex2, Version 2012.10-0, Bruker AXS Inc, Madison, Wisconsin, USA, 2012.
[22] Cosmo, Version 1.48, Bruker AXS Inc, Madison, Wisconsin, USA, 2003.
[23] SAINT-Plus, Version 8.27B (including XPREP), Bruker AXS, Inc, Madison, Wisconsin, USA, 2012.
[24] SADABS, Version 2012/1, Bruker AXS, Inc, Madison, Wisconsin, USA, 1998.
[25] G.M. Sheldrick, Acta Crystallogr, A64 (2008) 112-122.
[26] G.M. Sheldrick, SHELXL97, University of Göttingen, Göttingen, Germany, 1997.
[27] L.J. Farrugia, J. Appl. Crystallogr. 32 (1999) 837-838.
[28] K. Brandenburg, H. Putz, DIAMOND, release 3.1b, Crystal Impact GbR, Bonn, Germany, 2005.

Table 4.1: X-ray crystallographic data and refinement parameters for *fac*-[Mn(5-Me-Sal-CyPent)$(CO)_3]_2$ (1), *fac*-[Re(Sal-CyHex)$(CO)_3]_2$ (2), and *fac*-[Re(5-Me-Sal-EtPh)$(CO)_3$(MeOH)] (3).

	fac-[Mn(5-Me-Sal-CyPent) $(CO)_3]_2$ **(1)**	*fac*-[Re(Sal-CyHex) $(CO)_3]_2$ **(2)**	*fac*-[Re(5-Me-Sal-EtPh)$(CO)_3$(MeOH)] **(3)**
Empirical formula	$C_{32}H_{32}N_2O_8Mn_2$	$C_{32}H_{32}N_2O_8Re_2$	$C_{20}H_{20}NO_5Re$
Formula weight	682.47	944.99	540.57
Temperature/(K)	100(2)	100(2)	100 (2)
Wavelength Å	0.71073	0.71073	0.71073
Crystal system	Triclinic	Monoclinic	Monoclinic
Space group	$P\bar{1}$	$P2_1/c$	$C2/c$
a/Å	9.163(2)	9.2335(7)	21.5880(9)
b/Å	9.622(2)	9.3156(3)	14.9939(6)
c/Å	10.116(6)	18.1857(8)	14.2216(6)
α/°	106.023(7)	90	90
β/°	93.202(6)	96.197(5)	122.633(4)
γ/°	115.713	90	90
Volume/$Å^3$	756.3(7)	1555.11(15)	3876.7(3)
Z	1	2	8
Density ($g.cm^{-3}$)	1.498	2.018	1.852
μ(mm^{-1})	0.889	7.831	6.299
F(000)	352	904	2096
Crystal Color	Yellow	Yellow	Yellow
Crystal Morphology	Plate	Plate	Cuboid
Theta range (°)	4.158 to 27.998	2.219 to 32.968	2.717 to 27.998
Completeness(%) to θ	25.242, 99.3	25.242, 100.0	25.242, 99.9
Index ranges h k l	h = -12 to 11 k = -8 to 12 l = -13 to 13	h = -9 to 14 k = -13 to 7 l = -27 to 19	h = -26 to 28 k = -19 to 19 l = -18 to 15
Reflections collected	13167	13137	16061
Independent reflections	3623	5273	4691
R_{Int}	0.0286	0.0426	0.0451
Data/restraints/ parameters	3623 / 0 / 208	5273 / 0 / 207	4691 / 0 / 250
Goodness-of-fit on F^2	1.048	1.057	1.026
Final R indexes [I>=2σ (I)]	R1 = 0.0286, wR2 = 0.0741	R1 = 0.0343, wR2 = 0.0771	R1 = 0.0315, wR2 = 0.0653
Final R indexes [all data]	R1 = 0.0322 wR2 = 0.0767	R1 = 0.0414, wR2 = 0.0815	R1 = 0.0481, wR2 = 0.0735
ρ max, ρ min ($e.Å^{-3}$)	0.951, -0.278	3.187, -1.911	1.761, -1.735

Notes: 5-Me-Sal-Cypent = 2-(cyclopentyl)methyl-5-methylphenolato, Sal-CyHex = 2-(cyclohexyliminomethyl)phenolato, 5-Me-Sal-EtPh = 5-methyl-2-(phenylethyliminimethyl)phenolate.

4.3 Crystal structure of *fac*-[Mn(5-Me-Sal-CyPent)$(CO)_3]_2$

The solid state structure determination of the complex *fac*-[Mn(5-Me-Sal-CyPent)$(CO)_3]_2$ **(1)** (5-Me-Sal-Cypent = 2-(cyclopentyl)methyl-5-methylphenolato) was carried out with a yellow plate-like single crystal. The complex crystallizes in a triclinic crystal system in the $P\bar{1}$ space group, with one half of the molecule in the asymmetric unit cell. The other half is generated through the inversion symmetry operator. The molecular structure of **(1)** along with the numbering scheme is illustrated by Figure 4.2, while, relevant bond distances and bond angles are listed in Table 4.2.

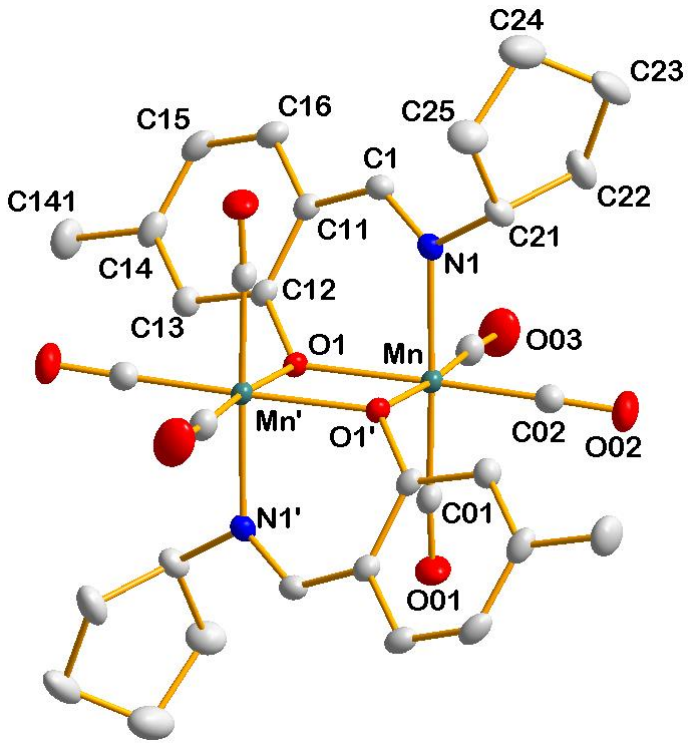

Figure 4.2: **Structural representation of *fac*-[Mn(5-Me-Sal-CyPent)$(CO)_3]_2$ (1) with atom numbering scheme and displacement ellipsoids at 50% probability level. For the aromatic rings, the first digit represents the ring number, while the second digit refers to the specific C-atom in the ring. Hydrogen atoms were omitted for clarity. (') indicates the symmetry generated subunit.**

Table 4.2: Selected bond lengths (Å) and angles (˚) of *fac*-[Mn(5-Me-Sal-CyPent)$(CO)_3]_2$ (1)

Atom	Bond Lengths (Å)	Atoms	Bond Angle (°)
Mn-O1	2.0427(13)	N1-Mn-O1	85.42(5)
Mn-O1'	2.0672(13)	N1-Mn-C01	177.07(6)
Mn'-O1	2.0672(13)	C03-Mn-O1'	175.13(6)
Mn-N1	2.0625(17)	Mn-O1-Mn'	101.95(5)
Mn-C01	1.8142(19)	O1-Mn-C03	97.72(7)
Mn-C02	1.8059(18)	O1-Mn-C02	175.12(6)
Mn-C03	1.7957(18)	O1-Mn-O1'	78.05(6)
Mn-Mn'	3.1930(18)	C01-Mn-C02	87.66(7)
N1-C1	1.281(2)	C01-Mn-C03	87.52(7)
C01-O01	1.145(2)	C02-Mn-C03	87.16(8)
C02-O02	1.149(2)	O01-C01-Mn	175.03(14)
C03-O03	1.148(2)	O02-C02-Mn	176.66(15)
		O03-C03-Mn	176.24(15)
		C1-N1-C21	116.71(13)

(') indicates the symmetry generated subunit

The coordination around the manganese centres in the dinuclear complex **(1)** forms a distorted octahedral geometry comprising of three carbonyl ligands that are facially coordinated to the metal centres and the O and N atoms of the 2-(cyclopentyl)methyl-5-methylphenolato ligand. The octahedron is completed by the bridging ligands through the phenolate oxygen atoms. A distortion from the ideal octahedral geometry around the Mn(I) centre is indicated by the N1-Mn-O1 bite angle of 85.42(5)° and the N1-Mn-C01 angle of 177.07(6)°. The Mn-N1 and Mn-O1 bond distances of 2.0625(17) Å and 2.0427(13) Å agree well with the related dinuclear manganese(I) complex with N,O chelating ligands with distances of 2.064(2) Å and 2.0325 (19) Å.[18] The central core of the dinuclear complex is defined by a four-membered planar system comprising of Mn-O1-Mn'-O1' atoms with the Mn-Mn' intermetallic distance of 3.1930(18) Å. This is in good comparison with the related dinuclear manganese(I) complexes with Mn-Mn' separation of 3.143 – 3.187 Å.[18,19,29] The two manganese atoms display an average out-of-plane distance of 0.0197(4) Å from the plane defined by the C-C-O-O atoms.

[29] C.M. Alvarez, R. Carrillo, R. Garcia-Rodriguez, D. Miguel, *Chem. Commun*. 48 (2012) 7705-7707

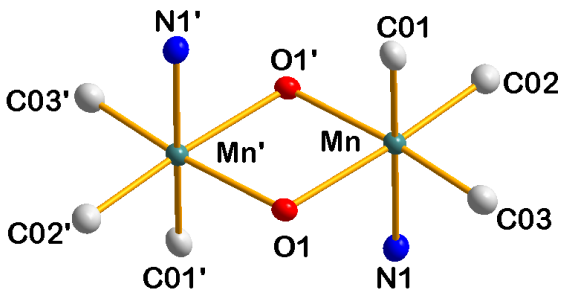

Figure 4.3: **A perspective view of the coordination octahedron around the manganese central atoms. (') indicates the symmetry generated atoms.**

The salicylidene backbone of the bidentate ligand indicated by C11, C12, C13, C14, C15, C16) (plane 1, purple) is bent relative to the plane defined by the atoms Mn, N1, O1, C01, C02 (plane 2, blue) with a dihedral angle of 40.062 (9)˚.

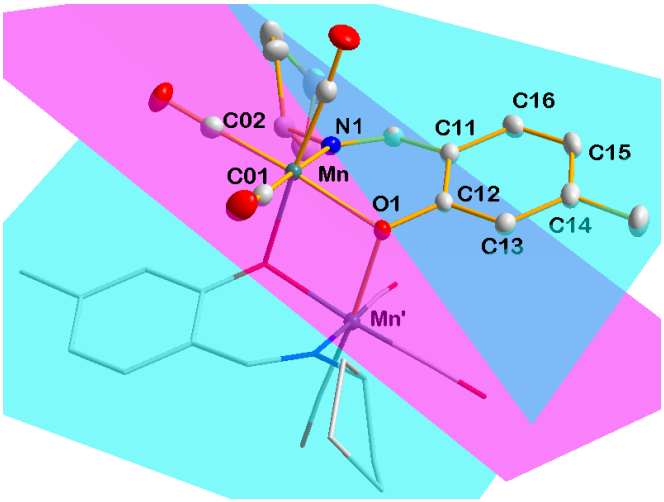

Figure 4.4: **Graphical representation of the bending aromatic backbone (Plane 1 is indicated in purple and Plane 2 indicated in blue). Hydrogen atoms were omitted for clarity**.

Two intermolecular hydrogen bonding interactions were observed and are indicated by the green dotted line in Figure 4.5. The related data is given in Table 4.3. There are weak π-π interactions between the salicylidene rings with a centroid-centroid distance of 5.607(3) **Å.**

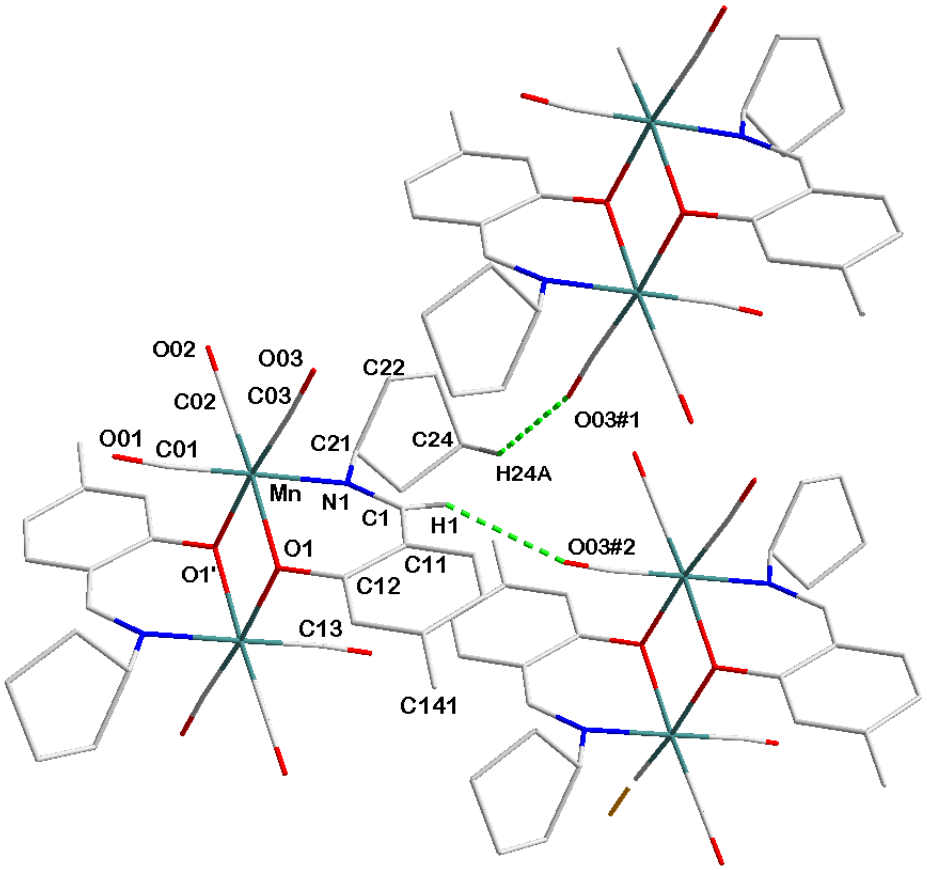

Figure 4.5: Graphical representation of hydrogen bonding interaction in C(1)-H(1)…O(03)$^{\#2}$ and C(24)-H(24)…O(03)$^{\#1}$. Some atom labels were omitted for clarity.

Table 4.3: Hydrogen bonds of *fac*-[Mn(5-Me-Sal-CyPent)(CO)$_3$]$_2$ (1) [Å and ˚].

D-H…A	d(D-H)	d(H…A)	d(D…A)	<(DHA)
C(1)-H(1)…O(03)#2	0.95(2)	2.59(2)	3.416(3)	145.4(15)
C(24)-H(24)…O(03)#1	0.97	2.59	3.394(3)	141

Symmetry transformations used to generate equivalent atoms
#1 1-x, -y, 1-2; #2 -1+ x, y, z,

The molecular packing in **(1)** is illustrated in Figure 4.6. The salicylidene rings pack in a "head-to-head" fashion on adjacent molecules with the methyl substituent pointing in opposite direction.

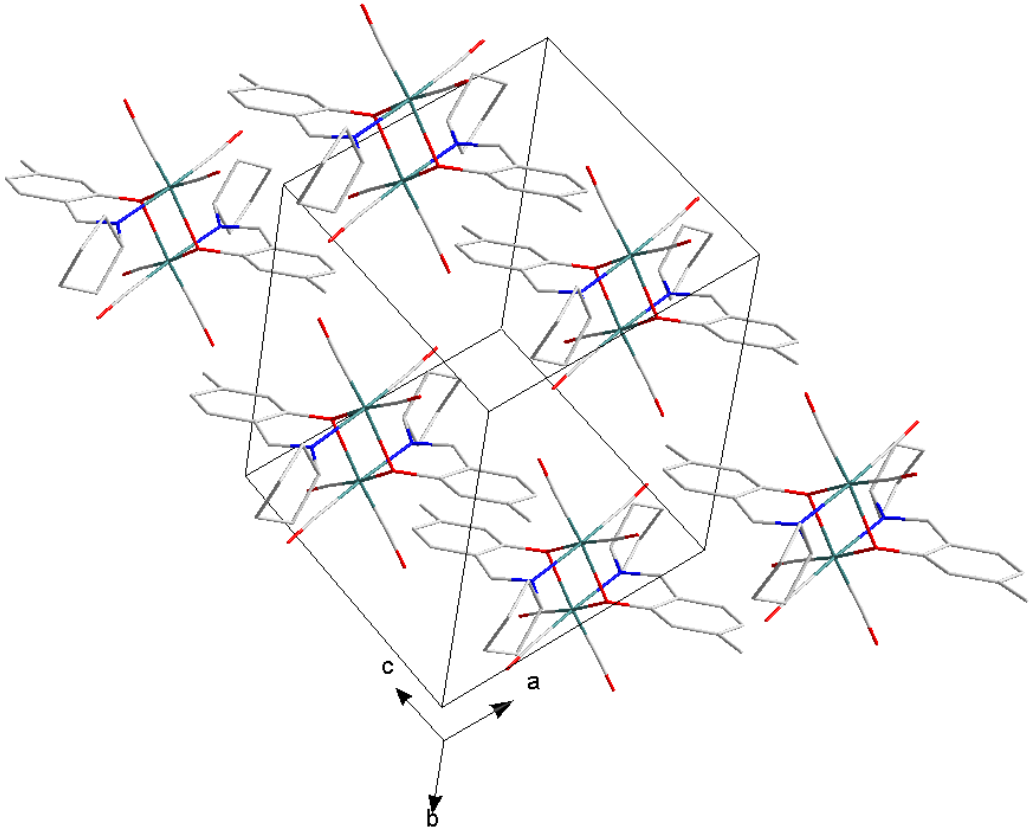

Figure 4.6: Molecular packing of *fac*-[Mn(5-Me-Sal-CyPent)$(CO)_3]_2$ (1).

4.4 Crystal structure of *fac*-[Re(Sal-CyHex)(CO)$_3$]$_2$

The molecular structure of the complex *fac*-[Re(Sal-CyHex)(CO)$_3$]$_2$ **(2),** (Sal-CyHex = 2-(cyclohexyliminomethyl)phenolate) is represented by Figure 4.7. The molecule crystallizes in a monoclinic crystal system in the $P2_1/c$ space group with two formula units in the unit cell (Z = 2). The asymmetric unit consists of one half of the molecule with the other half generated through symmetry. A structural representation of **(2)** along with the atom numbering scheme is illustrated by Figure 4.7. Selected bond angles and bond distances are listed in Table 4.4.

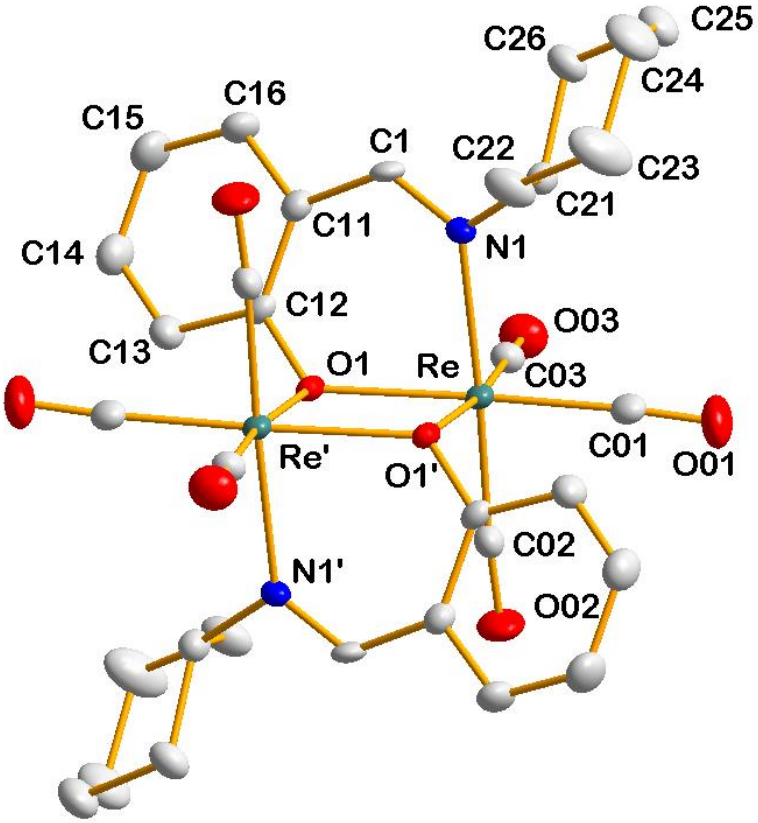

Figure 4.7: **Structural representation of *fac*-[Re(Sal-CyHex)(CO)$_3$]$_2$ (2) with atom numbering scheme and displacement ellipsoids at 50%. For the aromatic rings, the first digit represents the ring number, while the second digit refers to the specific C-atom in the ring. (‘) indicates the symmetry generated subunit.**

Table 4.4: Selected bond distances and angles of *fac*-[Re(Sal-CyHex)(CO)$_3$]$_2$ (2)-[Å and ˚].

Atoms	Bond Lengths (Å)	Atoms	Bond Angle (˚)
Re-N1	2.197(3)	N1-Re-O1	81.57(13)
Re'-O1	2.176(3)	N1-Re-C02	176.74(13)
Re-O1	2.149(3)	C01-Re-C02	84.45(16)
Re'-O1	2.149(3)	O1-Re-C01	172.77(14)
Re-C01	1.913(4)	Re-O1-Re'	106.17(11)
Re-C02	1.924(4)	O1-Re-C02	95.82(13)
Re-C03	1.902(4)	O1-Re-O1'	73.83(11)
Re-Re'	3.5478(4)	C01-Re-C03	88.38(17)
N1-C1	1.279(5)	C02-Re-C03	87.09(15)
C01-O01	1.146(4)	O01-C01-Re	176.6(3)
C02-O02	1.137(4)	O02-C02-Re	175.9(3)
C03-O03	1.154(5)	O03-C03-Re	178.2(3)
C1-C11	1.466(5)	C1-N1-C21	116.9(9)
N1-C21	1.503(5)		
O1-C12	1.359(4)		

(') indicates the symmetry generated subunit

The molecule adopts a six-coordinate distorted octahedral geometry around the rhenium centres with three carbonyl ligands facially coordinated to each metal centre and the two 2-(cyclohexyliminomethyl)phenolato ligands bridging via the phenolato oxygen atoms. The octahedron around the rhenium(I) centre is distorted as indicated by the N1-Re-O1 angle of 81.57(13)° and N1-Re-C02 angle of 176.74(13)°. The distortion around the rhenium centres can primarily be attributed to the constraints associated with the chelation of the ligand. The determined Re-N1 and Re-O1 bond distances of 2.197(3) Å and 2.149(3) Å compare well with literature example of dinuclear rhenium(I) tricarbonyl complexes having N,O donating atoms with bond distances ranging between 2.148-2.219 Å and 2.127-2.227 Å for Re-N1 and Re-O1 respectively.[30,31,32,33,34,35,36,37,38]

[30] S.M. Soares, S.S. Lemos, M.J.A.Sales, R.A. Burrow, *J. Organomet. Chem*. 750 (2014) 80-8.
[31] M. Grzegorczyk, A. Kapturkiewicz, J.Nowacki, A. Trojanowsk, *Inorg. Chem. Commun*. 14 (2011) 1773-1776.
[32] C.M. Alvarez, R. Carrillo, R. Garcia-Rodriguez, D. Miguel. *Chem. Eur. J.* 19 (2013) 8285-8293
[33] R. Wilberger, H. Piotrowski, P.Mayer, I.-P. Lorenz, *Inorg. Chem. Commun*. 5 (2002) 897-902.
[34] G.G. Aleksandrov, V.V. Derunov, A.A. Johansson, Yu.T. Struchkov, *J. Organomet. Chem*. 188 (1980) 367-371.
[35] H.C. Zhao, B. Mello, Bi-Li Fu, H. Chowdhury, D.J. Szalda, Ming-Kang Tsai, D.C. Grills, J. Rochford. *Organometallics*. 32 (2013) 1832-1841.
[36] G.G. Aleksandrov, V.V. Derunov, A.A.Johansson, Yu.T. Struchkov, *J. Organomet. Chem*. 188 (1980) 367-371.
[37] R. Wilberger, H. Piotrowski, P. Mayer, M. Vogt, I.-P. Lorenz. *Inorg. Chem. Commun*. 6 (2003) 845-851.

The molecule exhibits a coplanar central unit defined by a four-membered planar system made up of Re-O1-Re'-O1' atoms with a rhenium-rhenium distance of 3.5478(4) Å. The bidentate Schiff-base ligands are nitrogen bound to the rhenium(I) atoms at opposite ends of the diamond-shaped plane (Re'-O1-Re-O1') projecting the cyclohexyl rings away from the central core.

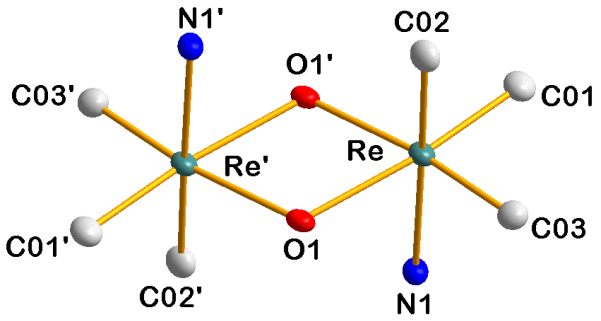

Figure 4.8: **View of the coordination octahedron around the rhenium atoms. The apostrophe (') indicates the symmetry generated subunit.**

The plane formed by the salicylidene backbone (Plane 1: C11, C12, C13, C14, C15, C16) is tilted out of the rhenium equatorial plane (Plane 2: Re, N1, O1, C01, C02) with a dihedral angle of 39.211˚.

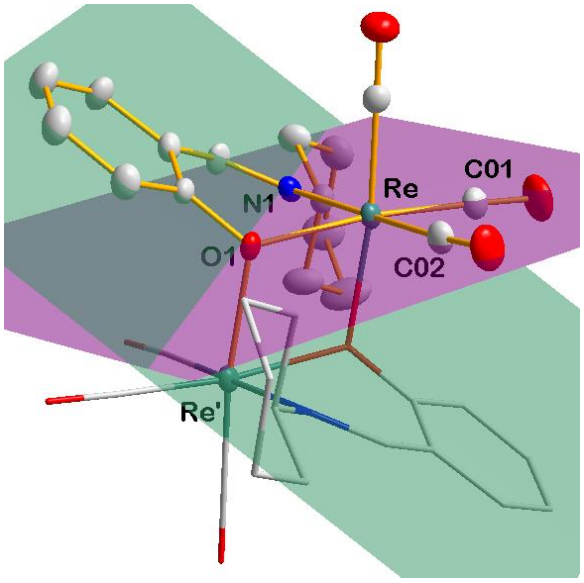

Figure 4.9: **Graphical representation of the bending of the salicylidene backbone (a) (Plane 1 is indicated in purple and plane 2 indicated in blue). Hydrogen atoms were omitted for clarity. (') indicates the symmetry generated subunit.**

[38] C.M.Alvarez, R.Carrillo, R.Garcia-Rodriguez, D.Miguel. *Chem. Commun*. 47 (2011)12765-12767.

The crystal lattice of **(2)** is stabilised by intermolecular hydrogen bonding observed in C(1)-H(1)…O(02)$^{\#1}$. The interaction is illustrated in Figure 4.10 and the related data is given in Table 4.5.

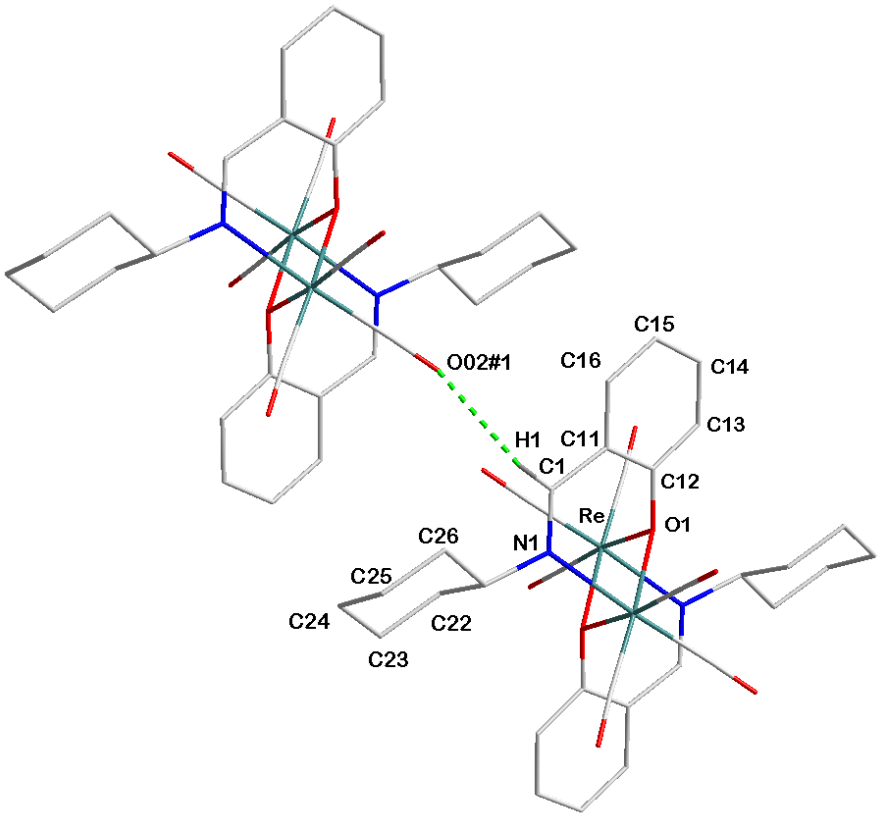

Figure 4.10: **Intermolecular hydrogen bond interaction. The interaction is illustrated by the green dotted line. Certain atoms were omitted for clarity.**

Table 4.5: **Hydrogen bonds for *fac*-[Re(Sal-CyHex)(CO)$_3$]$_2$ (2), [Å and °].**

D-H…A	d(H…A)	d(H…A)	d(D…A)	<(DHA)
C(1)-H(1)…O(02)$^{\#1}$	0.88(4)	2.50(4)	3.319(5)	155(3)

Symmetry transformation used to generate equivalent atoms:
#1 x, -1+y-1,z

The molecular packing in **(2)** is illustrated in Figure 4.11. The molecules pack in a head-to-head fashion with the carbonyl ligands pointing towards each other.

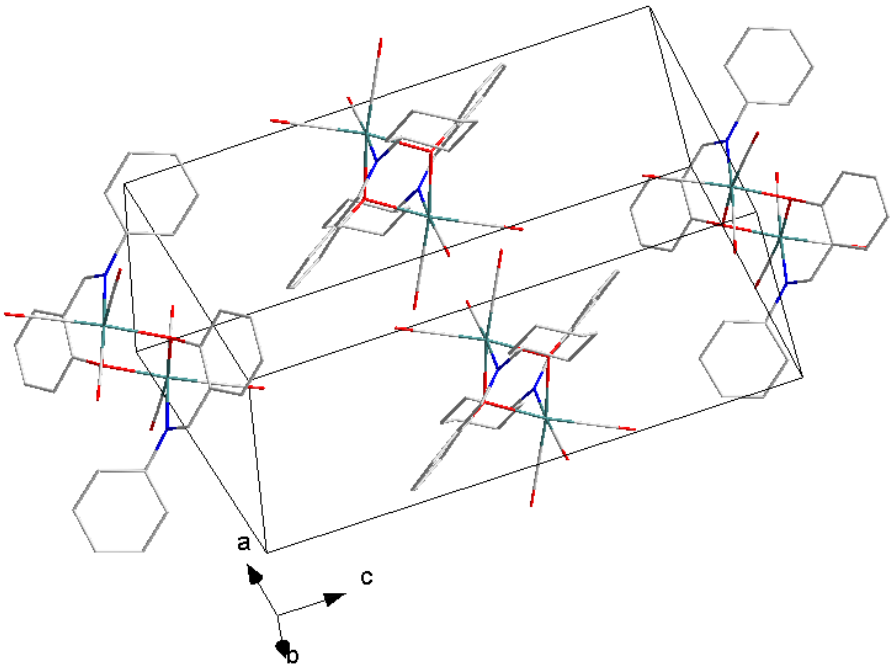

Figure 4.11: **Molecular packing of *fac*-[Re(Sal-CyHex)(CO)$_3$]$_2$ (2).**

4.5 Crystal structure of *fac*-[Re(5-Me-Sal-EtPh)(CO)$_3$(MeOH)]

The complex, *fac*-[Re(5-Me-Sal-EtPh)(CO)$_3$(MeOH)] **(3),** (5-Me-Sal-EtPh = 5-methyl-2-(phenylethyliminimethyl)phenolate) crystallizes in a monoclinic crystal system in the *C2/c* space group with eight formula units per unit cell (Z = 8). The asymmetric unit of **(3)** consists of one independent molecule, and the molecular structure is illustrated by Figure 4.12 along with the atom numbering scheme. Relevant bond distances and angles are listed in Table 4.6.

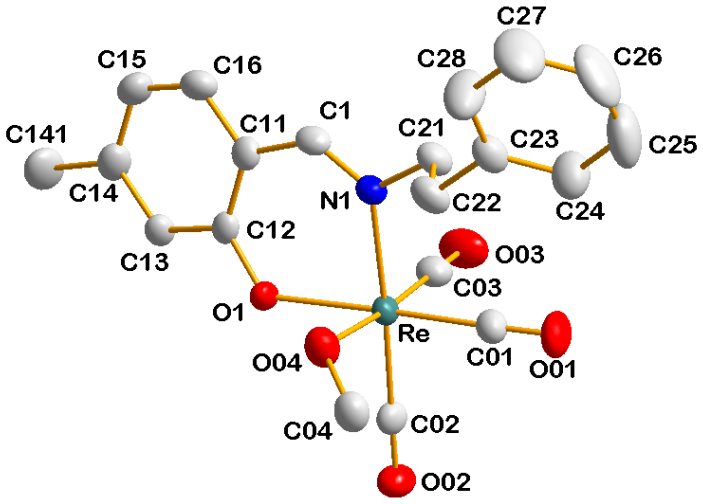

Figure 4.12: **Molecular structure of *fac*-[Re(5-Me-Sal-EtPh)(CO)$_3$(MeOH)] (3) showing atom numbering scheme and displacement ellipsoids at 50% probability level. For the aromatic rings, the first digit represents the ring number, while the second digit refers to the specific C-atom in the ring.**

Table 4.6: **Selected bond distances and angles of *fac*-[Re(5-Me-Sal-EtPh)(CO)$_3$(MeOH)] (3) [Å and ˚].**

Atoms	Bond Lengths (Å)	Atoms	Bond Angle (°)
Re-N1	2.173(4)	N1-Re-O1	84.88(14)
Re-O1	2.116(3)	N1-Re-C02	177.02(19)
Re-C01	1.904(6)	O04-Re-C03	175.2(2)
Re-C02	1.922(5)	O1-Re-C01	176.1(2)
Re-C03	1.893(7)	O1-Re-C02	92.53(17)
Re-O04	2.189(5)	C01-Re-C02	87.5(2)
N1-C1	1.287(7)	C01-Re-C03	87.6(3)
C01-O01	1.147(7)	C02-Re-C03	88.5(2)
C02-O02	1.139(6)	N1-Re-O04	83.13(16)
C03-O03	1.149(7)	O01-C01-Re	178.5(6)
C1-C11	1.436(7)	O02-C02-Re	178.4(5)
N1-C21	1.481(6)	O03-C03-Re	179.3(6)
O1-C12	1.322(6)	C1-N1-C21	115.6(4)

The molecule adopts a distorted octahedral configuration around the rhenium atom coordinated to the oxygen atom of the phenol group and the imine nitrogen atom, the three carbonyl ligands in facial arrangement and a methanol molecule. A distortion from the ideal octahedral geometry is indicated by the N1-Re-O1 bite angle of angle of 84.88(14)˚ and O04-Re-C03 angle of 175.2(2)˚. The Re-N1 and Re-O1 bond distances of 2.173(4) Å and 2.116(3) Å are consistent with related complexes in literature.[30-38] The rhenium carbonyl bond distances are comparable with bond distances of 1.904(6) Å, 1.922(5) Å and 1.893(7) Å for Re-C01, Re-C02 and Re-C03 respectively.

The plane formed by the salicylidene aromatic ring (Plane 1: C11, C12, C13, C14, C15, C16) is bending away from the plane rhenium equatorial plane (Plane 2: Re, N1, O1, C01, C02) with a dihedral angle of the 18.803˚ (2).

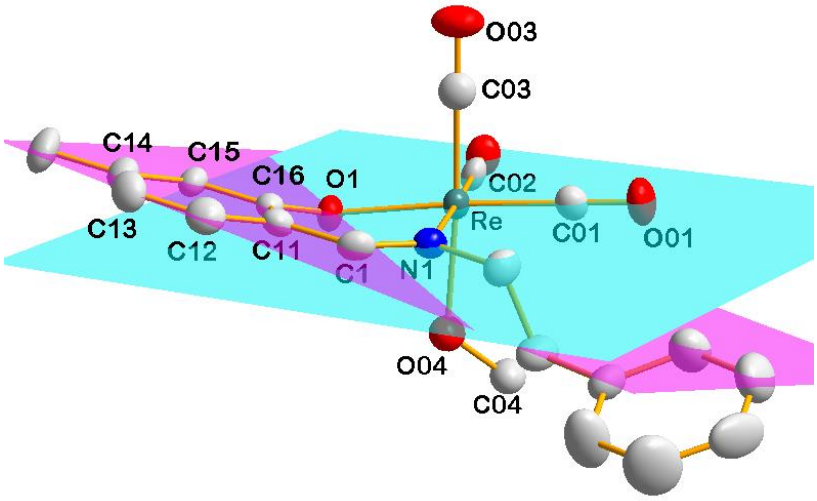

Figure 4.13: **Graphical representation of the bending of the salicylidene backbone from planarity in the equatorial plane. Hydrogen atoms were omitted for clarity.**

The molecular packing of **(3)** leads to the formation of classic intermolecular hydrogen bonding between the O04-H04 and the $O1^{\#1}$ of the phenolato oxygen atom. The interaction is indicated by the green dotted line in Figure 4.14, while related data is given by Table 4.7.

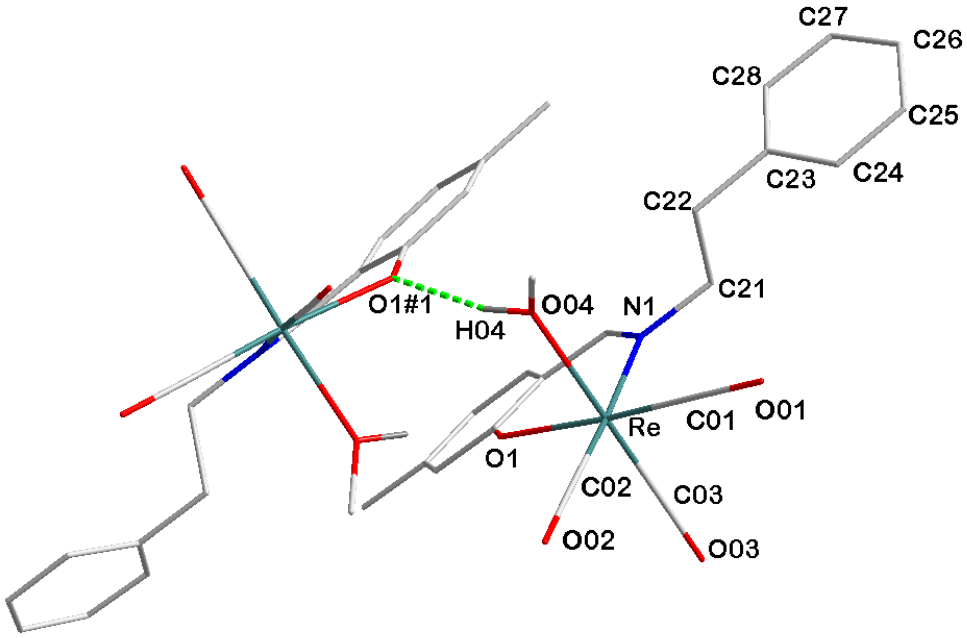

Figure 4.14: **Graphical representation of intermolecular hydrogen bond interaction indicated between O(04)-H(04)…$O(1)^{\#1}$. Hydrogen interaction is illustrated by the green dotted line. Certain hydrogen atoms were omitted for clarity.**

Table 4.7: Hydrogen bonds for *fac*-[Re(5Me-Sal-EtPh)$(CO)_3$(MeOH)] [Å and °].

D-H…A	d(D-H)	d(H…A)	d(D…A)	<(DHA)
O(04)-H(04)…O(1)#1	0.84(7)	1.84(7)	2.634(6)	166(8)

Symmetry transformations used to generate equivalent atoms:
#1 1-x, -y, 1.5 -z

An intermolecular π-π interaction is observed between the six-membered salicylidene rings of adjacent molecules with a centroid-to-centroid distance of 3.8860(11) Å as indicated in Figure 4.15.

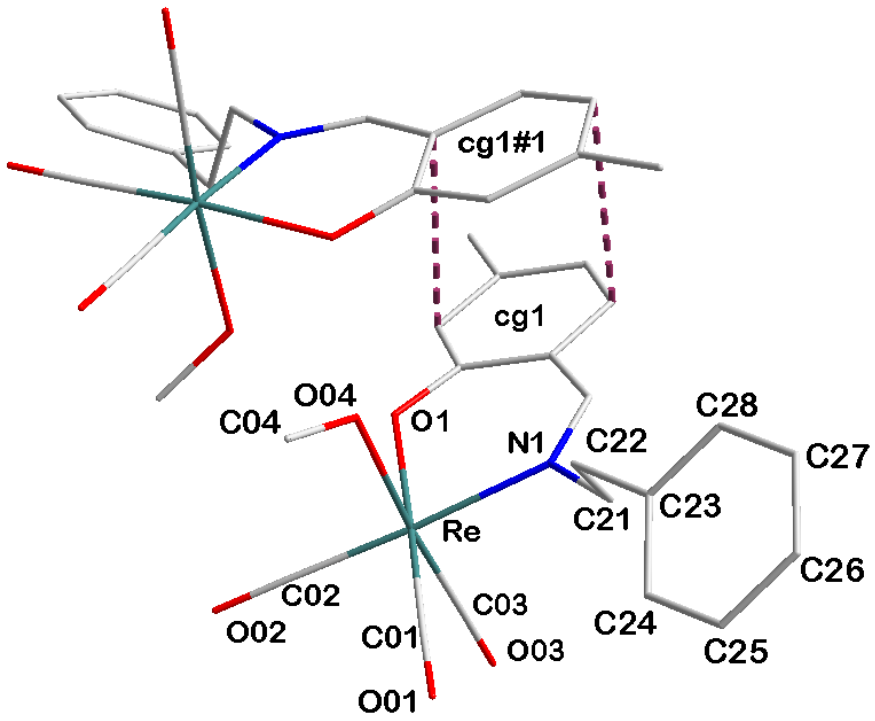

Figure 4.15: **Graphical representation of π-π interaction in *fac*-[Re(5Me-Sal-EtPh)(CO)$_3$(MeOH)] (3). Certain hydrogen atoms were omitted for clarity.**

Table 4.8: **π-π interaction in *fac*-[Re(5Me-Sal-EtPh)(CO)$_3$(MeOH)] (3) (Å).**

Centroid atom	**Centroid atom**	**Distance between centroid atoms** (Å)
Cg1	Cg1#1	3.886(11)

#1 1-x, -y, 1.5 –z; Cg1 centroid atom of C11, C12, C13, C14, C15, C16

The molecule displays C-O…π interaction between C01-O01…Cg1$^{\#1}$ (centroid of the phenyl ring), and is indicated by green dotted lines in Figure 4.16 and Table 4.9.

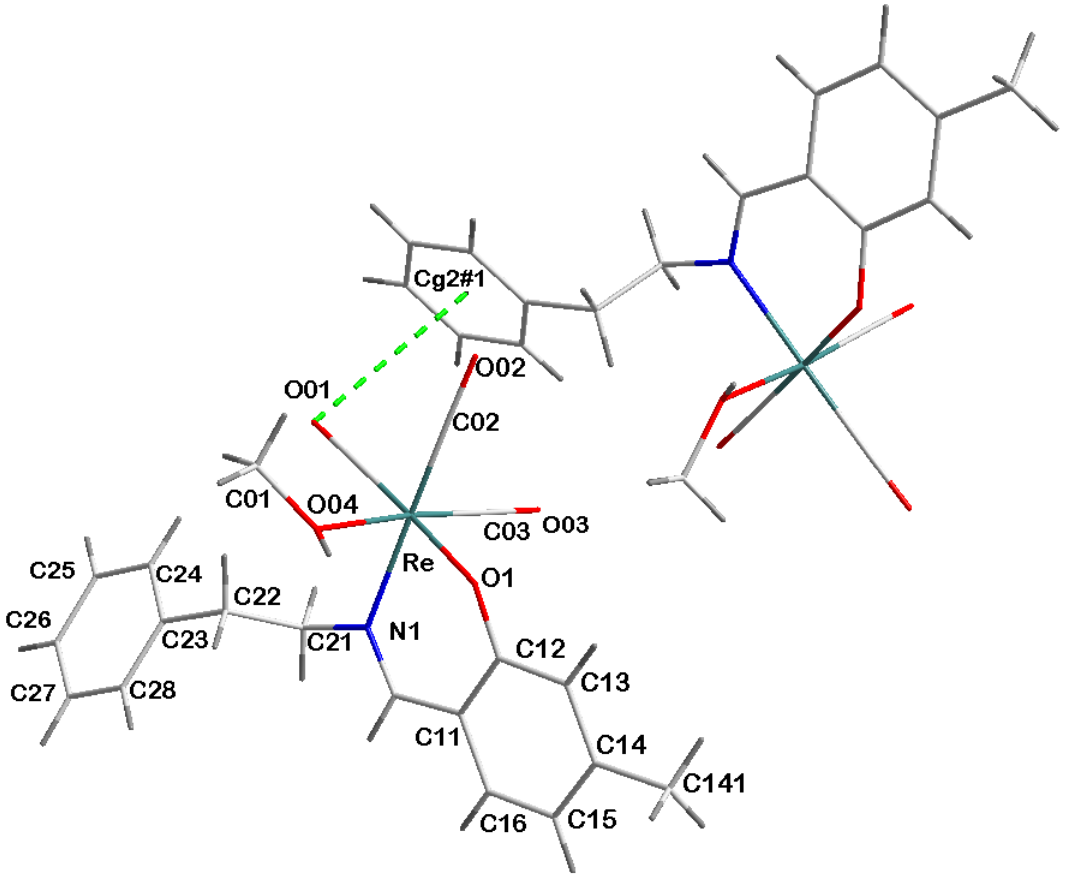

Figure 4.16: **Graphical representation of C-O…π interaction indicated by the green dotted lines. Hydrogen atoms were omitted for clarity.**

Table 4.9: **C-O…π interactions of *fac*-[Re(5Me-Sal-EtPh)(CO)$_3$(MeOH)] [Å and ˚].**

C-O…Cg	Centroid atom (Cg)	d(O…Cg)	d(C-H…Cg)	<(C-O…Cg)
C01-O01	Cg1#1	3.737(6)	4.062(7)	98.2(4)

Symmetry transformations:
#1 x, 1-Y,1/2+z
Cg1 = Centroid atom of C11, C12, C13, C14, C15, C16.

Figure 4.17 illustrates the molecular packing mode of complex **(3)** in the unit cell. The molecules pack in a head-to-tail fashion.

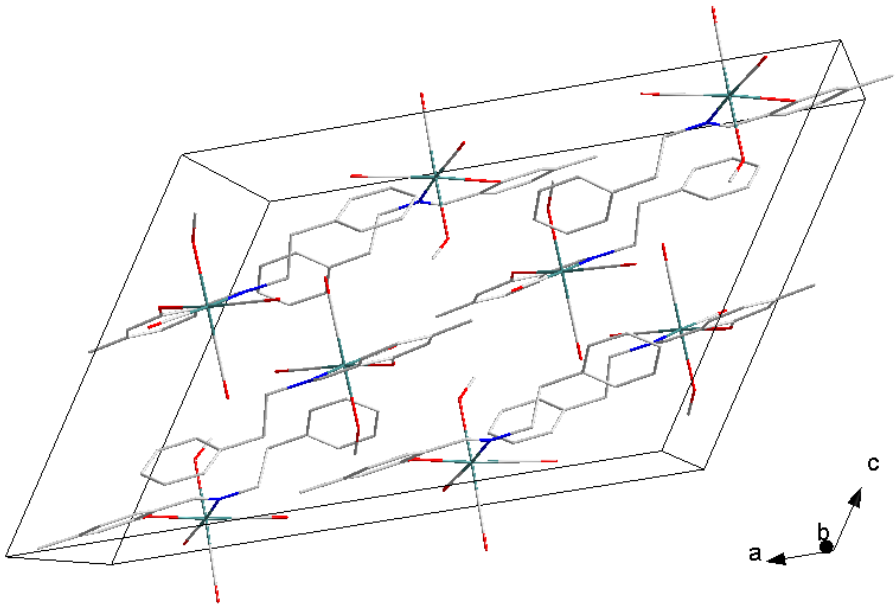

Figure 4.17: **Molecular packing of *fac*-[Re(5Me-Sal-EtPh)$(CO)_3$(MeOH)] (3). Hydrogen atoms were omitted for clarity.**

4.6 Discussion and conclusion

Three Schiff-base bidentate ligands with variation in the electronic and steric parameters, 2-(cyclopentyl)methyl-5-methylphenol, 2-(cyclohexyliminomethyl)-phenol and 5-methyl-2(phenylethyliminimethyl)phenol were coordinated to the *fac*-$[M(CO)_3]^+$(M = Mn, Re) core. The complexes were characterized by X-ray crystallography and a summary of bond distances and angles is given in Table 4.10.

Table 4.10: Comparison of selected bond distances and angles of *fac*-[Mn(5-Me-Sal-CyPent)$(CO)_3]_2$ (1), *fac*-[Re(Sal-CyHex)$(CO)_3]_2$ (2) and *fac*-[Re(5Me-Sal-EtPh)$(CO)_3$(MeOH)] (3)

Complex	*fac*-[Mn(5-Me-Sal-CyPent)$(CO)_3]_2$ (1)	*fac*-[Re(Sal-CyHex)$(CO)_3]_2$ (2)	*fac*-[Re(5Me-Sal-EtPh)$(CO)_3$(MeOH)] (3)
Bond Distance(Å)			
Re/Mn-O1	2.0427(13)	2.176(4)	2.116(3
Re/Mn-N1	2.0625(17)	2.176(4)	2.173(4)
Re/Mn-C01	1.8142(19)	1.913(4)	1.904(6)
Re/Mn-C02	1.8059(18)	1.924(4)	1.922(5)
Re/Mn-C03	1.7957(18)	1.902(4)	1.893(7)
N1-C1	1.281(2)	1.279(5)	1.287(7)
C01-O01	1.145(2)	1.146(4)	1.147(7)
Re/Mn-Re'/Mn'	3.1930(18)	3.5478(4)	-
M-O'/Re-O04	2.0672(13)	2.149(3)	2.189(5
Bond angle (°)			
N1-M-O1	85.42(5)	81.57(13)	84.88(14)
N1-M-C02	176.74(13	172.77(14)	177.02(19)
O1-M-O1'	78.05(6)	73.83(11)	-
O1-Mn-C02	175.12(6)	95.82(13)	
Mn-O1-Mn'	101.95(5)	106.17(11)	-

(') indicates the symmetry generated molecule.

The single crystal X-ray diffraction data as obtained in this study revealed that **(1)** and **(2)** are dinuclear complexes composed of two *fac*-[M(L,L'-Bid)$(CO)_3$] (M = Mn, Re and L,L'-Bid = N,O Sal bidentate ligand) subunits. The coordination around the metal centre in **(1)** and **(2)** exhibits a distorted octahedral geometry, while the bidentate ligand acts as both a chelate and a bridge using the nitrogen donor and the phenolate oxygen atom. The coordination geometry around the rhenium(I) centre in the mononuclear complex **(3)** resembles that of **(1)** and **(2)** with three facially coordinated carbonyl ligands and the chelating O and N atoms of the bidentate ligand. The octahedron in **(3)** is however completed by the coordinated methanol ligand. The inner core of the dinuclear species **(1)** and **(2)** consists of a

four membered planar system composed of the M-O-M'-O' ring, (M = Mn, Re). The intermetallic distances of **(1)** 3.1930(18) Å, is shorter than that of **(2)** 3.4578(4) Å.

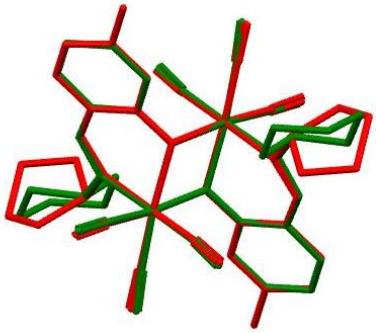

Figure 4.18: An overlay diagram of *fac*-[Mn(5-Me-Sal-CyPent)(CO)$_3$]$_2$ (1) (indicted in red) and the previously reported *fac*-[Mn(Sal-CyHex)(CO)$_3$]$_2$. (indicted in green) (RMS = 0.154 Å).[18] Overlays were drawn through the central core of Mn-Mn-O-O atoms.

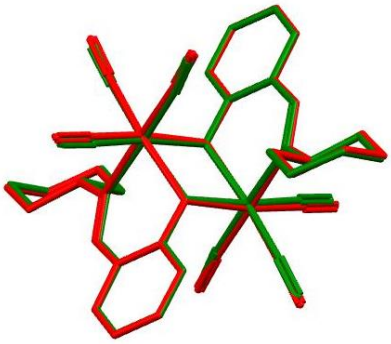

Figure 4.19: An overlay diagram of *fac*-[Mn(5-Me-Sal-CyPent)(CO)$_3$]$_2$ (1) (indicated in green) and *fac*-[Re(Sal-CyHex)(CO)$_3$]$_2$ (2) (indicated in red) (RMS = 0.107 Å). Overlays were drawn through the central core of M-M-O1-O1 atoms (M= Mn/Re).

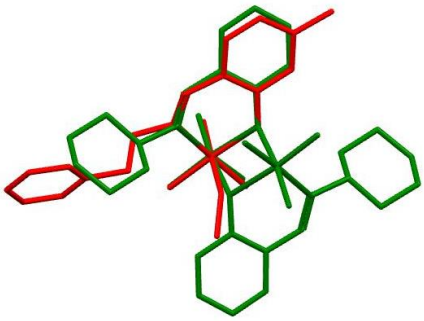

Figure 4.20: An overlay diagram of *fac*-[Re(Sal-CyHex)(CO)$_3$]$_2$ (2) (indicated in green) and *fac*-[Re(5Me-Sal-EtPh)(CO)$_3$(MeOH)] (3) (indicated in red) (RMS = 0.112 Å). Overlays were drawn through the central core of Re-Re-O1-O1 atoms.

The differences in the bond lengths obtained in **(1)** compared to **(2)** is possibly due to the larger atomic radius of 0.67 Å for rhenium compared to 0.60 Å for manganese in an octahedral geometry.[39] The differences in atomic radius are also apparent in the distortion at the bridging oxygen moiety indicated by the M-O1-M bond angle of 3-5˚ larger in **(1)** compared to **(2)**. The two metal centres in both complex **(1)** and **(2)** linked by two oxygen atom have comparable bond distances of M-O1 and M-O1' 2.0427(13), 2.0672(13) Å and 2.176(4), 2.197(3) Å for **(1)** and **(2)** respectively (where M = Mn, Re). The dinuclear complex **(1)** shows no intrinsic structural differences to the previously reported *fac*-[Mn(Sal-CyHex)$(CO)_3]_2$ with a similar inner core geometry defined by the Mn-O1-Mn'-O1' plane.[19] The inner core retains its rigidity in spite of the significant steric differences on the periphery of the molecules induced by the cyclopentyl substituent as well as the incorporation of a methyl group on the salicylidene backbone in **(1)** compared to the cyclohexyl substituent in the previously reported complex.[18] The intra-metallic Mn-Mn' distances in (**1**), 3.1992(9) Å is in good agreement with the 3.1930(18) Å for the reported complex bearing the cyclohexyl substituent on the imine nitrogen.

4.7 Conclusion

The solid state structures of three new Schiff-base metal complexes *fac*-[Mn(5-Me-Sal-CyPent)$(CO)_3]_2$ **(1)**, *fac*-[Re(Sal-CyHex)$(CO)_3]_2$ **(2)** and *fac*-[Re(5-Me-Sal-EtPh)$(CO)_3$(MeOH)] **(3)** were presented in this chapter. The investigation demonstrated the flexibility of the bidentate ligands with respect to their coordination mode and that the ligands are able to act as both chelates and a bridge between two metal centres. This behavior is particularly interesting in the context of designing theranostic radiopharmaceuticals which are essentially radiopharmaceutical agents which can integrate both therapeutic and imaging capabilities within a single molecule.

As an expansion and continuation of these investigations, the coordination of Schiff-base ligands to the rhenium congener, technetium-99, will be given in the following chapter.

[39] R.D. Shannon, *Acta Crystallogr*. A. 32 (1976) 751-767.

5 Crystallographic Study of *fac*-Technetium Tricarbonyl Complexes

5.1 Introduction

Chelators that are capable of providing sufficient *in vivo* stability to the *fac*-$[M(CO)_3]^+$ core are essential for the success in designing effective agents for application as single photon computed tomography (SPECT) imaging modality.[1,2,3] A variety of mono-, bi- and tridentate ligands have been investigated as potential chelators to form complexes of sufficient stability under physiological conditions. In this study, the investigation is aimed at the coordination behavior of bidentate Schiff-base ligands displaying varying steric and electronic parameters, to the *fac*-$[^{99}Tc(CO)_3]^+$ core. Schiff-base ligands are well-known ligand systems used in a broad range of applications due to their ease of preparation under mild conditions and their structural flexibility.[4,5,6]The structural flexibility of the ligands in this study particularly has the potential to incorporate a biomolecule or functional groups that are suitable for bioconjugation that could induce biological selectivity. This chapter presents the solid-state structures obtained from the single crystal X-ray diffraction investigations. The *fac*-^{99}Tc(I) tricarbonyl complexes described herein are all dinuclear in nature and are illustrated in Figure 5.1.

[1] J.L. Hickey, P.S. Donnelly, *Coord. Chem. Rev.* 256 (2012) 2367-2380.
[2] M.D. Bartholoma, A.S. Louie, J.F. Valliant, J. Zubieta, *Chem. Rev.* 110 (2010) 2903-2920.
[3] S. Banerjee, M.R.A. Pillai, N. Ramamoorthy, *Semin. Nucl. Med*. 31 (2001) 260-277.
[4] D.N. Dhar, C.L. Taploo, *J. Sci. Ind. Res*. 41 (1982) 501-506.
[5] W. Rehman, M.K. Baloch, B. Muhammad, A. Badshah, K.M. Khan, *Chin. Sci. Bull.* 49 (2004) 119-22.
[6] A.M. Abu-Dief, I.M.A. Mohamed, *Beni*-Seuf. *Univ. J. Apll. Sc*. 4 (2015) 119-133.

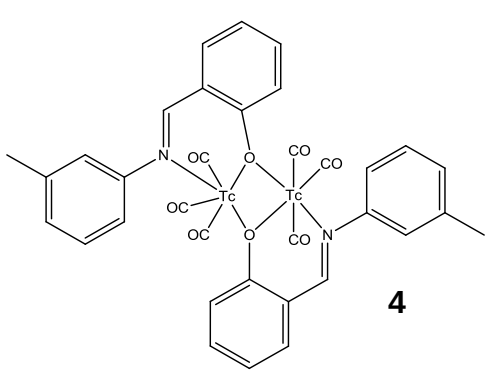

4

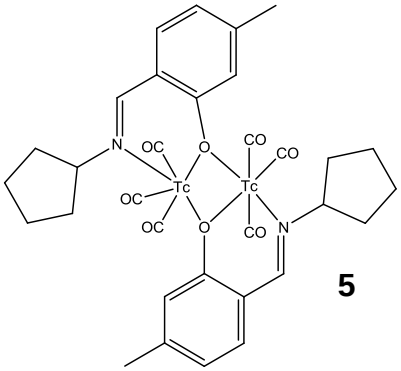

5

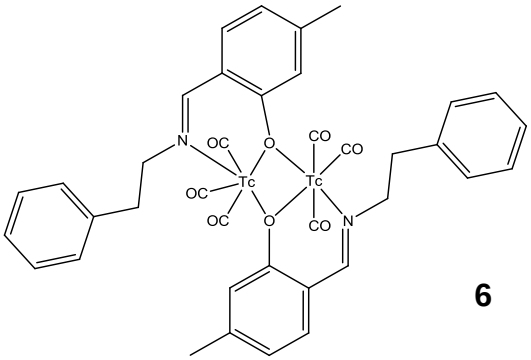

6

Figure 5.1: The two dimensional illustrations of *fac*-[^{99}Tc(Sal-*m*Tol)(CO)$_3$]$_2$ (4), *fac*-[^{99}Tc(5-Me-Sal-CyPent)(CO)$_3$]$_2$ (5) and *fac*-[^{99}Tc(5-Me-Sal-EtPh)(CO)$_3$] (6). Where Sal-*m*TolH = 2-(*m*-Tolyliminomethyl)phenol, 5-Me-SalH-CyPentH = 2-(cyclopentyl)methyl-5-methylphenol and 5-Me-Sal-EtPhH = and 5-methyl-2-(phenylethyliminimethyl)-phenol.

5.2 Experimental

Diffraction data of *fac*-[^{99}Tc(Sal-*m*Tol)$(CO)_3]_2$ **(4)** , *fac*-[^{99}Tc(5-Me-Sal-CyPent)$(CO)_3]_2$ **(5)** and *fac*-[^{99}Tc-(5-Me-Sal-EtPh)$(CO)_3]_2$ **(6)**, were collected at 100(2) K on an Oxford Diffraction Xcalibur 3 Crysalis CCD system[7] using MoKα radiation (λ = 0.71073 Å).[8] The structures were solved by direct methods and refined on F^2 using anisotropic displacement parameters for all non-hydrogen atoms. SHELXL-97[9,10] and WinGX[11] were used for structure solutions and refinements respectively, while the molecular graphics were prepared with DIAMOND.[12] All non-hydrogen atoms were refined with anisotropic displacement, while the methyl, methane and aromatic H atoms were placed in geometrically idealised positions and constrained to ride of their parent atoms, with (C-H distances of 0.98 – 0.95 Å and U_{iso}(H) = 1.2U_{eq}(C) and U_{iso}(H) = 1.5U_{eq}(C)) respectively. The N-bound hydrogen atom was located from the electron density map and refined without any constraints

Table 5.1 gives a summary of the general crystal data and refinement parameters for all three technetium(I) tricarbonyl Schiff-base complexes. The supplementary data for the atomic coordinates, bond distances and bond angles and anisotropic displacement parameters are given in the Appendix for each individual dataset.

[7] Crysalis CCD, Oxford Diffraction Ltd, Abingdon, Oxfordshire, U.K, 2005.
[8] Crysalis RED. Oxford Diffraction Ltd, Abingdon, Oxfordshire, U.K, 2005.
[9] G.M. Sheldrick, Acta Crystallogr, A64 (2008) 112-122.
[10] G.M. Sheldrick, SHELXL97, University of Göttingen, Göttingen, Germany, 1997.
[11] L.J. Farrugia, J. Appl. Crystallogr. 32 (1999) 837-838.
[12] K. Brandenburg, H. Putz, DIAMOND, release 3.1b, Crystal Impact GbR, Bonn, Germany, 2005.

Table 5.1: X-ray crystallographic data and refinement parameters for *fac*-[^{99}Tc(Sal-*m*Tol)(CO)$_3$]$_2$ (4), *fac*-[^{99}Tc(5-Me-Sal-CyPent)(CO)$_3$]$_2$ (5) and *fac*-[^{99}Tc(5-Me-Sal-EtPh)(CO)$_3$]$_2$ (6)

	fac-[^{99}Tc(Sal-*m*Tol)(CO)$_3$]$_2$ **(4)**	*fac*-[Tc(5-Me-Sal-CyPent)(CO)$_3$]$_2$ **(5)**	*fac*-[Tc-(5-Me-Sal-EtPh)(CO)$_3$] $_2$ **(6)**
Empirical formula	$C_{34}H_{24}N_2O_8Tc_2$	$C_{32}H_{30}N_2O_8Tc_2$	$C_{38}H_{32}N_2O_8Tc_2$
Formula weight	784.55	766.58	840.65
Temperature/(K)	183(2)	183(2)	183(2) K
Wavelength Å	0.71073	0.71073	0.71073
Crystal system	Triclinic	Triclinic	Monoclinic
Space group	$P\bar{1}$	$P\bar{1}$	$P2_1/n$
a/Å	7.7230(3)	8.5234(6)	7.5595(5)
b/Å	9.6213(5)	9.4839(4)	19.5030(9)
c/Å	11.4744(6)	10.3293(7)	12.0691(8)
α/°	103.910(4)	96.671(5)	90
β/°	102.384(4)	113.343(7)	97.395(7)
γ/°	99.338(4)	95.370(5)	90
Volume/Å^3	787.52(7)	752.46(9)	1764.58(19)
Z	1	1	2
Density (g.cm^{-3})	1.654	1.692	1.582
μ(mm^{-1})	0.933	0.974	0.838
F(000)	392	386	848
Crystal Colour	Yellow	Yellow	Yellow
Crystal Morphology	Plate	Plate	Plate
Theta range (°)	2.772 to 26.370	2.634 to 26.371	2.694 to 27.997
Completeness (%) to θ	99.9, 25.242	99.9, 25.242	99.9, 25.242
Index ranges	h = -8 to 9 k = -10 to 12 l= -13 to 14	h = -10 to 10 k = -11 to 7 l = -12 to 12	h = -9 to 9 k = -25 to 25 l = -15 to 15
Reflections collected	6179	6758	20701
Independent Reflections	3217	3074	4245
R_{Int}	0.0451	0.0391	0.0638
Data/Restraints/ parameters	3217 / 0 / 209	3074 / 18 / 231	4245 / 0 / 226
Goodness-of-fit on F^2	1.042	1.064	1.064
Final R indexes [I>=2σ (I)]	R1 = 0.0401 wR2 = 0.0727	R1 = 0.0321 wR2 = 0.0758	R1 = 0.0421 wR2 = 0.0712
Final R indexes [all data]	R1 = 0.0508 wR2 = 0.0779	R1 = 0.0370 wR2 = 0.0781	R1 = 0.0713 wR2 = 0.0833
ρ max, ρ min (e.Å^{-3})	0.777, -0.853	0.654, -0.515	0.720, -0.528

Where 2-(*m*-Tolyliminomethyl)phenol = SalH-*m*TolH, 2-(cyclopentyl)methyl-5-methylphenol = 5-Me-SalH-CyPentH, 5-methyl-2-(phenylethyliminimethyl)-phenol = 5-Me-Sal-EtPhH

5.3 Crystal structure of *fac*-[^{99}Tc(Sal-*m*Tol)(CO)$_3$]$_2$

The dinuclear complex *fac*-[^{99}Tc(Sal-*m*Tol)(CO)$_3$]$_2$ **(4)**, (Sal-*m*Tol = 2-[(*m*-tolyliminomethyl)]phenolato) crystallizes in the triclinic crystal system in the $P\bar{1}$ space group with one formula unit per unit cell (Z = 1). The asymmetric unit of **(4)** consists of one half of the molecule. A structural representation of **(4)** along with the numbering scheme is illustrated by Figure 5.2, while selected bond distances and angles are listed in Table 5.2.

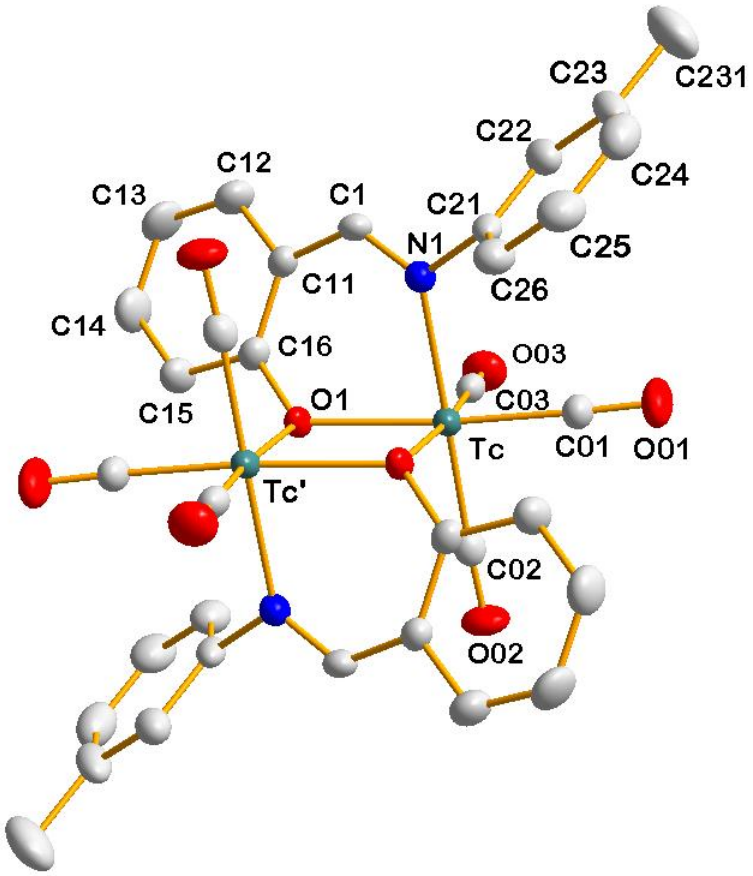

Figure 5.2: **Structural representation of *fac*-[^{99}Tc(Sal-*m*Tol)(CO)$_3$] with atom numbering scheme and displacement ellipsoids drawn at 50% probability level. The structure represents the full molecule generated by symmetry, indicated where appropriate by (‘). For the aromatic rings, the first digit represents the ring number, while the second digit refers to the specific C-atom in the ring.**

Table 5.2: Selected bond lengths (Å) and angles (˚) of *fac*-[^{99}Tc(Sal-*m*Tol)(CO)$_3$]$_2$ (4).

Atoms	Bond Lengths (Å)	Atoms	Bond Angles (°)
Tc-N1	2.188(3)	N1-Tc-O1	81.08(9)
Tc-O1	2.157(2)	N1-Tc-C02	179.31(13)
Tc'-O1'	2.157(2)	O1-Tc-C01	172.89(12)
Tc-C01	1.899(4)	Tc-O1-Tc'	103.84(9)
Tc-C02	1.922(4)	O1-Tc-C02	98.28(12)
Tc-C03	1.889(4)	O1-Tc-O1'	76.16(9)
Tc-Tc'	3.421(4)	C01-Tc-C02	87.49(14)
Tc-O1'	2.189(2)	C01-Tc-C03	87.72(15)
N1-C1	1.282(4)	C02-Tc-C03	87.51(13)
C01-O01	1.142(4)	O01-C01-Tc	177.5(3)
C02-O02	1.148(4)	O02-C02-Tc	177.6(3)
C03-O03	1.156(4)	O03-C03-Tc	178.1(3)
C1-C11	1.404(5)	C1-N1-C21	118.4(2)
N1-C21	1.148(4)		
O1-C16	1.360(4)		

(') indicates the symmetry generated part.

The basic coordination geometry around the technetium metal centres in the dinuclear complex **(4)** is a distorted octahedral geometry comprising of three carbonyl ligands that are facially coordinated to the metal centres and the oxygen and nitrogen atoms of the 2-[(*m*-tolyliminomethyl)]phenolato) ligand. The octahedral coordination is completed by the bridging ligands through the phenolate oxygen atoms.

The octahedral geometry around the metal centres is distorted as indicated by the N1-Tc-O1 bite angle of 81.08(9)˚ and O1-Tc-C01 with an angle of 172.89(12)˚. The Tc-N1 and Tc-O1 bond distances were determined as 2.188(3) Å and 2.157(2) Å respectively and are in good agreement with the bond distances reported for technetium complex containing N,O donor atoms with a range of 2.177-2.154 Å and 2.132-2.216 Å for Tc-N and Tc-O respectively.[13,14,15] The complexes exhibits an inner four-membered planar core defined by the atoms Tc-O1-Tc'-O1' with an intermetallic separation distance of 3.421(4) Å. The technetium-carbonyl bond distance of the carbonyl ligand trans to the nitrogen atom, Tc-C02 = 1.922(4) Å, is longer than the two Tc-CO bond distances for the carbonyl ligands that are trans to the bridging phenolato oxygen atoms, with bond distances of 1.899(4) Å and 1.889(4) Å for Tc-C01 and Tc-C03, respectively.

[13] T. Takayama, A. Harano, T. Sekine, H. Kudo, J. *Nucl. Radiochem. Sci*. 6 (2005) 149-151
[14] H.W. Schmalle, R. Alberto, *Acta Cryst*. E64 (2008) m1213-m1214.
[15] P. Kurz, B, Probst, B. Spingler, R. Alberto, *Eur. J. Inorg. Chem.* (2006) 2966-2974.

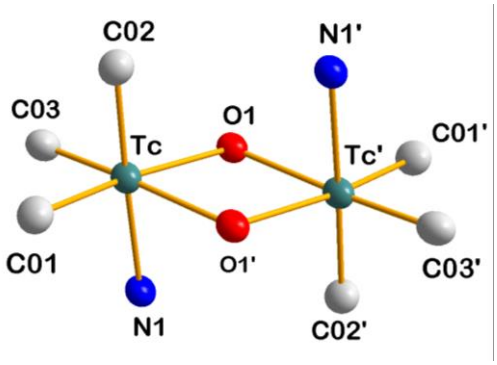

Figure 5.3: **View of the coordination octahedron around the technetium atoms. Atoms with an apostrophe were generated by symmetry.**

The plane formed through the salicylidene backbone (Plane 1: C11, C12, C13, C14, C15, C16) is twisted relative to the equatorial plane (Plane 2: Tc, N1, O1, C01, C02) with a dihedral angle of 27.71(2)˚, as illustrated in Figure 5.4.

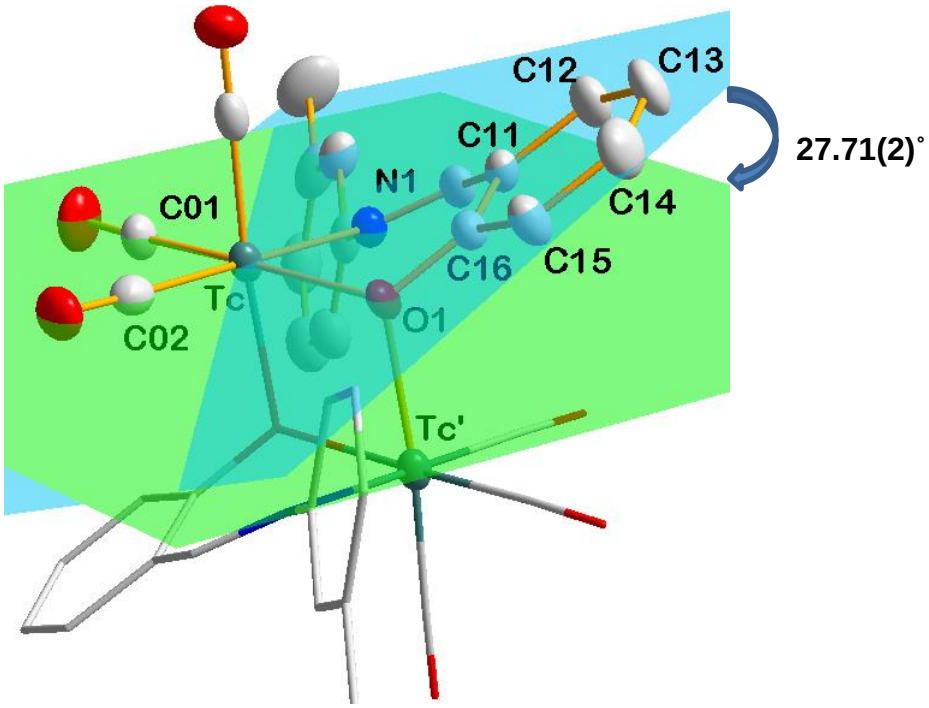

Figure 5.4: **Graphical representation of the bending aromatic backbone (Plane 1 is indicated in blue and Plane 2 indicated in green). Hydrogen atoms were omitted for clarity**.

Furthermore, the aromatic *m*Tol ring substituent on the imine nitrogen atom points away from the inner coordination geometry and is located nearly perpendicular with respect to plane (Plane 2: Tc, N1, O1, C01, C02) with a dihedral angle of 82.04˚(2), see Figure 5.5.

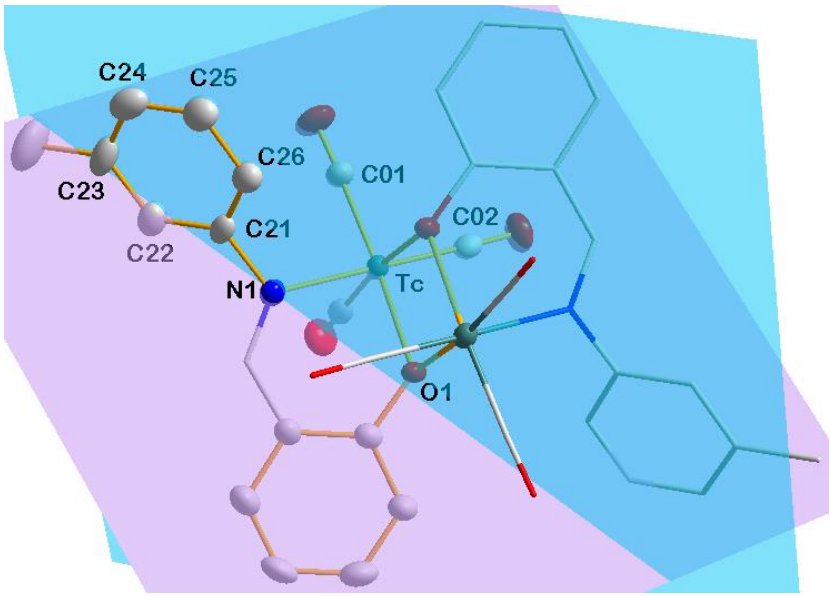

Figure 5.5: **Graphical representation of the bending *m*Tol aromatic ring (Plane 1 is indicated in blue and Plane 2 indicated in purple). Hydrogen atoms were omitted for clarity**.

The conformation in **(4)** leads to the formation of intra- and intermolecular hydrogen bonding as illustrated in Figure 5.6. The *inter*molecular hydrogen bonding is between the atom C13-H13 on the *m*Tol substituent and the $O01^{\#2}$ atom of the neighboring molecule. The *intra*molecular hydrogen bonding, on the other hand, is found between the *m*Tol substituent C26-H26 and the $O1^{\#1}$ atom of the phenolato oxygen atom. The interaction is indicated by the green dotted line in Figure 5.6 and the related data is given in Table 5.3.

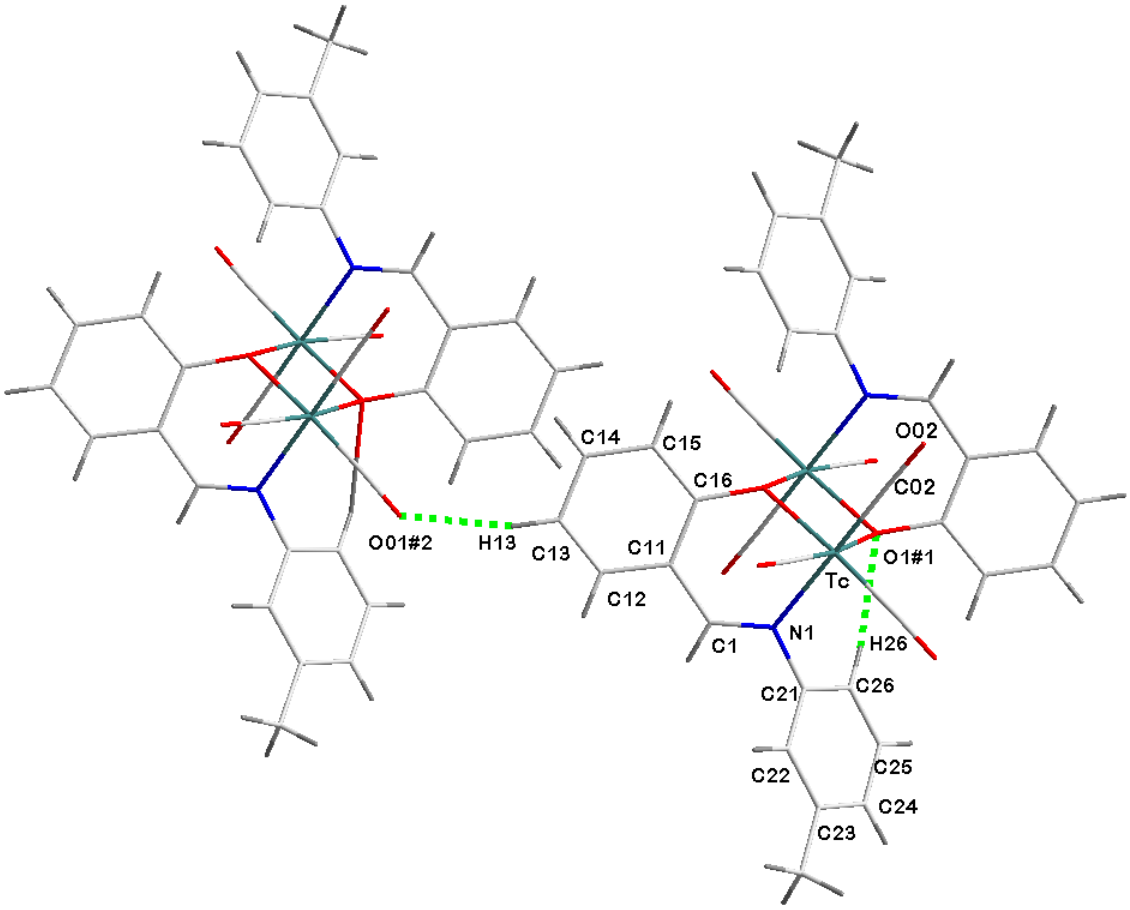

Figure 5.6: **Graphical representation of hydrogen bonding interaction between C26-H26…$O1^{\#1}$ and C13-H13…$O01^{\#2}$. Some atom labels were omitted for clarity.**

Table 5.3: **Hydrogen bonds of *fac*-[^{99}Tc(Sal-*m*Tol)$(CO)_3]_2$ (4) [Å and °].**

D-H…A	d(D-H)	d(H…A)	d(D…A)	<(DHA)
C(26)-H(26)…$O(1)^{\#1}$	0.95	2.52	3.236(5)	132(6)
C(13)-H(13)…$O(01)^{\#2}$	0.95	2.58	3.434(5)	149(5)

Symmetry transformations used to generate equivalent atoms
#1 1-x, 1-y,1-z; #2 x,y,1+z;

The complex is further stabilised by intra- and intermolecular C-O…π interaction as indicated by the green dotted lines in Figure 5.7. The related data is given in Table 5.4.

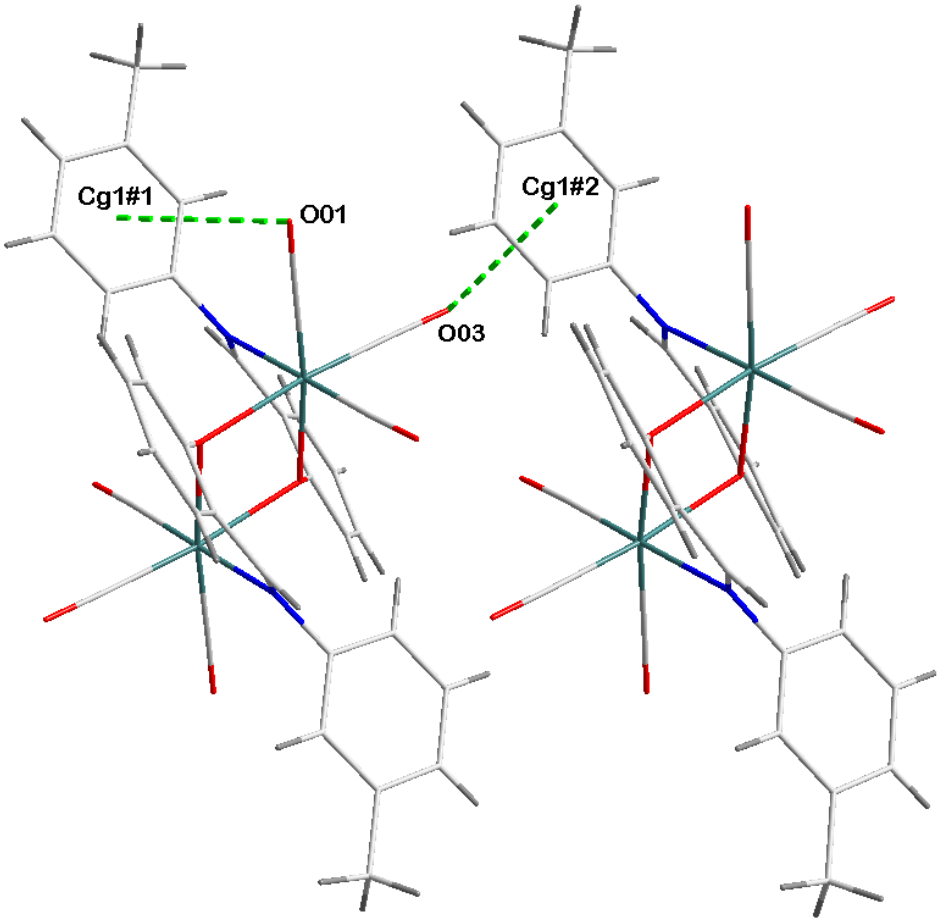

Figure 5.7: **Graphical representation of the C-O…π interaction indicated by the green dotted line. Some atom labels were omitted for clarity.**

Table 5.4: **C-O…π interactions of *fac*-[^{99}Tc(Sal-*m*Tol)(CO)$_3$]$_2$ (4) [Å and ˚].**

C-O…Cg	Centroid atom Cg	d(O…Cg) Å	d(C…Cg) Å	(C-O…Cg) (˚)
C01-O01	Cg1$^{\#1}$	3.878(4)	3.780(4)	76.6(3)
C03-O03	Cg1$^{\#2}$	3.510(4)	4.007(4)	107.2(3)

Symmetry transformation:
#1 x, y, z #2 x+1, y, z
Cg2 = centroid atom of C21, C22, C23, C24, C25, C26

The molecular packing of complex **(4)** is shown in Figure 5.8. The *m*Tol substituents are nicely arranged and well-defined in a “head-to-head” fashion.

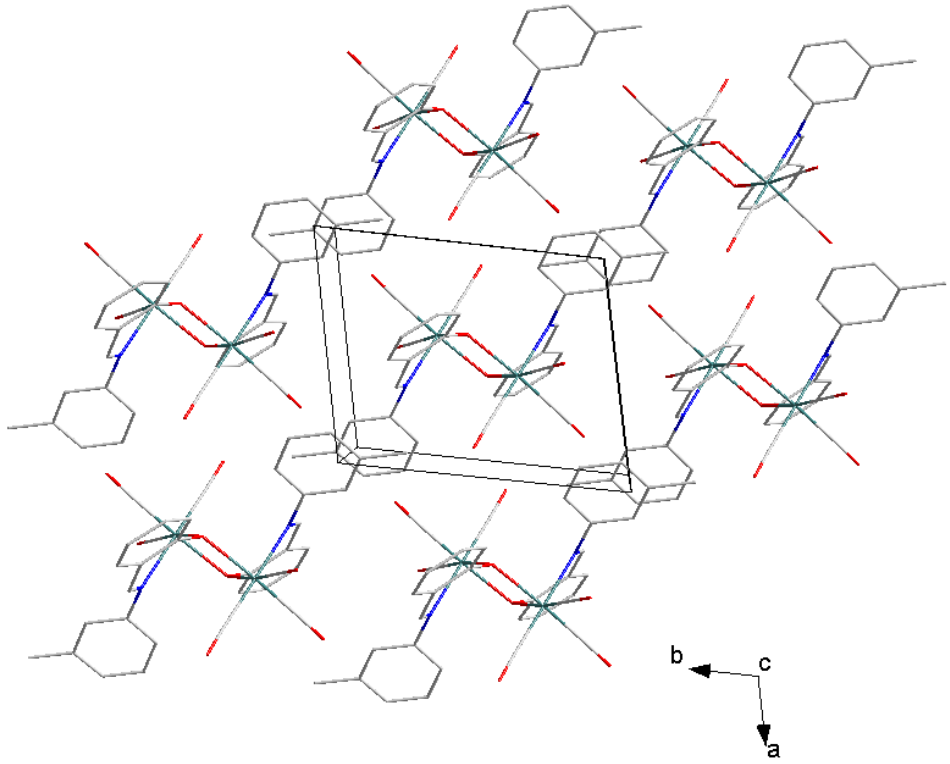

Figure 5.8: Molecular packing in *fac*-[^{99}Tc(Sal-*m*Tol)(CO)$_3$]$_2$ (4); viewed along the *c*-axis.

5.4 Crystal structure of *fac*-[^{99}Tc(5-Me-Sal-CyPent)(CO)$_3$]$_2$

The molecular structure of *fac*-[^{99}Tc(5-Me-Sal-CyPent)(CO)$_3$)]$_2$ **(5),** (5Me-Sal-CyPent = 2-(cyclopentyl)methyl-5-methylphenolate is illustrated in Figure 5.9. The molecule crystallizes in the triclinic crystal system in the $P\bar{1}$ space group with one half of the molecule present in the asymmetric unit. Relevant bond distances and angles are given in Table 5.5.

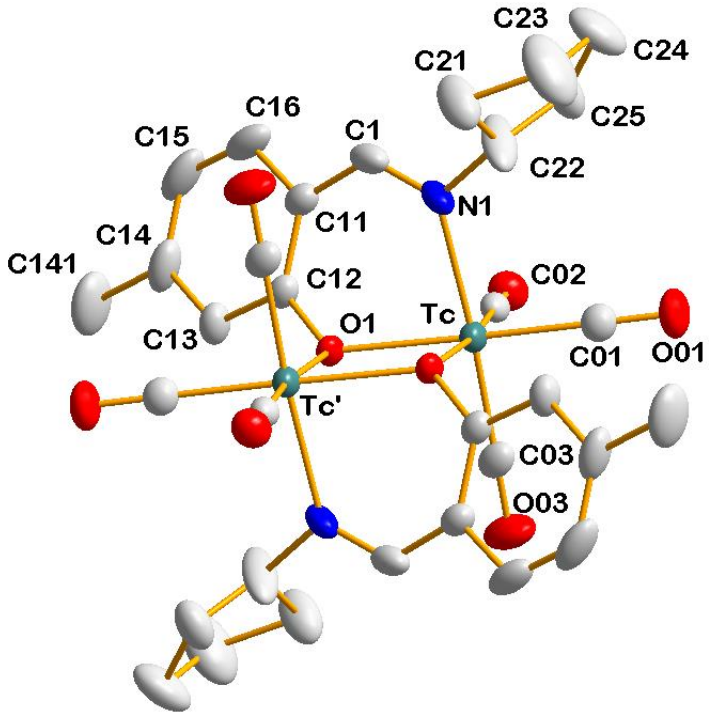

Figure 5.9: **Structural representation of *fac*-[^{99}Tc(5-Me-Sal-CyPent)(CO)$_3$]$_2$ (5), with atom numbering scheme and displacement ellipsoids drawn at 50%. The structure represents the full molecule generated by symmetry, indicated where appropriate by (‘). For the aromatic rings, the first digit represents the ring number, while the second digit refers to the specific C-atom in the ring.**

Table 5.5: Selected bond distances and angles of *fac*-[^{99}Tc(5-Me-Sal-CyPent)(CO)$_3$]$_2$ (5) [Å and °]

Atoms	Bond Lengths (Å)	Atoms	Bond Angles (°)
Tc-N1	2.195(3)	N1-Tc-O1	82.36(9)
Tc-O1	2.149(2)	N1-Tc-C02	91.68(12)
Tc'-O1'	2.149(2)	O1-Tc-C01	175.59(11)
Tc-C01	1.903(3)	Tc-O1-Tc'	104.09(8)
Tc-C02	1.894(3)	O1-Tc-C02	96.71(11)
Tc-C03	1.918(3)	O1-Tc-O1'	75.91(8)
Tc-Tc'	3.424(4)	C01-Tc-C02	87.65(13)
Tc-O1'	2.192(2)	C01-Tc-C03	88.15(14)
N1-C1	1.286(5)	C02-Tc-C03	87.65(13)
C01-O01	1.146(4)	O01-C01-Tc	179.1(3)
C02-O02	1.142(4)	O02-C02-Tc	178.9(3)
C03-O03	1.141(4)	O03-C03-Tc	176.9(3)
C1-C11	1.446(5)	C1-N1-C21	117.4(3)
N1-C21	1.480(5)		
O1-C12	1.356(4)		

(')Refers to the symmetry generated part.

Complex **(5)** adopts a six-coordinate distorted octahedral geometry around the technetium centres with three carbonyl ligands facially coordinated to each metal centre and the two 2-(cyclopentyl)methyl-5-methylphenolato ligands bridging via the oxygen atoms. The octahedral geometry around the technetium metal centre is distorted as indicated by the N1-Tc-O1 bite angle of 82.36(9)° and N1-Tc-C02 angle of 91.68(12). The Tc-N1 and Tc-O1 bond distances were determined as 2.195(3) Å and 2.149(2) Å respectively and are in good agreement with the average bond distances of the reported technetium complexes bearing N,O bidentate ligands with bond distances spanning around 2.177 - 2.154 Å for Tc-N and 2.132 - 2.216 Å for Tc-O.[13,14,15] The central unit forms a four-membered coplanar system defined by the Tc-O1-Tc'-O1 atoms. The two technetium centres are separated by an intermetallic distance of 3.424(4) Å.

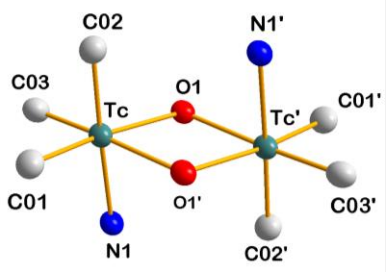

Figure 5.10: View of the coordination octahedron around the technetium atoms. The apostrophe indicates the symmetry generated subunit.

The plane defined by the salicylidene aromatic backbone (Plane 1: C11, C12, C13, C14, C15, C16) is bending relative to the technetium equatorial plane (Plane 2: Tc, N1, O1, C01, C02) with a dihedral angle of 41.75(2)˚ as indicated by Figure 5.11**(a)**. The cyclopentyl ring (plane 2: C21, C22, C23, C24, C25) on the imine nitrogen is rotated almost perpendicular to the equatorial plane defined by (Plane 2: Tc, N1, O1, C01, C02) with a dihedral angle of 64.36(1)˚. The ring points away from the inner coordination geometry as illustrated in Figure 5.11**(b)**.

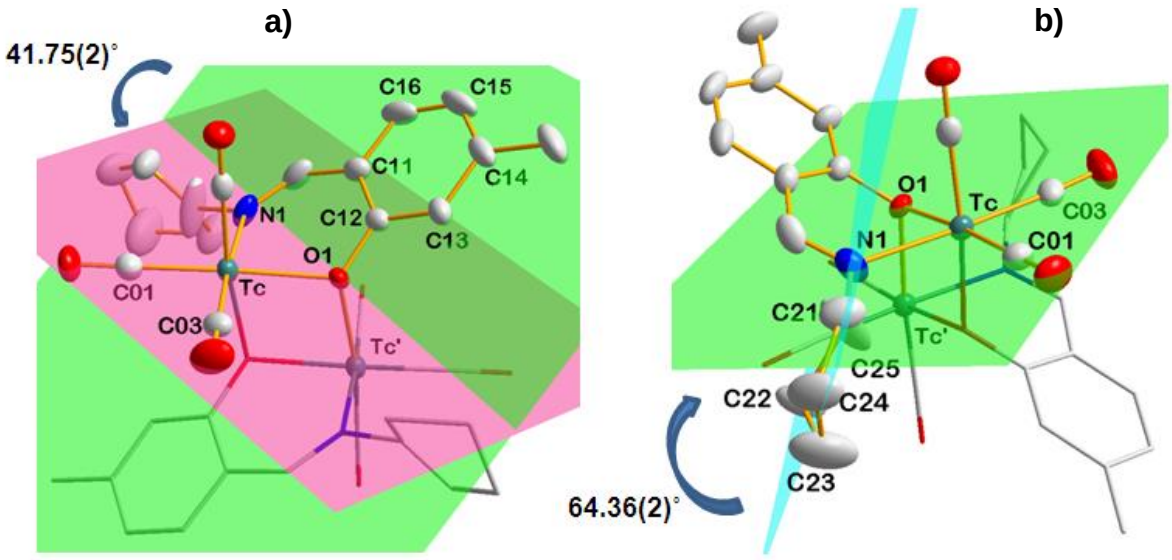

Figure 5.11: **Graphical representation of the bending salicylidene backbone (a) (Plane 1 is indicated in purple and plane 2 indicated in green) and (b) And the bending aromatic backbone (Plane 1 is indicated in green and plane 2 indicated in blue). Hydrogen atoms were omitted for clarity.**

An intermolecular C-O…π interaction is observed between the atoms C03-O03 and the salicylidene ring Cg1[#1]. The interaction is indicated by the green dotted line in Figure 5.12.

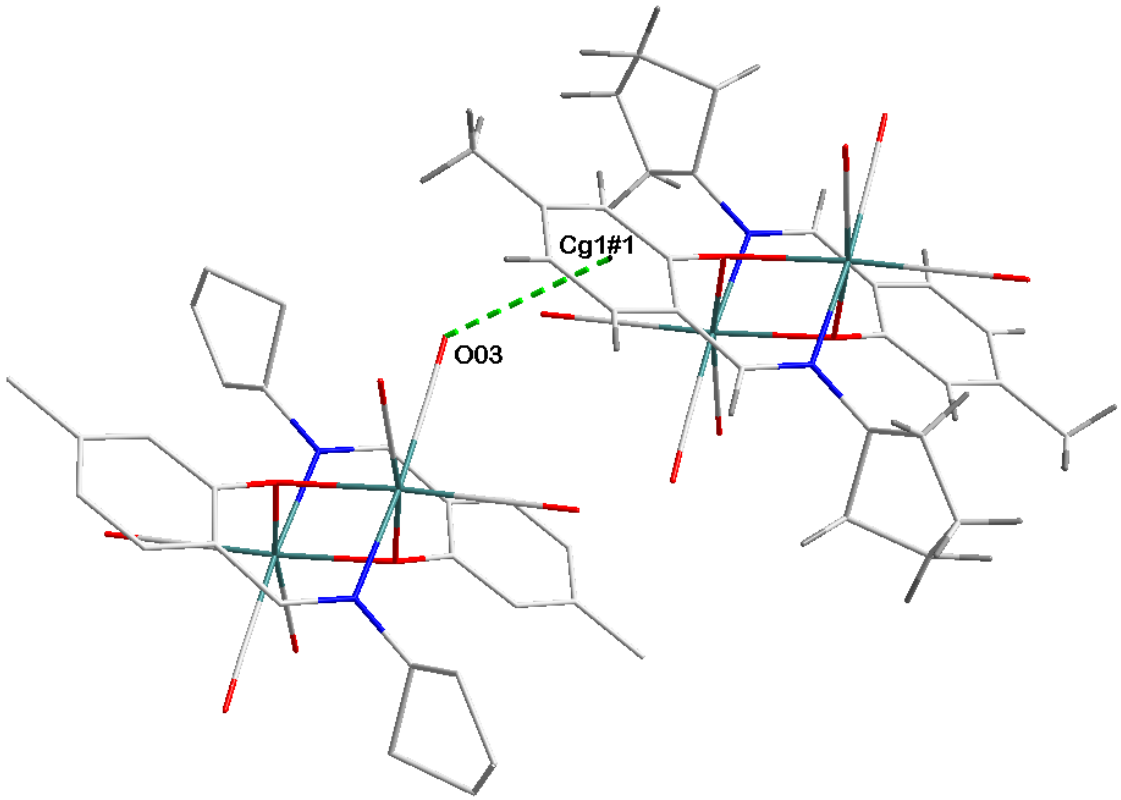

Figure 5.12: **Graphical Representation of the C-O…π interaction indicated by the green dotted line. Some atom labels were omitted for clarity.**

Table 5.6: **C-O…π interactions of *fac*-[^{99}Tc(5-Me-Sal-CyPent)(CO)$_3$)]$_2$ (5) [Å and °].**

C-O…Cg	Centroid atom	d(O…Cg) Å	d(O…Cg) Å	(C-O…Cg) (°)
C03-O03	Cg1[#1]	3.509	3.954(3)	104.6(4)

#1 -1+x,y,z

The molecular packing in complex **(5)** is illustrated in Figure 5.13. The molecules pack in a “head-to-head” fashion with the carbonyl ligands on adjacent molecules pointing towards each other.

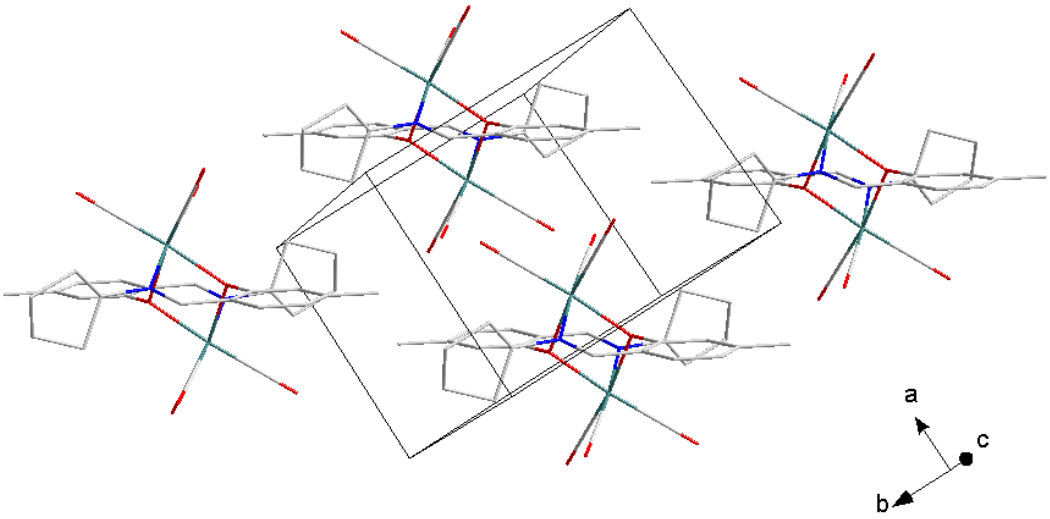

Figure 5.13: **Molecular packing of *fac*-[^{99}Tc(5-Me-Sal-CyPent)(CO)$_3$)]$_2$ (5).**

5.5 Crystal structure of *fac*-[^{99}Tc(5-Me-Sal-EtPh)(CO)$_3$]$_2$

The molecular structure of *fac*-[^{99}Tc(5-Me-Sal-EtPh)(CO)$_3$]$_2$ **(6)**, (5-Me-Sal-EtPh = (5-methyl-2-(phenylethyliminimethyl)phenolate) crystallizes in the monoclinic crystal system in the $P2_1/n$ space group with one half of the molecule present in the asymmetric unit. The molecular structure of **(6)** is illustrated by Figure 5.14 along with the atom numbering scheme. Relevant bond distances and angles are listed in Table 5.7.

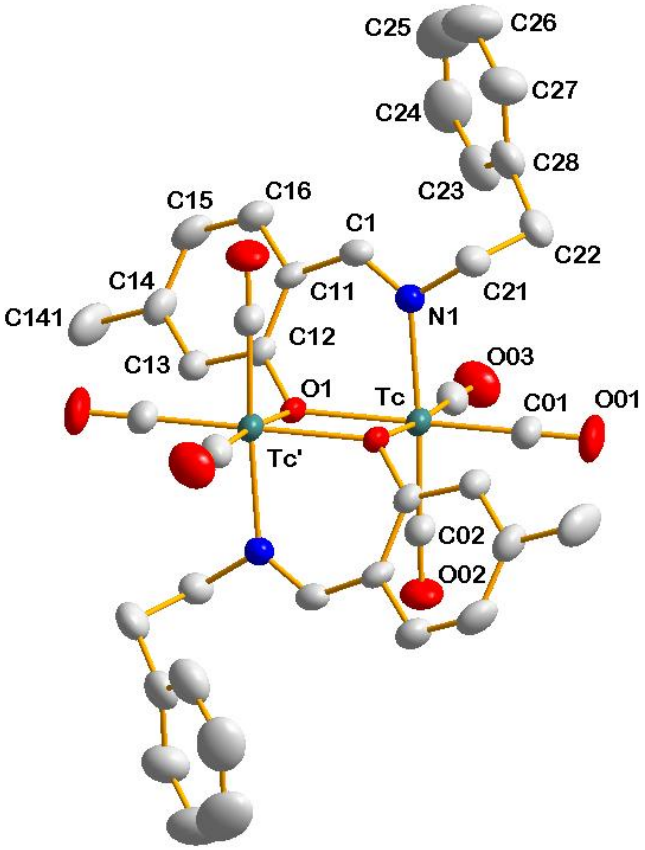

Figure 5.14: **Molecular structure of *fac*-[^{99}Tc(5-Me-Sal-EtPh)(CO)$_3$]$_2$ (6) showing atom numbering scheme and displacement ellipsoids drawn at 50% probability level. The structure represents the full molecule generated by symmetry, indicated where appropriate by (‘). For the aromatic rings, the first digit represents the ring number, and the second digit refers to the specific C-atom in the ring.**

Table 5.7: Selected bond distances and angles of *fac*-[^{99}Tc(5-Me-Sal-EtPh)(CO)$_3$]$_2$ (6) [Å and ˚]

Atoms	Bond Lengths (Å)	Atoms	Bond Angles (°)
Tc-N1	2.172(3)	N1-Tc-O1	82.01(9)
Tc-O1	2.158(2)	N1-Tc-C02	176.18(12)
Tc'-O1'	2.158)2)	O1-Tc-C01	172.02(12)
Tc-C01	1.892(4)	Tc-O1-Tc'	104.13(8)
Tc-C02	1.914(4)	O1-Tc-C02	94.59(11)
Tc-C03	1.899(4)	O1-Tc-O1'	75.87(8)
Tc-Tc'	3.434(2)	C01-Tc-C02	87.46(15)
Tc-O1'	2.195(2)	C01-Tc-C03	85.65(15)
N1-C1	1.286(4)	C02-Tc-C03	87.45(15)
C01-O01	1.147(4)	O01-C01-Tc	179.9(5)
C02-O02	1.149(4)	O02-C02-Tc	176.8(3)
C03-O03	1.142(4)	O03-C03-Tc	176.1(3)
C1-C11	1.455(5)	C1-N1-C21	116.3(3)
N1-C21	1.471(4)		
O1-C12	1.348(3)		

(') Indicates symmetry generated subunit.

The basic geometry in complex **(6)** is a distorted octahedral configuration around the technetium central atoms. The coordination around the central metal atoms consist of three carbonyl ligands in a facial arrangement, the oxygen and the imine nitrogen atoms of the bidentate chelate. The octahedron mode around the metal centres is completed by the bridging phenolato oxygen atoms linking together the two *fac*-[^{99}Tc(5-Me-Sal-EtPh)(CO)$_3$] subunits.

The deviation from the ideal octahedral geometry is indicated by the angles of 82.01(9)˚ and 176.18(12)˚ for N1-Tc-O1 and O1-Tc-C02 respectively. The Tc-N1 and Tc-O1 bond distances of 2.172(3) Å and 2.158(2) Å are good agreement with reported technetium(I) tricarbonyl complexes containing N,O bidentate ligands, with bond distances of around 2.177-2.154 Å for Tc-N and 2.132-2.216 Å for Tc-O.[13,14,15] The technetium-carbonyl bond distances were determined to be 1.892(4) Å, 1.914(4) Å and 1.899(4) Å for Tc-C01, Tc-C02 and Tc-C03 respectively. The central unit forms a four-membered coplanar system defined by the Tc-O1-Tc'-O1 atoms. The two technetium centres are separated by an intermetallic distance of 3.433(2) Å.

The plane formed by the salicylidene aromatic backbone (Plane 1: C11, C12, C13, C14, C15, C16) is tilted relative to the Tc equatorial plane (Plane 2: Tc, N1, O1, C01, C02) with a dihedral angle of the 39.19(1) as shown in Figure 5.15. On the other hand, the phenyl ring (Plane 1: C23, C24, C25, C26, C27, C28) is bending inwards, angled with respect to the equatorial plane 2 (Plane 2: Tc, N1, O1, C01, C02) with a dihedral angle of 56.81(2)˚, see Figure 5.16.

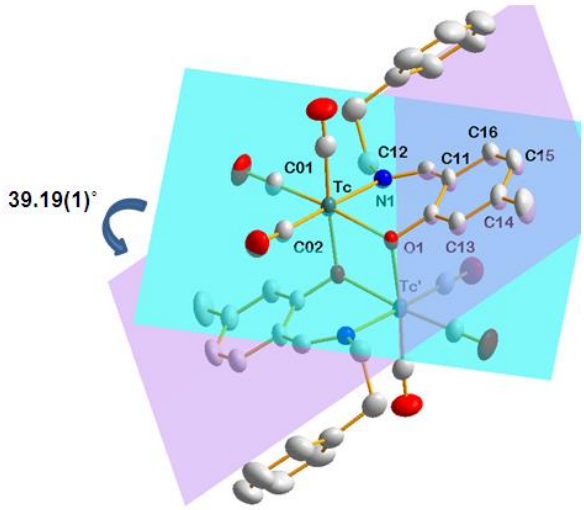

Figure 5.15: **Graphical representation of the bending of the salicylidene aromatic backbone (Plane 1 indicated by purple, Plane 2 indicated by blue). Hydrogen atoms were omitted for clarity.**

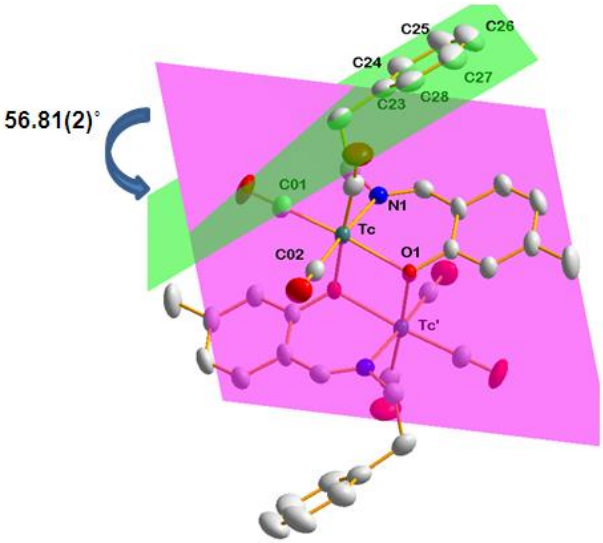

Figure 5.16: **Graphical representation of the bending of the phenyl ring (Plane 1 indicated by purple, plane 2 indicated by green). Hydrogen atoms were omitted for clarity.**

The molecular packing of **(6)** is stabilised by intermolecular hydrogen bonding as indicated by the green dotted line in Figure 5.17. The related data is given in Table 5.8.

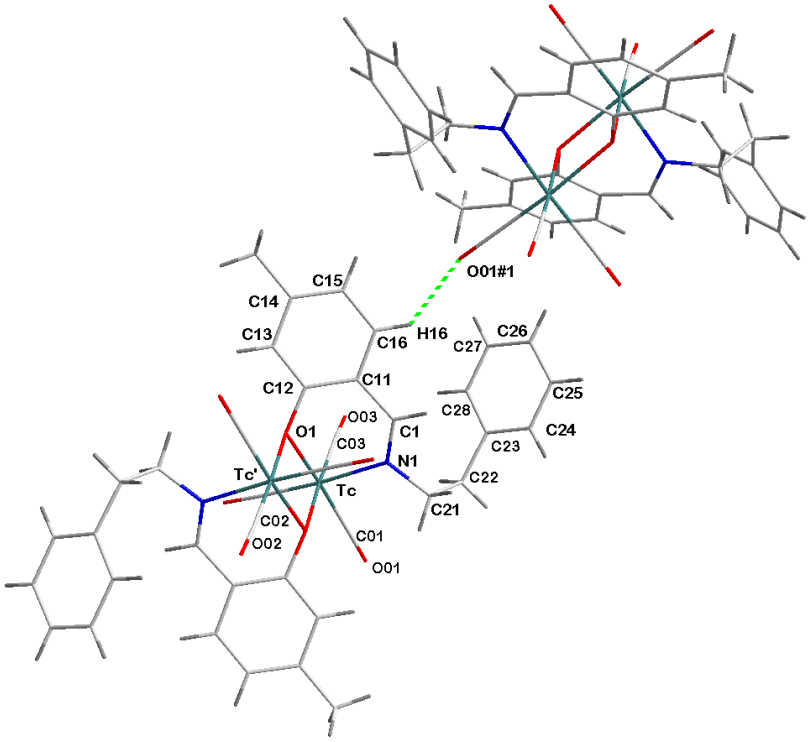

Figure 5.17: **Graphical representation of intermolecular hydrogen bond interaction indicated between C16-H16…O01$^{\#1}$. Hydrogen interaction is illustrated by the green dotted line.**

Table 5.8: **Hydrogen bonds for *fac*-[^{99}Tc(5-Me-Sal-EtPh)(CO)$_3$]$_2$ (7) [Å and ˚].**

D-H…A	d(D-H)	d(H…A)	d(D…A)	<(DHA)
C(16)-H(16)…O(01)#1	0.93	2.52	3.190(3)	130.5(3)

Symmetry transformations used to generate equivalent atoms:
#1 3/2-y, -1/2+y, 1/2-z

The molecular packing in complex **(6)** is illustrated in Figure 5.18. The molecules pack in a head-to-head fashion with the phenyl rings pointing towards each other in adjacent molecules.

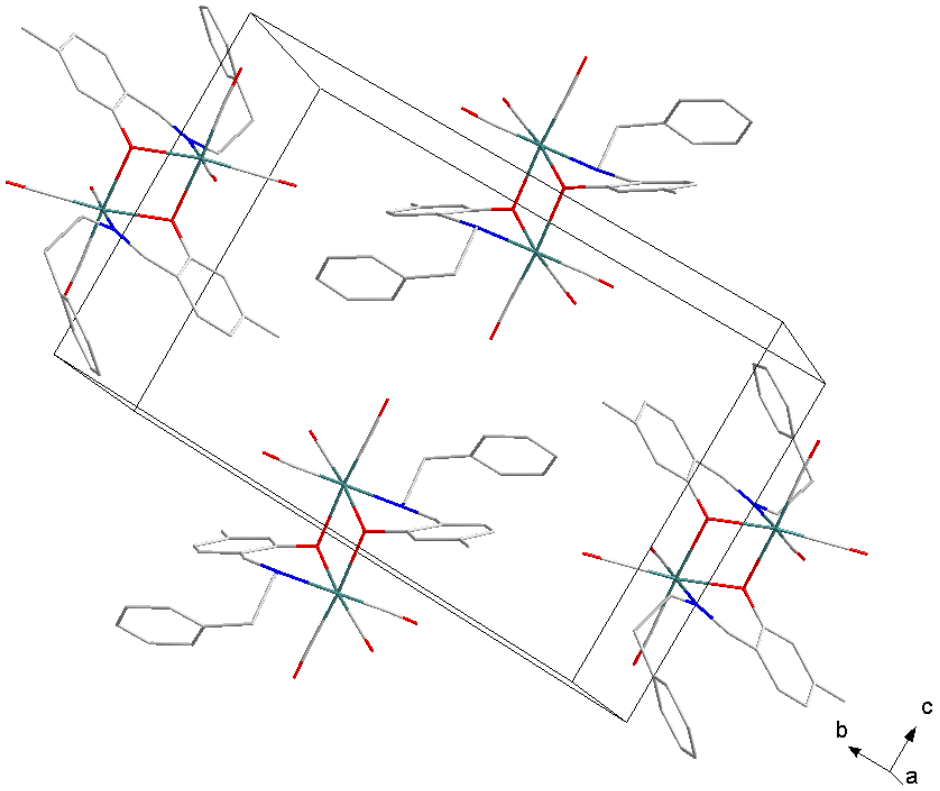

Figure 5.18: Molecular packing of *fac*-[^{99}Tc(5-Me-Sal-EtPh)(CO)$_3$]$_2$ (6).

5.6 Discussion

In this section, the solid state structures of three technetium-99 complexes were reported. Table 5.9 presents a summary of the selected parameters obtained for these dinuclear technetium(I) complexes, *fac*-[^{99}Tc(Sal-*m*Tol)(CO)$_3$]$_2$ **(4)**, *fac*-[^{99}Tc(5Me-Sal-CyPent)(CO)$_3$]$_2$ **(5)** and *fac*-[^{99}Tc(5Me-Sal-EtPh)(CO)$_3$] **(6)**. The complexes contain mono-anionic N,O Schiff-base bidentate ligands coordinated to the technetium as both chelators and as bridge linking the two metal centres. Each technetium(I) metal centre in the dinuclear complexes; **(4)**, **(5)** and **(6)** is hexa-coordinated by an imine nitrogen atom, the bridging phenolate oxygen atoms of the two bidentate ligands and by the three facially arranged carbonyl ligands.

Table 5.9: A comparison of selected geometric parameters of complexes *fac*-[^{99}Tc(Sal *m*Tol)(CO)$_3$]$_2$ (4), *fac*-[Mn(Sal-*m*Tol)(CO)$_3$]$_2$[16] (4a), *fac*-[^{99}Tc(5-Me-Sal-CyPent)(CO)$_3$]$_2$ (5), *fac*-[Mn(5-Me-Sal-CyPent)(CO)$_3$]$_2$ (1), *fac*-[Tc(5-Me-Sal-CyPent)(CO)$_3$]$_2$ (6), *fac*-[^{99}Tc(5Me-Sal-EtPh)(CO)$_3$] (6) and *fac*-[Re(5Me-Sal-EtPh)(CO)$_3$] (3).

Complex	(4)	4(a)[16]	(5)	(1)	(6)	(3)
Bond Distance (Å)						
M-N1	2.188(3)	2.033(2)	2.195(3)	2.176(4)	2.172(3)	2.173(4)
M-O1	2.157(2)	2.064(2)	2.149(2)	2.176(4)	2.158(2)	2.116(3)
M-C01	1.899(4))	1.815(3)	1.903(3)	1.814(2)	1.892(4)	1.904(6)
M-C02	1.922(4)	1.795(3)	1.894(3)	1.806(2)	1.914(4)	1.922(5)
N1-C1	1.282(4)	1.282(3)	1.286(5)	1.281(2)	1.286(4)	1.287(7)
Tc-Tc'	3.421(2)	3.187(2)	3.424(4)	3.193(2)	3.433(2)	-
Bond angle (°)						
N1-M-O1	81.08(9)	84.64(8)	82.36(9)	85.42(5)	82.01(9)	84.88(14)
O1-M-C01	172.89(12)	174.92(11)	175.59(11)	175.12(6)	172.02(12)	176.1(2)
O1-M-O1'	76.16(9)	77.96(8)	75.91(8)	78.05(6)	75.87(8)	-
M-O1-M'	103.841(3)	101.987(23)	104.094(2)	101.95(2)	104.127(2)	-

Where 2-(*m*-Tolyliminomethyl)phenol = SalH-*m*TolH, 2-(cyclopentyl)methyl-5-methylphenol = 5-Me-SalH-CyPentH, 5-methyl-2-(phenylethyliminimethyl)-phenol = 5-Me-Sal-EtPhH

Notes**:** M = Mn, Re and Tc).

4(a) = *fac*-[Mn(Sal *m*Tol)(CO)$_3$]$_2$[16]

(1) = *fac*-[Mn(5-Me-Sal-CyPent)(CO)$_3$]$_2$ (chapter 4)

(3) = *fac*-[Re(5-Me-Sal-EtPh)(CO)$_3$(MeOH)] (chapter 4).

The general geometry in the dinuclear technetium(I) complexes **(4)** and **(5)** are reminiscent to the manganese analogue **(1)** *fac*-[Mn(5-Me-Sal-CyPent)(CO)$_3$]$_2$, reported in the preceding chapter and the published *fac*-[Mn(Sal-*m*Tol)(CO)$_3$]$_2$ complex.[16] The central core in the analogues complexes form a diamond motif defined by the atoms M'-O1'-M-O1 (where M = Mn, Tc). The intermetallic distances in technetium complexes, averaging 3.423 Å, are longer than the average of around 3.190 Å obtained in analogues manganese complexes. The differences in the intermetallic distances are most likely due to the differences in ionic radius between the two elements in an octahedral coordination mode. The M(I)-N and M(I)-O bond distances obtained for the technetium complexes **(4)** and **(5)** are longer in comparison to the manganese complexes **(1)** and *fac*-[Mn(Sal-*m*Tol)(CO)$_3$]$_2$.[16]

[16] P.P. Mokolokolo, A. Brink, *Z. Kristallogr. NCS*. 231 (2016) 613-615.

The structures are compared visually by the structural overlay diagrams as given in Figures 5.20 and 5.21. The central core seems to be independent on the electronic and steric properties of the peripheral substituents on the ligand backbone introduced in terms of the *m*tolyl substituent in **(4)**, the methyl and cyclopentyl substituents in **(5)** as evidenced by the O1'-Tc-O1 bite angles of 76.16(9)◦ and 75.91(8)◦ for the technetium complexes **(4)** and **(5)** respectively. This effect is also manifested in the manganese(I) complexes **(1)** and *fac*-[Mn(Sal-*m*Tol)$(CO)_3]_2$ with O1'-Mn-O1 bite angles of 77.96(8) ◦ and 78.05(6) ◦respectively.[16]

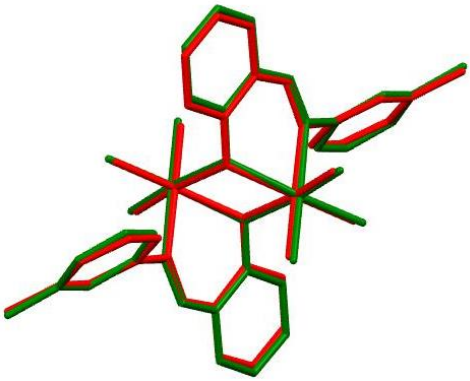

Figure 5.19: An overlay diagram of *fac*-[^{99}Tc(Sal-*m*Tol)$(CO)_3]_2$ (4) (indicted in red) and *fac*-[Mn(Sal-*m*Tol)$(CO)_3]_2$ (indicted in green) (RMS = 0.115 Å).[16]

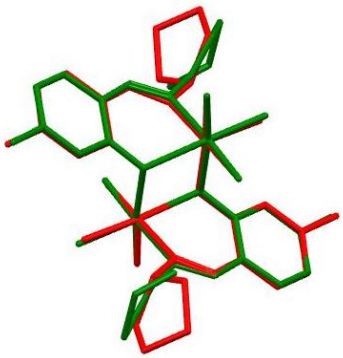

Figure 5.20: An overlay diagram of *fac*-[^{99}Tc(5-Me-Sal-CyPent)$(CO)_3]_2$ (5) (indicted in red) and *fac*-[Mn(5-Me-Sal-CyPent)$(CO)_3]_2$ (2) (indicted in green) (RMS = 0.0822 Å).

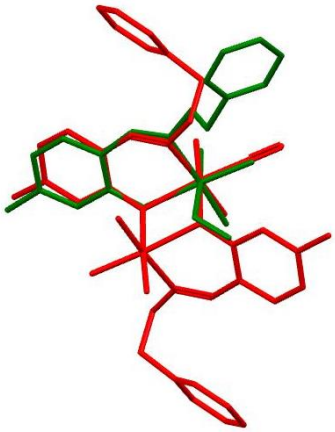

Figure 5.21: An overlay diagram of *fac*-[^{99}Tc(5-Me-Sal-EtPh)(CO)$_3$]$_2$ (6) (indicted in red) and *fac*-[Re(5-Me-Sal-EtPh)(CO)$_3$(MeOH)] (3) (indicted in green) (RMS = 0.134 Å).

The dinuclear complex **(6)** closely resembles that of the mononuclear complex **(3)**, *fac*-[Re(5-Me-Sal-EtPh)(CO)$_3$(MeOH)] reported in Chapter 4. The 6th position of the octahedral metal centre in **(3)** is occupied by the methanol molecule and by the bridging phenolate oxygen atom in **(6)**. An overlay diagram of complex **(6)** and *fac*-[Re(5Me-Sal-EtPh)(CO)$_3$(MeOH)] (Chapter 4) is given in Figure 5.21. The inner core in **(6)** forms a coplanar system defined by the atoms Tc-O1-Tc'-O1' with an intermetallic distance of 3.433(2) Å. The Tc-Tc distance is in good agreement with the bond distance of 3.408(2) for the only reported dinuclear technetium structure with O,N bidentate ligand as could be ascertained.[13] The Tc/Re-N and Tc/Re-O bond distances are in good agreement with bond distances of 2.172(3) Å and 2.158(2) Å and 2.173(4) Å and 2.116(3) Å for complex (6) and f*ac*-[Re(5Me-Sal-EtPh)(CO)$_3$(MeOH)] (chapter 4) respectively. There is however some strain experienced in the dinuclear binding mode as evidenced by the N1-Tc-O1 bite angle of 82.01(9)° compared to the less strained N1-Re-O1 bite angle of 84.88(14)° in *fac*-[Re(5-Me-Sal-EtPh)(CO)$_3$(MeOH)] (chapter 4).

5.7 Conclusion

As part of the ongoing investigations on Schiff-base bidentate ligands as potential bio-linkers in the [2+1] labeling strategy used in radiopharmaceutical design, involving the tricarbonyl complexes of the technetium and rhenium, the solid-state structures of three new ^{99}Tc(I) complexes were investigated and reported in this chapter. The complexes *fac*-[^{99}Tc(Sal-*m*Tol)$(CO)_3]_2$ **(4),** *fac*-[^{99}Tc(5-Me-Sal-CyPent)$(CO)_3]_2$ **(5)** and *fac*-[^{99}Tc(5-Me-Sal-EtPh)$(CO)_3$] **(6)** all exhibit distorted octahedral geometry around each technetium(I) centre in the dinuclear complexes with the coordination from three facially coordinated carbonyl ligands, the chelating nitrogen and oxygen atom of the bidentate ligand and the phenolate bridging oxygen atoms, linking together the subunits. The inner core of the dinuclear complexes is a four-membered planar system defined by Tc-O1-Tc'-O1'. The central core seems to be robust and relatively unaffected by the variations on the ligand peripheries as indicated by the small change in the bite angles within the three complexes. The formation of dinuclear complexes, together with the structurally flexible Schiff-base ligands offers an opportunity to explore the possibility of designing radioactive compounds that can incorporate more than one targeting unit. Also due to the structural flexibility of the ligand complexes, one technetium metal centre can potentially be replaced by a rhenium atom to form a doubly functioning complex for both radiotherapy and imaging.

The application of these Schiff-base ligands has been adequately illustrated in this chapter, augmented but that in Chapter 4. To further explore the versatile coordinative properties of these bidentate ligands, the coordinative and kinetic study of their effect on the important catalytic models pertaining to platinum group metals, and more specifically, oxidative addition reaction in rhodium(I) based complexes has been investigated and are reported in the ensuing chapters.

6 Crystallographic Study of Rhodium(I) Dicarbonyl Complexes

6.1 Introduction

There is ongoing interest in the use of intra- and intermolecular interactions for the development of new materials and technologies for catalytic, optical, electronic and medical applications.[1,2,3] One of the key areas of focus is on the d^8 square planar complexes exhibiting non-covalent, one-dimensional metal-metal interactions.[4,5,67] The metal ions' weak coordinating abilities may be utilized by carefully designed ligand systems in order to promote and induce these non-covalent metallophillic interactions. This highlights the invaluable role played by the supporting ligand systems towards the enhancement of the one-dimensional metal-metal interactions.

To study these metallophillic interactions, systems need to be designed wherein minimal steric effects in the *direction* of the interactions are present, i.e. perpendicular to the square plane in typical d^8 Platinum Group Metal complexes. Variation of steric demand *in-the-plane* of the square planar metal complex, such as the chelate bite angle, is of less importance, although it can significantly affect the electronics.

As to be discussed later, although the overarching focus of this PhD study was on Schiff-base ligands, the closely related oxine systems are also N,O-Bid ligands. They provide additional possibility to also, as in the case of the Schiff bases, introduce a

[1] H. Sun, K. Ye, C. Wang, H. Qi, F. Li, Y. Wang, *J. Phys. Chem. A.* 110 (2006) 10750-1075.
[2] M.J. Frampton, H.L. Anderson, *Angew. Chem. Int. Ed*. 46 (2007) 1028-1064.
[3] J.K. Bera, K.R. Dunbar, *Angew. Chem. Int. Ed.* 41 (2002) 4453-4457.
[4] W.J. Hunks, M.C. Jennings, R. Puddephatt, *J. Inorg. Chem*. 41 (2002) 4590-4598.
[5] V.W.-W. Yam, K.M.-C. Wong, N. Zhu, J*. Am. Chem. Soc*. 124 (2002) 6506-6507.
[6] V.W.-W. Yam, E.C.-C. Cheng, *Top. Curr. Chem*. 281 (2007) 269 - 309.
[7] M.M. Conradie, P. H.van Rooyen, C. Pretorius, A. Roodt, J. Conradie, *J. Mol. Struct*. 1144 (2017) 280-289.

subtle variation of the periphery of the ligand without significantly varying the steric effect thereby induced. Although they form *five-membered* chelates compared to the six-membered entities in the Schiff-base systems, they were particularly included in this study since they produce model complexes which can be much more readily crystallised. They can thus be studied in the solid state, contrary to the corresponding Schiff-base systems which proved to be quite challenging to crystallise. Manifestation of the latter stems from the fact that *only* one example of a Schiff-base complex could be crystallised after many attempts. This complex which was successfully isolated, is therefore presented and discussed here, in conjunction with the oxine based examples.

Thus, the metallophillic interactions in the rhodium(I) complexes of the type [Rh(L,L'-Bid)$(CO)_2$], (where L,L'-Bid = N,O-bidentate ligands; oxine- and Schiff-base chelates) have been studied. Both these ligand classes' complexes have been synthesized, and contain systematic variations in their electronic parameters/characteristics, while keeping their steric parameters perpendicular to the metal plane fairly constant although *significantly* varying the bite angle.

The aim is as indicated, the further understanding of the contribution of surrounding ligands on the extent of these metallophilic interactions. Figure 6.1 illustrates the rhodium(I) complexes utilized within this study. In particular, their solid-state structural properties will be the focus herein.

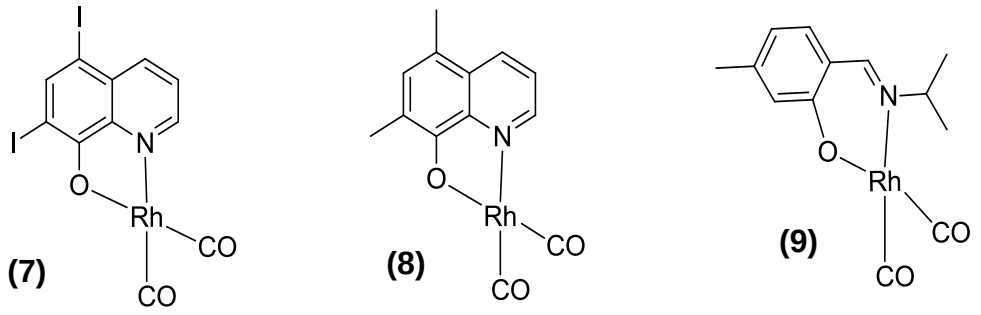

Figure 6.1: Schematic representation of the rhodium(I) complexes [Rh(5,7-Diido-Ox)$(CO)_2$] (7), [Rh(5,7-DiMe-Ox)$(CO)_2$] (8) and [Rh(5-Me-Sal-iProp)$(CO)_2$] (9), where 5,7-Diido-8-hydroxyquinoline = 5,7-Diido-OxH, 5,7-Dimethy-8-hydroxyquinoline = 5,7-Dimethyl-OxH, (iii) (5-Methyl-2 (isopropyliminomethyl)phenoline = 5-Me-Sal-IsoPropH). The complexes' numbering continues from the previous chapter.

6.2 Experimental

Diffraction data of [Rh(5,7-Diido-Ox)$(CO)_2$] **(7) ,** [Rh(5,7-DiMe-Ox)$(CO)_2$] **(8)** and [Rh(5-Me-Sal-iProp)$(CO)_2$] **(9)** were collected at 100(2) K on a Bruker X8 Apex II 4K diffractometer using MoKα radiation (λ=0.71073 Å).[8] The Apex II software package was utilized along with the optimum measurement method in collecting more than a hemisphere of reciprocal space as predicted by COSMO[9]. The cell parameters were refined by the SAINT-Plus[10] program, while SADABS[11] was used for the absorption corrections. The structures were solved by direct methods and refined on F^2 using anisotropic displacement parameters for all non-hydrogen atoms. SHELXL-97[12,13] and WinGX[14] were used for structure solutions and refinements respectively. The molecular graphics were prepared with DIAMOND.[15] All non-hydrogen atoms were refined with anisotropic displacement, while the methyl, methane and aromatic H atoms were placed in geometrically idealised positions and constrained to ride of their parent atoms, with (C-H distances of 0.98 – 0.95 Å and U_{iso}(H) = 1.2U_{eq}(C) and U_{iso}(H) = 1.5U_{eq}(C)) respectively. The N-bound hydrogen atom was located from the electron density map and refined without any constraints.

Table 6.1 gives a summary of the general crystal data and refinement parameters for all three rhodium(I) complexes. The supplementary data for the atomic coordinates, bond distances and bond angles and anisotropic displacement parameters are given in the Appendix for each individual dataset.

[8] Apex2, Version 2012.10-0, Bruker AXS Inc, Madison, Wisconsin, USA, 2012.
[9] Cosmo, Version 1.48, Bruker AXS Inc, Madison, Wisconsin, USA, 2003.
[10] SAINT-Plus, Version 8.27B (including XPREP), Bruker AXS, Inc, Madison, Wisconsin, USA, 2012.
[11] SADABS, Version 2012/1, Bruker AXS, Inc, Madison, Wisconsin, USA, 1998.
[12] G.M. Sheldrick, Acta Crystallogr, A64 (2008) 112-122.
[13] G.M. Sheldrick, SHELXL97, University of Göttingen, Göttingen, Germany, 1997.
[14] L.J. Farrugia, J. Appl. Crystallogr. 32 (1999) 837-838.
[15] K. Brandenburg, H. Putz, DIAMOND, release 3.1b, Crystal Impact GbR, Bonn, Germany, 2005.

Table 6.1: X-ray crystallographic data and refinement parameters for [Rh(5,7-Diido-Ox)(CO)$_2$] (7), [Rh(5,7-DiMe-Ox)(CO)$_2$] (8) and [Rh(5-Me-Sal-IsoProp)(CO)$_2$] (9).

	Rh(5,7-Diido-Ox)(CO)$_2$] (7)	**[Rh(5,7-DiMe-Ox)(CO)$_2$] (8)**	**[Rh(5-Me-Sal-IsoProp)(CO)$_2$] (9)**
Empirical formula	$C_{11}H_4NO_3I_2Rh$	$C_{13}H_{10}NO_3Rh$	$C_{13}H_{14}NO_3Rh$
Formula weight	554.86	331.13	335.16
Temperature/(K)	100(2)	100(2)	100(2)
Wavelength (Å)	0.71073	0.71073	0.71073
Crystal system	Orthorhombic	Orthorhombic	Monoclinic
Space group	*Pnma*	*Pbca*	$P2_1/c$
a/Å	18.032(2)	7.303(8)	9.1622(9)
b/Å	6.507(8)	16.176(2)	16.776(2)
c/Å	10.721(1)	20.064(3)	8.3470(7)
α/°	90	90	90
β/°	90	90	90.449(3)
γ/°	90	90.	90
Volume/Å^3	1257.9(12)	2370.1(19)	1282.9(11)
Z	8	8	4
Density (g.cm^{-3})	2.930	1.856	1.735
μ(mm^{-1})	6.263	1.439	1.330
F(000)	1008	1312	672
Crystal Colour	Red	Red	Yellow
Crystal Size (mm)	0.110 x 0.126 x 0.278	0.364 x 0.374 x 0.444	0.092 x 0.126 x 0.278
Crystal Morphology	Plate	Cuboid	Cuboid
Theta range (°) to θ	4.305 to 27.995	3.894 to 27.997	4.449 to 27.996
Completeness (%)	99.0, 25.242	99.4, 25.242	99.3, 25.242
Index ranges h k l	h = -17 to 23 k = -8 to 8 l = -13 to 14	h = -9 to 9, k = -15 to 21 l = -26 to 26	h = -12 to 12 k = -22 to 22 l = -11 to 7
Reflections collected	17902	38440	20461
Independent reflections	1642	2849	3083
R_{Int}	0.0567	0.0490	0.0638
Data/restraints/ parameters	1642 / 0 / 109	2849 / 0 / 163	3083 / 0 / 171
Goodness-of-fit on F^2	1.138	1.129	1.032
Final R indexes [I>=2σ (I)]	R1 = 0.0329 wR2 = 0.0812	R1 = 0.0261 wR2 = 0.0679	R1 = 0.0208 wR2 = 0.0481
Final R indexes [all data]	R1 = 0.0367 wR2 = 0.0857	R1 = 0.0270 wR2 = 0.0689	R1 = 0.0264 wR2 = 0.0508
ρ max, ρ min (e.Å^{-3})	2.523 and -1.749	0.730 and -1.272	0.385 and -0.466

5,7-Diido-OxH = 5,7-Diido-8-hydroxyquinoline; 5,7-Dimethyl-OxH = 5,7-Dimethy-8-hydroxyquinoline =5-Me-Sal-IsoPropH = (5-Methyl-2-(isopropyliminomethyl)phenol.

6.3 Crystal structure of [Rh(5,7-Diido-Ox)(CO)$_2$]

The complex, [Rh(5,7-Diido-Ox)(CO)$_2$] **(7),** (5,7-Diido-Ox = 5,7-Diiodo-8-hydroxyquinolinate) is illustrated in Figure 6.2. The molecule crystallizes in the orthorhombic crystal system in the *Pnma* space group with one independent molecule in the asymmetric unit and eight formula units per unit cell (Z = 8). Selected bond distances and angles are given in Table 6.2.

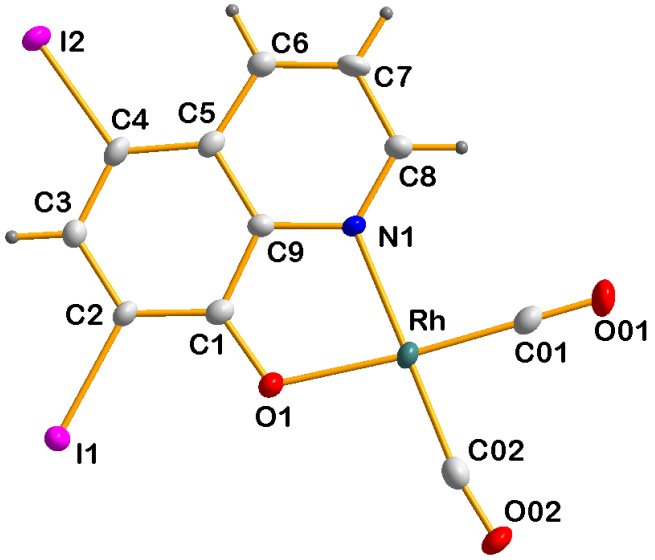

Figure 6.2: **Structural representation of [Rh(5,7-Diido-Ox)(CO)$_2$] (7), with atom numbering scheme and displacement ellipsoids drawn at 50% probability level.**

Table 6.2: **Selected bond distances and angles of [Rh(5,7-diido)-Ox(CO) [Å and ˚]**

Atoms	Bond Lengths (Å)	Atoms	Bond Angle [°]
Rh-N1	2.068(5)	C02-Rh-C01	84.3(3)
Rh-O1	2.052(5)	C02-Rh-O1	99.6(2)
Rh-C01	1.837(7)	C01-Rh-O1	176.1(3)
Rh-C02	1.860(8)	C02-Rh-N1	179.6(2)
Rh···Rh	3.4602(24)	C01-Rh-N1	96.1(3)
C02-O02	1.142(9)	O1-Rh-N1	80.02(19)
C1-C2	1.397(9)	O01-C01-Rh	179.9(6)
C9-N1	1.376(8)	O02-C02-Rh	170.6(18)
C1-O1	1.316(8)	Rh···Rh···Rh angle	140.193(2)
N1···O1	2.914(2)		
I2-C4	2.106(7)		
I1-C2	2.083(6)		

Complex (**7**) adopts a distorted square-planar geometry around the central rhodium(I) which is coordinated to two carbonyl ligands and the nitrogen and oxygen atoms of the bidentate chelate. The square planar orientation around the rhodium atom is distorted from the ideal geometry as indicated by the C02-Rh-C01 and O1-Rh-N1 angles of 84.3(3)° and 80.02(19)° respectively. The rhodium central atom is located perfectly on the plane constructed through O1-N1-C01-C02. The Rh-N and Rh-O bond lengths 2.068(5) Å and 2.052(5) Å are comparable to those found in rhodium(I) complexes with N,O donor atoms with bond distances around 2.018 - 2.092 Å and 2.027 - 2.077 Å for Rh-N and Rh-O respectively.[16,17,18] The Rh-C01 and Rh-C02 bond distances were determined to be 1.837(7) Å and 1.860(8) Å respectively.

The rhodium molecules display extended metallophilic interactions with an intermolecular Rh···Rh distance of 3.4602(24) Å repeating throughout the crystal lattice. The Rh···Rh distance is within range of 3.25 - 3.68 Å distances found in literature.[19,20,21] The interaction is illustrated by the green dotted lines in Figure 6.3, and the Rh···Rh···Rh chains are quite strained forming a zig-zag with a Rh-Rh-Rh angle of 140.193(2)˚.

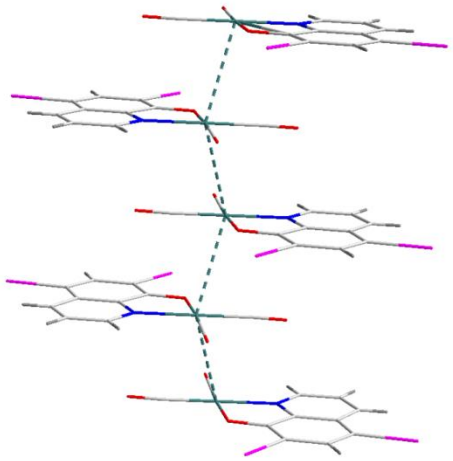

Figure 6.3: **Illustration of the observed Rh○○○Rh interactions indicated by the green dotted line.**

[16] J. Janse van Rensburg, A. Muller, A. Roodt, *Acta Cryst*. E67 (2007) m3015-m3016.
[17] J. Janse van Rensburg, A. Roodt, *Acta Cryst. E62* (2006) m2981-m2983.
[18] J.G. Leipoldt, S.S. Basson, E.C. Grobler, A. Roodt, *Inorganica Chim. Acta*. 99 (1985) 13-17.
[19] M. Jakonen, L. Oresmaa, M. Haukka, *Crystal Growth & Design*. 7 (2007) 2620-2026.
[20] E. Laurila, R. Tatikonda, L. Oresmaa, P. Hirva, M. Haukka, *CrystEngcomm*. 14 (2012) 8401-8408.
[21] E. Laurila, L. Oresmaa, J. Hassinen, P. Hirva, M. Haukka, *Dalton Trans*. 42 (2013) 395-398.

Various other interactions contribute to the stabilisation of the crystal lattice. Inter- and intra-molecular hydrogen bond interactions are indicated by the green dotted lines in Figure 6.4, while related data to the hydrogen bonds is given in Table 6.3.

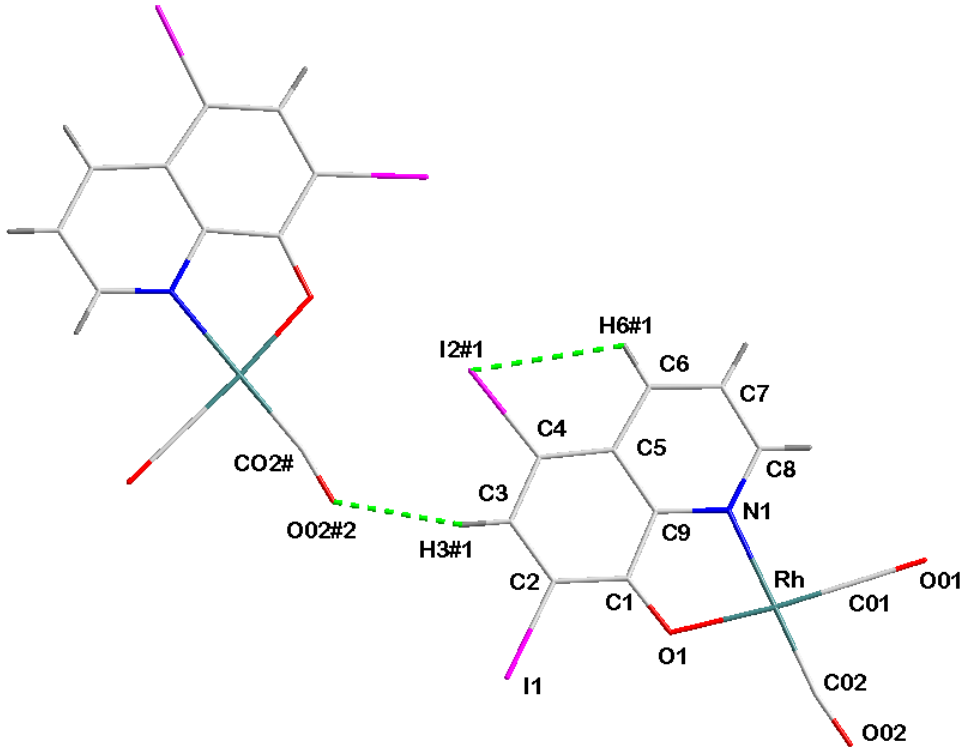

Figure 6.4: **Graphical representation of observed intermolecular hydrogen bonding interaction in [Rh(5,7-Diido-Ox)(CO)$_2$] (7).**

Table 6.3: **Hydrogen bonds of [Rh(5,7-Diido-Ox)(CO)$_2$] (7) [Å and °].**

D-H…A	d(D-H)	d(H…A)	d(D…A)	<(DHA)
C(6)-H(6)…I2(1)$^{\#1}$	0.93	2.96	3.397(7)	111(2)
C(3)-H(3)…O02(1)$^{\#2}$	0.93	2.46	3.368(9)	165(3)

Symmetry transformations used to generate equivalent atoms
#1 x, y, z; #2 -1/ 2-x, 1/2-y, 1/2-z

Furthermore, the crystal lattice is also stabilised by significant halogen bonding involving the iodine atoms on the ligand backbone. These interactions are indicated by the green dotted line in Figure 6.5 with the related data given in Table 6.4. The halogen interaction extends along the 1D chain in a head-to-tail manner for further stabilisation of the crystal lattice.

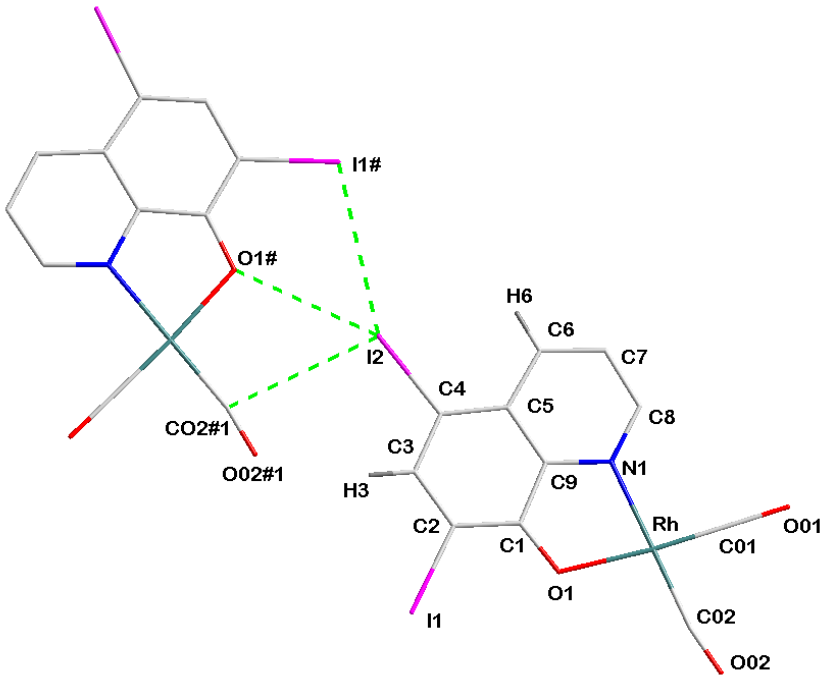

Figure 6.5: **Graphical representation of observed halogen bonding interaction in [Rh(5,7-Diido-Ox)$(CO)_2$] (7)**

Table 6.4: **Halogen bonding of [Rh(5,7-Diido-Ox)$(CO)_2$] (7) [Å and °].**

D-I…A	d(D-I)	d(I…A)	d(D…A)	<(DIA)
C(4)-I(2)…I(1)$^{\#1}$	2.1058(6)	3.839(3)	5.8105(16)	103.1(2)
C(4)-I(2)…O(1)$^{\#1}$	2.1058(6)	3.319(6)	5.2771(13)	152.5(2)
C(4)-I(2)…C(02)$^{\#1}$	2.1058(6)	3.568(7)	4.4809(15)	101.2(2)

Symmetry transformations used to generate equivalent atoms
#1 -1/2 + x, 1/2-y, 1/2-z

The molecular packing is in addition to the above further stabilised by several C-O…π interactions between neighboring molecules as indicated by the green dotted lines in Figure 6.6. The related data is given in Table 6.5.

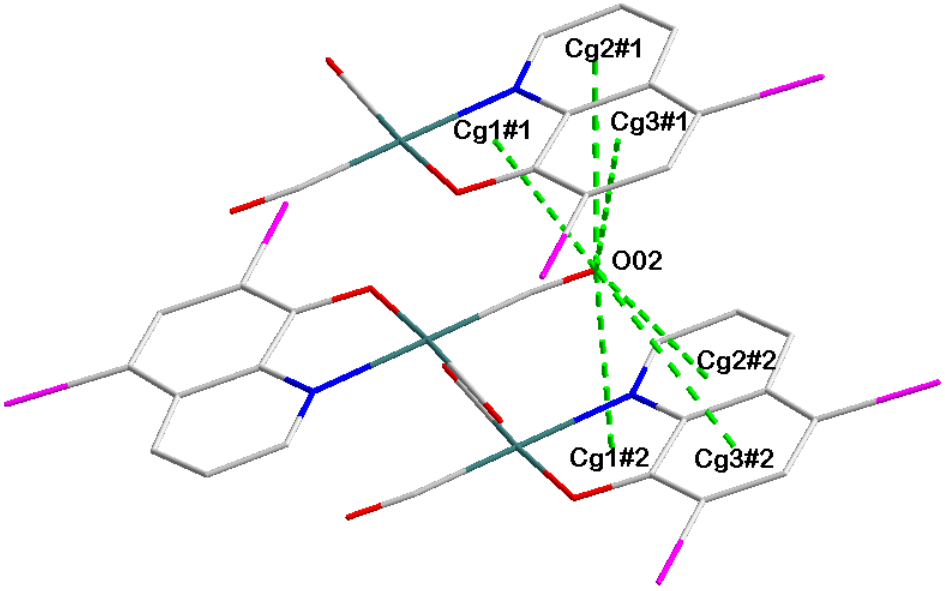

Figure 6.6: **Graphical representation of the CO …π interactions indicated by the green dotted lines. Hydrogen bonds were omitted for clarity.**

Table 6.5: **C-O…π interactions of [Rh(5,7-Diido-Ox)$(CO)_2$] (7) [Å and ˚].**

C-O…Cg	Centroid atom	d(O…Cg) Å	d(C…Cg) Å	(C-O…Cg) (˚)
C02-O02	$Cg1^{\#1}$	3.356(3)	3.283(3)	76.5(1)
C02-O02	$Cg2^{\#1}$	3.5961(3)	4.110(6)	108.9(2)
C02-O02	$Cg3^{\#1}$	3.7288(22)	4.224(6)	108.0(2)
C02-O02	$Cg1^{\#2}$	3.356(3)	3.283(3)	76.5(1)
C02-O02	$Cg2^{\#2}$	3.5961(3)	4.110(6)	108.9(2)
C02-O02	$Cg3^{\#2}$	3.7288(22)	4.224(6)	108.0(2)

Symmetry transformations used to generate equivalent atoms
#1 2-x, ½+y; 1-z #2 2-x, -1/2+y, 1-z;
Cg1; Rh, O1, C1, C9, N1;
Cg2: N1, C8, C7, C6, C5, C9
Cg3: C1, C2, C3, C4, C5, C9.

There are various noncovalent interactions coexisting in the molecular packing of complex (**7**). The molecules pack in a “head-to-head” arrangement with the carbonyl ligands pointing away from each other in neighboring molecules. The molecular packing is given in Figure 6.7 below.

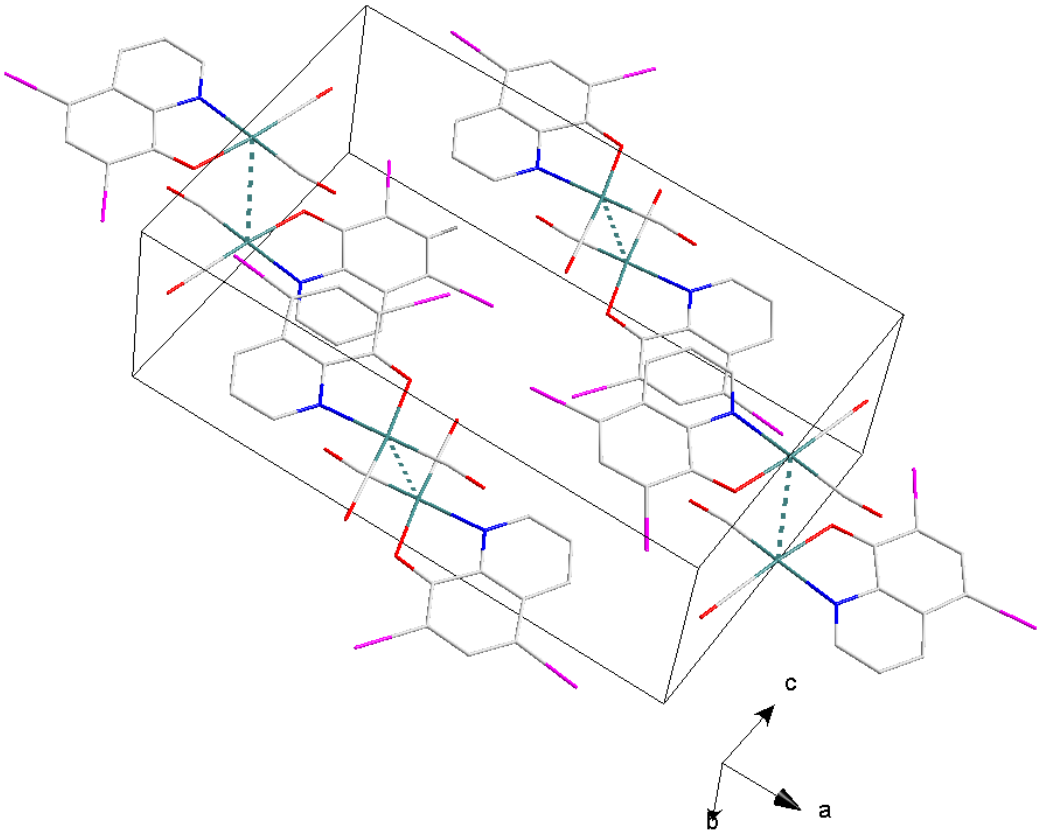

Figure 6.7: Molecular packing of [Rh(5,7-Diido-Ox)$(CO)_2$] (7).

6.4 Crystal structure of [Rh(5,7-DiMe-Ox)(CO)$_2$]

The complex, [Rh(5,7-DiMe-Ox)(CO)$_2$] **(8)**, (5,7-DiMe-Ox = 5,7-Dimethyl-8-hydroxyquinolinato) is illustrated by Figure 6.8. The molecule crystallizes in the orthorhombic crystal system in the *Pbca* space group with one independent molecule in the asymmetric unit and 8 formula units per unit cell (Z = 8). Selected bond distances and angles are given in Table 6.6.

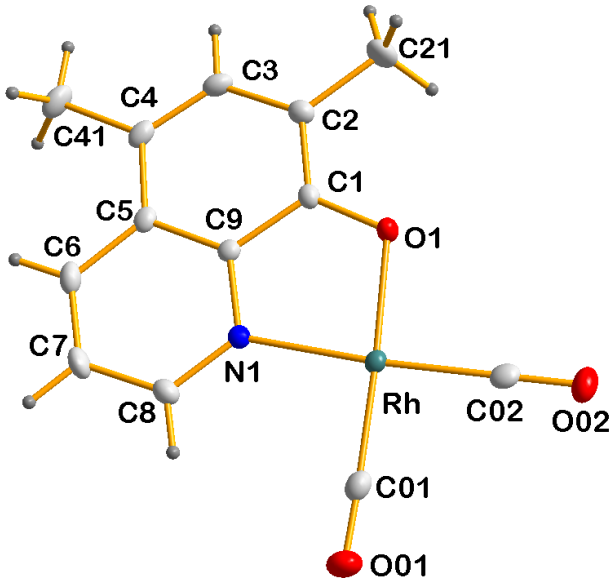

Figure 6.8: Structural representation of [Rh(5,7-DiMe-Ox)(CO)$_2$] with atom numbering scheme and displacement ellipsoids drawn at 50% probability level.

Table 6.6: Selected bond lengths (Å) and angles (˚) of [Rh(5,7-DiMe-Ox)(CO)$_2$] (8).

Atoms	Bond Lengths (Å)	Atoms	Bond Angle [°]
Rh-N1	2.075(2)	C02-Rh-C01	89.23(10)
Rh-O1	2.0333(17)	C02-Rh-O1	93.82(9)
Rh-C01	1.844(2)	C01-Rh-O1	176.27(9)
Rh-C02	1.866(2)	C02-Rh-N1	173.58(9)
Rh···Rh	3.1345(17)	C01-Rh-N1	95.76(9)
C02-O02	1.135(3)	O1-Rh-N1	81.04(7)
C1-C2	1.391(3)	O01-C01-Rh	177.7(2)
C9-N1	1.375(3)	O02-C02-Rh	179.1(18)
C1-O1	1.329(3)		
N1···O1	2.679(8)		

The rhodium(I) atom in complex **8** is coordinated by two carbonyl ligands and the oxygen and nitrogen atoms of the bidentate chelate. The rhodium central atom is located 0.0508(2) Å out of the plane constructed through O1-N1-C01-C02. The distortion from the ideal square planar geometry is indicated by the angles of 89.23(10)˚ and 81.04(7)˚ for C02-Rh-C01 and O1-Rh-N1 respectively. The Rh-N and Rh-O bond distances of 2.075(2) and 2.0333(17) Å obtained compare well with related rhodium(I) complexes with N,O donating ligand. Rh-$C_{(CO)}$ bond distances were determined to be 1.844(2) Å and 1.866(2) Å and are within the range expected for rhodium(I) carbonyl complexes with bond distances ranging between 1.791(10)-1.872(2) Å.[16,17,18,22]

The square planar complex shows rhodium-rhodium metallophillic interaction between adjacent molecules. The interaction is illustrated by the green dotted lines in Figure 6.9. The metal-metal interactions in (**8)** are however, contrary to **(7)** see Par. 6.3, restricted between two neighboring molecules and do not form extended chains but rather dimers with a Rh···Rh interaction of 3.1345(17) Å, (Figure 6.9). Thus, 'dimeric' pairs are observed in the case of **(8)**, which illustrates another kind of metallophillic interaction. This behavior is in contrast to that of complex (**7**) where an extended chain of metal-metal interactions is observed. The reason for this phenomenon is not presently clear and will be investigated in future as to why varying virtually identically sized substituents leads to different type of interaction.

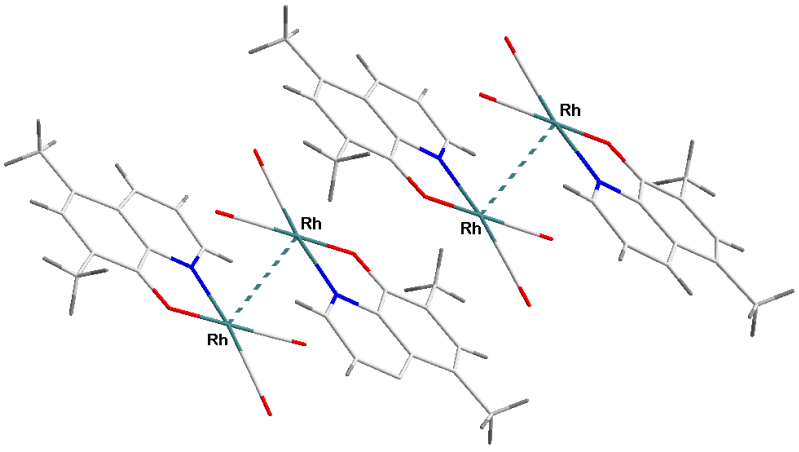

Figure 6.9: Graphical representation of the Rh···Rh interactions indicated by the green dotted lines. Hydrogen atoms were omitted for clarity.

[22] G.J.S. Venter, G. Steyl, A. Roodt, *J. Coord. Chem*. 67 (2014) 176-193.

The conformation of **(8)** leads to the formation of intermolecular hydrogen C-H…O bond interactions between neighboring molecules. The interactions are indicated by the green dotted lines in Figure 6.10 with the related data in Table 6.7

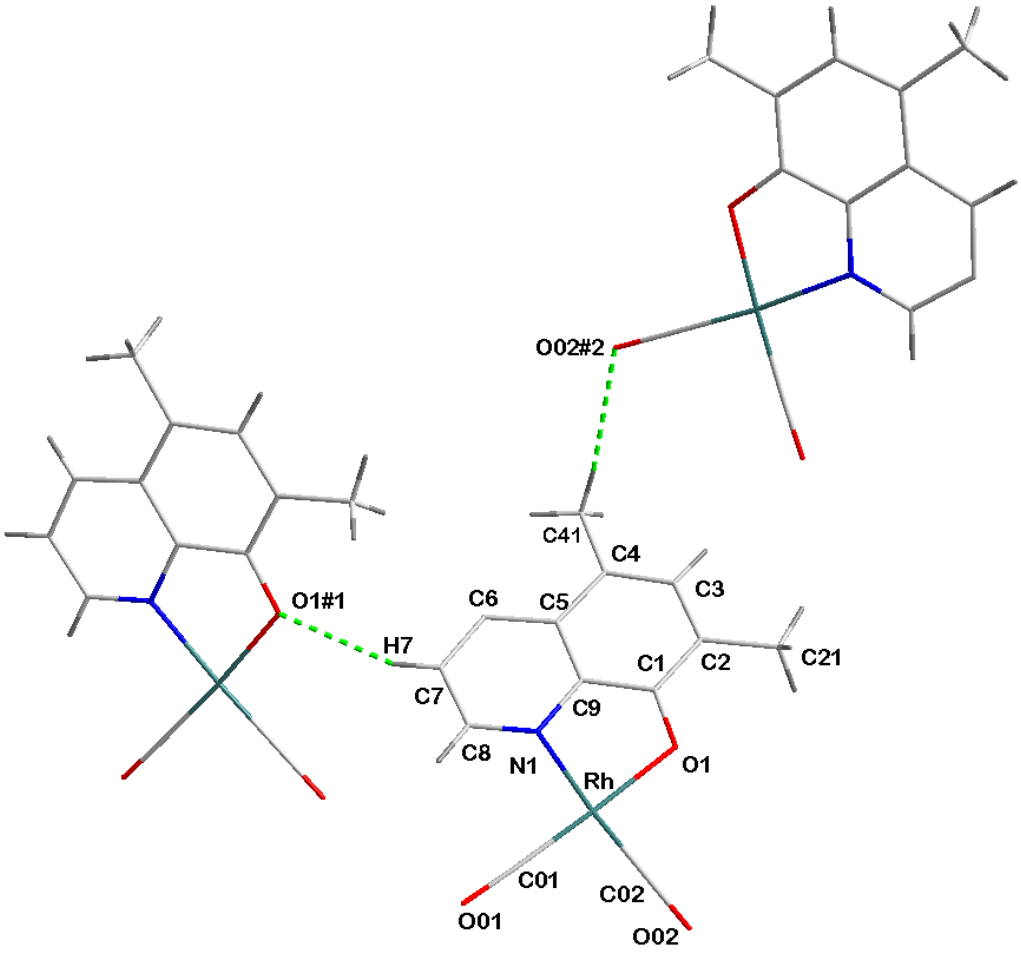

Figure 6.10: **Graphical representation of hydrogen bonding interaction. Some atom labels were omitted for clarity.**

Table 6.7: **Hydrogen bonds of [Rh(5,7-DiMe-Ox)(CO)$_2$] [Å and °].**

D-H…A	d(D-H)	d(H…A)	d(D…A)	<(DHA)
C(7)-H(7)…O(1)$^{\#1}$	0.93	2.39	3.275(4)	158(2)
C(41)-H(41C)…O(02)$^{\#2}$	0.96	2.50	3.440(4)	168(2)

Symmetry transformations used to generate equivalent atoms
#1 ½ - x, ½+ y, x; #2 ½-x, -y, ½ + z

The molecular structure is further stabilised by C-O…π interaction between C02-O02 and the aromatic ring defined by the atoms (Cg2: C1, C2, C3, C4, C5, C9) as indicated by the green dotted line in Figure 6.11 and listed in Table 6.8. The molecule is also further supported by π-π interactions as indicated in Figure 6.12 and the related data in Table 6.9.

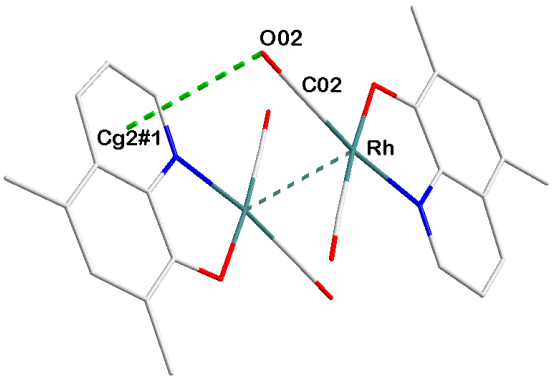

Figure 6.11: **Graphical representation of the CO …π indicated by the green dotted line. Hydrogen bonds were omitted for clarity.**

Table 6.8: **C-O …π interactions of [Rh(5,7-DiMe-Ox)(CO)$_2$] (8) [Å and ˚].**

C-O…Cg	Centroid atom	d(O…Cg) Å	d(O…Cg) Å	(C-O…Cg) (˚)
C02-O02	Cg2$^{\#1}$	3.380(3)	3.563(3)	89.90

Symmetry transformations used to generate equivalent atoms
#1 -x,-y,-z Cg2 = centroid atom of C1, C2, C3, C4, C5, C9.

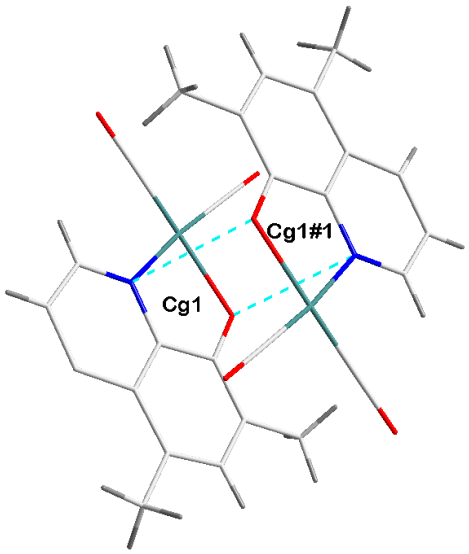

Figure 6.12: **Graphical representation of the π …π interaction indicated by the blue dotted lines. Some atom labels were omitted for clarity.**

Table 6.9: π…π interaction in [Rh(5,7-DiMe-Ox)(CO)$_2$] (8) (Å)

Centroid atom	Centroid atom	Distance between centroid atoms (Å)
Cg1	Cg1$^{\#1}$	3.886(11)

Symmetry transformations used to generate equivalent atoms
#1 -x,-y,-z Cg1 = centroid atom of Rh, O1, C1, C9, N1

Based on the structure of **(7)** as described in Par 6.3, it was anticipated that this molecule would form extended one dimensional Rh···Rh chains. However, the molecular packing in the unit cell clearly overrode this interaction between every two molecule pairs and formed dimeric units instead. This is possibly due to the interference of other noncovalent interactions such as hydrogen bonding, π···π and CO···π, as found within the molecule. The molecular packing is illustrated in Figure 6.13. However, it could also be manifested in the fact that the Rh--Rh observed in **(8)** is much shorter (and stronger) than that shown in **(8)**. The implication of this might be that much more electron density is focused between the two Rh centers in **(8)**, thus leaving less on the other side, which is required to drive the formation of infinite chains.

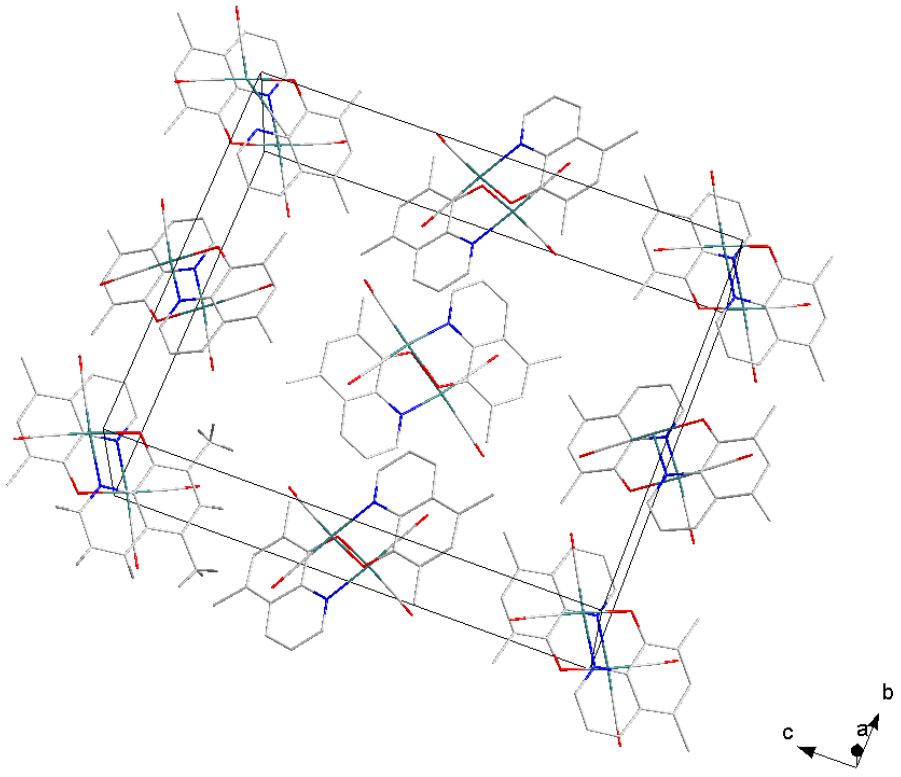

Figure 6.13: Molecular packing of [Rh(5,7-DiMe-Ox)(CO)$_2$] (8).

6.5 Crystal structure of Rh(5-Me-Sal-IsoProp)$(CO)_2$]

The complex, [Rh(5-Me-Sal-IsoProp)$(CO)_2$] **(9)**, **(**5-Me-Sal-IsoProp = 5-Methyl-2-(isopropyliminomethyl)phenolate) crystallizes in the monoclinic crystal system in the $P2_1/c$ space group with four formula units per unit cell (Z = 4). The asymmetric unit of complex **9** consists of one independent molecule. The molecular structure of **9** is illustrated by Figure 6.14 along with atom numbering scheme. Selected bond distances and angles are listed in Table 6.10.

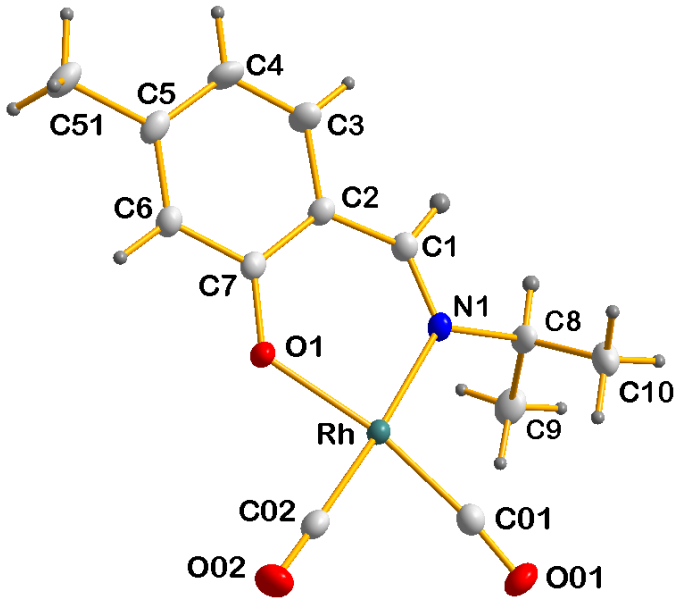

Figure 6.14: **Molecular structure of Rh(5-Me-Sal-IsoProp)$(CO)_2$] (9) showing atom numbering scheme and displacement ellipsoids drawn at 50% probability level.**

Table 6.10: **Selected bond lengths (Å) and angles (˚) of [Rh(5-Me-Sal-IsoProp)$(CO)_2$] (9).**

Atoms	Bond Lengths (Å)	Atoms	Bond Angle [°]
Rh-N1	2.0880(17)	C02-Rh-C01	85.61(10)
Rh-O1	2.0182(16)	C02-Rh-O1	85.73(8)
Rh-C01	1.846(2)	C01-Rh-O1	170.34(7)
Rh-C02	1.865(2)	C02-Rh-N1	175.88(7)
Rh···Rh	3.6007(10)	C01-Rh-N1	98.37(9)
C02-O02	1.138(3)	O1-Rh-N1	90.38(7)
C1-C2	1.437(3)	O01-C01-Rh	173.46(19)
C1-N1	1.295(3)	O02-C02-Rh	178.34(2)
O1-C7	1.305(2)	C1-C2-C7	124.09(18)
N1···O1	2.914(2)		

The rhodium(I) atom in complex (**9)** lies at the centre of a distorted square planar configuration with two carbonyl ligands and the coordinated 5Me-Sal-IsoProp through the imine N atoms and the phenolato O atoms. The deviation from the ideal square planar is evidenced by the observed angles of 85.61(10), 85.73(8) and 90.38(7)˚ for C02-Rh-C01, C02-Rh-O1 and O1-Rh-N1 respectively. The rhodium central atom is located 0.0246(2) Å out of the plane constructed through O1-N1-C01-C02. The Rh-N1 and Rh-O1 bond distances of 2.0880(17) Å and 2.0182(16) Å are typical for related complexes containing N,O donor atom. The Rh-CO bond lengths 1.846(2) Å and 1.865(2) Å are within the expected range for rhodium(I) carbonyl systems.[18,20,21,22] The plane formed by the salicylidene aromatic backbone (Plane 1: C2, C3, C4, C5, C6, C7) is bending relative to the rhodium(I) plane (Plane 2: O1-N1-C01-C02) with a dihedral angle of the 13.457(2)˚. The bending is illustrated in Figure 6.15.

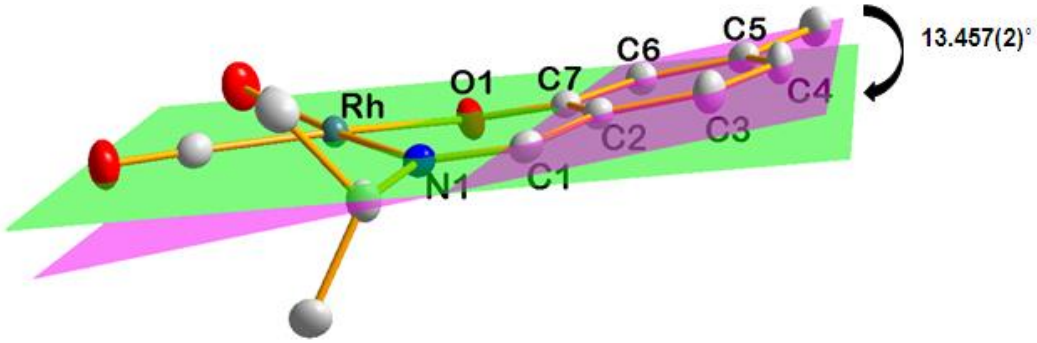

Figure 6.15: **Graphical representation of the twisting of the aromatic backbone (Plane 1 green, Plane 2 purple). Hydrogen atoms were omitted for clarity.**

The molecule packing displays quite long rhodium-rhodium interactions between neighboring molecules with a Rh···Rh distance of 3.6007(10) Å illustrated by the blue dotted line in Figure 6.16. In contrast to the infinite Rh···Rh chains displayed in complex **(7)**, complex **(9)** also displays interactions that are limited to the two immediate molecules, forming dimeric units. A similar behavior of constrained interactions was observed in complex **(8).** However, an argument was made in Par. 6.4 above that the shorter (and stronger) Rh--Rh metallophilic interactions observed in **8** might be a reason for forming dinuclear pairs. Considering the very long Rh--Rh observed in **9**, it suggests that this is not the case and driving force, and other factors are responsible for the formation of dinuclear entities, see discussion below.

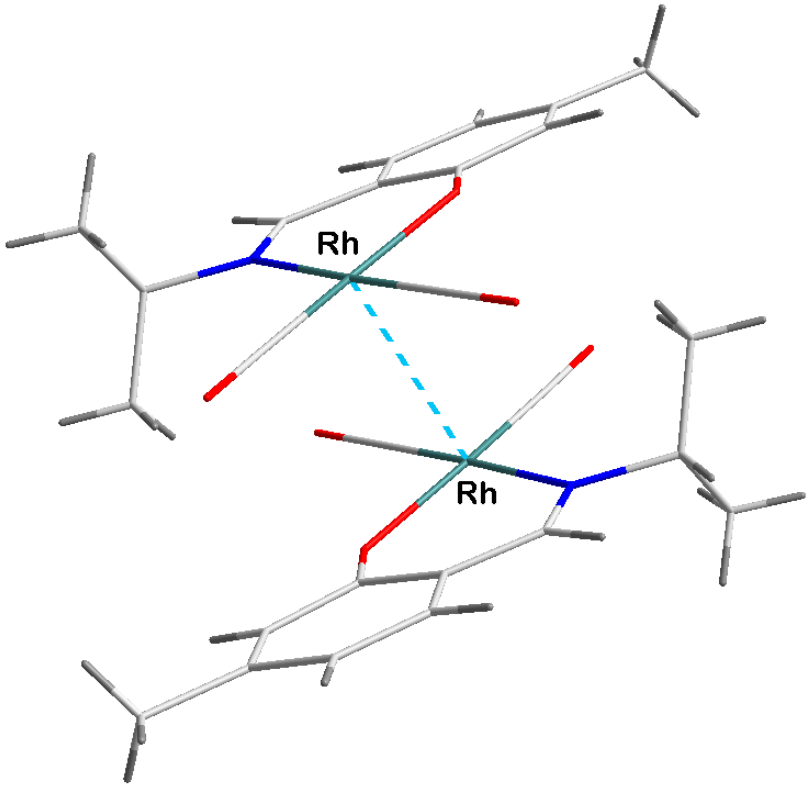

Figure 6.16: **Graphical representation of the Rh···Rh interactions indicated by the green dotted lines. Hydrogen atoms were omitted for clarity**.

Complex (**9)** displays a C-O…π interaction between C01-O01…Cg2$^{\#1}$ and the salicylidene C1 backbone aromatic ring, as indicated by the green dotted lines in Figure 6.17 and values in Table 6.11.

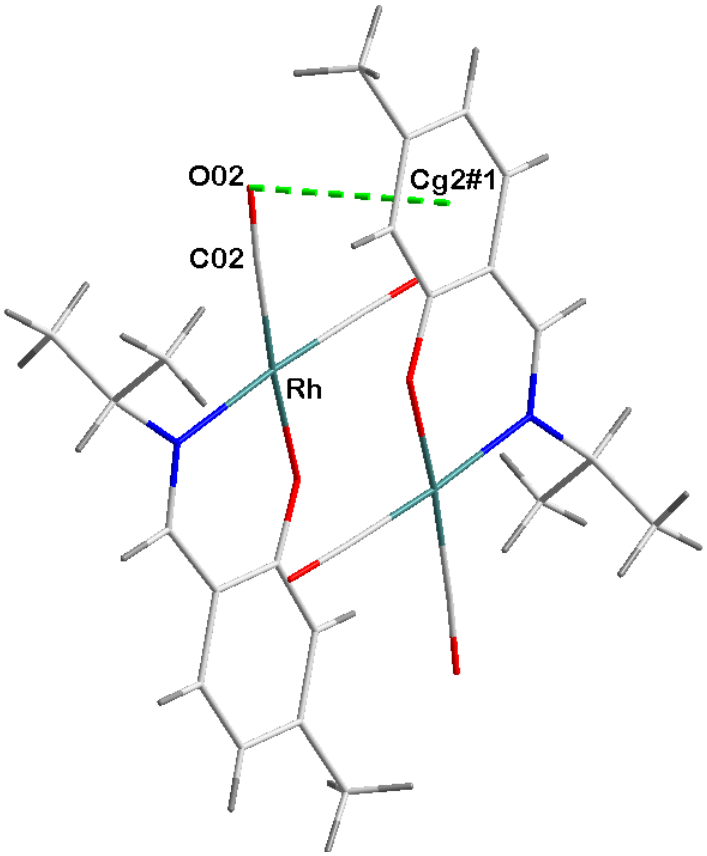

Figure 6.17: **Graphical representation of the C-O…π interaction in Rh(5-Me-Sal-IsoProp)$(CO)_2$] (9)**

Table 6.11: **C-O…π interactions of Rh(5-Me-Sal-IsoProp)$(CO)_2$] [Å and °].**

C-O…Cg	Centroid atom (Cg)	d(O…Cg) Å	d(C…Cg)	d(C-O…Cg)
C(02)-O(02)…Cg2$^{\#1}$	Cg2 #1	3.3234(9)	3.5321(10)	91.03(13)

Symmetry transformations:
#2 -x,-y,-z
Cg1 = Centroid atom of C2, C3, C4, C5, C6, C7.

Figure 6.18 illustrates the molecular packing of complex **(9)**. The figure shows the formation of the dimers through the rhodium-rhodium interactions. It was anticipated that the interactions might form a one dimensional chain along a specific axis,

however, this was not the case. Upon closer inspection of the packing motif, the metal-metal interaction occurs between units where the substituents on the imine nitrogen, i.e. the isopropyl group, is somewhat pointing away from the face. It is thus concluded with the current data in hand that the isopropyl interferes with extended rhodium-rhodium interactions.

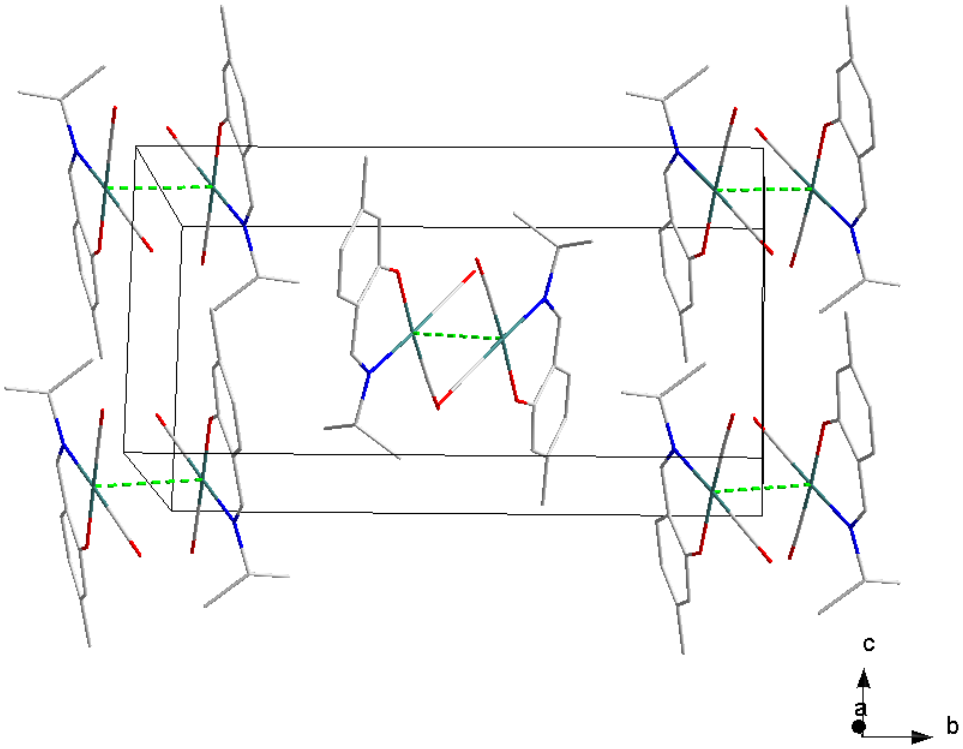

Figure 6.18: **Molecular packing of [Rh(5-Me-Sal-IsoProp)$(CO)_2$]. Hydrogen atoms were omitted for clarity.**

6.6 Discussion

Three new complexes of the general formula [Rh(N,O'-Bid)$(CO)_2$] were synthesized and characterized by X-ray crystallography and their solid-state structures were presented in this chapter. These complexes were synthesized to investigate and superficially evaluate effects from electronic and steric parameters on the extent of metal-metal interactions displayed by these rhodium(I) square-planar complexes. The coordination around the rhodium(I) centre in all three complexes consisted of two carbonyl ligands and the N,O'-bidentate chelate. The selected bidentate ligands have varying electronic and steric parameters. The ligand skeletons of **(7)** 5,7-Diido-8-hydroxyquinolinate = 5,7-Diido-Ox and **(8)** 5,7-Dimethy-8-hydroxyquinolinate = 5,7-Dimethyl-Ox contain a methyl and an iodo group respectively. An overlay structure of complex **(7)** and **(8)** is shown in Figure 6.19. These structures show good correlation with a RMS values of 0.0108 Å, and N-Rh-O ligand bite angles of 80.02(19) and 81.04(7)˚, respectively. The third ligand **(9)** (5-Methyl-2-(isopropyliminomethyl)phenolate = 5-Me-SalH-IsoProp) forms a 6-membered ring with the rhodium(I) centre in comparison to the to the 5-membered rings formed by the ligands **(7)** and **(8)**, and a corresponding N-Rh-O bite angle of 90.38(7) ˚, basically 10 ˚ larger than the oxine type ligands.

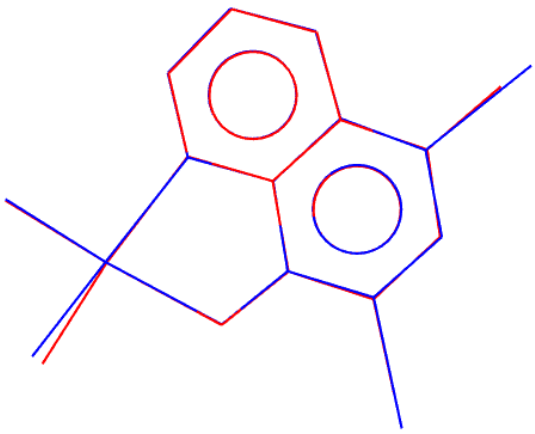

Figure 6.19: Overlay figures of the complexes [Rh(5,7-Diido)$(CO)_2$] (7) Blue), [Rh(5,7-DiMe)$(CO)_2$] (8). (Overlay drawn through the 5-memembered ring made up of atoms Rh, O1, C1, C2, C9, N1 (RMS = 0.0108 Å).

Selected bond distances and angles for the complexes–[Rh(5,7-Diido)$(CO)_2$] **(7)**, [Rh(5,7-DiMe)$(CO)_2$] **(8)** and [Rh(5-Me-Sal-IsoProp)$(CO)_2$] **(9)** are given in Table 6.12.

Table 6.12: Selected bond distances and angles of [Rh(5,7-Diido)$(CO)_2$] (7), [Rh(5,7-DiMe)$(CO)_2$] (8) and [Rh(5-Me-Sal-IsoProp)$(CO)_2$] (9) [Å and ˚].

Complex	**(7)**	**(8)**	**(9)**
Bond length (Å)			
Rh-N1	2.068(5)	2.075(2)	2.0880(17)
Rh-O1	2.052(5)	2.0333(17)	2.0182(16)
Rh…Rh	3.4602(24)	3.1345(17	3.6007(10)
Rh-C01	1.837(7)	1.844(2)	1.846(2)
Rh-C02	1.860(8)	1.866(2)	1.865(2)
C9-N1	1.376(8)	1.391(3)	1.437(3)
C1-C2	1.397(9)	1.375(3)	1.295(3)
C1-01	1.316(8)	1.329(3)	1.305(2)
N1…O1	2.914(2)	2.679(8)	2.914(2)
Bond angle (^{o})			
C02-Rh-C01	84.3(3)	89.23(10)	85.61(10)
C02-Rh-O1	99.6(2)	93.82(9)	85.73(8)
C01-Rh-O1	176.1(3)	176.27(9)	170.34(7)
C02-Rh-N1	179.6(2)	173.58(9)	175.88(7)
C01-Rh-N1	96.1(3)	95.76(9)	98.37(9)
O1-Rh-N1	80.02(19)	81.04(7)	90.38(7)
O01-C01-Rh	179.9(6)	177.7(2)	173.46(19)
O02-C02-Rh	170.6(18)	179.1(18)	178.34(2)
C1-C2-C7			124.09(18)

A distortion from the ideal square planar geometry was observed in all three complexes as evidenced by the reduction of the C01-Rh-O1 bond angles of 176.1(3), 176.27(9), 170.34(7)˚ for **(7), (8)** and **(9)** respectively. The bond angles of 80.02(19), 81.04(7) and 90.38(7)˚ were obtained for O1-Rh-N1 bite angle, and indicate that there is more strain in the 5-membered ring, **(7)** and **(8)** in comparison to the clearly less stressed 6-membered ring in **(9)**, formed by the Rh-O1-C1-C9-N1-Rh atoms, 5-membered versus the Rh-O1-C1-C2-C9-N1-Rh atoms for the 6-membered ring.

The physical crystals obtained for the complexes have intense coloring reminiscent of metal-metal interactions which was confirmed by X-ray diffraction analysis. Two types of metal-metal interactions were found in the three complexes. Firstly, an infinite one dimensional chain was observed in complex **(7)** and a restricted type of

interaction were observed in complexes **(8)** and **(9)**. The metal-metal interactions in complex **(8)** and **(9)** are confined between two neighboring molecules forming dimeric units. This effect might result in the disruption of other "competing" intermolecular interactions in the crystal packing of **(8)** and **(9)**. This suggests that the rhodium-rhodium interactions dominated in strength for complex **(7)**. The rhodium-rhodium distances of 3.4602(24) Å, 3.1345(17) Å and 3.600(7(10) Å were obtained for **(7)**, **(8)** and (**9)** respectively. The observed Rh···Rh distance in **(8)** is shorter than that in **(7)** and this difference can be attributed to the steric and electronic contribution of substituents on the 8-hydroxyquinoline skeleton in **(7)** versus **(8)**. Complex **(7)** has iodine substituents on the ligand backbone, whilst complex **(8)** contained methyl groups attached to the 8-hydroxyquinoline backbone. In the case of **(8)**, the two methyl groups are electron donating in comparison to the electron withdrawing iodine substituents in **(7)**. The iodine substituents reduce the electron density at the rhodium centre leading to less effective orbital overlap and consequently weaker and longer rhodium-rhodium interactions. The metal-metal chains are further supported by other weak interactions such as hydrogen and halogen bonding, and π-π interactions.

6.7 Conclusion

In this chapter three rhodium(I) complexes of the general formula [Rh(N,O-Bid)$(CO)_2$] (where N,O'-Bid = mononegative N,O-bidentate ligands) were presented. The objective was to evaluate the N,O-ligands as chelators for the Rh(I) metal centre and evaluate possible contributions of steric and electronic properties on the metallophillic interactions. The three structures showed two types of rhodium-rhodium interactions. In the one mode, the interactions form infinite chains in one direction and in the other mode, the rhodium-rhodium interactions are restricted between two adjacent molecules forming pseudo dinuclear units. These results obtained imply that the coordinated ligand influences not only the magnitude of the metal-metal interactions, but also the stacking arrangement.

At present, the main challenge associated with these complexes is obtaining additional suitable single crystals for X-ray analysis involving a broad range of N,O'-bidentate ligands systems. More attempts to obtain suitable single crystals will be

undertaken in future in order to have a more broader study that may contribute towards the understanding and control of metallophilic interactions.

The forthcoming chapter presents the reactivity of rhodium(I) Schiff-base complexes as model catalysts by evaluating a fundamental catalytic reaction, i.e. the iodomethane oxidative addition. The reason for this is that it is imperative to not only understand the structural information, but also the reactivity, pathways and the formation of intermediates in order to design more effective compounds for application in fields such as homogeneous catalysis and nuclear medicine and thus, structure-activity relationships.

7 Kinetic Study of the Iodomethane Oxidative Addition to [Rh(N,O-Schiff-Base)(CO)(PPh_3)] Complexes

7.1 Introduction

The oxidative addition reaction represents a key step in a variety of catalytic reactions such as carbonylation of alcohols, hydroformylation of alkenes and cross-coupling reactions.[1,2] An important example is the rhodium-iodide supported carbonylation of methanol to produce acetic acid, i.e the Monsanto process.[3,4,5] Numerous studies have been undertaken in order to improve the catalytic activity of the rhodium based complex by introducing ligands with different electronic and steric properties and evaluating their effect on the overall catalytic activity.[6,7]

The rhodium(I) square planar complexes of the type [Rh(L,L-Bid)(CO)(PPX_3)], where L,L-Bid = monoanionic bidentate ligands and PX_3 are tertiary phosphine ligands, have been investigated extensively as potential catalyst precursors.[8,9,10,11,12,13,14,15,16] These [Rh(L,L'-Bid)(CO)(PPX_3)] complexes are in

[1] J. A. Labinger, *Organometallics*. 34 (2015) 4784-479.
[2] F.O. Arp, G.C. Fu, *J. Am. Chem. Soc*. 127 (2005) 10482-10483.
[3] P.M. Maitlis, A. Haynes, G.J. Sunley, M.J. Howard, *J. Chem. Soc. Dalton Trans*. (1996) 2187-2196
[4] M. Gauss, A. Seidel, P. Torrence, and P. Heymans, Applied Homogeneous Catalysis with Organometallic Compunds, ed. B. Cornils, and W.A. Herrmann, VCH, New York, 1996
[5] D. Forster*, J. Am. Chem. Soc*. 98 (1976) 846-848
[6] L.M. Rendina, R. J. Puddephatt, *Chem. Rev.* 97 (1997) 1737-1754.
[7] D. Foster, *J. Am. Chem. Soc*. 98 (1976) 846-848.
[8] A. Roodt , H. G. Visser, A. Brink. *Crystallogr.* Rev. 17 (2011) 241-280.
[9] S. Warsink, F.G. Fessha, W. Purcell, J.A. Venter, *J. Organomet. Chem*. 726 (2013) 14-20.
[10] M.M. Conradie, J. Conradie, *Dalton Trans*. 40 (2011) 8226-8237.
[11] A Brink, A. Roodt, G. Steyl, H.G. Visser, *Dalton Trans*. 39 (2010) 5572–5578.
[12] S.S. Basson, J. G. Leipoldt, A. Roodt, J.A. Venter, T.J. Van Der Walt, *Inorg. Chim. Acta*. 119 (1986) 35-38.
[13] J. Conradie, G.J. Lamprecht, A. Roodt, J.C. Swarts, *Polyhedron*. 23 (2007) 5075-5087.
[14] A. Roodt, G.J.J. Steyn, Recent Res. Devel*. Inorganic. Chem*. 2 (2000) 1-23.

general easily obtained from the substitution of one carbonyl ligand in the parent complex Rh(L,L'-Bid)$(CO)_2$], by monodentate tertiary phosphines. The complexes described and discussed in Chapter 7 are good examples of these precursors. The substitution of one carbonyl ligand from the parent dicarbonyl complex may lead to the formation of two isomers as illustrated in Figure 7.1. Studies have indicated the high selectivity of the carbonyl substitution when there is a pronounced difference in the nature of the donating and accepting properties between the donor atoms L and L'.[17,18,8,19] The atom with the lowest electronegativity (stronger donor) directs the substitution, *i.e*, the major isomer will contain the phosphine ligand trans to the stronger donor e,g (sulphur or nitrogen if O,S or O,N). If the donor atoms have comparable donor capabilities, the isomers form in comparable ration, specifically for complexes such as asymmetrical β-diketonenates.[20,21] However, since the kinetics of Rh(I) is usually extremely fast, reorganization of the [Rh(L,L-Bid)(CO)(PX_3)] to form the more stable thermodynamic isomer will primarily determine the pathway of the next steps.

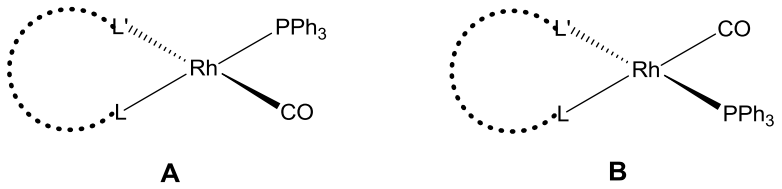

Figure 7.1: Illustration of the possible isomers in the substitution reaction of complex Rh(L,L'-Bid)$(CO)_2$] with a monodentate tertiary(PPX_3) phosphines

This present study serves as a continuation of the investigations on the effect(s) of coordinated bidentate ligands on the oxidative addition reaction, specifically evaluating the model Schiff base ligand systems' effects on the fundamental oxidative addition reaction.

---

[15] S.S. Basson, J.G. Leipoldt, A. Roodt, J.A. Venter, *Inorg. Chim. Acta*.128 (1987) 31-37.
[16] S.S. Basson, J.G. Leipoldt, J.A. Venter, Acta Crystallogr. C46 (1990) 1324-1326.

[17] J.G. Leipoldt, S.S. Basson, S.S, C.R. Dennis, *Inorg. Chim. Acta*. 50 (1981) 121-124.
[18] J.G. Leipoldt, S.S. Basson, J.T. Nel, *Inorg. Chim Acta*. 74 (1983) 85-88.
[19] J.G. Leipoldt, L.D.C. Bok, J.S. van Vollenhoven, A.I. Pieterse, J*. Inorg. Nucl. Chem*. 40 (1978) 61-63.
[20] I.A. Poletaeva, T.G. Cherkasova, L.V. Osetrova, Y.S. Varshavsky, A. Roodt, J.G. Leipoldt, *Rhodium Express*. 3 (1994) 21-27.
[21] A.M. Treciak, J.J. Ziolkowski, *Inorg. Chim. Acta*. 96 (1985) 15-20.

Chapter 7

The synthesis and characterization of the complexes used for the evaluations has been presented in the Chapter 3, where the starting complexes were characterized by IR and ^{31}P-NMR spectroscopies. The crystallographic characterization of the starting [Rh(L,L-Bid)(CO)(PPX_3)] complexes and the oxidative addition products has not yet been successful. However, the range of the Schiff base complexes which were successfully synthesized are pure and is the topic covered in this chapter.

The selected Schiff-base ligands have varying electronic and steric parameters as informed by the cyclopentyl, isopropyl, cyclohexyl and the methyl substituents attached to the imine nitrogen atom. The effects of these various factors on the rate of oxidative addition will be evaluated in order to further understand the role of the coordinated ligand on the oxidative addition reaction. Figure 7.2 illustrates the ligands selected for preparing the corresponding Rh(I) complexes for evaluation in the kinetic study.

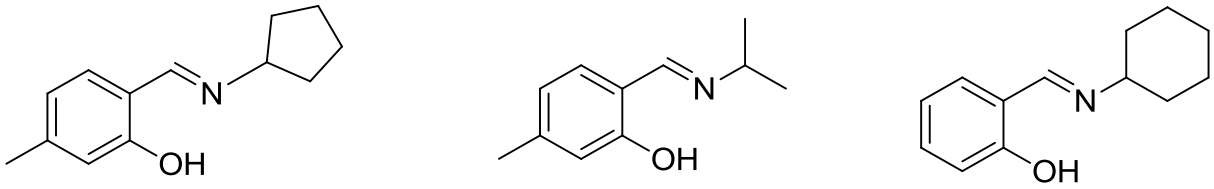

a **b** **c**

Figure 7.2: The general formula the Schiff-base ligands used for the oxidative addition investigations. (a) (5-Me-Sal-CyPentH = 2-(cyclopentyl)methyl-5-methylphenol, (b) (5-Me-Sal-IsoPropH = 5-Methyl-2-(isopropyliminomethyl)phenol and (c) (Sal-CyHexH = 2-(cyclohexyliminomethyl)phenol.

7.2 Experimental

All chemicals used in this study were of analytical grade and used as purchased from Sigma-Aldrich, South Africa, unless stated otherwise. The rhodium metal complexes were synthesised, characterized and purified as described in Chapter 3. The UV-vis measurements were collected using a Varian 50 Conc UV/Vis spectrophotometer, equipped with a Julabo F12-mV temperature cell regulator (accurate within 0.1°C) in 1.000 $\pm$ 0.001 cm tandem quartz cuvette cells. ^{31}P NMR spectra were recorded on a 400 MHz Bruker spectrometer. ^{31}P NMR spectra were recorded on a 400 MHz Bruker spectrometer operating at the ^{31}P frequency of 161.98 MHz (2074 scans, pulse of 30° and delay time of 1.89 s). The FT-IR spectra were recorded as liquid samples in dry dichloromethane in a NaCl cell on a Bruker Tensor 27 spectrometer in the range of 2350-1600 cm^{-1}, equipped with a temperature cell regulator accurate within ±0.3 °C.

All the kinetic experiments were performed under *pseudo* first order conditions and the data was processed using the Scientist Micromath version 2.01 software package.[22]

7.3 General rate laws

The Beer-Lambert Law relates the absorption of light to the concentration of a solution, by the following equation:

$$\boldsymbol{A_t = A_\infty(A_\infty - A_0)e^{k_{obs}t}} \qquad \textbf{...7.1}$$

Where A_0 and A_t are the absorbance's at time 0 and t, A_∞ is the absorbance at time infinity and k_{obs} is the pseudo first-order rate constant of the reaction determined from a least-squares fit of absorbance *vs* time data.

[22] Micromath Scientist for Windows, Version 2.01, copyright © 1986-1995, MicorMath, Inc

A direct relationship of the observed pseudo first-order rate constants on the iodomethane concentration was observed in this study in preliminary measurements, as found in many literature examples, see Par 7.4 below..[7,9,23] The results are thus consistent with the rate expression given by Equation 7.2, defining the oxidative addition and the reductive elimination steps in the mechanism.

$$k_{obs} = k_1[\mathrm{CH_3I}] + k_{-1} \qquad \textbf{…7.2}$$

In Eq. 7.2 k_1 and k_{-1} represent the first-order rate constant of the oxidative addition and reductive elimination steps, respectively.

Once the second order rate constants have been determined as a function of temperature, these data is then translated into the linear Eyring relationship (Equation 7.3) from which the standard activation enthalpy ($\Delta H^{\neq}$) and the standard activation entropy changes ($\Delta S^{\neq}$) are determined.

$$\ln\frac{k}{T} = \frac{-\Delta H^{\neq}}{RT} + \ln\frac{k_B}{h} + \frac{\Delta S^{\neq}}{\mathrm{R}} \qquad \textbf{…7.3}$$

A plot of $\ln\frac{k}{T}$ vs $\frac{1}{T}$ gives a linear relation with a slope defined by $\frac{-\Delta H^{\neq}}{R}$ and intercept of $\ln\frac{k_B}{h} + \frac{\Delta S^{\neq}}{\mathrm{R}}$

Here k is the experimentally determined second-order rate constant at temperature *T*, determined from Eq. 7.7, *R* is the Universal Gas Constant, k_B the Boltzmann Constant and *h* Planck's Constant.

[23] J.J.C. Erasmus, J. Conradie, *Dalton Trans.* 42 (2013) 8655-8666.

7.4 Results and discussion

7.4.1 Reaction mechanism

The general mechanism for the oxidative addition of iodomethane to [Rh(L,L'-Bid)(CO)(PX_3)] complexes has been determined previously and is given by Scheme 1.[9] The mechanism includes the formation of two succeeding species, namely, rhodium alkyl and acyl species as illustrated in Scheme 7.1. The iodomethane is oxidatively added to the rhodium(I) complex leading to the formation of the alkyl (d) species, followed by the migratory insertion of the CO ligand into the Rh-methyl bond to the form the acyl product (c). In some cases, a solvent dependent pathway is observed as indicated in Scheme 7.1.[9]

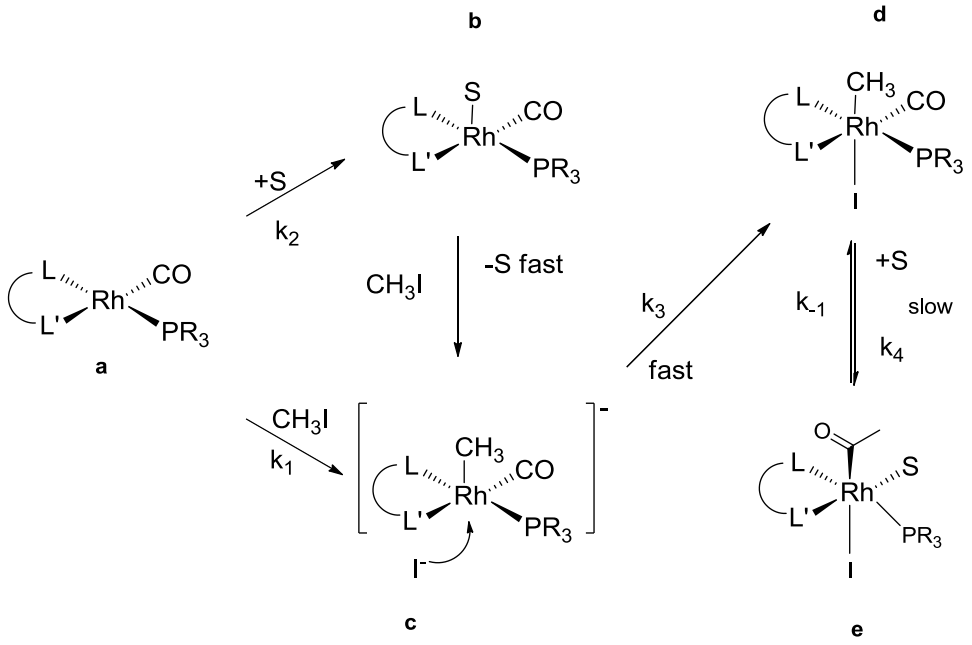

Scheme 7.1: A representation of a typical scheme for the oxidative addition of iodomethane to the rhodium [Rh(L,L'-Bid)(CO)(PX_3)], PX_3 = tertiary phosphine complexes.[9] S = solvent molecule.

The oxidative addition of iodomethane to the rhodium(I) complexes [Rh(5-Me-Sal-CyPent)(CO)(PPh_3)] **(1)**, [Rh(5-Me-Sal-IsoProp)(CO)(PPh_3)] **(2)** and [Rh(Sal-

CyHex)(CO)(PPh_3)] **(3)** was monitored by IR, ^{31}P-NMR, and UV/Vis spectroscopies for the identification of reaction intermediates and products.

In this study, the oxidative addition of iodomethane to the rhodium(I) Schiff-base complexes indicated the rapid formation of the alkyl(III) product and no subsequent formation of the acyl product was observed as evidenced by the FT-IR and ^{31}P-NMR spectra. This is possibly due to the very slow rate of formation of the acyl species relative to the alkyl product. The investigations of this study will thus only focus on the oxidative addition step. Figure 7.3 **(i)** illustrates the disappearance of the [Rh(5-Me-Sal-CyPent)(CO)(PPh_3)] Rh(I) complex at $\mathbf{\nu_{(CO)}}$ = 1955 cm^{-1} with the corresponding simultaneous growth of the Rh(III) at $\mathbf{\nu_{(CO)}}$ = 2056 cm^{-1} upon the addition of iodomethane. A similar trend was obtained in complexes **(2)** and **(3)**. The absence of the corresponding acyl product was confirmed by ^{31}P NMR investigations as shown in Figure 7.4.

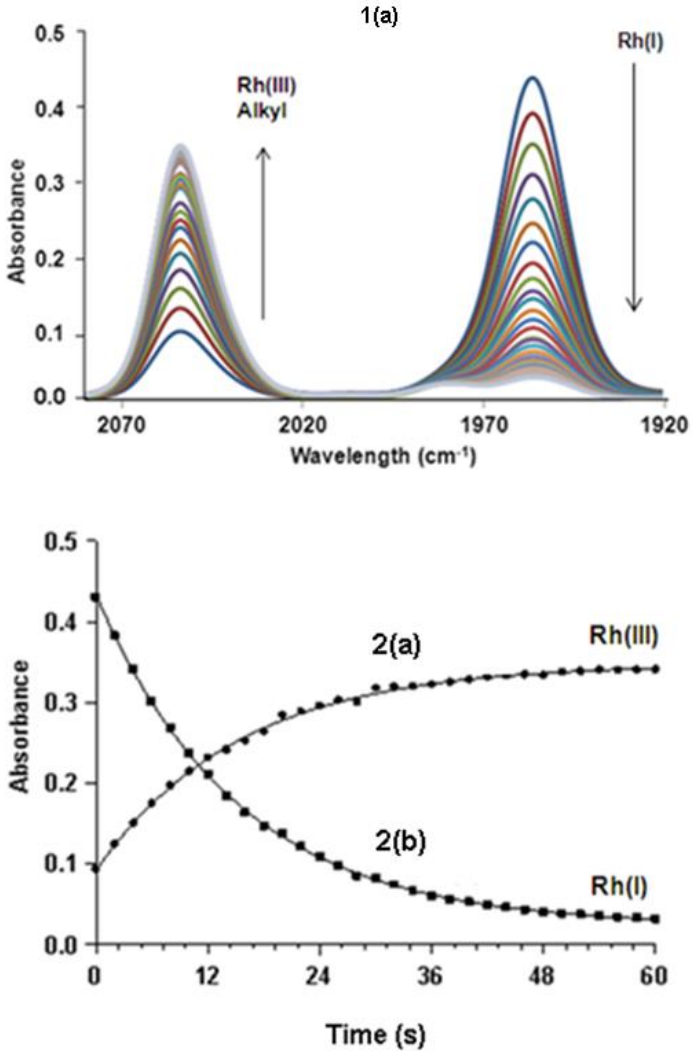

Figure 7.3: **IR scans 1(a) for the oxidative addition of iodomethane to [Rh(5-Me-Sal-CyPent)(CO)(PPh_3)] (1) in dichloromethane at 25 °C, 2(b) illustrates the disappearance of the Rh(I) (k_{obs} = 0.0657(5)) species with the simultaneous growth 2(a) of the Rh(III) (k_{obs} = 0.0650(1)) alkyl species. [Rh(5-Me-Sal-CyPent)(CO)(PPh_3)] = 9 x 10^{-3} M, [MeI] = 0.12 M, Δt = 2 s.**

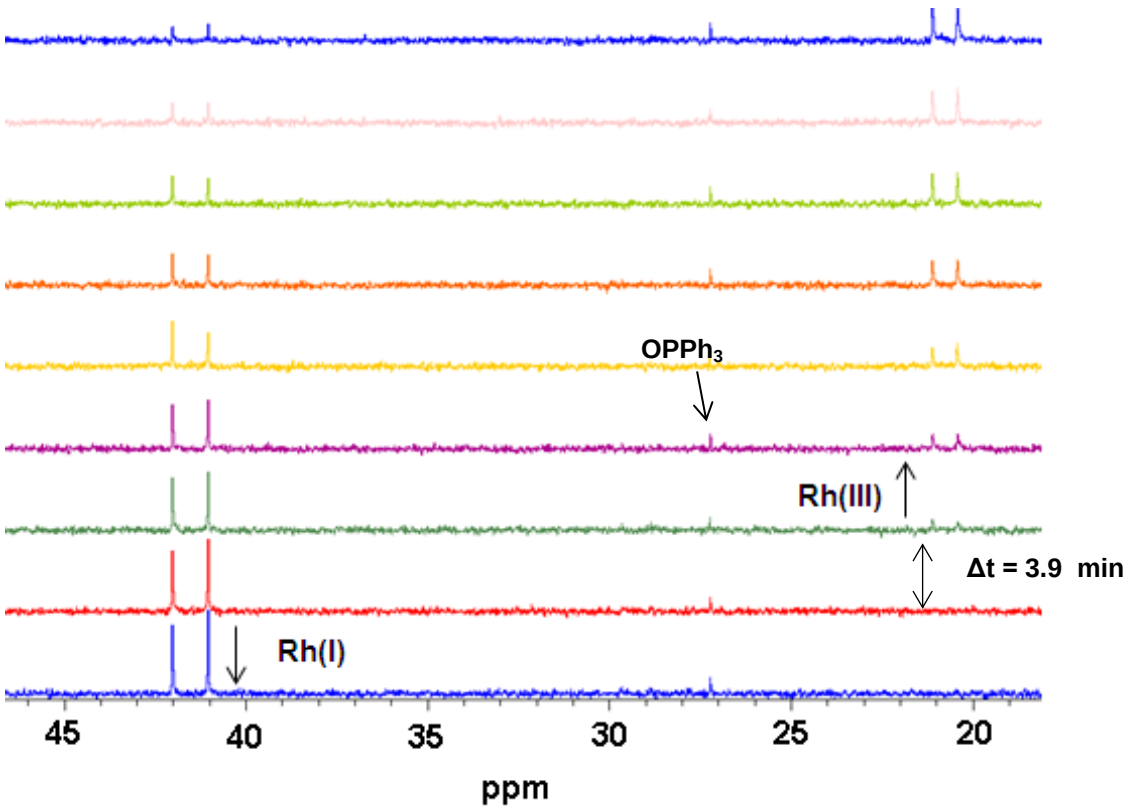

Figure 7.4: **Successive ^{31}P-NMR spectra for the disappearance of Rh(I) species and the simultaneous formation of the Rh(III) alkyl species for the reaction of [Rh(5-Me-Sal-CyPent)(CO)(PPh$_3$)] (1) with iodomethane in dichloromethane at 25 °C; [Rh(I) = 6 x 10^{-3} M, [MeI] =0.06 M. Δt = 2 min.**

A summary of the FT-IR data for the reaction of the three complexes [Rh(5-Me-Sal-CyPent)(CO)(PPh$_3$)] **(1)**, [Rh(5-Me-Sal-IsoProp)(CO)(PPh$_3$)] **(2)** and [Rh(Sal-CyHex)(CO)(PPh$_3$)] **(3)** with iodomethane is given in Table 7.1.

Table 7.1: **IR kinetic data for the oxidative addition of iodomethane to the complexes [Rh(5-Me-Sal-CyPent)(CO)(PPh$_3$)] (1), [Rh(5-Me-Sal-IsoProp)(CO)(PPh$_3$)] (2) and [Rh(Sal-CyHex)(CO)(PPh$_3$)] (3) in dichloromethane at 25 °C; [Rh] =9 x 10^{-3} M, λ = 432 nm and [MeI] = 0.12 M**

Complex		$\nu_{(CO)}$ (cm^{-1})	k_{obs}(s^{-1})	$^1J_{Rh-P}$(Hz)
[Rh(5-Me-Sal-CyPent)(CO)(PPh$_3$)]	Rh(I)	1955	0.0657(5)	157.6
(1)	Rh(III) alkyl	2054	0.0650(1)	109.8
[Rh(5-Me-Sal-IsoProp)(CO)(PPh$_3$)]	Rh(I)	1955	0.0558(6)	158.5
(2)	Rh(III) alkyl	2054	0.0540(1)	111.0
[Rh(Sal-CyHex)(CO)(PPh$_3$)]	Rh(I)	1957	0.0590(1)	155.8
(3)	Rh(III) alkyl	2054	0.0490(3)	111.4

From the results presented in Table 7.1, it is clear that the rate of Rh(I) disappearance for all three complexes is the same as the rate of Rh(III) alkyl formation. The values are comparable within experimental error. The observed rates for the oxidative addition step are comparable with an approximate increase of about 1.3 times in the order of **(1)** > **(2)** > **(3)** .. This result implies that there is not much electronic variation introduced on the metal centre by the three ligands in spite of the variations of the steric and electronic parameters of the ligand backbone as manifested by the methyl group and the cyclopentyl, isopropyl and the cyclohexyl groups, respectively as attached to the imine nitrogen atom. This is corroborated by the first order coupling constant of the complexes which were found to be 109.8, 111.0 and 111.4 Hz for complex (1), (2) and (3) respectively. This is further supported by the $\nu_{(CO)}$ stretching frequencies The FT-IR spectrum obtained for the oxidative addition reactions indicate an equilibrium reaction inferring a solvent independent pathway. A solvent dependency study will be done in future.

The electronic and steric influence of the ligands on the rate of oxidative addition reaction between iodomethane and the rhodium(i) Schiff-base complexes, [Rh(5-Me-Sal-CyPent)(CO)(PPh_3)] **(1)**, [Rh(5-Me-Sal-IsoProp)(CO)(PPh_3)] **(2)** and [Rh(Sal-CyHex)(CO)(PPh_3)] **(3)** was also evaluated with UV/Vis spectroscopy. Figure 7.5 illustrates the overall spectral changes for both the disappearance of the Rh(I) starting complex and the formation of the Rh(II) alkyl species. It is difficult to discriminate between the two species in solution because of the spectra overlap. A similar spectral trend was obtained in all three complexes

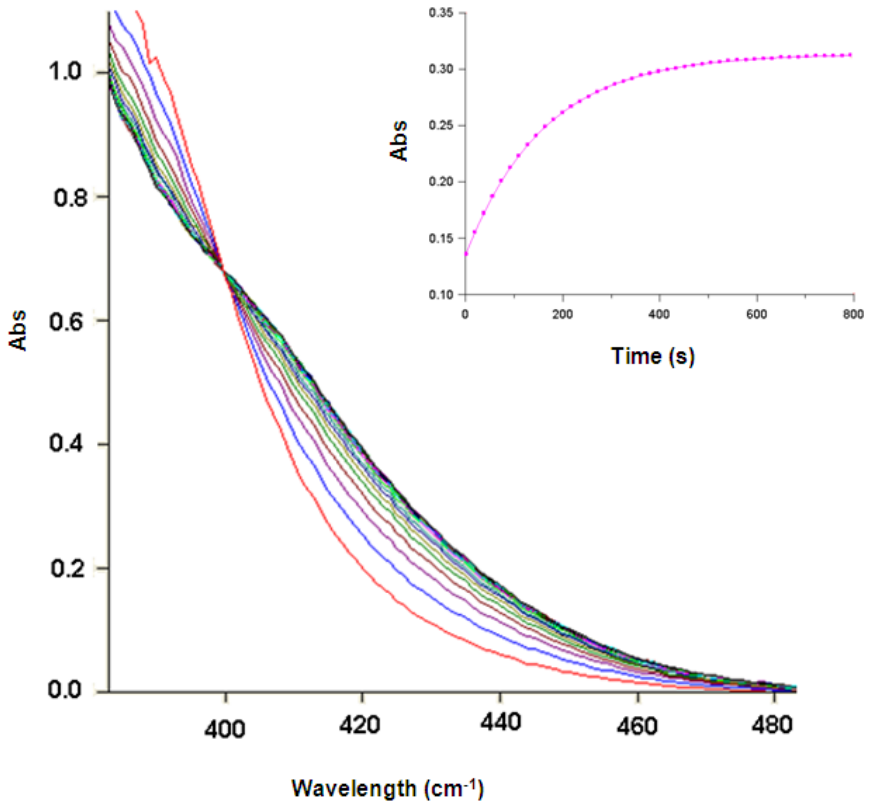

Figure 7.5: **Typical Uv/Vis spectral change for the reaction between iodomethane and [Rh(5-Me-Sal-CyPent)(CO)(PPh_3)] in dichloromethane at 25 °C, [Rh] = 3 x 10^{-4} M, λ = 432 nm, Δt = 20 s and [MeI] = 0.12 M.**

A summary of the UV/Vis kinetic study obtained for the reaction of iodomethane with the complexes [Rh(5-Me-Sal-CyPent)(CO)(PPh_3)] **(1)**, [Rh(5-Me-Sal-IsoProp)(CO)(PPh_3)] **(2)** and [Rh(Sal-CyHex)(CO)(PPh_3)] **(3)**. The related data is presented in Table 7.2

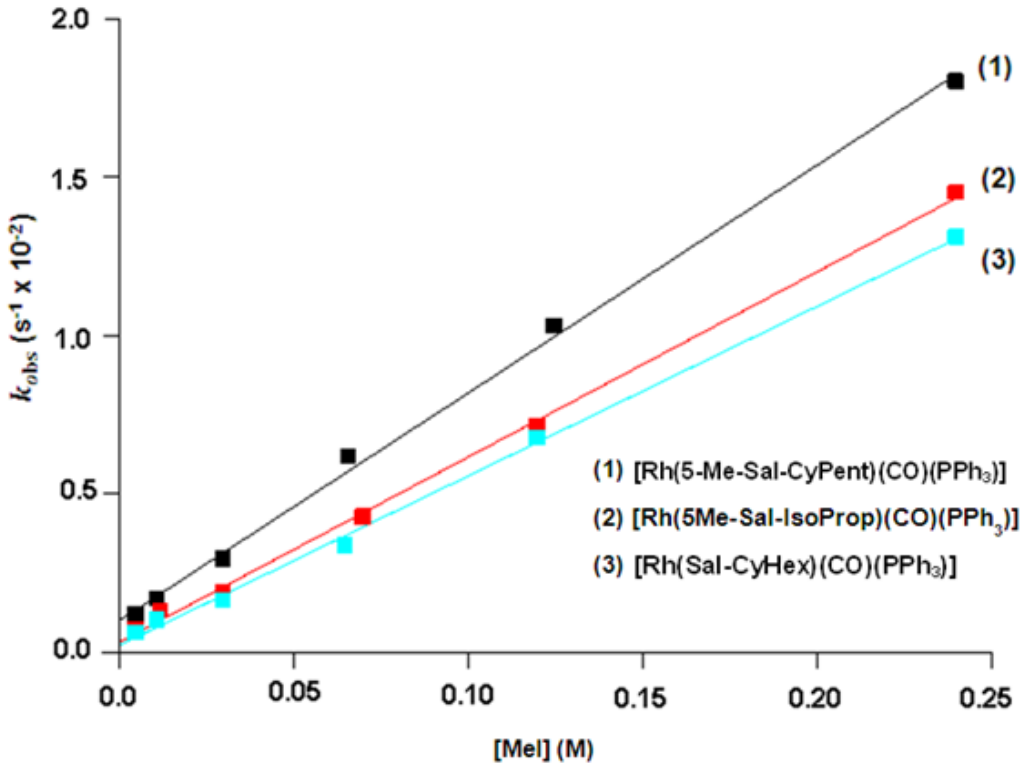

Figure 7.6: **Plots of the observed rate constants *vs* iodomethane concentrations for the iodomethane oxidative addition to complexes [Rh(5-Me-Sal-CyPent)(CO)(PPh_3)] (1), [Rh(5-Me-Sal-IsoProp)(CO)(PPh_3)] (2) and [Rh(Sal-CyHex)(CO)(PPh_3)] (3) in dichloromethane at 25 °C; [Rh] = 3 x 10^{-4} M, λ = 432 nm and [MeI] = 0.004-0.24 M.**

Table 7.2: **Kinetic data obtained for the iodomethane oxidative addition to [Rh(5-Me-Sal-CyPent)(CO)(PPh_3)] (1), [Rh(5-Me-Sal-IsoProp)(CO)(PPh_3)] (2) and [Rh(Sal-CyHex)(CO)(PPh_3)] (3) in dichloromethane at 25 °C. [Rh] = 3 x 10^{-4} M, λ = 432 nm and [MeI] = 0.004-0.24 M.**

Complex	k_1 ($M^{-1}.s^{-1}$)	k_{-1} (M^{-1})	$^1J_{Rh-P}$ (Hz)
[Rh(5-Me-Sal-CyPent)(CO)(PPh_3)] (1)	0.072(2)	0.001(2)	157.6
[Rh(5-Me-Sal-Iso)(CO)(PPh_3)] (2)	0.058(1)	0.0003(1)	158.5
[Rh(Sal-CyHex)(CO)(PPh_3)] (3)	0.054(1)	0.0002(1)	155.8

The UV/Vis kinetic study for the three rhodium(I) Schiff-base complexes show a liner dependency between the observed rate constant and the iodomethane concentration. The results obtained are consistent with those obtained for the FT-IR kinetic study in that, there is approximately 1 order of magnitude difference in rate

in the order of (1) > (2) > (3). The relatively small intercepts k_{-1} values obtained supports the proposed notion of a direct mechanism with no solvent dependent pathway.

7.4.2 Temperature dependence of oxidative addition

A variable temperature study for the oxidative addition of iodomethane to the complex [Rh(5-Me-Sal-CyPent)(CO)(PPh_3)] was conducted. The data was treated using Equations 7.2 and 7.3 the observed rate constants are given in Table 7.3. Figure 7.7 illustrates the overall spectral changes observed in the UV-Vis scans for the oxidative addition of iodomethane to [Rh(5-Me-Sal-CyPent)(CO)(PPh_3)]. Due to the slow rate of formation of the Rh(III) acyl product relative to the alkyl(III), only the oxidative addition step was evaluated. Because of the overlapping spectral changes between the disappearance of Rh(I) starting material and the formation of the Rh(III) alkyl species, the combined effect of the two processes is thus observed and illustrated in Figure 7.7.

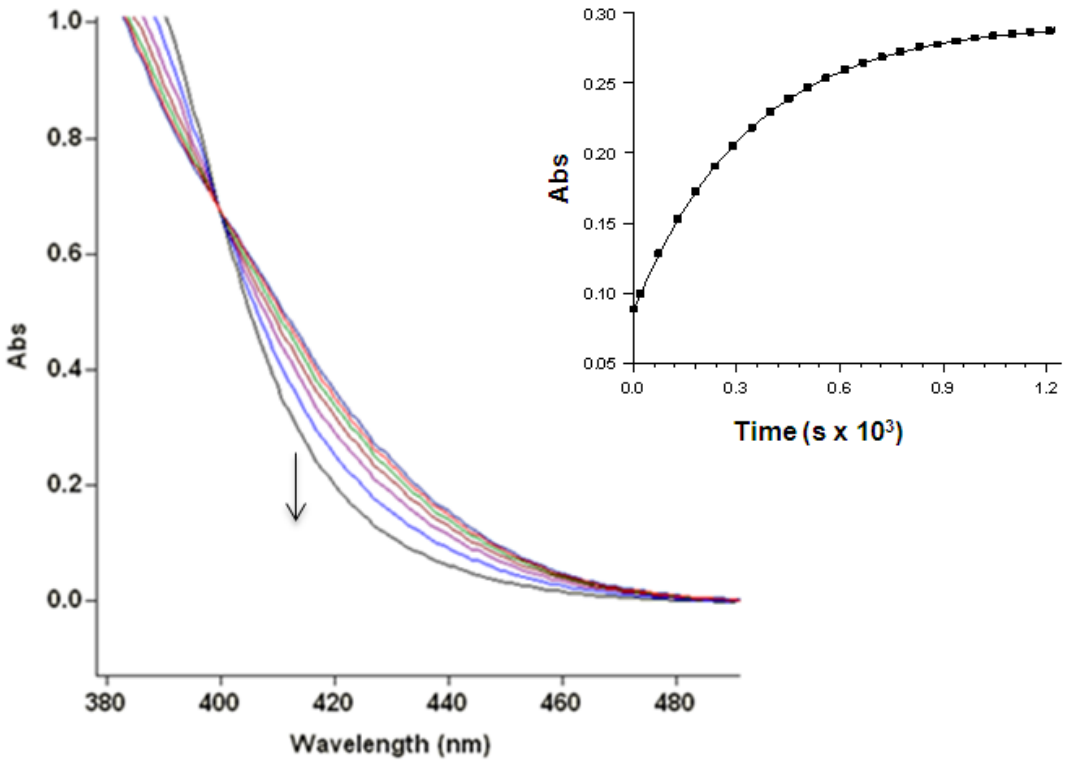

Figure 7.7: Typical Uv/Vis spectral change for the reaction between iodomethane and [Rh(5-Me-Sal-CyPent)(CO)(PPh_3)] in dichloromethane at 25 °C, [Rh] = 3.26 x 10^{-4} M, λ = 432 nm, Δt = 20 s and [MeI] = 0.24 M.

Figure 7.8 illustrates the linear relationship between the observed pseudo-first order rate constants and the iodomethane concentration at different temperatures.

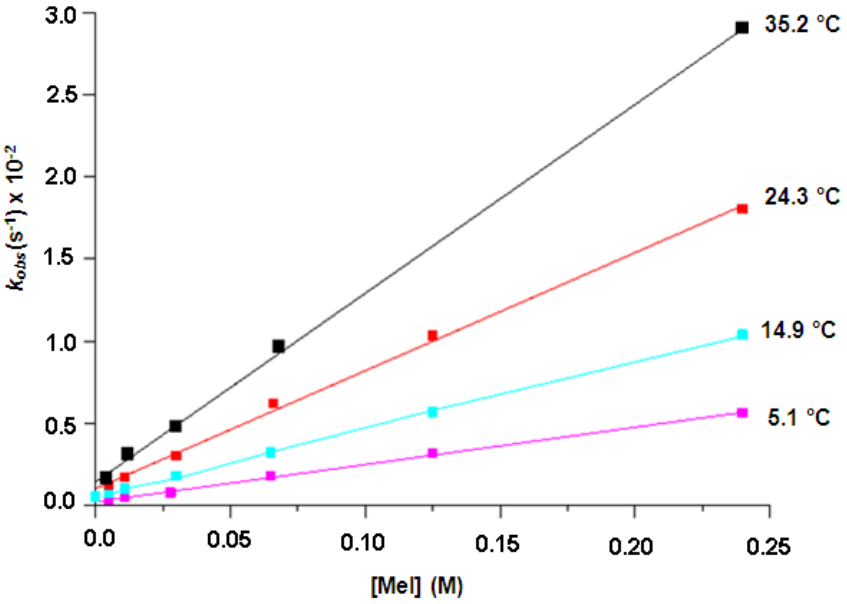

Figure 7.8: **Plots of the observed rate constants *vs* iodomethane concentrations for the iodomethane oxidative addition to [Rh(5-Me-Sal-CyPent)(CO)(PPh_3)] at various temperatures; [Rh] = 3.26 x 10^{-4} M, λ = 432 nm and [MeI] = 0.004-0.24 M.**

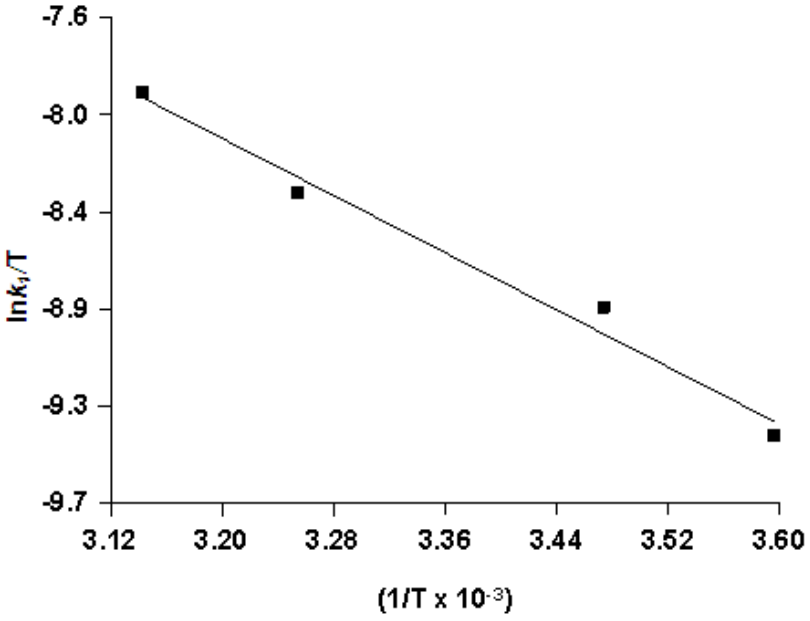

Figure 7.9: **Eyring plot of the pseudo-first order rate constants (k_1) for the formation of [Rh(5-Me-Sal-CyPent)(CH_3)(I)(CO)(PPh_3)] in dichloromethane.**

Table 7.3: A summary of the rate constant and activation parameters for the reaction of [Rh(5-Me-Sal-CyPent)(CO)(PPh_3)] and iodomethane at various temperatures; [Rh] = 3.26 x 10^{-4} M, λ = 432 nm and [MeI] = 0.004-0.24 M.

Constants	5.1 ^{0}C	14.9 ^{0}C	24.3 ^{0}C	35.2 ^{0}C
$10^2 k_1$ ($M^{-1}.s^{-1}$)	2.27(5)	4.11(6)	7.2(2)	11.5(2)
$10^3 k_1$ ($M^{-1}.s^{-1}$)	0.195(6)	0.49(6)	1.0(2)	1.4(2)
K_1 (M^{-1})	116(9)[a]	84(16)[a]	72(15)	82(12)
$\Delta H^{\neq}$ (kJ mol^{-1})			36(1)	
$\Delta S^{\neq}$ (J K^{-1} mol)			-145(5)	

[a] values should be treated as estimation

The activation parameters for the oxidative addition of iodomethane to the complex [Rh(5-Me-Sal-CyPent)$(CO)_2(PPh_3)$] were determined from the variable temperature study in dichloromethane. The data was fitted to the Eyring Equation 7.3. The values were found to be $\Delta H^{\neq}$ = 36(1) kJ mol^{-1} and $\Delta S^{\neq}$ = -145(5) (J K^{-1} mol). The relatively small $\Delta H^{\neq}$ and the large negative $\Delta S^{\neq}$ value are characteristic of an associative type mechanism. The UV-vis variable temperature study (k_{obs} *vs.* [MeI] *vs*. Temp] gave straight lines, see Figure 7.8, with relatively small intercepts. These values indicate that the oxidative addition reaction in these rhodium(I) Schiff-base complexes is probably not solvent assisted [product b in Scheme 7.1 negligible within conditions studied herein]. This is supported by the data obtained from the IR studies indicating an equilibrium between the disappearance of the rhodium(I) starting complex and the formation of the rhodium(III) alkyl product.

$$\ln\frac{k}{T} = \frac{-\Delta H^{\neq}}{RT} + \ln\frac{k_B}{h} + \frac{\Delta S^{\neq}}{\mathrm{R}} \qquad \textbf{...7.3}$$

The oxidative addition of alkyl halides to metal complexes is an important reaction in many catalytic processes. Herein, the reactivity of rhodium(I) Schiff-base complex towards oxidative addition of iodomethane was evaluated. The contribution of steric and electronic parameters on the rate of oxidative addition of iodomethane to rhodium(I) complexes of the type was investigated. Due to the slow rate of formation of the rhodium(III) acyl species, only the rhodium(III) intermediate was assessed in this study. As mentioned above, unexpected irregularity was observed,

similarly pointed out in other related reactivity studies.[11] The rate of the reaction was expected to be decelerated through systematic replacement of the phenyl rings in the phosphine ligands by sterically bulkier and more electron rich cyclohexyl groups. The results obtained herein, (see following Paragraph) which clearly do not yield a systematic change, imply that there is still much work to do with regards to understanding the structure and reactivity correlation of these [Rh(L,L'-Bid)(CO)(PX_3)] type complexes.

7.4.3 The effect of tertiary aryl phosphine ligands on the oxidative addition of iodomethane to [Rh(5-Me-Sal-CyPent)(CO)(PPX_3)] , PPX_3 = PPh_3, PCY_3, PPh_2Cy, $PPhCy_2$

A major application of phosphine containing metal complexes is in homogenous catalysis. It has been shown in many studies that the activity of the metal centres can be manipulated by affecting changes on the steric and electronic parameters of a phosphine ligand. In order to expand the understanding of the contributions of electronic and steric parameters in the reactivity of rhodium(I) complexes towards oxidative addition reactions, a preliminary UV/vis kinetic study of the oxidative addition of iodomethane to the a series of rhodium(I) complexes, [Rh(5-Me-Sal-CyPent)(CO)(PPX_3)], (PPX_3 = PPh_3 **1(a), 1(b)** PPh_2Cy, **1(c)** $PPhCy_2$ and **1(d)** PCy_3, was conducted. Sterically demanding ligands have been shown to retard the rate of oxidative addition, whilst ligands with electron-donating properties have the ability to enhance the reaction rate. The electronic and steric differences in the phosphine ligands used herein are manifested by the systematic replacement of the weaker electron donating phenyl rings by the electron rich and sterically demanding cyclohexyl rings.

The selected monophosphine ligands for the investigations are presented in Figure 7.10.

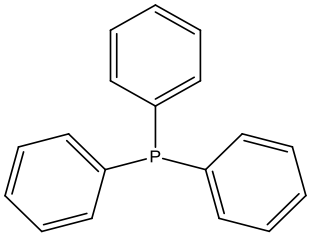

a

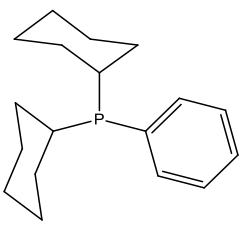

c

b **d**

Figure 7.10. **Tertiary phosphine ligands used in this study; (a) triphenylphosphine (PPh_3); (b) Cyclohexyldiphenylphosphine = PPh_2Cy, (c) dicyclohexyl-phenylphosphine = $PPhCy_2$ and (d) tricyclohexylphosphine = PCy_3.**

The rhodium(I) complexes; [Rh(5-Me-SalCyPent)(CO)(PPh_3)] **1(a)**, Rh(5-Me-Sal-CyPent)(CO)(PPh_2Cy)] **1(b)**, [Rh(5-Me-Sal-CyPent)(CO)($PPhCy_2$)] **1(c)** and [Rh(5-Me-Sal-CyPent)(CO)(PCy_3)] **1(d)** were obtained from the reaction of the parent complex, [Rh(5-Me-Sal-CyPent)$(CO)_2$)] with the series of the tertiary phosphine ligands. The oxidative addition reaction of iodomethane with the rhodium(I) complexes was studied at different methyl iodide concentrations as illustrated in Figure 7.12 . The data was fitted to Equation 7.2 and the results are given in Table 7.4.

From Figure 7.11, it can be clearly seen that all three rhodium(I) Schiff base complexes react with iodomethane to form exclusively the rhodium(III) alkyl product. Previous studies have indicated the tendency of complexes of the type [Rh(L,L-Bid)(CO)(PX_3)] to form the alkyl species as the final product when the donor atoms are oxygen and nitrogen, L,L'-Bid= N,O-Bid.[24] The alkyl Rh(I)-CO stretching frequencies are at about 2054, 2054, 2039 and 2035 cm^{-1} for complexes **1(a)**, **1(b)**, **1(c)** and **1(d)** respectively.

[24] D.E. Graham, G.J. Lamprecht, I.M. Potgieter, A. Roodt, J.G. Leipoldt, *Trans. Met. Chem*. 16 (1991) 193-195.

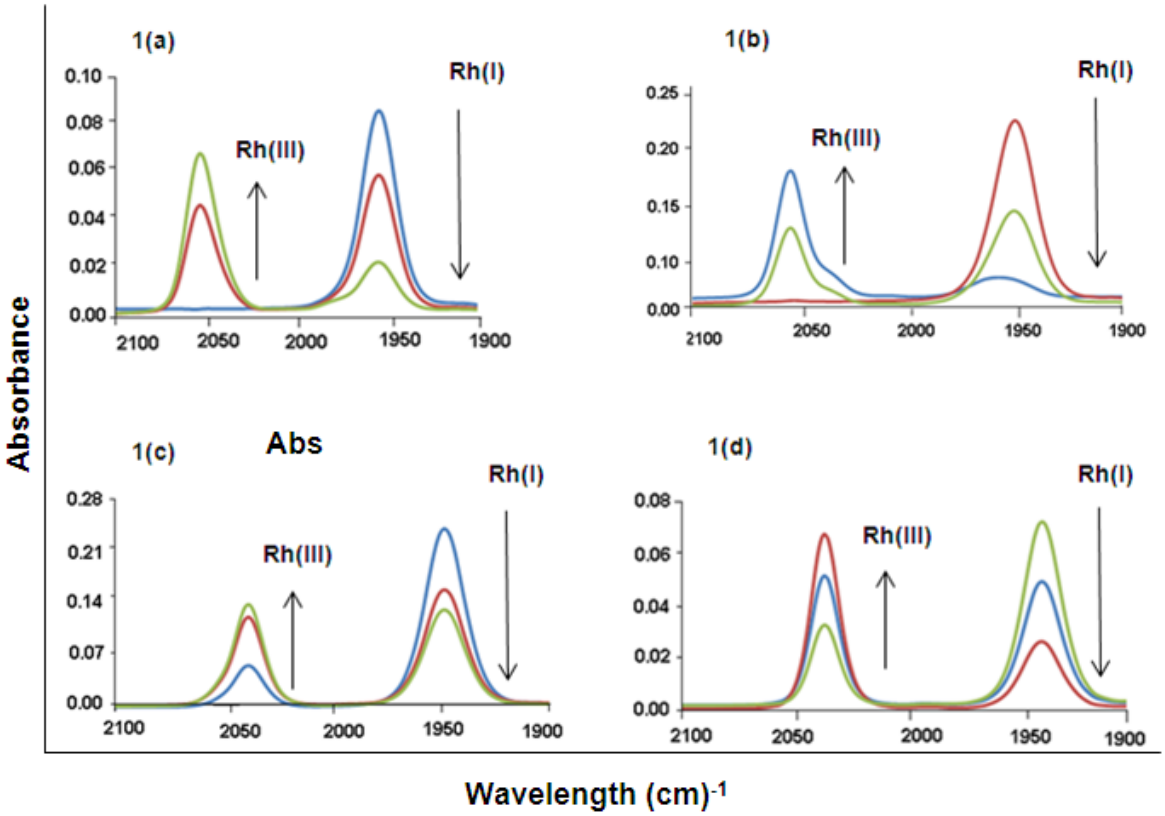

Figure 7.11 **Illustration of the IR scans for the conversion of the rhodium(I) complexes to the rhodium(III) alkyl species. [Rh(5-Me-Sal-CyPent)(CO)(PPh_3)] 1(a), Rh(5-Me Sal-CyPent)(CO)(PPh_2Cy)] 1(b), [Rh(5-Me-Sal-CyPent)(CO)($PPhCy_2$)] 1(c) and [Rh(5-Me-Sal-CyPent)(CO)(PCy_3)] 1(d) in dichloromethane at 25 °C. [Rh] = 9 x 10^{-3} M, [MeI] = 0.12 M, Δt = 2 s.**

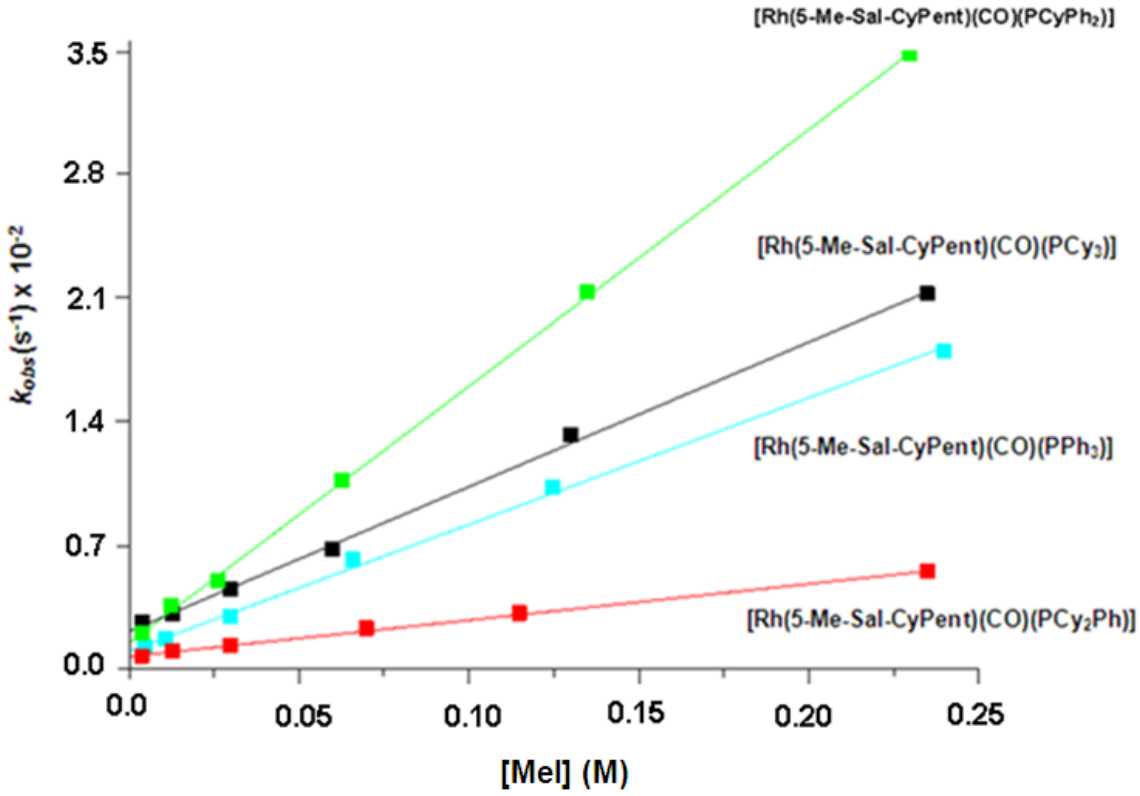

Figure 7.12: **The effect of tertiary phosphine ligands on the oxidative addition of iodomethane to [Rh(5-Me-Sal-CyPent)(CO)(PPX_3)] (PPX_3 = PPh_3, PCY_3, PPh_2Cy, $PPhCy_2$) in dichloromethane at 25 °C using the UV/Vis spectroscopy. [Rh] = 3 x 10^{-4} M, λ = 432 nm and [MeI] = 0.004-0.24 M for all reactions.**

Table 7.4: **A summary of the rate constants for the reaction of [Rh(5-Me-Sal-CyPent)(CO)(PPX_3)] (PPX_3 = PPh_3, PCY_3, PPh_2Cy, $PPhCy_2$) with iodomethane in dichloromethane using the UV/Vis spectroscopy. [Rh] = 3 x 10^{-4} M, λ = 432 nm and [MeI] = 0.004-0.24 M for all reactions.**

PPX_3	PPh_3	PPh_2Cy	$PPhCy_2$	PCy_3
k_1 ($M^{-1}.s^{-1}$)	0.072(2)	0.146(1)	0.026(5)	0.082(1)
$10^3 k_{-1}$ ($M^{-1}.s^{-1}$)	1.0(2)	1.47(2)	0.71(5)	2.13(2)
K_1 (M^{-1})	72(5)	99 (14)	37(7)	39(4)
Effective cone angle(°)	150	163	151	170

The UV/Vis kinetic study of the oxidative addition corroborated the IR evidence on the absence of the second reaction, i.e. the formation of the acyl product. This again can be attributed to the slow rate of formation of the acyl product as well as the small extinction coefficient of the rhodium(III) acyl product. Since the rhodium(I) centre acts as a nucleophile under the oxidative addition reaction, naturally one expects an increase in activation of the metal centre towards oxidative addition when replacing weaker electron donating phenyl rings of the phosphine ligands by the larger cyclohexyl rings.

However, the results obtained for the different phosphine ligands suggest otherwise. According to Figure 7.6 and Table 7.3, a decrease in the rate of formation is observed in the order [Rh(5-Me-SalCyPent)(CO)(PPh_2Cy)] > [Rh(5-Me-SalCyPent)(CO)(PCy_3)] > [Rh(5-Me-SalCyPent)(CO)(PPh_3)]> [Rh(5-Me-SalCyPent)(CO)(PPh_2Cy)]. A difference of about 3 times is observed between [Rh(5-Me-SalCyPent)(CO)(PPh_2Cy)] > [Rh(5-Me-SalCyPent)(CO)(PCy_3)]. These results suggest interplay between the steric and electronic parameters in these complexes. A more detailed kinetic study of the electronic and steric contribution of the tertiary phosphine ligands will be conducted in future.

7.5 Conclusion

In this study rhodium(I) Schiff-base complexes of the type [Rh(L,L-Bid)(CO)(PPX_3)] were synthesized via the facile substitution of the carbonyl ligand in the parent complex Rh(L,L'-Bid)$(CO)_2$], by monodentate tertiary phosphines. ^{31}P-NMR spectra of the complexes exhibit a single doublet, which is indicative of the presence of only one specific isomer while IR also clearly show the formation of one product. The formation of only one isomer product from the carbonyl substitution in the parent complex [Rh(L,L'-Bid)$(CO)_2$] simplifies the kinetic investigations. The complexes were synthesized to evaluate how factors such as electronic and steric characteristics of the bidentate ligands, the differences in the monodentate tertiary phosphines and the temperature influence the rate of oxidative addition reaction.

Chapter 7

The understanding of structure and reactivity dynamics is important in the development of more effective catalysts. Herein, variations in electron density around the rhodium(I) metal centre were accomplished by introducing varying substituents on the Schiff-base bidentate ligands. The data obtained for the iodomethane oxidative addition reaction in complexes **(1)**, **(2)** and **(3)** are comparable in spite of the varying electronic and steric parameters on the ligand backbone. There is about a factor of 2 increase in second-order rate constants between complex **(1)** and **(2)**. Apart from the steric contribution of the substituents, the effect may also be electronic contribution of the methyl group attached in the ligand backbone of complex **(1)** and **(2)**. The methyl group donates electron density to the ligand backbone, consequently increasing the electron density around the metal centre activating it towards the oxidative addition of the iodomethane.

A systematic replacement of the phenyl groups from the electron poor ligand PPh_3 to the more steric demanding cyclohexyl groups showed a decrease in oxidative addition rate as opposed to the expected increase. There is approximately 6-times increase of the reaction rate from $PPhCy_2$ to PPh_2Cy tertiary phosphine ligands. A possibility may be the “competition” of the contribution of steric *vs*. electronic parameters of the tertiary phosphine ligands. More elaborate studies on the contribution of the tertiary phosphine on the rate of oxidative addition will be conducted in future. The temperature effect on the reaction of [Rh(5-Me-Sal-CyPent)(CO)(PPh_3)] (**1**) with iodomethane was studied at four different temperatures in dichloromethane. The values obtained for the activation parameters ($\Delta H^{\neq}, \Delta S^{\neq}$) indicate an associative type mechanism as characterized by large negative $\Delta S^{\neq}$ accompanied by a small $\Delta H^{\neq}$. The results imply that there is still much work to do with regards to understanding the structure and reactivity correlation of [Rh(L,L-Bid)(CO)(PPX_3)] type complexes.

To this effect, a preliminary attempt is made utilizing solid state NMR, as described in Chapter 8, to take the study of these complexes forward by introducing the data obtained in the solid state via advance NMR and further correlate the aspects of importance and identify aspects to be investigated in future.

8 Preliminary Solid-State NMR Investigation on [Rh(L,L'-Bid)(CO)(PX_3)] Complexes

8.1 Introduction

As indicated in Chapter 7 above, the rhodium(I) square planar complexes of the type [Rh(L,L'-Bid)(CO)(PPX_3)], where L,L'-Bid = monoanionic bidentate ligands and PPX_3 are tertiary phosphine ligands, have been extensively investigated as potential catalyst precursors[1,2,3,4,5,6,7,8,9,10] in different conversion reactions. These rhodium(I) complexes are in general obtained from the substitution of one carbonyl ligand in the complexes [Rh(L,L'-Bid)($CO)_2$] (Chapter 6), by simple stoichiometric reaction with monodentate tertiary phosphines.

The accurate characterization of crystalline material is important for the understanding of their structural dynamics, and solution state NMR spectroscopy and X-ray diffraction (XRD) are the two most commonly used techniques for structural determination in chemical applications.

Unfortunately, the crystallographic characterization of the starting complexes (and the corresponding oxidative addition products as described in Chapter 7) has not yet been successful. For current unknown reasons, suitable crystals of none of the

[1] A. Roodt , H. G. Visser, A. Brink. *Crystallogr. Rev*. 17 (2011) 241-280.
[2] S. Warsink, F.G. Fessha, W. Purcell, J.A. Venter, *J. Organomet. Chem.* 726 (2013) 14-20.
[3] M.M. Conradie, J. Conradie, *Dalton Trans*. 40 (2011) 8226-8237.
[4] A Brink, A. Roodt, G. Steyl, H.G. Visser, *Dalton Trans*. 39 (2010) 5572–5578.
[5] S.S. Basson, J. G. Leipoldt, A. Roodt, J.A. Venter, T.J. Van Der Walt, *Inorg. Chim. Acta*. 119 (1986) 35-38.
[6] J. Conradie, G.J. Lamprecht, A. Roodt, J.C. Swarts, *Polyhedron.* 23 (2007) 5075-5087.
[7] A. Roodt, G.J.J. Steyn, Recent Res. Devel. Inorganic. Chem. 2 (2000) 1-23.
[8] J.J.G. Gideon, A. Roodt, I. Poletaeva, Y.S. Varshavsky, *J. Organomet. Chem*. 536-537 (1997) 197-205
[9] S.S. Basson, J.G. Leipoldt, A. Roodt, J.A. Venter, *Inorg. Chim. Acta*. 128 (1987) 31-37.
[10] S.S. Basson, J.G. Leipoldt, J.A. Venter, *Acta Crystallogr*. C46 (1990) 1324-1326.

rhodium(I) Schiff base complexes [Rh(L,L'-Bid)(CO)(PPX_3)], where L,L'-Bid = monoanionic bidentate Schiff-base ligands and PPX_3 are tertiary phosphine ligands, could be isolated in the present study, in spite of significant efforts to this regard (see Chapter 3). Reasons are assumed to be due to the dynamics of substituents on the periphery of the molecules, coupled with the fact that they readily undergo oxidative addition reactions (for example, with molecular oxygen and also different solvents).

It was thus identified that solid-state NMR spectroscopy techniques may in this study serve as a bridge between solution state NMR and X-ray diffraction to generate more knowledge on the structures. Solid-state NMR studies may thus provide an opportunity to have a closer look at the solid *vs*. solution state behavior of the compounds which might enable a better prediction and translation to the solution state and possible structural relationship(s).

Hence, in a preliminary attempt to circumvent the problem of non-crystalline compounds of the Schiff-base compounds, in this chapter a solid-state ^{31}P NMR study is introduced. This aims to contribute to the overall understanding of the coordination environment around the metal centre and are essential for the rationale synthesis of highly selective catalysts and also drugs, such as radiopharmaceutical models. (For example, a large number of administered drugs are solids, but their developmental processes are mainly in the solution state.)

Thus, preliminary investigations on the solid and solution state ^{31}P NMR relationship in the tertiary phosphine complexes of these [Rh(L,L'-Bid)(CO)(PPX_3)] (L,'L-Bid = monoanionic bidentate Schiff-base ligands) as shown below in Figure 8.1, were conducted and are reported herein. The synthesis and characterization of the complexes used in this chapter have been presented in Chapter 3 and all complexes were characterized by IR and ^{31}P-NMR spectroscopies.

The data is then compared with solid-state NMR spectra of other related rhodium(I) complexes and solid-state structures reported elsewhere to attempt correlations as described below.

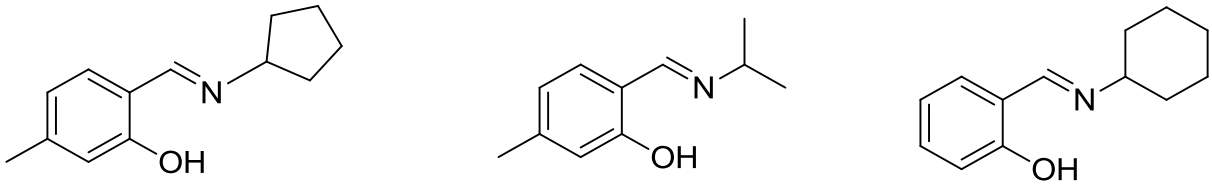

a **b** **c**

Figure 8.1: **The general formula the Schiff-base ligands used for the solid-state investigations. (a) (5-Me-Sal-CypentH = 2-(cyclopentyl)methyl-5-methylphenol, (b) (5-Me-Sal-IsoPropH = 5-Methyl-2-(isopropyliminomethyl)phenol and (c) (Sal-CyHexH = 2-(cyclohexyliminomethyl)phenol.**

8.2 Experimental

All chemicals used in this study were of analytical grade and used as purchased from Sigma-Aldrich, South Africa, unless stated otherwise. The rhodium metal complexes were synthesised, characterized and purified as described in Chapter 3.
All chemicals used in this study were of analytical grade and used as purchased from Sigma-Aldrich, South Africa, unless stated otherwise. The rhodium metal complexes were synthesised, characterized and purified as described in Chapter 3.
The solution and solid state ^{31}P NMR spectra were collected on a Bruker 400. spectrometer operating at the ^{31}P frequency of 161.98 MHz. The cross-polarisation and magic angle spinning techniques (CP/MAS) were implemented and the spectra were acquired at a spinning speed of 14 kHz.

All the data was processed using the Scientist Micromath version 2.01 software package.[11]

[11] Micromath Scientist for Windows, Version 2.01, copyright © 1986-1995, MicorMath, Inc

8.3 Results and discussion

As indicated, in this study the aim was to use ^{31}P NMR and X-ray crystallography in conjunction to investigate the structure and reactivity relationship of the rhodium(I) complexes for potential application in catalysis.

Solution and solid ^{31}P NMR spectra of rhodium(I) complexes were recorded and the corresponding data is summarized in Table 8.1 below. Cross polarization/magic angle spinning (CP/MAS) was used for solid samples. As expected, typical broad lines were obtained for many of the solid-state spectra, characteristic of data collected by CP/MAS. Figure 8.2 indicates typical spectra for solution and solid-state NMR.

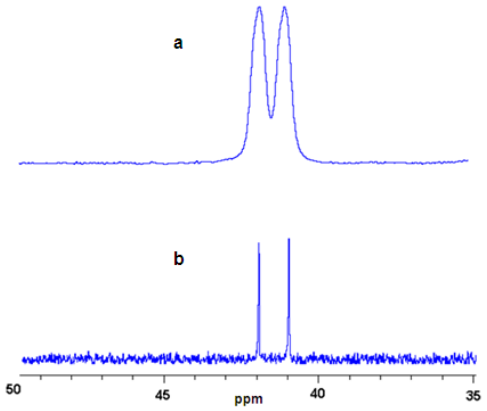

Figure 8.2: **Solid-state (a) and solution state (b) ^{31}P NMR spectra of [Rh(Sal-CyHex)(CO)(PPh$_3$)].**

Table 8.1: Comparison of Rh-P bond distances and NMR parameters obtained in solution and solid-state for [Rh(L,L-Bid)(CO)(PPX_3)] complexes

	Bond distance		Solution State		Solid-state	
Complex	**Rh-P Å**	***V* (CO) cm^{-1}**	**$\delta^{31}P$ ppm**	**$^1J_{Rh-P}$ Hz**	**$\delta^{31}P$ ppm**	**$^1J_{Rh-P}$ Hz**
[12]Trop-PPh_3	2.232(2)	1978	48.7	173.6	52.7	176.2
[13]Cup-PPh_3	2.232(2)	1982	48.9	170.3	53.6	171.1
CyHex-PPh_3	-	1957	41.6	152.9	41.4	156.9
Ox-PPh_3	2.261(2)	1991	41.4	157.3	41.6	161.6
5,7-dCl-PPh_3	-	1970	41.1	157.5	45.6	165.2
Ox-PPh2Cy	2.280(1)	1953	47.9	158.2	50.6	162.0
5-Cl-Ox-PCy_3	2.248(1)	1964	40.7	155.9	41.1	157.0
5,7-dMe-PPh_3	-	1952	**-**	161.1	41.4	163.6
5,7-dI-PPh3	-	1956	**-**	160.0	41.8	164.1
[4]acac-PPh	2.242(9)	1977	48.6	173.4	46.6	175.7
acac-PP_2Cy	2.243(6)	1948	58.8	177.7	60.0	171.3
acac-PCy_3	2.254(4)	1945	59.1	166.1	60.8	164.3

Notes: L,L-BidH: TropH = Tropolone, CupH = Cupferron, CyHexH = 2-(Cyclohexyliminomethyl)phenol, OxH = 8-hydroxyquinoline, 5,7-dClH = 5,7-dichloro-8-hydroxyquinoline, 5-Cl-OxH = 5-Chloro-8-hydroxyquionoline, 5,7-dMeH = 5,7-dimethyl-8-hydroxyquinolineH, 5,7-dI-PPh3H= 5,7-diido-8-hydroxyquinoline, AcacH = acetylacetone.

The results from Table 8.1 were used to construct correlations between the metal-phosphorus coupling constant ($^1J_{Rh-P}$), the chemical shift ($\delta^{31}P$), and the metal-phosphorus bond distances d(Rh-P).

As mentioned, unfortunately, suitable crystals of the rhodium(I) Schiff base complexes [Rh(L,L-Bid)(CO)(PPX_3)] where L,L-Bid = monoanionic Schiff base ligands and PPX_3 are tertiary phosphine ligands, in the present study have not yet been isolated to permit correlation with the bond distances of these. Nevertheless, below are given a variation of correlations which will now be systematically discussed. Solid NMR spectra of related rhodium(I) complexes were also included and correlated as far as possible.

[12] G.J.J. Steyn, A. Roodt, A, J.G. Leipoldt, Rhodium Express. 1 (1993) 25–29.
[13] D.E. Graham, G.J. Lamprecht, I.M. Potgieter, A. Roodt, J.G. Leipoldt, Transition Met. Chem. 16 (1991) 193–195.

8.3.1 Correlation between the first-order coupling constant ($^1J_{Rh\text{-}P}$) and the Rh-P bond distances

Correlation is firstly made between the first-order coupling constant $^1J_{Rh\text{-}P}$ in both the liquid and solid states as illustrated in Figure 8.3.

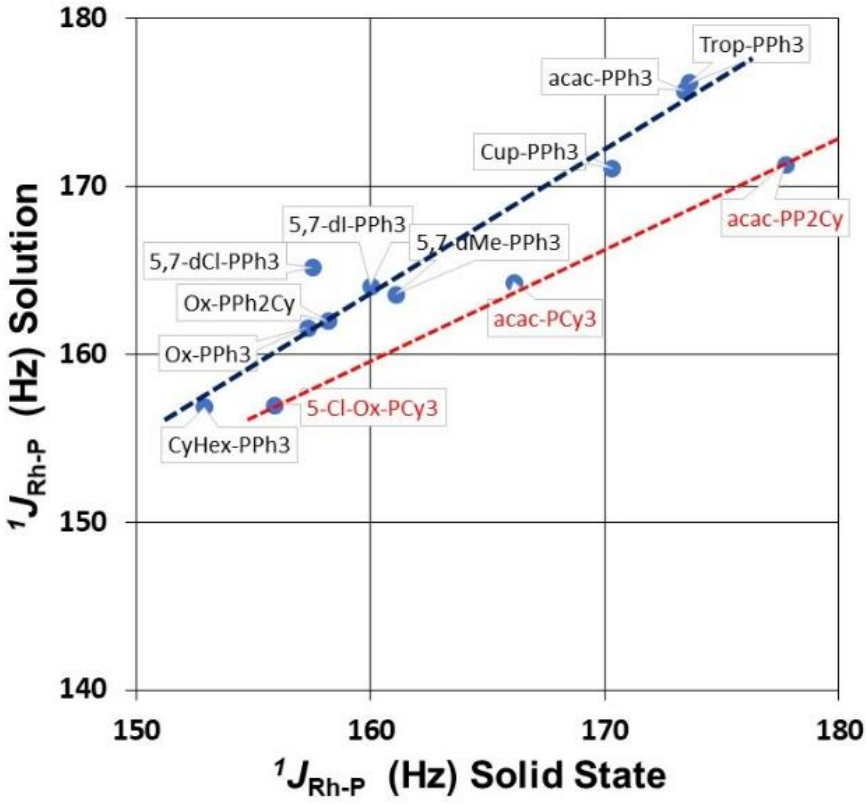

Figure 8.3: Correlation between $^1J_{Rh\text{-}P}$ (Solution) and $^1J_{Rh\text{-}P}$ (Solid-state) from the data in Table 8.1.

It is clear from Figure 8.3 that an interesting phenomenon occurs. A quite reasonable correlation within tertiary phosphine ligands comparable to PPh_3 holds (blue dotted line in Figure 8.3). As soon as additional more bulky entities such as cyclohexyl instead of phenyl, as in the PPh_2Cy, $PPhCy_3$ and PCy_3 ligands are introduced, a second correlation related to the more bulky P-ligands seems to emerge (red dotted line in Figure 8.3), although not convincingly.

This is even more readily observed when considering the separate correlations of the coupling constants (both solution and solid-state, see (a) and (b) in Figure 8.4) with the XRD-measured Rh-P bond distances. Superficially the correlation between the solid-state coupling constant and the Rh-P bond length is better. This is to be expected since the physical measurement of the XRD structure and the NMR is on the exact same (solid-state) sample; not in solution.

However, the same tendency of two possible relationships emerges (although even less convincingly as in Figure 8.3 above). There are in addition also clear outliers not agreeing with any of the two lines (blue or red in both (a) and (b) in Figure 8.4).

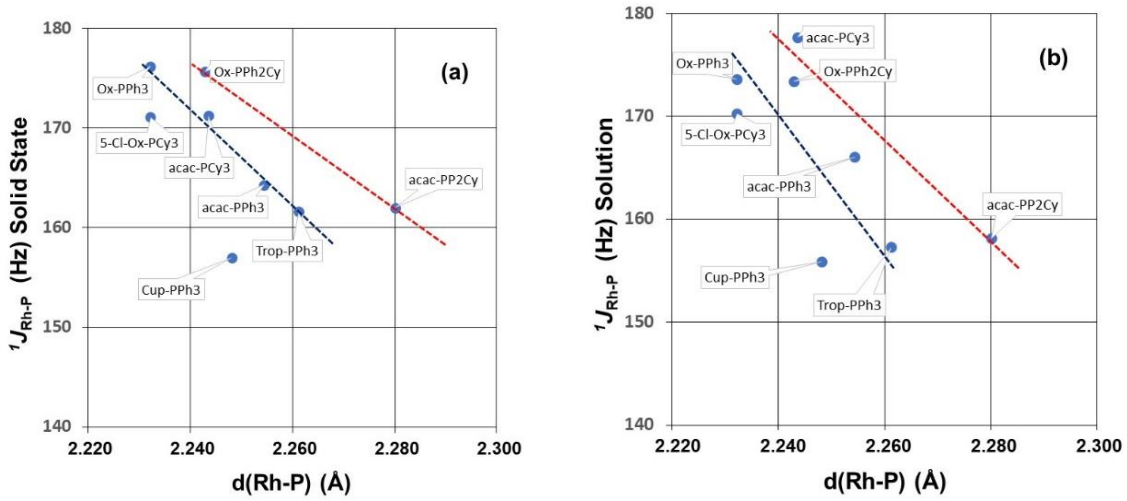

Figure 8.4: Correlation between (a) $^1J_{Rh-P}$ (Solid-state) *vs*. d(Rh-P) and (b) $^1J_{Rh-P}$ (Solution) vs. d(Rh-P) from the data in Table 8.1

Again, there is a somewhat better correlation in the solid-state NMR and the XRD data (Figure 8.4(a)).

The same tendency of different possible relationships emerges from the bar graphs shown in Figure 8.5. Superficially here too, as in Figure 8.4, the general trend observed from the solid-state NMR data (Figure 8.5(a)) is better that the correlation with the solution data.

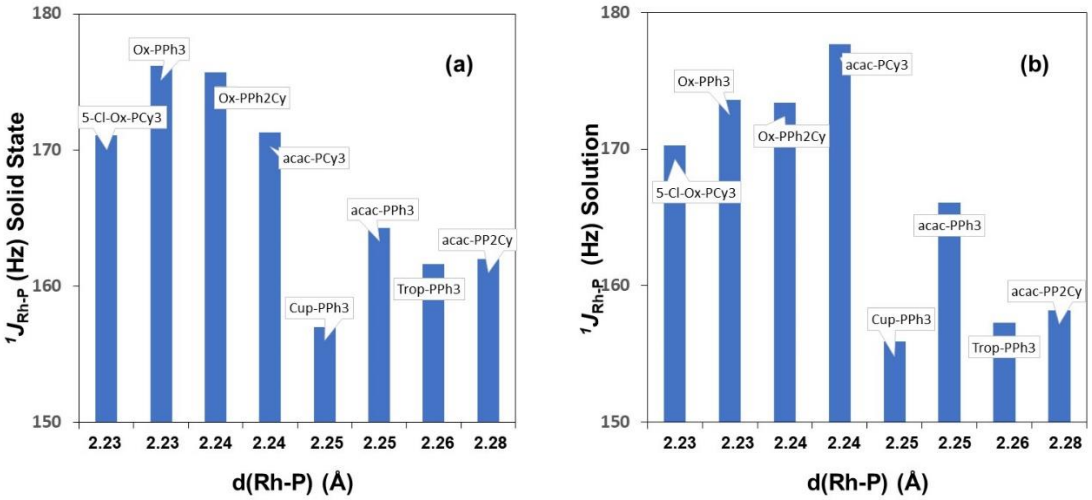

Figure 8.5: **Bar graph for correlation between (a) $^1J_{Rh-P}$ (Solid-state) vs. d(Rh-P) and (b) $^1J_{Rh-P}$ (Solution) *vs*. d(Rh-P) from the data in Table 8.1**

It is clear from Figures 8.3-8.5 that reasonable tendencies are observed and a fair correlation between these parameters surfaced, at least within in the data sample which has been studied.

Thus, although promising, significantly more data needs to be generated to enable a more detailed analysis of the relationships (if at all) between these parameters.

8.3.2 Correlation between the ^{31}P chemical shift and the Rh-P bond distances

Next, correlations are made between the chemical shift in the solution and solid states, and are then correlated with the Rh-P bond distances.

First, the correlation between the chemical shifts in both the solution and solid states is illustrated in Figure 8.6. It is clear that quite a good correlation is obtained, at least in the data sample which has been studied.

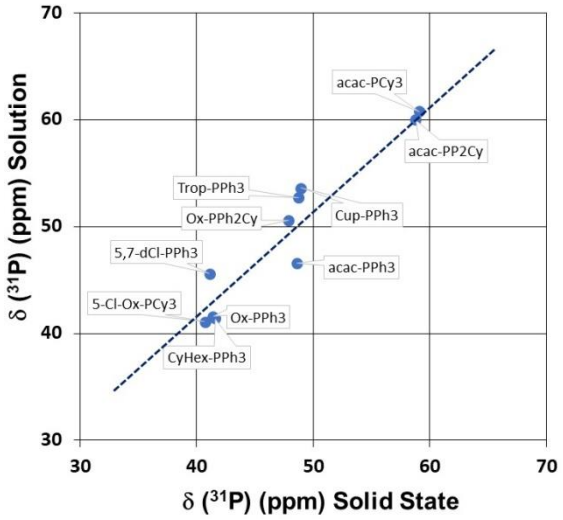

Figure 8.6: Correlation between δ^{31}P (Solution) and δ^{31}P (Solid-state) from the data in Table 8.1

Next, a comparison between both the chemical shift in the solution and solid states are correlated with the Rh-P bond distance, see Figure 8.7. It is clear that in this case a very weak correlation, in fact, questionable if at all, is obtained.

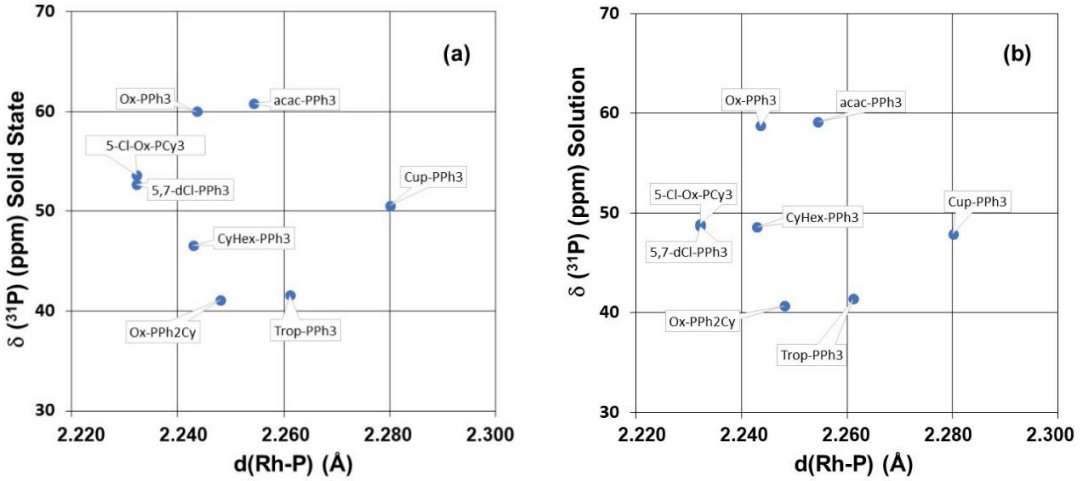

Figure 8.7: Correlation between (a) δ^{31}P (Solid-state) vs. d(Rh-P) and (b) δ^{31}P (Solution) vs. d(Rh-P) from the data in Table 8.1

The comparison between both the chemical shift in the solution and solid states are further illustrated by the bar graphs in Figure 8.8 and it is clear that the questionable correlation is also manifested here, as in Figure 8.7.

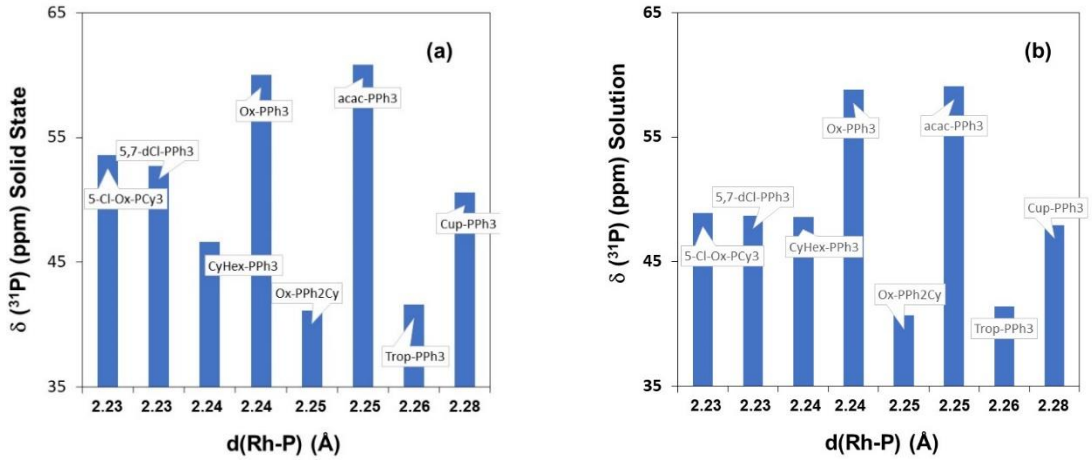

Figure 8.8: Bar graph for possible correlation between (a) δ^{31}P (Solid-state) vs. d(Rh-P) and (b) δ^{31}P (Solution) vs. d(Rh-P) from the data in Table 8.1

8.4 Conclusion

The first-order coupling constant and chemical shift together with the rhodium-phosphorus bond distances in these complexes can provide important information pertaining to the nature of the metal-phosphorus bond.[1,7] Inspection of the data in Table 8.1 and Figures 8.3-8.8 shows some good comparisons of the solid-state NMR data with the solution state ^{31}P NMR spectra, but also less convincing ones. The apparent difference in chemical shift between the solid and solution state are relatively small and may be used to conclude that there is no significant structural difference between solid and solution states.

From Table 8.1, a slight decrease in the first-order coupling constant $^{1}J_{\text{Rh-P}}$ is observed in solid-state relative to solution state. This may be brought about the rigidity in the solid-state which is lost in solution state. The difference may also be attributed to substituents on the ligand backbone via factors such as the fixed conformation in the solid-state.

Be as it may, the experiments described within this chapter, and the results obtained, warrants expansion to a significant wider statistical sample of complexes. This is envisaged for the future.

9 Evaluation of Study

9.1 Introduction

The overarching objective of this PhD study was to investigate the coordination behavior of Schiff-base and closely related oxine-type ligands (both N,O-donor bidentate ligands; N,O-Bid) to selected middle and late transition metal carbonyl cores. Firstly, an integrated in-depth study of the N,O-Bid coordination to the octahedral *fac*-$[M(CO)_3]^+$ (M = manganese, technetium or rhenium) core was pursued as the primary thrust. Then secondly, the electronic and steric influence of these coordinated N,O-Bid ligands in rhodium(I) square planar carbonyl complexes was pursued with primary aim the construction of one dimensional metallophilic interaction networks. Although the Schiff-base ligands were the initial prime focus, it was during the course of the study realized that the subtle sterics and stability of the Schiff-base ligands might not be ideal in the soft Rh(I) complexes. The closely related oxine ligand systems were thus incorporated in the investigation of the influence of steric and electronic parameters on the metallophilic interactions. The oxine ligands systems, just like the Schiff-base ligands utilized in this study, contain N,O donor atoms but vary in the metallocycle (five-membered in oxines *vs*. six membered for the Schiff-base ligands) and thus provide additional possibilities of increasing subtle variations in the total steric effect but also on the periphery of the ligands without significantly varying the steric contribution within the specific ligand system chosen.

9.2 Evaluation

9.2.1 Synthesis of metal complexes and characterization

The coordination behavior of Schiff-base bidentate ligands towards the *fac*-$[M(CO)_3]^+$ (M = manganese, technetium and rhenium) core was evaluated in the context of model radiopharmaceutical design. The synthesis of these analogous complexes are reported in Chapter 3. The Schiff-base ligands in this study are derived from a salicylidene backbone and contain varying aromatic and aliphatic substituents on the imine nitrogen atom. It was demonstrated through detailed single crystal X-ray diffraction experiments that the nuclearity of rhenium(I) complexes could be manipulated to form either mononuclear or dinuclear complexes. This was however not the case with respect to manganese and technetium complexes since only dinuclear complexes could be isolated, in spite of employing relatively similar synthetic procedures in the synthesis of the metal complexes as for the Re(I). The coordination geometry around the metal centre in the dinuclear complexes is reminiscent to that of the mononuclear species with respect to the metal atoms situated in the centre of a distorted octahedron surrounded by three facially coordinated carbonyl ligands and the chelating O and N atoms of the bidentate ligand. The octahedron in the mononuclear complex is then completed by the coordinated methanol ligand, and by the bridging phenolato oxygen atom in the dinuclear complexes. This study highlighted further the structural flexibility of the Schiff-base ligands with respect to their multi-functional ability to act as both a chelating and a bridging ligand towards the two metal centres.

The Schiff-base ligands were also coordinated to a rhodium(I) dicarbonyl moiety to form complexes of the type, $[Rh(N,O\text{-}Bid)(CO)_2]$ (where N,O-Bid = mononegative Schiff-base and oxine-type bidentate ligands) to gain insight into the effects of the coordinated ligands towards the formation of metal-metal interactions which can occur within square planar rhodium complexes. Oxine ligand systems were included in these evaluations and as indicated above, these chelates form six membered entities compared to the six membered entities in the Schiff-base systems. However, they were particularly chosen since they produce model Rh(I)

complexes which can be much more readily crystallized than the corresponding Schiff-base systems. They could thus be readily studied in the solid state, contrary to the corresponding Schiff-base systems which proved to be quite challenging to crystallize. The steric and electronic parameters were varied and their influence on the rhodium-rhodium interactions were carefully evaluated by monitoring the rhodium-rhodium intermolecular distances in the solid state. The crystallographic studies of these rhodium(I) complexes indicated two types of metallophilic interactions. The first type of interactions consisted of an infinite array of metal-metal interactions throughout the crystal lattice, while in the second type, the metal-metal interactions are restricted between two adjacent molecules forming pseudo *dinuclear* units.

9.2.2 Oxidative addition study

Rhodium(I) complexes of the type [Rh(L,L-Bid)(CO)(PPX_3)], (where L,L-Bid = monoanionic bidentate Schiff base ligands and PPX_3 = tertiary phosphine) were synthesized in order to evaluate the influence of bidentate ligands on the rate of iodomethane oxidative addition as a fundamental, model reaction associated with Homogeneous Catalysis. The electronic manipulation on the metal centre was firstly achieved by introducing varying substituents on the imine nitrogen atom in the ligands (5-Me-Sal-CyPentH = 2-(cyclopentyl)methyl-5-methylphenol, (5-Me-Sal-IsoPropH = 5-Methyl-2-(isopropyliminomethyl)phenol and (Sal-CyHexH = 2-(cyclohexyliminomethyl)phenol. The IR and NMR spectroscopy investigations indicated a rapid decay of the rhodium(I) accompanied by the simultaneous formation of the rhodium(III) alkyl species with no detection of the rhodium (III) acyl product, assumed to be due to its slow rate of formation relative to the alkyl product. The observed rates for the oxidative addition step were comparable within all three the rhodium(I) Schiff-base complexes in spite of the variations of the steric and electronic parameters of the ligands as manifested by the methyl group, the cyclopentyl, isopropyl and the cyclohexyl groups attached to the imine nitrogen atom.

The effect of entering different tertiary phosphine ligands (PPh_3, PCY_3, PPh_2Cy and $PPhCy_2$) on the oxidative addition reaction was also evaluated. A decrease in the

overall rate was observed when replacing the weaker electron donating phenyl ring of the phosphine ligands by the larger cyclohexyl rings. The results are contrary to what was anticipated. The rhodium(I) centre acts as a nucleophile under the oxidative addition reaction, naturally one expects an increase in activation of the metal centre towards oxidative addition when increasing the electron density around the metal centre. In attempt to gain more insight on the coordination environment around the rhodium centre, preliminary solid state ^{31}P NMR studies were conducted. Solid state NMR spectroscopy as technique may serve as a bridge between solution and solid, non-crystalline compounds, such as in this case, the Schiff-base systems. Information pertaining to the first-order coupling constant and chemical shift may provide more insight into the electronic and steric influences on the metal centre. Thus, preliminary correlations were made based on the ^{31}P NMR studies in the different states, and although not conclusive, the results obtained showed a good agreement between the solution and solid-state characteristics, which must be expanded in future.

9.3 Future work

The relationship between structure and reactivity is important in the development and understanding and behavior of general chemical processes, and in particular also for radiopharmaceutical models. Important information with regards to the preparation, administration in patients, *in vivo* uptake and clearance of the radiopharmaceutical agents can in principle be estimated from these mechanistic studies. Thus, a detailed kinetic-mechanistic study on the formation of the manganese, technetium and rhenium Schiff-base tricarbonyl complexes should be conducted in future. These kinetic evaluations will shed some light unto the formation of the mononuclear and dinuclear complexes obtained in this present study and the factors governing this process. The possibility of synthesizing radiopharmaceutical agents which integrate both therapeutic and imaging capabilities within a single molecule should also be further explored. In addition, *in vitro* cancer screening and biological distribution studies of the Schiff-base complexes should be conducted, including studies with additional aggressive functionalization of the ligand's periphery. The structural flexibility of the ligands

allows for variations of the steric and electronic properties which can be used to manipulate the different characteristics of the resulting complexes including the lipophilicity.

For the rhodium(I) complexes, the current range of Schiff-base and oxine metal complexes should be expanded to include more variations on the electronic and steric parameters, but also extended to other ligand systems to probe the complete accessible range of bond distances as reported in literature. These investigations could be further substantiated by the inclusion of computational investigations for improved understanding of the nature of the metallophilic interactions. Electron conductivity studies on the present rhodium(I) complexes, which will incorporate the determination of the temperature effects and photochemical activation on the metallophilic interactions should be considered with relation to the field of forming nano-wire materials which are able to selectively direct and conduct electrons. The ultimate goal is to investigate the future applications of these rhodium(I) complexes in optoelectronic technologies. Furthermore, in-depth kinetic investigations of the reactivity of the complexes with respect to substitution and oxidative addition reactions should be expanded in particularly for its application in the fields of homogenous catalysis.

Appendix

Supplementary Data of Crystal Structures

Supplementary data of *fac*-[Mn(5-Me-Sal-Cypent)$(CO)_3]_2$ for the atomic coordinates, bond distances and angles and anisotropic displacement parameters are given in appendix tables.

Table 1.A: Atomic coordinates (x 10^4) and equivalent isotropic displacement parameters ($Å^2$ x 10^3) for *fac*-[Mn(5-Me-Sal-Cypent)$(CO)_3]_2$. U(eq) is defined as one third of the trace of the orthogonalized U^{ij} tensor.

	x	y	z	U(eq)
Mn(1)	9439(1)	3086(1)	4520(1)	13(1)
O(01)	12745(2)	3387(2)	5314(1)	31(1)
O(03)	8241(2)	432(2)	5728(2)	41(1)
O(1)	9789(1)	4986(1)	6251(1)	15(1)
O(02)	9053(2)	504(2)	1925(1)	33(1)
N(1)	7084(2)	2803(2)	4065(1)	16(1)
C(13)	9185(2)	5657(2)	8528(2)	20(1)
C(02)	9190(2)	1530(2)	2910(2)	21(1)
C(11)	6954(2)	3789(2)	6522(2)	17(1)
C(16)	5840(2)	3614(2)	7438(2)	21(1)
C(1)	6275(2)	3035(2)	5021(2)	18(1)
C(01)	11498(2)	3343(2)	5012(2)	19(1)
C(15)	6388(2)	4414(2)	8868(2)	23(1)
C(03)	8694(2)	1498(2)	5292(2)	23(1)
C(141)	8638(2)	6443(2)	10980(2)	31(1)
C(25)	4997(2)	2731(2)	2184(2)	29(1)
C(14)	8066(2)	5479(2)	9427(2)	22(1)
C(12)	8664(2)	4803(2)	7078(2)	16(1)
C(21)	6153(2)	2055(2)	2585(2)	21(1)
C(22)	5018(2)	192(2)	2222(2)	30(1)
C(23)	3448(2)	-207(3)	1257(2)	40(1)

C(24)	3239(2)	1306(3)	1815(2)	42(1)

Table 1.B: Bond lengths (Å) and angles (°) for *fac*-[Mn(5-Me-Sal-Cypent)(CO)$_3$]$_2$.

Bond	Distance	Bond	angle
Mn(1)-C(03)	1.7957(18)	C(03)-Mn(1)-C(02)	87.16(8)
Mn(1)-C(02)	1.8059(18)	C(03)-Mn(1)-C(01)	87.52(7)
Mn(1)-C(01)	1.8142(19)	C(02)-Mn(1)-C(01)	87.66(7)
Mn(1)-O(1)	2.0427(13)	C(03)-Mn(1)-O(1)	97.72(7)
Mn(1)-N(1)	2.0625(17)	C(02)-Mn(1)-O(1)	175.12(6)
Mn(1)-O(1)#1	2.0672(13)	C(01)-Mn(1)-O(1)	92.58(6)
Mn(1)-Mn(1)#1	3.1930(18)	C(03)-Mn(1)-N(1)	90.62(7)
O(01)-C(01)	1.145(2)	C(02)-Mn(1)-N(1)	94.52(6)
O(03)-C(03)	1.148(2)	C(01)-Mn(1)-N(1)	177.07(6)
O(1)-C(12)	1.3471(18)	O(1)-Mn(1)-N(1)	85.42(5)
O(1)-Mn(1)#1	2.0672(13)	C(03)-Mn(1)-O(1)#1	175.13(6)
O(02)-C(02)	1.149(2)	C(02)-Mn(1)-O(1)#1	97.07(7)
N(1)-C(1)	1.281(2)	C(01)-Mn(1)-O(1)#1	95.05(6)
N(1)-C(21)	1.489(2)	O(1)-Mn(1)-O(1)#1	78.05(6)
C(13)-C(14)	1.395(2)	N(1)-Mn(1)-O(1)#1	86.64(5)
C(13)-C(12)	1.403(2)	C(03)-Mn(1)-Mn(1)#1	136.97(6)
C(13)-H(13)	0.9300	C(02)-Mn(1)-Mn(1)#1	135.82(5)
C(11)-C(16)	1.404(2)	C(01)-Mn(1)-Mn(1)#1	94.92(5)
C(11)-C(12)	1.413(2)	O(1)-Mn(1)-Mn(1)#1	39.30(3)
C(11)-C(1)	1.453(2)	N(1)-Mn(1)-Mn(1)#1	84.90(4)
C(16)-C(15)	1.381(2)	O(1)#1-Mn(1)-Mn(1)#1	38.75(4)
C(16)-H(16)	0.9300	C(12)-O(1)-Mn(1)	120.68(9)
C(1)-H(1)	0.960(19)	C(12)-O(1)-Mn(1)#1	119.45(9)
C(15)-C(14)	1.396(3)	Mn(1)-O(1)-Mn(1)#1	101.95(6)
C(15)-H(15)	0.9300	C(1)-N(1)-C(21)	116.71(13)
C(141)-C(14)	1.512(2)	C(1)-N(1)-Mn(1)	122.37(11)
C(141)-H(14A)	0.9600	C(21)-N(1)-Mn(1)	120.22(10)
C(141)-H(14B)	0.9600	C(14)-C(13)-C(12)	121.64(15)
C(141)-H(14C)	0.9600	C(14)-C(13)-H(13)	119.2
C(25)-C(24)	1.532(3)	C(12)-C(13)-H(13)	119.2
C(25)-C(21)	1.552(2)	O(02)-C(02)-Mn(1)	176.66(15)
C(25)-H(25A)	0.9700	C(16)-C(11)-C(12)	119.18(14)
C(25)-H(25B)	0.9700	C(16)-C(11)-C(1)	117.93(14)

C(21)-C(22)	1.551(2)	C(12)-C(11)-C(1)	122.63(13)
C(21)-H(21)	0.970(19)	C(15)-C(16)-C(11)	121.16(15)
C(22)-C(23)	1.525(3)	C(15)-C(16)-H(16)	119.4
C(22)-H(22A)	0.9700	C(11)-C(16)-H(16)	119.4
C(22)-H(22B)	0.9700	N(1)-C(1)-C(11)	125.63(14)
C(23)-C(24)	1.508(3)	N(1)-C(1)-H(1)	118.5(11)
C(23)-H(23A)	0.9700	C(11)-C(1)-H(1)	115.9(11)
C(23)-H(23B)	0.9700	O(01)-C(01)-Mn(1)	175.03(14)
C(24)-H(24A)	0.9700	C(16)-C(15)-C(14)	120.33(15)
C(24)-H(24B)	0.9700	C(16)-C(15)-H(15)	119.8
		C(14)-C(15)-H(15)	119.8
		O(03)-C(03)-Mn(1)	176.24(15)
		C(14)-C(141)-H(14A)	109.5
		C(14)-C(141)-H(14B)	109.5
		H(14A)-C(141)-H(14B)	109.5
		C(14)-C(141)-H(14C)	109.5
		H(14A)-C(141)-H(14C)	109.5
		H(14B)-C(141)-H(14C)	109.5
		C(24)-C(25)-C(21)	105.70(16)
		C(24)-C(25)-H(25A)	110.6
		C(21)-C(25)-H(25A)	110.6
		C(24)-C(25)-H(25B)	110.6
		C(21)-C(25)-H(25B)	110.6
		H(25A)-C(25)-H(25B)	108.7
		C(13)-C(14)-C(15)	118.96(15)
		C(13)-C(14)-C(141)	121.09(16)
		C(15)-C(14)-C(141)	119.94(15)
		O(1)-C(12)-C(13)	119.72(14)
		O(1)-C(12)-C(11)	121.66(13)
		C(13)-C(12)-C(11)	118.61(13)
		N(1)-C(21)-C(22)	110.83(13)
		N(1)-C(21)-C(25)	116.57(14)
		C(22)-C(21)-C(25)	105.09(14)
		N(1)-C(21)-H(21)	105.4(11)
		C(22)-C(21)-H(21)	109.5(11)
		C(25)-C(21)-H(21)	109.4(11)

		C(23)-C(22)-C(21)	105.77(16)
		C(23)-C(22)-H(22A)	110.6
		C(21)-C(22)-H(22A)	110.6
		C(23)-C(22)-H(22B)	110.6
		C(21)-C(22)-H(22B)	110.6
		H(22A)-C(22)-H(22B)	108.7
		C(24)-C(23)-C(22)	103.31(15)
		C(24)-C(23)-H(23A)	111.1
		C(22)-C(23)-H(23A)	111.1
		C(24)-C(23)-H(23B)	111.1
		C(22)-C(23)-H(23B)	111.1
		H(23A)-C(23)-H(23B)	109.1
		C(23)-C(24)-C(25)	104.68(16)
		C(23)-C(24)-H(24A)	110.8
		C(25)-C(24)-H(24A)	110.8
		C(23)-C(24)-H(24B)	110.8
		C(25)-C(24)-H(24B)	110.8
		H(24A)-C(24)-H(24B)	108.9

Table 1.C: Anisotropic displacement parameters ($Å^2$ x 10^3) *fac*-[Mn(5-Me-Sal-Cypent)$(CO)_3]_2$. The anisotropic displacement factor exponent takes the form: $-2\pi^2$ [$h^2a^{*2}U^{11}$ + ... + 2 h k a* b* U^{12}]

	U^{11}	U^{22}	U^{33}	U^{23}	U^{13}	U^{12}
Mn(1)	14(1)	13(1)	13(1)	4(1)	4(1)	7(1)
O(01)	23(1)	32(1)	40(1)	7(1)	2(1)	18(1)
O(03)	58(1)	31(1)	46(1)	24(1)	24(1)	21(1)
O(1)	16(1)	16(1)	14(1)	5(1)	5(1)	8(1)
O(02)	42(1)	27(1)	26(1)	-2(1)	6(1)	19(1)
N(1)	16(1)	15(1)	16(1)	4(1)	2(1)	6(1)
C(13)	22(1)	20(1)	17(1)	6(1)	4(1)	10(1)
C(02)	20(1)	20(1)	24(1)	7(1)	5(1)	10(1)
C(11)	19(1)	19(1)	17(1)	7(1)	6(1)	11(1)
C(16)	20(1)	25(1)	25(1)	11(1)	10(1)	13(1)
C(1)	15(1)	19(1)	21(1)	6(1)	4(1)	7(1)
C(01)	23(1)	17(1)	19(1)	4(1)	5(1)	11(1)
C(15)	29(1)	29(1)	23(1)	13(1)	15(1)	20(1)

C(03)	25(1)	22(1)	22(1)	6(1)	8(1)	12(1)
C(141)	41(1)	35(1)	18(1)	5(1)	9(1)	20(1)
C(25)	27(1)	38(1)	26(1)	16(1)	3(1)	15(1)
C(14)	34(1)	24(1)	18(1)	9(1)	10(1)	19(1)
C(12)	19(1)	17(1)	16(1)	8(1)	7(1)	11(1)
C(21)	18(1)	23(1)	16(1)	5(1)	1(1)	5(1)
C(22)	30(1)	21(1)	24(1)	2(1)	1(1)	2(1)
C(23)	20(1)	49(1)	22(1)	-3(1)	1(1)	0(1)
C(24)	28(1)	62(1)	30(1)	12(1)	4(1)	19(1)

Supplementary data of *fac*-[ReSal-CyHex)$(CO)_3]_2$ for the atomic coordinates, bond distances and angles and anisotropic displacement parameters are given in appendix tables

Table 2.A: Atomic coordinates (x 10^4) and equivalent isotropic displacement parameters (Å^2 x 10^3) for *fac*-[ReSal-CyHex)$(CO)_3]_2$. U(eq) is defined as one third of the trace of the orthogonalized U^{ij} tensor.

	x	y	z	U(eq)
Re(1)	1758(1)	443(1)	9841(1)	16(1)
C(01)	3465(4)	1107(4)	10434(2)	23(1)
N(1)	2099(3)	-1876(3)	9998(2)	16(1)
O(1)	-293(3)	-293(2)	9301(1)	16(1)
C(14)	-1467(4)	-2292(4)	7627(2)	30(1)
C(12)	-344(4)	-1345(4)	8781(2)	17(1)
C(22)	2178(5)	-2753(5)	11290(2)	33(1)
C(21)	3077(4)	-2423(4)	10652(2)	20(1)
C(03)	2848(4)	450(4)	9012(2)	20(1)
O(01)	4458(3)	1572(4)	10787(2)	42(1)
C(24)	4202(6)	-4323(5)	11871(3)	41(1)
C(13)	-1391(4)	-1252(4)	8164(2)	25(1)
C(26)	4010(4)	-3725(4)	10517(2)	26(1)
C(23)	3185(6)	-3074(6)	11998(2)	47(1)
C(1)	1602(4)	-2804(4)	9518(2)	21(1)
O(03)	3486(4)	481(3)	8500(2)	34(1)

C(16)	442(4)	-3597(4)	8307(2)	26(1)
C(11)	573(4)	-2536(4)	8860(2)	19(1)
C(25)	5033(4)	-4055(5)	11220(2)	31(1)
O(02)	1275(4)	3649(3)	9543(2)	38(1)
C(02)	1399(4)	2450(4)	9650(2)	22(1)
C(15)	-556(5)	-3468(5)	7687(2)	32(1)

Table 2.B: Bond lengths [Å] and angles [°] for *fac*-[ReSal-CyHex)$(CO)_3]_2$.

Bond	Distance	Bond	Angle
Re(1)-C(03)	1.902(4)	C(03)-Re(1)-C(01)	88.38(17)
Re(1)-C(01)	1.913(4)	C(03)-Re(1)-C(02)	87.09(15)
Re(1)-C(02)	1.924(4)	C(01)-Re(1)-C(02)	84.45(16)
Re(1)-O(1)	2.149(3)	C(03)-Re(1)-O(1)	98.86(14)
Re(1)-O(1)#1	2.176(3)	C(01)-Re(1)-O(1)	172.77(14)
Re(1)-N(1)	2.197(3)	C(02)-Re(1)-O(1)	95.82(13)
C(01)-O(01)	1.146(4)	C(03)-Re(1)-O(1)#1	172.59(13)
N(1)-C(1)	1.279(5)	C(01)-Re(1)-O(1)#1	98.94(14)
N(1)-C(21)	1.503(5)	C(02)-Re(1)-O(1)#1	94.80(13)
O(1)-C(12)	1.359(4)	O(1)-Re(1)-O(1)#1	73.83(11)
O(1)-Re(1)#1	2.176(3)	C(03)-Re(1)-N(1)	91.45(12)
C(14)-C(13)	1.372(5)	C(01)-Re(1)-N(1)	98.43(13)
C(14)-C(15)	1.378(6)	C(02)-Re(1)-N(1)	176.74(13)
C(14)-H(14)	0.9500	O(1)-Re(1)-N(1)	81.51(10)
C(12)-C(11)	1.394(5)	O(1)#1-Re(1)-N(1)	86.29(9)
C(12)-C(13)	1.403(5)	O(01)-C(01)-Re(1)	176.6(3)
C(22)-C(21)	1.528(5)	C(1)-N(1)-C(21)	116.9(3)
C(22)-C(23)	1.535(6)	C(1)-N(1)-Re(1)	122.7(3)
C(22)-H(22A)	0.9900	C(21)-N(1)-Re(1)	120.1(2)
C(22)-H(22B)	0.9900	C(12)-O(1)-Re(1)	120.7(2)
C(21)-C(26)	1.523(5)	C(12)-O(1)-Re(1)#1	118.3(2)
C(21)-H(21)	0.97(4)	Re(1)-O(1)-Re(1)#1	106.17(11)
C(03)-O(03)	1.154(5)	C(13)-C(14)-C(15)	121.4(4)

C(24)-C(25)	1.500(6)	C(13)-C(14)-H(14)	119.3
C(24)-C(23)	1.529(7)	C(15)-C(14)-H(14)	119.3
C(24)-H(24A)	0.9900	O(1)-C(12)-C(11)	121.9(3)
C(24)-H(24B)	0.9900	O(1)-C(12)-C(13)	118.8(3)
C(13)-H(13)	0.9500	C(11)-C(12)-C(13)	119.3(3)
C(26)-C(25)	1.536(5)	C(21)-C(22)-C(23)	110.3(4)
C(26)-H(26A)	0.9900	C(21)-C(22)-H(22A)	109.6
C(26)-H(26B)	0.9900	C(23)-C(22)-H(22A)	109.6
C(23)-H(23A)	0.9900	C(21)-C(22)-H(22B)	109.6
C(23)-H(23B)	0.9900	C(23)-C(22)-H(22B)	109.6
C(1)-C(11)	1.466(5)	H(22A)-C(22)-H(22B)	108.1
C(1)-H(1)	0.88(4)	N(1)-C(21)-C(26)	116.4(3)
C(16)-C(15)	1.383(5)	N(1)-C(21)-C(22)	109.8(3)
C(16)-C(11)	1.405(5)	C(26)-C(21)-C(22)	109.0(3)
C(16)-H(16)	0.9500	N(1)-C(21)-H(21)	106(2)
C(25)-H(25A)	0.9900	C(26)-C(21)-H(21)	108(2)
C(25)-H(25B)	0.9900	C(22)-C(21)-H(21)	106(2)
O(02)-C(02)	1.137(4)	O(03)-C(03)-Re(1)	178.2(3)
C(15)-H(15)	0.9500	C(25)-C(24)-C(23)	111.6(4)
		C(25)-C(24)-H(24A)	109.3
		C(23)-C(24)-H(24A)	109.3
		C(25)-C(24)-H(24B)	109.3
		C(23)-C(24)-H(24B)	109.3
		H(24A)-C(24)-H(24B)	108.0
		C(14)-C(13)-C(12)	120.3(3)
		C(14)-C(13)-H(13)	119.9
		C(12)-C(13)-H(13)	119.9
		C(21)-C(26)-C(25)	109.5(3)
		C(21)-C(26)-H(26A)	109.8
		C(25)-C(26)-H(26A)	109.8
		C(21)-C(26)-H(26B)	109.8
		C(25)-C(26)-H(26B)	109.8
		H(26A)-C(26)-H(26B)	108.2

		C(24)-C(23)-C(22)	110.3(4)
		C(24)-C(23)-H(23A)	109.6
		C(22)-C(23)-H(23A)	109.6
		C(24)-C(23)-H(23B)	109.6
		C(22)-C(23)-H(23B)	109.6
		H(23A)-C(23)-H(23B)	108.1
		N(1)-C(1)-C(11)	126.5(3)
		N(1)-C(1)-H(1)	122(2)
		C(11)-C(1)-H(1)	111(2)
		C(15)-C(16)-C(11)	121.4(4)
		C(15)-C(16)-H(16)	119.3
		C(11)-C(16)-H(16)	119.3
		C(12)-C(11)-C(16)	118.8(3)
		C(12)-C(11)-C(1)	123.5(3)
		C(16)-C(11)-C(1)	117.5(3)
		C(24)-C(25)-C(26)	111.7(4)
		C(24)-C(25)-H(25A)	109.3
		C(26)-C(25)-H(25A)	109.3
		C(24)-C(25)-H(25B)	109.3
		C(26)-C(25)-H(25B)	109.3
		H(25A)-C(25)-H(25B)	108.0
		O(02)-C(02)-Re(1)	175.9(3)
		C(14)-C(15)-C(16)	118.7(4)
		C(14)-C(15)-H(15)	120.7
		C(16)-C(15)-H(15)	120.7

Table 2.C: Anisotropic displacement parameters ($Å^2 x\ 10^3$) for *fac*-[ReSal-CyHex)$(CO)_3]_2$. The anisotropic displacement factor exponent takes the form: $-2\pi^2[\ h^2 a^{*2} U^{11} + ... + 2\ h\ k\ a^*\ b^*\ U^{12}\ ]$

	U^{11}	U^{22}	U^{33}	U^{23}	U^{13}	U^{12}
Re(1)	16(1)	10(1)	21(1)	1(1)	1(1)	-1(1)
C(01)	23(2)	15(2)	30(2)	2(2)	1(1)	-1(1)
N(1)	15(1)	12(1)	22(1)	3(1)	2(1)	1(1)
O(1)	18(1)	11(1)	18(1)	-2(1)	-2(1)	-1(1)
C(14)	34(2)	28(2)	26(2)	0(2)	-7(2)	-3(2)
C(12)	19(2)	13(2)	19(2)	-2(1)	2(1)	-3(1)
C(22)	35(2)	36(2)	28(2)	8(2)	9(2)	14(2)
C(21)	21(2)	18(2)	20(2)	1(1)	-2(1)	0(1)
C(03)	20(2)	18(2)	22(2)	1(1)	0(1)	3(1)
O(01)	26(2)	44(2)	51(2)	4(2)	-14(1)	-9(1)
C(24)	43(3)	44(3)	33(2)	16(2)	-2(2)	15(2)
C(13)	25(2)	21(2)	27(2)	2(2)	-5(1)	2(2)
C(26)	23(2)	29(2)	26(2)	5(2)	1(1)	7(2)
C(23)	61(3)	60(3)	21(2)	10(2)	4(2)	29(3)
C(1)	24(2)	8(1)	29(2)	-2(1)	-1(1)	3(1)
O(03)	36(2)	36(2)	32(2)	4(1)	12(1)	1(1)
C(16)	30(2)	19(2)	28(2)	-7(2)	-1(2)	4(2)
C(11)	21(2)	15(2)	21(2)	0(1)	-1(1)	-3(1)
C(25)	25(2)	31(2)	36(2)	8(2)	-2(2)	6(2)
O(02)	40(2)	15(1)	59(2)	7(1)	1(2)	1(1)
C(02)	18(2)	21(2)	26(2)	1(2)	-4(1)	1(1)
C(15)	36(2)	29(2)	29(2)	-10(2)	-3(2)	-1(2)

Appendix

Supplementary data of *fac*-[Re(5-Me-Sal-EtPh)$(CO)_3$(MeOH)] **(3)**, for the atomic coordinates, bond distances and angles and anisotropic displacement parameters are given in appendix tables

Table 3.A: Atomic coordinates (x 10^4) and equivalent isotropic displacement parameters (Å^2 x 10^3) for *fac*-[Re(5-Me-Sal-EtPh)$(CO)_3$(MeOH)] (3). U(eq) is defined as one third of the trace of the orthogonalized U^{ij} tensor.

	x	y	z	U(eq)
Re(1)	6459(1)	4494(1)	9135(1)	25(1)
O(1)	5517(2)	3799(2)	8842(3)	29(1)
O(01)	7767(2)	5512(3)	9399(4)	51(1)
O(02)	5965(2)	6235(3)	9662(4)	42(1)
N(1)	6755(2)	3236(3)	8721(4)	27(1)
C(02)	6144(3)	5591(3)	9450(5)	30(1)
C(12)	5448(3)	2934(3)	8942(4)	25(1)
O(03)	7398(3)	4148(3)	11636(4)	52(1)
C(11)	5872(3)	2287(3)	8822(5)	29(1)
C(1)	6455(3)	2476(4)	8647(5)	29(1)
C(14)	4787(3)	1752(4)	9230(5)	36(1)
C(01)	7269(3)	5139(4)	9292(5)	34(1)
C(03)	7045(3)	4274(4)	10690(6)	36(1)
C(13)	4913(3)	2650(3)	9147(4)	27(1)
C(16)	5732(3)	1385(4)	8892(5)	37(1)
C(15)	5209(3)	1120(4)	9098(6)	40(2)
O(04)	5755(2)	4632(3)	7318(4)	42(1)
C(21)	7370(3)	3221(4)	8543(5)	35(1)
C(22)	7171(3)	3601(4)	7444(5)	41(1)
C(23)	7796(3)	3471(4)	7247(5)	37(1)
C(24)	8391(4)	4041(5)	7736(6)	54(2)
C(28)	7775(4)	2784(5)	6622(8)	69(2)
C(25)	8956(4)	3898(7)	7552(8)	75(3)
C(26)	8926(4)	3196(7)	6917(7)	74(3)
C(27)	8352(5)	2647(6)	6475(8)	81(3)
C(141)	4200(4)	1492(4)	9432(6)	50(2)
C(04)	5746(3)	5438(4)	6717(6)	42(1)

Table 3. B: Bond lengths [Å] and angles [°] for *fac*-[Re(5-Me-Sal-EtPh)$(CO)_3$(MeOH)] (3).

Bond	Distance	Bond	Angle
Re(1)-C(03)	1.893(7)	C(03)-Re(1)-C(01)	87.6(3)
Re(1)-C(01)	1.904(6)	C(03)-Re(1)-C(02)	88.5(2)
Re(1)-C(02)	1.922(5)	C(01)-Re(1)-C(02)	87.5(2)
Re(1)-O(1)	2.116(3)	C(03)-Re(1)-O(1)	96.3(2)
Re(1)-N(1)	2.173(4)	C(01)-Re(1)-O(1)	176.1(2)
Re(1)-O(04)	2.189(5)	C(02)-Re(1)-O(1)	92.54(17)
O(1)-C(12)	1.322(6)	C(03)-Re(1)-N(1)	93.2(2)
O(01)-C(01)	1.147(7)	C(01)-Re(1)-N(1)	94.9(2)
O(02)-C(02)	1.139(6)	C(02)-Re(1)-N(1)	177.02(19)
N(1)-C(1)	1.287(7)	O(1)-Re(1)-N(1)	84.88(14)
N(1)-C(21)	1.481(6)	C(03)-Re(1)-O(04)	175.2(2)
C(12)-C(13)	1.401(7)	C(01)-Re(1)-O(04)	95.7(2)
C(12)-C(11)	1.406(7)	C(02)-Re(1)-O(04)	95.0(2)
O(03)-C(03)	1.149(7)	O(1)-Re(1)-O(04)	80.38(16)
C(11)-C(16)	1.402(7)	N(1)-Re(1)-O(04)	83.14(16)
C(11)-C(1)	1.436(7)	C(12)-O(1)-Re(1)	127.9(3)
C(1)-H(1)	0.9500	C(1)-N(1)-C(21)	115.5(4)
C(14)-C(13)	1.390(7)	C(1)-N(1)-Re(1)	125.6(4)
C(14)-C(15)	1.395(8)	C(21)-N(1)-Re(1)	118.8(3)
C(14)-C(141)	1.494(8)	O(02)-C(02)-Re(1)	178.4(5)
C(13)-H(13)	0.9500	O(1)-C(12)-C(13)	118.4(5)
C(16)-C(15)	1.368(8)	O(1)-C(12)-C(11)	123.0(5)
C(16)-H(16)	0.9500	C(13)-C(12)-C(11)	118.6(5)
C(15)-H(15)	0.9500	C(16)-C(11)-C(12)	118.5(5)
O(04)-C(04)	1.474(7)	C(16)-C(11)-C(1)	116.4(5)
O(04)-H(04)	0.83(2)	C(12)-C(11)-C(1)	125.0(5)
C(21)-C(22)	1.492(8)	N(1)-C(1)-C(11)	127.6(5)
C(21)-H(21A)	0.9900	N(1)-C(1)-H(1)	116.2

C(21)-H(21B)	0.9900	C(11)-C(1)-H(1)	116.2
C(22)-C(23)	1.531(8)	C(13)-C(14)-C(15)	118.3(5)
C(22)-H(22A)	0.9900	C(13)-C(14)-C(141)	119.5(5)
C(22)-H(22B)	0.9900	C(15)-C(14)-C(141)	122.1(5)
C(23)-C(28)	1.345(9)	O(01)-C(01)-Re(1)	178.5(6)
C(23)-C(24)	1.378(9)	O(03)-C(03)-Re(1)	179.4(6)
C(24)-C(25)	1.394(10)	C(14)-C(13)-C(12)	122.2(5)
C(24)-H(24)	0.9500	C(14)-C(13)-H(13)	118.9
C(28)-C(27)	1.385(10)	C(12)-C(13)-H(13)	118.9
C(28)-H(28)	0.9500	C(15)-C(16)-C(11)	122.0(5)
C(25)-C(26)	1.365(12)	C(15)-C(16)-H(16)	119.0
C(25)-H(25)	0.9500	C(11)-C(16)-H(16)	119.0
C(26)-C(27)	1.331(12)	C(16)-C(15)-C(14)	120.3(5)
C(26)-H(26)	0.9500	C(16)-C(15)-H(15)	119.8
C(27)-H(27)	0.9500	C(14)-C(15)-H(15)	119.8
C(141)-H(14A)	0.9800	C(04)-O(04)-Re(1)	123.0(4)
C(141)-H(14B)	0.9800	C(04)-O(04)-H(04)	110(6)
C(141)-H(14C)	0.9800	Re(1)-O(04)-H(04)	117(7)
C(04)-H(04A)	0.9800	N(1)-C(21)-C(22)	113.3(4)
C(04)-H(04B)	0.9800	N(1)-C(21)-H(21A)	108.9
C(04)-H(04C)	0.9800	C(22)-C(21)-H(21A)	108.9
		N(1)-C(21)-H(21B)	108.9
		C(22)-C(21)-H(21B)	108.9
		H(21A)-C(21)-H(21B)	107.7
		C(21)-C(22)-C(23)	111.0(5)
		C(21)-C(22)-H(22A)	109.4
		C(23)-C(22)-H(22A)	109.4
		C(21)-C(22)-H(22B)	109.4
		C(23)-C(22)-H(22B)	109.4
		H(22A)-C(22)-H(22B)	108.0
		C(28)-C(23)-C(24)	119.9(6)
		C(28)-C(23)-C(22)	119.9(6)
		C(24)-C(23)-C(22)	120.2(6)

		C(23)-C(24)-C(25)	118.8(7)
		C(23)-C(24)-H(24)	120.6
		C(25)-C(24)-H(24)	120.6
		C(23)-C(28)-C(27)	120.0(7)
		C(23)-C(28)-H(28)	120.0
		C(27)-C(28)-H(28)	120.0
		C(26)-C(25)-C(24)	120.6(7)
		C(26)-C(25)-H(25)	119.7
		C(24)-C(25)-H(25)	119.7
		C(27)-C(26)-C(25)	119.2(7)
		C(27)-C(26)-H(26)	120.4
		C(25)-C(26)-H(26)	120.4
		C(26)-C(27)-C(28)	121.5(8)
		C(26)-C(27)-H(27)	119.3
		C(28)-C(27)-H(27)	119.3
		C(14)-C(141)-H(14A)	109.5
		C(14)-C(141)-H(14B)	109.5
		H(14A)-C(141)-H(14B)	109.5
		C(14)-C(141)-H(14C)	109.5
		H(14A)-C(141)-H(14C)	109.5
		H(14B)-C(141)-H(14C)	109.5
		O(04)-C(04)-H(04A)	109.5
		O(04)-C(04)-H(04B)	109.5
		H(04A)-C(04)-H(04B)	109.5
		O(04)-C(04)-H(04C)	109.5
		H(04A)-C(04)-H(04C)	109.5
		H(04B)-C(04)-H(04C)	109.5

Table 3.C: Anisotropic displacement parameters ($Å^2 x\ 10^3$) for *fac*-[Re(5-Me-Sal-EtPh)$(CO)_3$(MeOH)] (3). The anisotropic displacement factor exponent takes the form: $-2\pi^2[\ h^2 a^{*2} U^{11} + ... + 2\ h\ k\ a^*\ b^*\ U^{12}\ ]$

	U^{11}	U^{22}	U^{33}	U^{23}	U^{13}	U^{12}
Re(1)	22(1)	27(1)	28(1)	-2(1)	16(1)	-1(1)
O(1)	26(2)	24(2)	39(2)	4(2)	20(2)	-1(1)
O(01)	37(2)	58(3)	67(3)	-11(2)	34(2)	-16(2)
O(02)	47(2)	34(2)	58(3)	-4(2)	36(2)	2(2)
N(1)	26(2)	29(2)	26(3)	-1(2)	14(2)	3(2)
C(02)	31(3)	30(3)	37(3)	2(2)	24(3)	-3(2)
C(12)	23(2)	29(2)	18(3)	1(2)	9(2)	-4(2)
O(03)	61(3)	56(3)	30(3)	3(2)	18(2)	14(2)
C(11)	26(3)	34(3)	22(3)	-4(2)	11(2)	-3(2)
C(1)	33(3)	31(3)	26(3)	-3(2)	17(3)	6(2)
C(14)	36(3)	38(3)	33(3)	9(3)	17(3)	-3(2)
C(01)	30(3)	37(3)	36(3)	-6(3)	19(3)	-1(2)
C(03)	38(3)	33(3)	41(4)	-1(3)	23(3)	5(2)
C(13)	27(2)	30(3)	26(3)	6(2)	15(2)	1(2)
C(16)	37(3)	32(3)	37(4)	4(3)	17(3)	7(2)
C(15)	42(3)	28(3)	47(4)	5(3)	21(3)	-1(2)
O(04)	36(2)	49(2)	38(2)	2(2)	18(2)	-2(2)
C(21)	31(3)	41(3)	38(4)	5(3)	22(3)	8(2)
C(22)	34(3)	52(4)	35(4)	6(3)	19(3)	11(3)
C(23)	34(3)	50(3)	35(3)	7(3)	22(3)	5(3)
C(24)	49(4)	66(4)	53(5)	-17(4)	32(4)	-10(3)
C(28)	63(5)	71(5)	95(7)	-40(5)	58(5)	-16(4)
C(25)	41(4)	120(7)	63(6)	-11(5)	28(4)	-25(4)
C(26)	41(4)	144(8)	55(5)	-3(5)	38(4)	11(5)
C(27)	74(6)	98(6)	97(8)	-32(6)	63(6)	4(5)
C(141)	52(4)	47(3)	61(5)	18(3)	36(4)	-3(3)
C(04)	36(2)	49(2)	38(2)	2(2)	18(2)	-2(2)

Appendix

Supplementary data of *fac*-[^{99}Tc(Sal-*m*Tol)$(CO)_3]_2$ **(4)**, for the atomic coordinates, bond distances and angles and anisotropic displacement parameters are given in appendix tables

Table 4.A: Atomic coordinates (x 10^4) and equivalent isotropic displacement parameters ($Å^2$x 10^3) for *fac*-[^{99}Tc(Sal-*m*Tol)$(CO)_3]_2$ (4). U(eq) is defined as one third of the trace of the orthogonalized U^{ij} tensor.

	x	y	z	U(eq)
Tc(1)	5677(1)	3597(1)	4115(1)	24(1)
C(16)	5794(5)	4005(3)	6887(3)	26(1)
C(15)	6857(5)	4640(4)	8106(3)	35(1)
C(14)	6759(6)	3924(4)	9013(4)	45(1)
C(13)	5600(6)	2553(4)	8716(4)	45(1)
C(12)	4515(5)	1945(4)	7535(4)	39(1)
C(11)	4575(5)	2638(3)	6594(3)	27(1)
C(1)	3233(5)	1979(3)	5408(3)	27(1)
C(21)	1765(5)	1542(4)	3311(3)	29(1)
C(26)	745(5)	2387(4)	2766(4)	37(1)
C(25)	-709(5)	1726(4)	1737(4)	45(1)
C(24)	-1151(6)	216(5)	1258(4)	48(1)
C(23)	-155(5)	-653(4)	1787(4)	43(1)
C(22)	1329(5)	30(4)	2838(4)	37(1)
C(01)	5139(5)	2553(4)	2403(4)	30(1)
C(02)	7775(5)	4776(3)	3894(3)	27(1)
C(03)	7142(5)	2274(4)	4455(3)	29(1)
N(1)	3288(4)	2276(3)	4384(3)	25(1)
O(1)	5928(3)	4744(2)	6027(2)	24(1)
O(01)	4810(4)	1880(3)	1384(3)	49(1)
O(02)	9026(3)	5440(3)	3726(3)	42(1)
O(03)	8080(4)	1492(3)	4662(3)	43(1)
C(231)	-626(7)	-2290(4)	1268(5)	68(2)

Table 4.B: Bond lengths [Å] and angles [°] for *fac*-[^{99}Tc(Sal-*m*Tol)(CO)$_3$]$_2$ (4).

Bond	Distance	Bond	Angle
Tc(1)-C(03)	1.889(4)	C(03)-Tc(1)-C(01)	87.71(15)
Tc(1)-C(01)	1.898(4)	C(03)-Tc(1)-C(02)	87.52(14)
Tc(1)-C(02)	1.922(4)	C(01)-Tc(1)-C(02)	87.49(15)
Tc(1)-O(1)	2.157(2)	C(03)-Tc(1)-O(1)	96.64(12)
Tc(1)-N(1)	2.188(3)	C(01)-Tc(1)-O(1)	172.87(12)
Tc(1)-O(1)#1	2.189(2)	C(02)-Tc(1)-O(1)	98.31(12)
C(16)-O(1)	1.360(4)	C(03)-Tc(1)-N(1)	92.82(12)
C(16)-C(15)	1.391(5)	C(01)-Tc(1)-N(1)	93.10(13)
C(16)-C(11)	1.407(4)	C(02)-Tc(1)-N(1)	179.33(13)
C(15)-C(14)	1.387(5)	O(1)-Tc(1)-N(1)	81.08(9)
C(15)-H(15)	0.9500	C(03)-Tc(1)-O(1)#1	172.78(12)
C(14)-C(13)	1.388(5)	C(01)-Tc(1)-O(1)#1	99.50(12)
C(14)-H(14)	0.9500	C(02)-Tc(1)-O(1)#1	92.98(11)
C(13)-C(12)	1.362(5)	O(1)-Tc(1)-O(1)#1	76.16(9)
C(13)-H(13)	0.9500	N(1)-Tc(1)-O(1)#1	86.62(9)
C(12)-C(11)	1.403(5)	O(1)-C(16)-C(15)	119.0(3)
C(12)-H(12)	0.9500	O(1)-C(16)-C(11)	122.1(3)
C(11)-C(1)	1.447(5)	C(15)-C(16)-C(11)	118.8(3)
C(1)-N(1)	1.283(4)	C(14)-C(15)-C(16)	120.9(3)
C(1)-H(1)	0.9500	C(14)-C(15)-H(15)	119.6
C(21)-C(22)	1.381(4)	C(16)-C(15)-H(15)	119.6
C(21)-C(26)	1.384(5)	C(15)-C(14)-C(13)	120.4(4)
C(21)-N(1)	1.445(4)	C(15)-C(14)-H(14)	119.8
C(26)-C(25)	1.377(5)	C(13)-C(14)-H(14)	119.8
C(26)-H(26)	0.9500	C(12)-C(13)-C(14)	119.1(3)
C(25)-C(24)	1.380(5)	C(12)-C(13)-H(13)	120.4
C(25)-H(25)	0.9500	C(14)-C(13)-H(13)	120.4
C(24)-C(23)	1.383(5)	C(13)-C(12)-C(11)	122.0(3)

C(24)-H(24)	0.9500	C(13)-C(12)-H(12)	119.0
C(23)-C(22)	1.407(5)	C(11)-C(12)-H(12)	119.0
C(23)-C(231)	1.496(5)	C(12)-C(11)-C(16)	118.7(3)
C(22)-H(22)	0.9500	C(12)-C(11)-C(1)	117.7(3)
C(01)-O(01)	1.143(4)	C(16)-C(11)-C(1)	123.3(3)
C(02)-O(02)	1.148(4)	N(1)-C(1)-C(11)	126.1(3)
C(03)-O(03)	1.156(4)	N(1)-C(1)-H(1)	117.0
O(1)-Tc(1)#1	2.189(2)	C(11)-C(1)-H(1)	117.0
C(231)-H(23A)	0.9800	C(22)-C(21)-C(26)	120.5(4)
C(231)-H(23B)	0.9800	C(22)-C(21)-N(1)	121.0(3)
C(231)-H(23C)	0.9800	C(26)-C(21)-N(1)	118.6(3)
		C(25)-C(26)-C(21)	120.2(4)
		C(25)-C(26)-H(26)	119.9
		C(21)-C(26)-H(26)	119.9
		C(26)-C(25)-C(24)	119.7(4)
		C(26)-C(25)-H(25)	120.2
		C(24)-C(25)-H(25)	120.2
		C(25)-C(24)-C(23)	121.3(4)
		C(25)-C(24)-H(24)	119.4
		C(23)-C(24)-H(24)	119.4
		C(24)-C(23)-C(22)	118.7(3)
		C(24)-C(23)-C(231)	121.5(4)
		C(22)-C(23)-C(231)	119.8(4)
		C(21)-C(22)-C(23)	119.7(4)
		C(21)-C(22)-H(22)	120.2
		C(23)-C(22)-H(22)	120.2
		O(01)-C(01)-Tc(1)	177.6(3)
		O(02)-C(02)-Tc(1)	177.6(3)
		O(03)-C(03)-Tc(1)	178.1(3)
		C(1)-N(1)-C(21)	117.4(3)
		C(1)-N(1)-Tc(1)	123.8(2)
		C(21)-N(1)-Tc(1)	118.4(2)
		C(16)-O(1)-Tc(1)	121.29(19)

		C(16)-O(1)-Tc(1)#1	118.7(2)
		Tc(1)-O(1)-Tc(1)#1	103.84(9)
		C(23)-C(231)-H(23A)	109.5
		C(23)-C(231)-H(23B)	109.5
		H(23A)-C(231)-H(23B)	109.5
		C(23)-C(231)-H(23C)	109.5
		H(23A)-C(231)-H(23C)	109.5
		H(23B)-C(231)-H(23C)	109.5

Table 4.C: Anisotropic displacement parameters ($Å^2 x\ 10^3$) for *fac*-[^{99}Tc(Sal-*m*Tol)(CO)$_3$]$_2$. The anisotropic displacement factor exponent takes the form: $-2\pi^2[\ h^2a^{*2}U^{11} + ... + 2\ h\ k\ a^*\ b^*\ U^{12}\ ]$

	U^{11}	U^{22}	U^{33}	U^{23}	U^{13}	U^{12}
Tc(1)	27(1)	21(1)	19(1)	3(1)	6(1)	-2(1)
C(16)	32(2)	26(2)	22(2)	9(2)	9(2)	7(1)
C(15)	44(2)	33(2)	24(2)	11(2)	5(2)	0(2)
C(14)	54(3)	53(2)	22(2)	9(2)	3(2)	5(2)
C(13)	61(3)	50(2)	30(3)	24(2)	14(2)	7(2)
C(12)	48(3)	37(2)	34(3)	16(2)	15(2)	1(2)
C(11)	34(2)	25(2)	23(2)	6(2)	11(2)	3(2)
C(1)	30(2)	23(2)	28(2)	7(2)	11(2)	-2(1)
C(21)	27(2)	32(2)	22(2)	0(2)	10(2)	-7(2)
C(26)	33(2)	40(2)	33(2)	10(2)	7(2)	-4(2)
C(25)	33(2)	56(3)	42(3)	16(2)	7(2)	-3(2)
C(24)	36(2)	67(3)	31(3)	7(2)	7(2)	-3(2)
C(23)	34(2)	39(2)	42(3)	-10(2)	15(2)	-9(2)
C(22)	37(2)	33(2)	35(2)	2(2)	14(2)	-1(2)
C(01)	33(2)	31(2)	21(2)	5(2)	7(2)	1(2)
C(02)	28(2)	28(2)	23(2)	6(2)	1(2)	6(2)
C(03)	33(2)	29(2)	21(2)	5(2)	10(2)	-3(2)
N(1)	27(2)	24(1)	22(2)	4(1)	7(1)	1(1)
O(1)	34(1)	21(1)	15(1)	5(1)	5(1)	2(1)
O(01)	48(2)	61(2)	23(2)	-4(1)	8(1)	-1(1)
O(02)	35(2)	39(1)	56(2)	19(1)	20(1)	-1(1)
O(03)	50(2)	34(1)	51(2)	16(1)	16(2)	14(1)

C(231)	60(3)	44(3)	72(4)	-16(2)	11(3)	-4(2)

Supplementary data of *fac*-[^{99}Tc(5-Me-Sal-CyPent)$(CO)_3]_2$ **(5)** for the atomic coordinates, bond distances and angles and anisotropic displacement parameters are given in appendix tables

Table 5.A: Atomic coordinates (x 10^4) and equivalent isotropic displacement parameters (Å^2 x 10^3) for *fac*-[^{99}Tc(5-Me-Sal-CyPent)$(CO)_3]_2$ (5) U(eq) is defined as one third of the trace of the orthogonalized U^{ij} tensor.

	x	y	z	U(eq)
Tc(1)	8025(1)	4782(1)	3583(1)	22(1)
C(01)	5849(4)	3582(4)	2920(4)	31(1)
O(01)	4534(3)	2863(3)	2502(3)	43(1)
C(03)	7119(4)	6197(4)	4459(3)	31(1)
O(03)	6570(4)	7070(3)	4929(3)	51(1)
C(02)	7098(4)	5586(3)	1891(4)	26(1)
O(02)	6528(3)	6087(2)	882(3)	35(1)
N(1)	9210(4)	3275(3)	2608(3)	33(1)
O(1)	10570(3)	6011(2)	4425(2)	22(1)
C(12)	11339(4)	6249(3)	3530(3)	25(1)
C(13)	12239(4)	7610(4)	3696(4)	32(1)
C(14)	13047(5)	7918(4)	2800(4)	41(1)
C(15)	12968(5)	6836(5)	1747(4)	49(1)
C(16)	12114(5)	5498(5)	1583(4)	42(1)
C(11)	11246(4)	5170(4)	2446(3)	30(1)
C(1)	10392(5)	3712(4)	2205(4)	38(1)
C(141)	14003(6)	9413(5)	3018(5)	60(1)
C(21)	8497(6)	1728(4)	2245(7)	74(2)
C(23)	8397(8)	-672(5)	2487(7)	85(2)
C(22A)	8538(11)	987(7)	3165(8)	45(2)
C(24A)	8573(12)	-671(7)	1177(8)	44(2)
C(25A)	9319(9)	831(6)	1188(7)	38(2)
C(22B)	9803(13)	650(9)	2969(11)	53(3)
C(24B)	7213(18)	-549(9)	957(11)	61(3)
C(25B)	7264(11)	1085(9)	1042(9)	44(2)

Table 5.B: Bond lengths [Å] and angles [°] for *fac*-[^{99}Tc(5-Me-Sal-CyPent)(CO)$_3$]$_2$ (5).

Bond	Distance	Bond	Angle
Tc(1)-C(02)	1.894(3)	C(02)-Tc(1)-C(01)	87.21(13)
Tc(1)-C(01)	1.903(3)	C(02)-Tc(1)-C(03)	87.65(13)
Tc(1)-C(03)	1.918(3)	C(01)-Tc(1)-C(03)	88.15(14)
Tc(1)-O(1)	2.149(2)	C(02)-Tc(1)-O(1)	96.77(11)
Tc(1)-O(1)#1	2.192(2)	C(01)-Tc(1)-O(1)	175.59(11)
Tc(1)-N(1)	2.195(3)	C(03)-Tc(1)-O(1)	93.90(12)
C(01)-O(01)	1.146(4)	C(02)-Tc(1)-O(1)#1	172.50(10)
C(03)-O(03)	1.141(4)	C(01)-Tc(1)-O(1)#1	100.07(11)
C(02)-O(02)	1.142(4)	C(03)-Tc(1)-O(1)#1	94.35(11)
N(1)-C(1)	1.286(5)	O(1)-Tc(1)-O(1)#1	75.91(8)
N(1)-C(21)	1.480(5)	C(02)-Tc(1)-N(1)	91.68(12)
O(1)-C(12)	1.356(4)	C(01)-Tc(1)-N(1)	95.65(12)
O(1)-Tc(1)#1	2.192(2)	C(03)-Tc(1)-N(1)	176.10(12)
C(12)-C(13)	1.393(4)	O(1)-Tc(1)-N(1)	82.36(9)
C(12)-C(11)	1.398(4)	O(1)#1-Tc(1)-N(1)	85.83(9)
C(13)-C(14)	1.396(5)	O(01)-C(01)-Tc(1)	179.1(3)
C(13)-H(13)	0.9500	O(03)-C(03)-Tc(1)	176.9(3)
C(14)-C(15)	1.382(6)	O(02)-C(02)-Tc(1)	178.9(3)
C(14)-C(141)	1.513(5)	C(1)-N(1)-C(21)	118.4(3)
C(15)-C(16)	1.360(6)	C(1)-N(1)-Tc(1)	121.8(2)
C(15)-H(15)	0.9500	C(21)-N(1)-Tc(1)	119.3(3)
C(16)-C(11)	1.408(5)	C(12)-O(1)-Tc(1)	119.51(18)
C(16)-H(16)	0.9500	C(12)-O(1)-Tc(1)#1	120.27(18)
C(11)-C(1)	1.446(5)	Tc(1)-O(1)-Tc(1)#1	104.09(8)
C(1)-H(1)	0.94(4)	O(1)-C(12)-C(13)	118.8(3)
C(141)-H(14A)	0.9800	O(1)-C(12)-C(11)	121.7(3)
C(141)-H(14B)	0.9800	C(13)-C(12)-C(11)	119.5(3)
C(141)-H(14C)	0.9800	C(12)-C(13)-C(14)	121.3(3)
C(21)-C(22A)	1.238(9)	C(12)-C(13)-H(13)	119.4
C(21)-C(25B)	1.300(9)	C(14)-C(13)-H(13)	119.4
C(21)-C(22B)	1.604(9)	C(15)-C(14)-C(13)	118.7(4)
C(21)-C(25A)	1.706(8)	C(15)-C(14)-C(141)	121.8(4)

C(23)-C(24A)	1.419(9)	C(13)-C(14)-C(141)	119.4(4)
C(23)-C(24B)	1.526(12)	C(16)-C(15)-C(14)	120.6(3)
C(23)-C(22B)	1.535(10)	C(16)-C(15)-H(15)	119.7
C(23)-C(22A)	1.619(8)	C(14)-C(15)-H(15)	119.7
C(23)-H(23A)	0.9900	C(15)-C(16)-C(11)	121.7(4)
C(23)-H(23B)	0.9900	C(15)-C(16)-H(16)	119.1
C(22A)-H(22A)	0.9900	C(11)-C(16)-H(16)	119.1
C(22A)-H(22B)	0.9900	C(12)-C(11)-C(16)	118.1(3)
C(24A)-C(25A)	1.502(9)	C(12)-C(11)-C(1)	124.0(3)
C(24A)-H(24A)	0.9900	C(16)-C(11)-C(1)	117.8(3)
C(24A)-H(24B)	0.9900	N(1)-C(1)-C(11)	127.0(3)
C(25A)-H(25A)	0.9900	N(1)-C(1)-H(1)	118(3)
C(25A)-H(25B)	0.9900	C(11)-C(1)-H(1)	115(3)
C(22B)-H(22C)	0.9900	C(14)-C(141)-H(14A)	109.5
C(22B)-H(22D)	0.9900	C(14)-C(141)-H(14B)	109.5
C(24B)-C(25B)	1.537(12)	H(14A)-C(141)-H(14B)	109.5
C(24B)-H(24C)	0.9900	C(14)-C(141)-H(14C)	109.5
C(24B)-H(24D)	0.9900	H(14A)-C(141)-H(14C)	109.5
C(25B)-H(25C)	0.9900	H(14B)-C(141)-H(14C)	109.5
C(25B)-H(25D)	0.9900	C(22A)-C(21)-N(1)	122.5(6)
		C(25B)-C(21)-N(1)	125.9(6)
		C(25B)-C(21)-C(22B)	111.0(6)
		N(1)-C(21)-C(22B)	116.7(4)
		C(22A)-C(21)-C(25A)	106.8(5)
		N(1)-C(21)-C(25A)	110.8(4)
		C(24B)-C(23)-C(22B)	104.1(6)
		C(24A)-C(23)-C(22A)	107.2(5)
		C(24A)-C(23)-H(23A)	110.3
		C(22A)-C(23)-H(23A)	110.3
		C(24A)-C(23)-H(23B)	110.3
		C(22A)-C(23)-H(23B)	110.3
		H(23A)-C(23)-H(23B)	108.5
		C(21)-C(22A)-C(23)	107.6(6)
		C(21)-C(22A)-H(22A)	110.2
		C(23)-C(22A)-H(22A)	110.2
		C(21)-C(22A)-H(22B)	110.2
		C(23)-C(22A)-H(22B)	110.2
		H(22A)-C(22A)-H(22B)	108.5
		C(23)-C(24A)-C(25A)	107.1(5)

		C(23)-C(24A)-H(24A)	110.3
		C(25A)-C(24A)-H(24A)	110.3
		C(23)-C(24A)-H(24B)	110.3
		C(25A)-C(24A)-H(24B)	110.3
		H(24A)-C(24A)-H(24B)	108.6
		C(24A)-C(25A)-C(21)	98.2(5)
		C(24A)-C(25A)-H(25A)	112.1
		C(21)-C(25A)-H(25A)	112.1
		C(24A)-C(25A)-H(25B)	112.1
		C(21)-C(25A)-H(25B)	112.1
		H(25A)-C(25A)-H(25B)	109.8
		C(23)-C(22B)-C(21)	95.0(6)
		C(23)-C(22B)-H(22C)	112.7
		C(21)-C(22B)-H(22C)	112.7
		C(23)-C(22B)-H(22D)	112.7
		C(21)-C(22B)-H(22D)	112.7
		H(22C)-C(22B)-H(22D)	110.2
		C(23)-C(24B)-C(25B)	102.1(6)
		C(23)-C(24B)-H(24C)	111.4
		C(25B)-C(24B)-H(24C)	111.4
		C(23)-C(24B)-H(24D)	111.4
		C(25B)-C(24B)-H(24D)	111.4
		H(24C)-C(24B)-H(24D)	109.2
		C(21)-C(25B)-C(24B)	109.2(7)
		C(21)-C(25B)-H(25C)	109.8
		C(24B)-C(25B)-H(25C)	109.8
		C(21)-C(25B)-H(25D)	109.8
		C(24B)-C(25B)-H(25D)	109.8
		H(25C)-C(25B)-H(25D)	108.3

Table 5.C; Anisotropic displacement parameters ($Å^2 x\ 10^3$) for *fac*-[^{99}Tc(5-Me-Sal-CyPent)(CO)$_3$]$_2$ (5). The anisotropic displacement factor exponent takes the form: $-2\pi^2[\ h^2 a^{*2} U^{11} + ... + 2\ h\ k\ a^*\ b^*\ U^{12}\ ]$

	U^{11}	U^{22}	U^{33}	U^{23}	U^{13}	U^{12}
Tc(1)	21(1)	20(1)	26(1)	3(1)	11(1)	0(1)
C(01)	32(2)	31(2)	32(2)	9(2)	13(2)	5(2)
O(01)	30(1)	42(1)	53(2)	9(1)	15(1)	-9(1)

C(03)	27(2)	41(2)	25(2)	9(2)	10(1)	10(2)
O(03)	51(2)	63(2)	46(2)	4(1)	22(1)	31(2)
C(02)	25(2)	21(1)	32(2)	-2(1)	13(1)	-1(1)
O(02)	41(1)	34(1)	31(1)	9(1)	14(1)	4(1)
N(1)	27(2)	23(1)	37(2)	-7(1)	5(1)	2(1)
O(1)	22(1)	25(1)	21(1)	4(1)	12(1)	-1(1)
C(12)	22(2)	32(2)	23(2)	7(1)	10(1)	5(1)
C(13)	27(2)	36(2)	33(2)	11(2)	12(2)	-2(1)
C(14)	26(2)	59(2)	44(2)	28(2)	16(2)	3(2)
C(15)	35(2)	85(3)	44(2)	32(2)	27(2)	18(2)
C(16)	36(2)	71(3)	27(2)	10(2)	18(2)	22(2)
C(11)	26(2)	38(2)	26(2)	4(1)	13(1)	7(1)
C(1)	32(2)	39(2)	33(2)	-10(2)	7(2)	10(2)
C(141)	46(2)	72(3)	70(3)	37(3)	29(2)	-5(2)
C(21)	36(2)	19(2)	141(5)	-14(3)	17(3)	0(2)
C(23)	87(4)	36(2)	99(5)	18(3)	5(4)	-10(2)
C(22A)	62(5)	23(3)	40(4)	0(3)	17(4)	-11(3)
C(24A)	59(5)	27(3)	40(4)	-2(3)	16(4)	8(3)
C(25A)	49(4)	28(3)	39(4)	2(3)	22(3)	8(3)
C(22B)	45(6)	29(4)	65(6)	11(4)	0(5)	7(4)
C(24B)	92(9)	28(5)	46(6)	-3(4)	17(6)	-7(5)
C(25B)	43(5)	38(4)	36(5)	7(4)	3(4)	-7(4)

Supplementary data of *fac*-[^{99}Tc(5-Me-Sal-EtPh)$(CO)_3$] **(6)** for the atomic coordinates, bond distances and angles and anisotropic displacement parameters are given in appendix tables

Table 6.A: Atomic coordinates (x 10^4) and equivalent isotropic displacement parameters (Å^{2}x 10^3) for *fac*-[^{99}Tc(5-Me-Sal-EtPh)$(CO)_3$] (6). U(eq) is defined as one third of the trace of the orthogonalized U^{ij} tensor.

	x	y	z	U(eq)
Tc(1)	5318(1)	5461(1)	1221(1)	28(1)
O(1)	3942(3)	4571(1)	478(2)	27(1)
O(02)	2090(3)	6415(1)	764(2)	54(1)

N(1)	7472(4)	4725(1)	1583(2)	30(1)
O(03)	4524(4)	5426(2)	3626(2)	60(1)
C(15)	3905(6)	2737(2)	2185(3)	47(1)
C(02)	3311(5)	6059(2)	904(3)	36(1)
C(141)	669(5)	2548(2)	1461(4)	64(1)
C(16)	5456(5)	3107(2)	2244(3)	42(1)
C(13)	2425(4)	3571(2)	951(3)	35(1)
C(1)	7225(5)	4083(2)	1753(3)	33(1)
C(12)	3969(4)	3974(2)	1041(3)	30(1)
C(21)	9327(4)	4969(2)	1778(3)	38(1)
C(14)	2374(5)	2955(2)	1533(3)	42(1)
C(11)	5514(5)	3733(2)	1680(3)	33(1)
C(03)	4783(5)	5420(2)	2715(3)	39(1)
C(23)	10003(5)	4484(2)	3733(3)	48(1)
C(22)	9866(5)	5125(2)	3025(3)	48(1)
C(28)	8610(6)	4263(2)	4291(3)	59(1)
C(24)	11497(6)	4069(2)	3787(4)	61(1)
C(27)	8715(8)	3649(3)	4855(4)	74(1)
C(25)	11584(7)	3460(3)	4364(4)	79(2)
C(26)	10200(9)	3253(3)	4887(4)	86(2)
C(01)	6686(5)	6245(2)	1692(3)	39(1)
O(01)	7515(4)	6720(1)	1977(3)	61(1)

Table 6.B: Bond lengths [Å] and angles [°] for *fac*-[^{99}Tc(5-Me-Sal-EtPh)(CO)$_3$] (6).

Bond	Distance	Bond	Angle
Tc(1)-C(01)	1.892(4)	C(01)-Tc(1)-C(03)	85.65(15)
Tc(1)-C(03)	1.899(4)	C(01)-Tc(1)-C(02)	87.46(15)
Tc(1)-C(02)	1.914(4)	C(03)-Tc(1)-C(02)	87.45(15)
Tc(1)-O(1)	2.158(2)	C(01)-Tc(1)-O(1)	172.02(12)
Tc(1)-N(1)	2.172(3)	C(03)-Tc(1)-O(1)	102.14(12)
Tc(1)-O(1)#1	2.195(2)	C(02)-Tc(1)-O(1)	94.59(11)
O(1)-C(12)	1.348(3)	C(01)-Tc(1)-N(1)	96.15(13)
O(1)-Tc(1)#1	2.195(2)	C(03)-Tc(1)-N(1)	91.55(13)

O(02)-C(02)	1.149(4)	C(02)-Tc(1)-N(1)	176.18(12)
N(1)-C(1)	1.286(4)	O(1)-Tc(1)-N(1)	82.01(9)
N(1)-C(21)	1.471(4)	C(01)-Tc(1)-O(1)#1	96.23(12)
O(03)-C(03)	1.142(4)	C(03)-Tc(1)-O(1)#1	175.28(11)
C(15)-C(16)	1.370(5)	C(02)-Tc(1)-O(1)#1	96.95(11)
C(15)-C(14)	1.381(5)	O(1)-Tc(1)-O(1)#1	75.87(8)
C(15)-H(15)	0.9300	N(1)-Tc(1)-O(1)#1	83.95(9)
C(141)-C(14)	1.507(5)	C(12)-O(1)-Tc(1)	120.69(19)
C(141)-H(14A)	0.9600	C(12)-O(1)-Tc(1)#1	117.23(17)
C(141)-H(14B)	0.9600	Tc(1)-O(1)-Tc(1)#1	104.13(8)
C(141)-H(14C)	0.9600	C(1)-N(1)-C(21)	116.3(3)
C(16)-C(11)	1.402(4)	C(1)-N(1)-Tc(1)	123.7(2)
C(16)-H(16)	0.9300	C(21)-N(1)-Tc(1)	119.5(2)
C(13)-C(14)	1.395(4)	C(16)-C(15)-C(14)	121.1(3)
C(13)-C(12)	1.399(4)	C(16)-C(15)-H(15)	119.5
C(13)-H(13)	0.9300	C(14)-C(15)-H(15)	119.5
C(1)-C(11)	1.455(5)	O(02)-C(02)-Tc(1)	176.8(3)
C(1)-H(7)	0.9300	C(14)-C(141)-H(14A)	109.5
C(12)-C(11)	1.395(5)	C(14)-C(141)-H(14B)	109.5
C(21)-C(22)	1.538(5)	H(14A)-C(141)-H(14B)	109.5
C(21)-H(13A)	0.9700	C(14)-C(141)-H(14C)	109.5
C(21)-H(13B)	0.9700	H(14A)-C(141)-H(14C)	109.5
C(23)-C(24)	1.383(5)	H(14B)-C(141)-H(14C)	109.5
C(23)-C(28)	1.389(5)	C(15)-C(16)-C(11)	120.9(4)
C(23)-C(22)	1.512(5)	C(15)-C(16)-H(16)	119.5
C(22)-H(21A)	0.9700	C(11)-C(16)-H(16)	119.5
C(22)-H(21B)	0.9700	C(14)-C(13)-C(12)	121.4(3)
C(28)-C(27)	1.375(6)	C(14)-C(13)-H(13)	119.3
C(28)-H(28)	0.9300	C(12)-C(13)-H(13)	119.3
C(24)-C(25)	1.374(6)	N(1)-C(1)-C(11)	126.3(3)
C(24)-H(24)	0.9300	N(1)-C(1)-H(7)	116.8
C(27)-C(26)	1.359(7)	C(11)-C(1)-H(7)	116.8
C(27)-H(27)	0.9300	O(1)-C(12)-C(11)	121.7(3)
C(25)-C(26)	1.351(7)	O(1)-C(12)-C(13)	119.2(3)
C(25)-H(25)	0.9300	C(11)-C(12)-C(13)	119.1(3)
C(26)-H(26)	0.9300	N(1)-C(21)-C(22)	110.3(3)
C(01)-O(01)	1.147(4)	N(1)-C(21)-H(13A)	109.6
		C(22)-C(21)-H(13A)	109.6
		N(1)-C(21)-H(13B)	109.6

		C(22)-C(21)-H(13B)	109.6
		H(13A)-C(21)-H(13B)	108.1
		C(15)-C(14)-C(13)	118.5(3)
		C(15)-C(14)-C(141)	121.3(3)
		C(13)-C(14)-C(141)	120.2(4)
		C(12)-C(11)-C(16)	119.0(3)
		C(12)-C(11)-C(1)	123.4(3)
		C(16)-C(11)-C(1)	117.5(3)
		O(03)-C(03)-Tc(1)	176.1(3)
		C(24)-C(23)-C(28)	117.5(4)
		C(24)-C(23)-C(22)	120.5(4)
		C(28)-C(23)-C(22)	121.9(4)
		C(23)-C(22)-C(21)	112.3(3)
		C(23)-C(22)-H(21A)	109.1
		C(21)-C(22)-H(21A)	109.1
		C(23)-C(22)-H(21B)	109.1
		C(21)-C(22)-H(21B)	109.1
		H(21A)-C(22)-H(21B)	107.9
		C(27)-C(28)-C(23)	120.7(4)
		C(27)-C(28)-H(28)	119.7
		C(23)-C(28)-H(28)	119.7
		C(25)-C(24)-C(23)	121.0(4)
		C(25)-C(24)-H(24)	119.5
		C(23)-C(24)-H(24)	119.5
		C(26)-C(27)-C(28)	120.3(5)
		C(26)-C(27)-H(27)	119.9
		C(28)-C(27)-H(27)	119.9
		C(26)-C(25)-C(24)	120.3(5)
		C(26)-C(25)-H(25)	119.8
		C(24)-C(25)-H(25)	119.8
		C(25)-C(26)-C(27)	120.2(5)
		C(25)-C(26)-H(26)	119.9
		C(27)-C(26)-H(26)	119.9
		O(01)-C(01)-Tc(1)	179.9(5)

Table 6.C: Anisotropic displacement parameters ($Å^2$ x 10^3) for *fac*-[^{99}Tc(5-Me-Sal-EtPh)$(CO)_3$] (6).The anisotropic displacement factor exponent takes the form: $-2\pi^2[h^2a^{*2}U^{11} + ... + 2 h k a^* b^* U^{12}]$

	U^{11}	U^{22}	U^{33}	U^{23}	U^{13}	U^{12}
Tc(1)	29(1)	20(1)	34(1)	-3(1)	0(1)	0(1)
O(1)	28(1)	18(1)	33(1)	1(1)	-1(1)	0(1)
O(02)	45(2)	51(2)	65(2)	-7(1)	0(2)	22(1)
N(1)	30(2)	28(1)	31(2)	-1(1)	-1(1)	3(1)
O(03)	57(2)	83(2)	40(2)	-6(2)	13(2)	3(2)
C(15)	58(3)	26(2)	58(3)	12(2)	14(2)	3(2)
C(02)	36(2)	30(2)	43(2)	-6(2)	3(2)	2(2)
C(141)	54(3)	34(2)	107(4)	10(2)	19(3)	-9(2)
C(16)	47(2)	29(2)	48(2)	6(2)	2(2)	5(2)
C(13)	30(2)	27(2)	48(2)	0(2)	2(2)	1(2)
C(1)	35(2)	31(2)	32(2)	1(2)	1(2)	10(2)
C(12)	33(2)	21(2)	35(2)	-1(1)	6(2)	1(2)
C(21)	31(2)	37(2)	44(2)	3(2)	2(2)	1(2)
C(14)	44(2)	27(2)	55(3)	-1(2)	13(2)	-4(2)
C(11)	33(2)	20(2)	45(2)	3(2)	7(2)	6(2)
C(03)	30(2)	39(2)	46(2)	-6(2)	1(2)	0(2)
C(23)	48(3)	54(2)	39(2)	-7(2)	-8(2)	-3(2)
C(22)	34(2)	53(2)	55(3)	-9(2)	-7(2)	-3(2)
C(28)	56(3)	77(3)	42(2)	-9(2)	-1(2)	-4(2)
C(24)	58(3)	69(3)	55(3)	7(2)	2(2)	11(2)
C(27)	97(4)	82(3)	43(3)	7(3)	16(3)	-13(3)
C(25)	90(4)	85(4)	62(3)	21(3)	8(3)	32(3)
C(26)	133(5)	75(3)	49(3)	17(3)	10(3)	12(4)
C(01)	39(2)	29(2)	47(2)	-7(2)	2(2)	2(2)
O(01)	61(2)	35(1)	83(2)	-23(2)	0(2)	-17(1)

Appendix

Supplementary data of [Rh(5,7-Diido-Ox)$(CO)_2$] **(7)**, for the atomic coordinates, bond distances and angles and anisotropic displacement parameters are given in appendix tables

Table 7.A: Atomic coordinates (x 10^4) and equivalent isotropic displacement parameters ($Å^2$ x 10^3) for [Rh(5,7-Diido-Ox)$(CO)_2$] (7). U(eq) is defined as one third of the trace of the orthogonalized U^{ij} tensor.

	x	y	z	U(eq)
I(2)	5997(1)	2500	3110(1)	20(1)
I(1)	8991(1)	2500	694(1)	21(1)
Rh(1)	9797(1)	2500	5430(1)	16(1)
O(1)	9463(3)	2500	3600(4)	19(1)
O(01)	10173(3)	2500	8148(5)	30(1)
C(6)	7111(4)	2500	5665(6)	19(1)
C(2)	8368(3)	2500	2331(6)	17(1)
O(02)	11452(3)	2500	5240(5)	27(1)
C(7)	7497(4)	2500	6767(6)	23(1)
C(02)	10819(4)	2500	5204(6)	22(1)
C(5)	7487(4)	2500	4510(6)	16(1)
C(1)	8737(4)	2500	3477(6)	17(1)
N(1)	8659(3)	2500	5667(5)	16(1)
C(8)	8269(4)	2500	6743(6)	20(1)
C(4)	7159(4)	2500	3316(6)	20(1)
C(01)	10029(4)	2500	7098(7)	21(1)
C(9)	8280(4)	2500	4553(6)	16(1)
C(3)	7585(4)	2500	2257(6)	17(1)

Table 7.B: Bond lengths (Å) and angles (°) for [Rh(5,7-Diido-Ox)$(CO)_2$] (7).

Bond	Distance	Bond	Angle
I(2)-C(4)	2.106(7)	C(01)-Rh(1)-C(02)	84.3(3)
I(1)-C(2)	2.083(6)	C(01)-Rh(1)-O(1)	176.1(3)
Rh(1)-C(01)	1.837(7)	C(02)-Rh(1)-O(1)	99.6(2)
Rh(1)-C(02)	1.860(8)	C(01)-Rh(1)-N(1)	96.1(3)
Rh(1)-O(1)	2.052(5)	C(02)-Rh(1)-N(1)	179.6(2)
Rh(1)-N(1)	2.068(5)	O(1)-Rh(1)-N(1)	80.02(19)
O(1)-C(1)	1.316(8)	C(1)-O(1)-Rh(1)	112.8(4)
O(01)-C(01)	1.155(8)	C(7)-C(6)-C(5)	120.7(6)
C(6)-C(7)	1.370(9)	C(7)-C(6)-H(6)	119.6
C(6)-C(5)	1.412(9)	C(5)-C(6)-H(6)	119.6
C(6)-H(6)	0.9300	C(1)-C(2)-C(3)	121.6(6)
C(2)-C(1)	1.397(9)	C(1)-C(2)-I(1)	119.0(5)
C(2)-C(3)	1.414(8)	C(3)-C(2)-I(1)	119.4(5)
O(02)-C(02)	1.142(9)	C(6)-C(7)-C(8)	119.5(6)
C(7)-C(8)	1.394(9)	C(6)-C(7)-H(7)	120.2
C(7)-H(7)	0.9300	C(8)-C(7)-H(7)	120.2
C(5)-C(4)	1.411(9)	O(02)-C(02)-Rh(1)	170.6(6)
C(5)-C(9)	1.430(9)	C(4)-C(5)-C(6)	126.4(6)
C(1)-C(9)	1.418(9)	C(4)-C(5)-C(9)	116.7(6)
N(1)-C(8)	1.350(8)	C(6)-C(5)-C(9)	116.9(6)
N(1)-C(9)	1.376(8)	O(1)-C(1)-C(2)	124.2(6)
C(8)-H(8)	0.9300	O(1)-C(1)-C(9)	119.7(6)
C(4)-C(3)	1.371(9)	C(2)-C(1)-C(9)	116.1(6)
C(3)-H(3)	0.9300	C(8)-N(1)-C(9)	119.0(6)
		C(8)-N(1)-Rh(1)	128.4(4)
		C(9)-N(1)-Rh(1)	112.7(4)
		N(1)-C(8)-C(7)	122.3(6)
		N(1)-C(8)-H(8)	118.8
		C(7)-C(8)-H(8)	118.8
		C(3)-C(4)-C(5)	121.1(6)
		C(3)-C(4)-I(2)	118.1(5)
		C(5)-C(4)-I(2)	120.9(5)

		O(01)-C(01)-Rh(1)	179.9(6)
		N(1)-C(9)-C(1)	114.7(6)
		N(1)-C(9)-C(5)	121.6(6)
		C(1)-C(9)-C(5)	123.7(6)
		C(4)-C(3)-C(2)	120.9(6)
		C(4)-C(3)-H(3)	119.5
		C(2)-C(3)-H(3)	119.5

Table 7.C: Anisotropic displacement parameters ($Å^2$ x 10^3) for Rh(5,7-Diido-Ox)$(CO)_2$] (7).The anisotropic displacement factor exponent takes the form: $-2\pi^2[h^2a^{*2}U^{11} + ... + 2 h k a^* b^* U^{12}]$

	U^{11}	U^{22}	U^{33}	U^{13}
I(2)	11(1)	26(1)	23(1)	-1(1)
I(1)	15(1)	33(1)	15(1)	1(1)
Rh(1)	13(1)	21(1)	15(1)	-4(1)
O(1)	12(2)	28(3)	17(2)	-1(2)
O(01)	26(3)	43(3)	20(2)	-10(2)
C(6)	15(3)	22(3)	21(3)	1(2)
C(2)	11(3)	21(3)	18(3)	-3(2)
O(02)	11(2)	42(3)	28(3)	-3(2)
C(7)	18(3)	30(4)	20(3)	8(3)
C(02)	26(4)	24(3)	17(3)	-1(3)
C(5)	13(3)	13(3)	22(3)	-2(2)
C(1)	14(3)	17(3)	21(3)	0(3)
N(1)	9(2)	24(3)	15(2)	1(2)
C(8)	15(3)	26(3)	18(3)	2(2)
C(4)	13(3)	23(3)	23(3)	-5(3)
C(01)	14(3)	25(3)	25(3)	-3(3)
C(9)	13(3)	18(3)	17(3)	2(2)
C(3)	16(3)	18(3)	17(3)	-3(2)

Appendix

Supplementary data of [Rh(5,7-DiMe-Ox)$(CO)_2$] **(8)** for the atomic coordinates, bond distances and angles and anisotropic displacement parameters are given in appendix tables

Table 8.A: Atomic coordinates (x 10^4) and equivalent isotropic displacement parameters ($Å^2$x 10^3) for [Rh(5,7-DiMe-Ox)$(CO)_2$] (8). U(eq) is defined as one third of the trace of the orthogonalized U^{ij} tensor.

	x	y	z	U(eq)
Rh(1)	1910(1)	-90(1)	-348(1)	11(1)
O(02)	1111(3)	-1675(1)	-1069(1)	24(1)
O(1)	2917(2)	-674(1)	471(1)	14(1)
O(01)	649(3)	874(1)	-1529(1)	27(1)
C(01)	1109(3)	493(2)	-1083(1)	18(1)
C(6)	3949(3)	2149(1)	1075(1)	17(1)
C(5)	4164(3)	1308(1)	1252(1)	13(1)
C(9)	3500(3)	713(1)	792(1)	11(1)
C(7)	3165(3)	2361(2)	478(1)	19(1)
C(02)	1399(3)	-1074(2)	-797(1)	16(1)
C(2)	4353(3)	-408(1)	1522(1)	15(1)
N(1)	2738(3)	938(1)	192(1)	12(1)
C(21)	4488(4)	-1313(2)	1686(1)	24(1)
C(4)	4976(3)	1033(2)	1858(1)	15(1)
C(1)	3580(3)	-153(1)	923(1)	12(1)
C(8)	2596(3)	1735(1)	41(1)	16(1)
C(41)	5727(3)	1646(2)	2353(1)	22(1)
C(3)	5039(3)	196(2)	1969(1)	16(1)

Table 8.B: Bond lengths (Å) and angles (°) for [Rh(5,7-DiMe-Ox)$(CO)_2$] (8).

Bond	Distance	Bond	Angle
Rh(1)-C(01)	1.844(2)	C(01)-Rh(1)-C(02)	89.23(10)
Rh(1)-C(02)	1.866(2)	C(01)-Rh(1)-O(1)	176.27(9)
Rh(1)-O(1)	2.0333(17)	C(02)-Rh(1)-O(1)	93.82(9)
Rh(1)-N(1)	2.075(2)	C(01)-Rh(1)-N(1)	95.76(9)
Rh(1)-Rh(1)#1	3.1345(17)	C(02)-Rh(1)-N(1)	173.58(9)
O(02)-C(02)	1.135(3)	O(1)-Rh(1)-N(1)	81.04(7)
O(1)-C(1)	1.329(3)	C(01)-Rh(1)-Rh(1)#1	91.51(8)
O(01)-C(01)	1.139(3)	C(02)-Rh(1)-Rh(1)#1	96.68(7)
C(6)-C(7)	1.370(4)	O(1)-Rh(1)-Rh(1)#1	90.25(6)
C(6)-C(5)	1.415(3)	N(1)-Rh(1)-Rh(1)#1	87.24(6)
C(6)-H(6)	0.9300	C(1)-O(1)-Rh(1)	112.89(14)
C(5)-C(9)	1.418(3)	O(01)-C(01)-Rh(1)	177.7(2)
C(5)-C(4)	1.425(3)	C(7)-C(6)-C(5)	120.4(2)
C(9)-N(1)	1.375(3)	C(7)-C(6)-H(6)	119.8
C(9)-C(1)	1.427(3)	C(5)-C(6)-H(6)	119.8
C(7)-C(8)	1.403(3)	C(6)-C(5)-C(9)	116.8(2)
C(7)-H(7)	0.9300	C(6)-C(5)-C(4)	124.1(2)
C(2)-C(1)	1.391(3)	C(9)-C(5)-C(4)	119.0(2)
C(2)-C(3)	1.417(3)	N(1)-C(9)-C(5)	121.9(2)
C(2)-C(21)	1.503(3)	N(1)-C(9)-C(1)	115.93(19)
N(1)-C(8)	1.328(3)	C(5)-C(9)-C(1)	122.2(2)
C(21)-H(21A)	0.9600	C(6)-C(7)-C(8)	119.3(2)
C(21)-H(21B)	0.9600	C(6)-C(7)-H(7)	120.4
C(21)-H(21C)	0.9600	C(8)-C(7)-H(7)	120.4
C(4)-C(3)	1.373(3)	O(02)-C(02)-Rh(1)	179.1(2)
C(4)-C(41)	1.507(3)	C(1)-C(2)-C(3)	119.0(2)
C(8)-H(8)	0.9300	C(1)-C(2)-C(21)	120.3(2)
C(41)-H(41A)	0.9600	C(3)-C(2)-C(21)	120.6(2)
C(41)-H(41B)	0.9600	C(8)-N(1)-C(9)	119.2(2)
C(41)-H(41C)	0.9600	C(8)-N(1)-Rh(1)	129.46(16)
C(3)-H(3)	0.9300	C(9)-N(1)-Rh(1)	111.31(14)
		C(2)-C(21)-H(21A)	109.5
		C(2)-C(21)-H(21B)	109.5

		H(21A)-C(21)-H(21B)	109.5
		C(2)-C(21)-H(21C)	109.5
		H(21A)-C(21)-H(21C)	109.5
		H(21B)-C(21)-H(21C)	109.5
		C(3)-C(4)-C(5)	117.4(2)
		C(3)-C(4)-C(41)	122.1(2)
		C(5)-C(4)-C(41)	120.5(2)
		O(1)-C(1)-C(2)	123.3(2)
		O(1)-C(1)-C(9)	118.8(2)
		C(2)-C(1)-C(9)	117.9(2)
		N(1)-C(8)-C(7)	122.4(2)
		N(1)-C(8)-H(8)	118.8
		C(7)-C(8)-H(8)	118.8
		C(4)-C(41)-H(41A)	109.5
		C(4)-C(41)-H(41B)	109.5
		H(41A)-C(41)-H(41B)	109.5
		C(4)-C(41)-H(41C)	109.5
		H(41A)-C(41)-H(41C)	109.5
		H(41B)-C(41)-H(41C)	109.5
		C(4)-C(3)-C(2)	124.4(2)
		C(4)-C(3)-H(3)	117.8
		C(2)-C(3)-H(3)	117.8

Table 8.C: Anisotropic displacement parameters ($Å^2$ x 10^3) for [Rh(5,7-DiMe-Ox)$(CO)_2$] (8). The anisotropic displacement factor exponent takes the form: $-2\pi^2[h^2a^{*2}U^{11} + ... + 2 h k a^* b^* U^{12}]$

	U^{11}	U^{22}	U^{33}	U^{23}	U^{13}	U^{12}
Rh(1)	11(1)	12(1)	11(1)	-1(1)	0(1)	0(1)
O(02)	30(1)	22(1)	21(1)	-7(1)	2(1)	-6(1)
O(1)	18(1)	11(1)	14(1)	-1(1)	-3(1)	-1(1)
O(01)	37(1)	28(1)	16(1)	3(1)	-4(1)	4(1)
C(01)	18(1)	19(1)	16(1)	-4(1)	1(1)	-1(1)
C(6)	16(1)	13(1)	24(1)	-5(1)	4(1)	-2(1)
C(5)	9(1)	15(1)	14(1)	-3(1)	4(1)	-1(1)
C(9)	9(1)	13(1)	11(1)	-1(1)	2(1)	0(1)

C(7)	22(1)	10(1)	26(1)	0(1)	3(1)	-1(1)
C(02)	14(1)	22(1)	12(1)	0(1)	3(1)	0(1)
C(2)	14(1)	16(1)	16(1)	2(1)	1(1)	1(1)
N(1)	11(1)	12(1)	12(1)	0(1)	2(1)	0(1)
C(21)	30(1)	18(1)	25(1)	6(1)	-5(1)	1(1)
C(4)	10(1)	22(1)	14(1)	-5(1)	1(1)	-2(1)
C(1)	11(1)	11(1)	14(1)	-1(1)	2(1)	-1(1)
C(8)	16(1)	14(1)	18(1)	3(1)	2(1)	0(1)
C(41)	16(1)	32(1)	19(1)	-9(1)	-1(1)	-4(1)
C(3)	14(1)	24(1)	12(1)	1(1)	0(1)	0(1)

Supplementary data of [Rh(5-Me-Sal-iProp)$(CO)_2$] **(9)** for the atomic coordinates, bond distances and angles and anisotropic displacement parameters are given in appendix tables

Table 9.A: Atomic coordinates (x 10^4) and equivalent isotropic displacement parameters ($Å^2$ x 10^3) for [Rh(5-Me-Sal-iProp)$(CO)_2$] (9) U(eq) is defined as one third of the trace of the orthogonalized U^{ij} tensor.

	x	y	z	U(eq)
Rh(1)	3720(1)	791(1)	380(1)	15(1)
O(01)	1067(2)	456(1)	-1594(2)	30(1)
O(02)	2144(2)	-141(1)	2894(2)	32(1)
O(1)	5225(2)	994(1)	2111(2)	21(1)
C(1)	6301(2)	1646(1)	-940(2)	17(1)
C(5)	8969(2)	1395(1)	3220(2)	20(1)
C(4)	9533(2)	1677(1)	1764(3)	25(1)
N(1)	4975(2)	1427(1)	-1260(2)	16(1)
C(2)	7147(2)	1533(1)	500(2)	17(1)
C(9)	3150(2)	2230(1)	-2742(3)	26(1)
C(8)	4431(2)	1662(1)	-2883(2)	20(1)
C(10)	4103(2)	934(1)	-3918(3)	25(1)
C(02)	2720(2)	215(1)	1936(2)	21(1)
C(3)	8637(2)	1752(1)	452(3)	24(1)

C(6)	7516(2)	1189(1)	3299(2)	19(1)
C(01)	2125(2)	588(1)	-922(2)	21(1)
C(7)	6573(2)	1229(1)	1953(2)	16(1)
C(51)	9957(2)	1303(1)	4663(3)	27(1)

Table 9.B: Bond lengths (Å) and angles (°) for [Rh(5-Me-Sal-iProp)$(CO)_2$] (9).

Bond	Distance	Bond	Angle
Rh(1)-C(01)	1.846(2)	C(01)-Rh(1)-C(02)	85.61(10)
Rh(1)-C(02)	1.865(2)	C(01)-Rh(1)-O(1)	170.34(7)
Rh(1)-O(1)	2.0182(16)	C(02)-Rh(1)-O(1)	85.73(8)
Rh(1)-N(1)	2.0880(18)	C(01)-Rh(1)-N(1)	98.37(9)
O(01)-C(01)	1.138(3)	C(02)-Rh(1)-N(1)	175.88(7)
O(02)-C(02)	1.131(3)	O(1)-Rh(1)-N(1)	90.38(7)
O(1)-C(7)	1.305(2)	C(7)-O(1)-Rh(1)	128.34(13)
C(1)-N(1)	1.295(3)	N(1)-C(1)-C(2)	129.34(19)
C(1)-C(2)	1.437(3)	N(1)-C(1)-H(1)	116.0(14)
C(1)-H(1)	0.99(2)	C(2)-C(1)-H(1)	114.6(14)
C(5)-C(6)	1.378(3)	C(6)-C(5)-C(4)	119.18(19)
C(5)-C(4)	1.406(3)	C(6)-C(5)-C(51)	120.64(19)
C(5)-C(51)	1.509(3)	C(4)-C(5)-C(51)	120.16(19)
C(4)-C(3)	1.369(3)	C(3)-C(4)-C(5)	120.0(2)
C(4)-H(4)	0.9300	C(3)-C(4)-H(4)	120.0
N(1)-C(8)	1.493(3)	C(5)-C(4)-H(4)	120.0
C(2)-C(3)	1.415(3)	C(1)-N(1)-C(8)	114.76(16)
C(2)-C(7)	1.420(3)	C(1)-N(1)-Rh(1)	122.01(14)
C(9)-C(8)	1.517(3)	C(8)-N(1)-Rh(1)	123.23(13)
C(9)-H(9A)	0.9600	C(3)-C(2)-C(7)	118.74(18)
C(9)-H(9B)	0.9600	C(3)-C(2)-C(1)	117.17(18)
C(9)-H(9C)	0.9600	C(7)-C(2)-C(1)	124.09(18)
C(8)-C(10)	1.524(3)	C(8)-C(9)-H(9A)	109.5
C(8)-H(8)	0.94(2)	C(8)-C(9)-H(9B)	109.5
C(10)-H(10A)	0.9600	H(9A)-C(9)-H(9B)	109.5
C(10)-H(10B)	0.9600	C(8)-C(9)-H(9C)	109.5
C(10)-H(10C)	0.9600	H(9A)-C(9)-H(9C)	109.5
C(3)-H(3)	0.9300	H(9B)-C(9)-H(9C)	109.5
C(6)-C(7)	1.414(3)	N(1)-C(8)-C(9)	110.41(17)

C(6)-H(6)	0.9300	N(1)-C(8)-C(10)	111.47(17)
C(51)-H(51A)	0.9600	C(9)-C(8)-C(10)	113.47(18)
C(51)-H(51B)	0.9600	N(1)-C(8)-H(8)	103.1(13)
C(51)-H(51C)	0.9600	C(9)-C(8)-H(8)	107.1(14)
		C(10)-C(8)-H(8)	110.7(14)
		C(8)-C(10)-H(10A)	109.5
		C(8)-C(10)-H(10B)	109.5
		H(10A)-C(10)-H(10B)	109.5
		C(8)-C(10)-H(10C)	109.5
		H(10A)-C(10)-H(10C)	109.5
		H(10B)-C(10)-H(10C)	109.5
		O(02)-C(02)-Rh(1)	178.34(19)
		C(4)-C(3)-C(2)	121.8(2)
		C(4)-C(3)-H(3)	119.1
		C(2)-C(3)-H(3)	119.1
		C(5)-C(6)-C(7)	122.29(19)
		C(5)-C(6)-H(6)	118.9
		C(7)-C(6)-H(6)	118.9
		O(01)-C(01)-Rh(1)	173.46(19)
		O(1)-C(7)-C(6)	118.53(18)
		O(1)-C(7)-C(2)	123.54(17)
		C(6)-C(7)-C(2)	117.93(18)
		C(5)-C(51)-H(51A)	109.5
		C(5)-C(51)-H(51B)	109.5
		H(51A)-C(51)-H(51B)	109.5
		C(5)-C(51)-H(51C)	109.5
		H(51A)-C(51)-H(51C)	109.5
		H(51B)-C(51)-H(51C)	109.5

Table 9.C: Anisotropic displacement parameters ($Å^2$ x 10^3) for [Rh(5-Me-Sal-iProp)$(CO)_2$] (9)The anisotropic displacement factor exponent takes the form: $-2\pi^2[h^2a^{*2}U^{11} + ... + 2 h k a^* b^* U^{12}]$

	U^{11}	U^{22}	U^{33}	U^{23}	U^{13}	U^{12}
Rh(1)	14(1)	17(1)	13(1)	0(1)	-1(1)	-1(1)
O(01)	23(1)	40(1)	29(1)	-2(1)	-9(1)	-6(1)
O(02)	27(1)	42(1)	26(1)	10(1)	3(1)	-7(1)
O(1)	15(1)	33(1)	14(1)	1(1)	-2(1)	-3(1)
C(1)	21(1)	15(1)	16(1)	2(1)	-1(1)	-2(1)
C(5)	22(1)	16(1)	23(1)	-1(1)	-8(1)	0(1)
C(4)	17(1)	27(1)	32(1)	3(1)	-5(1)	-7(1)
N(1)	19(1)	16(1)	14(1)	2(1)	-2(1)	-1(1)
C(2)	18(1)	15(1)	18(1)	1(1)	-3(1)	-1(1)
C(9)	32(1)	21(1)	26(1)	5(1)	-8(1)	2(1)
C(8)	21(1)	24(1)	14(1)	6(1)	-3(1)	-3(1)
C(10)	27(1)	32(1)	17(1)	-1(1)	-1(1)	4(1)
C(02)	17(1)	25(1)	20(1)	-1(1)	-4(1)	-1(1)
C(3)	21(1)	26(1)	24(1)	5(1)	-2(1)	-6(1)
C(6)	21(1)	20(1)	16(1)	1(1)	-3(1)	-1(1)
C(01)	23(1)	21(1)	18(1)	0(1)	1(1)	-1(1)
C(7)	17(1)	15(1)	16(1)	-3(1)	-2(1)	1(1)
C(51)	23(1)	28(1)	29(1)	1(1)	-12(1)	-2(1)